Mathematical modelling and life-cycle energy and financial analysis of solar kilns for wood drying

A thesis submitted in fulfilment of the requirements for the degree of

Doctor of Philosophy

By

Mahmudul Hasan

B.Sc. (Mechanical Engineering)

School of Chemical and Biomolecular Engineering

Faculty of Engineering and Information Technologies

The University of Sydney, Australia

June 2017

Declaration

I, Mahmudul Hasan, declare that the entire contents of this thesis are, to the best of my knowledge and belief, original, except where otherwise acknowledged. This thesis contains no material that has been submitted previously, in whole or in part, for the award of any other academic degree or diploma.

………………………

Mahmudul Hasan

June 2017

Dedications

Dedicated

To

My parents and wife who are my inspirations.

Acknowledgment

I would like to express my heartiest gratefulness and indebtedness to my principal supervisor, Professor Timothy Langrish, for his scholastic supervision, inestimable help, proper guidance/suggestions throughout my study and research at The University of Sydney. His constant encouragement, time-to-time feedback, and immense knowledge in the research context were the key motivation and inspiration throughout my study. I have been especially fortunate to work with such a great supervisor.

I also express my sincere gratitude to my co-supervisor, A/Prof. Ali Abbas, for his insightful suggestions and valuable advice. As an auxiliary supervisor, he was strong and supportive.

I would also like to express my special thanks to Dr. Nawshad Haque (CSIRO, Australia) for his insightful advice and intellectual support. I gratefully acknowledge the financial support from The University of Sydney for this research. I extend my extreme thankfulness to all the members in our research group for their help and valuable support.

Finally, I feel highly indebted to my beloved wife, Umma, and other family members for her unconditional support, patience, and love.

List of publications

Book chapter:

1. **Hasan, M.** and Langrish, T.A.G. (2017). Solar dryers: A green technology for the Australian agricultural and forest industries. In Rasul, M., Azad, A.K., and Sharma, S. (Eds.), Clean Energy for Sustainable Development. Academic Press, Elsevier, Oxford, United Kingdom.

Peer-reviewed journal papers:

1. **Hasan, M.**, Langrish, T.A.G (2016). Development of a sustainable methodolgy for life-cycle performance evaluation of solar dryers. ***Solar Energy***, 135, 1-13. doi: 10.1016/j.solener.2016.05.036

2. **Hasan, M.**, Zhang, M., Wu, W., and Langrish, T.A.G. (2016). Discounted cash flow analysis of greenhouse-type solar kilns. ***Renewable Energy***, 95, 404-412. doi: 10.1016/j.renene.2016.04.050

3. **Hasan, M.**, Langrish, T.A.G. (2016). Time-valued net energy analysis of solar kilns for wood drying: A solar thermal application. ***Energy***, 96, 415-426. doi: http://dx.doi.org/10.1016/j.energy.2015.11.081

4. **Hasan, M.**, Langrish, T.A.G. (2015). Embodied energy and carbon analysis of solar kilns for wood drying. ***Drying Technology***, 33 (8), 973-985. doi: 10.1080/07373937.2015.1010207

5. **Hasan, M**., Langrish, T.A.G. (2014b). Performance comparison of two solar kiln designs for wood drying using a numerical simulation. *Drying Technology*, 33(6), 634-645. doi: 10.1080/07373937.2014.968254

6. **Hasan, M**., Langrish, T.A.G. (2014a). Numerical simulation of a solar kiln design for drying timber with different geographical and climatic conditions in Australia. *Drying Technology*, 32 (13), 1632-1639. doi: 10.1080/07373937.2014.915556

Conferences/Seminars:

1. **Hasan, M**. and T.A.G. Langrish. (2014b). Timber drying by solar kilns: A performance comparison. Conference proceedings, *Energy Conversion and Clean Energy Technology*, paper 0004, BSME-ICTE, 19-21 December, 2014, **Dhaka**, Bangladesh.

2. **Hasan, M**. (2014a). Mathematical modelling and time-valued energy analysis of solar kilns for wood drying. *A Research Seminar*, October 31, 2014, University of Sydney, **Australia**.

Abbreviations

Symbol	Description		Symbol	Description
FSP	Fibre saturation point $(kgkg^{-1})$		D_r	reference diffusion coefficient $(m^2\ s^{-1})$
X	moisture content $(kgkg^{-1})$		D_E	activation energy (K)
P_{vd}	vapour pressure at dry-bulb temperature (Pa)		E	modulus of elasticity (Pa)
P_{vw}	vapour pressure at wet-bulb temperature (Pa)		C_I	instantaneous compliance (Pa^{-1})
Y_w	saturation humidity at dry-bulb temperature $(kgkg^{-1})$		E_0	modulus of elasticity for bone-dry timber (Pa)
Y	bulk-air humidity $(kgkg^{-1})$		E_g	Green modulus of elasticity (Pa)
T_d	dry-bulb temperature (K)		M	thermal mass $(J\ K^{-1})$
D_b	diffusion coefficient for bound water $(m^2\ s^{-1})$		m	Mass (kg)
D	diffusion coefficient $(m^2\ s^{-1})$		E_n	net energy flow rate (W)
p_v	partial pressure of water vapor at local temperature and moisture content (Pa)		W_n	net water flow rate $(kg\ s^{-1})$
			SG	solar gain (W)
			CL	convection losses (W)
			RL	radiation losses (W)
			C	convection heat transfer (W)

Symbol	Description	Symbol	Description
TR	thermal radiation heat transfer (W)	g	acceleration due to gravity (m s^{-2})
SR	solar radiation heat transfer (W)	VR	venting rate (kg s^{-1})
$Evap$	evaporation rate (kg s^{-1})	z	distance through the timber thickness (m)
$Cond$	condensation rate (kg s^{-1})	G_r	recirculating air mass flow rate (kg h^{-1})
T_p	plate temperature (K)		
$Hvap$	latent heat of vaporization (J kg^{-1})	G	air mass flow rate (kg h^{-1})
		SLD	scaled linear dimension (m)
WS	water spray rate (kg s^{-1})	OLD	original linear dimension (m)
LR	leakage rate (kg s^{-1})	SSA	scaled surface area (m^2)
Q	radiation energy flow rate (W)	OSA	original surface area (m^2)
		SV	scaled volume (m^3)
A	surface area (m^2)	OV	original volume (m^3)
I_T	total solar radiation (W m^{-2})	OSV	original stack volume (m^3)
G_{cb}	beam radiation (W m^{-2})	U_{stack}	stack velocity (m s^{-1})
R_b	ratio of the beam radiation on a tilted surface to that on a horizontal surface	EE	Embodied energy (J)
		OE	operational energy (J)
		LCEE	life cycle embodied energy (J)
G_{cd}	diffuse radiation (W m^{-2})		
h	heat transfer coefficient (W m^2 K^{-1})	LCEC	life cycle embodied carbon (kg CO$_2$-e)

Symbol	Description	Symbol	Description
EU	European Union	NEA	net energy analysis
ISO	International Organization for Standardization	FEV	future energy value (J)
		PEV	Present energy value (J)
LCA	life cycle assessment	d	discount rate (%)
AusLCI	Australian Life Cycle Inventory	*TPEPV*	total present energy production value (J)
AIM-CED	Australian Impact Method with Normalization including Cumulative Energy Demand	*TPECV*	total present energy consumption value (J)
		FEPV	future energy production value (J)
EoL	End of life	*FECV*	future energy consumption value (J)
GWP	global warming potential (t-CO_2-e)	NPEV	net present energy value (J)
GHG	greenhouse gas	TPELV	total present energy loss value (J)
ICE	Inventory of Carbon and Energy	NBLR	Net benefit to loss ratio
LCNE	life-cycle net energy	PVEL	present value of energy losses (J)
MARR	minimum attractive rate of return (%)	PDEV	Present drying energy value (J)
MC	moisture content ($kg kg^{-1}$)		
n	time into the kiln service life (years)	PVFE	Present value of fan energy (J)

Symbol	Description
PVLE	Present value of loading/unloading energy (J)
PVEE	Present value of embodied energy (J)
DEPP	discounted energy payback period (years)
IRR	Internal rate of return (%)
DCF	discounted cash flow
LCCF	life-cycle cash flow
FC	future cost (AUD)
FB	future benefit (AUD)
PC	Present cost (AUD)
PB	Present benefit (AUD)
DPB	discounted present benefits (AUD)
TPB	total present benefit (AUD)
TPC	total present cost (AUD)
i	inflation rate (%)
NPCB	net present cash benefits (AUD)
PELC	Present energy losses costs (AUD)

Symbol	Description
PDEB	Present drying energy benefits (AUD)
PFEC	Present fan energy costs (AUD)
PLC	Present loading/unloading costs (AUD)
PMLC	Present material & labor costs (AUD)

Greek symbols

Symbol	Description
γ	the slope angle (radians)
ε_s	shrinkage strain (mm/mm)
σ	Stress (Pa)
C_p	specific heat capacity (J kg^{-1} K^{-1})
ρ_g	reflectance of the ground
ε_p	emissivity of the panel
τ	transmissivity of cover
βp	reflectivity of the panel
βc	reflectivity of the cover
μ_G	dynamic viscosity of the air (kg m^{-1} s^{-1})

Symbol	Description	Symbol	Description
β	thermal expansion coefficient (m m^{-1} K^{-1})	*Subscripts*	
		f	floor
η_p	pick-up efficiency (%)	*air*	internal air
η_d	drying efficiency (%)	*nr*	north roof
η_{d1}	first-day drying efficiency (%)	*sr*	south roof
		na	north absorber
η_{pd}	present drying efficiency (%)	*sa*	south absorber
k	thermal conductivity (W m^{-1} K^{-1})	*intw*	internal walls
		intf	internal floor
ρ_t	Density of the timber (kg m^{-3})	*int*	internal
		w	walls
C_{pt}	specific heat capacity of the timber (J kg^{-1} K^{-1})	*a*	ambient
		extsr	external south roof
ζ_i	free shrinkage of the ith layer	*intsr*	internal south roof
α	the shrinkage coefficient (m m^{-1}/kg kg^{-1})	*extnr*	external north roof
		intnr	internal north roof
σ	Stefan-Boltzmann constant (W m^{-2} K^{-4})	*intsa*	internal south absorber
		intna	internal north absorber

Abstract

There is a general challenge to improve the designs of solar dryers for the direct drying of various materials through the uses of robust models in conjunction with methods incorporating an appropriately defined set of performance parameters for evaluating the performance of solar kilns. However, the use of prevailing methods is unlikely to provide a sustainable means of comparison between various solar-kiln designs, unless a whole life-cycle perspective is taken into consideration. The key tasks involved in this thesis were to develop a robust mathematical model and its simulation procedure for predicting the performance of solar kilns, to build a life cycle assessment (LCA) model for assessing the embodied energy and embodied carbon of solar kilns, to develop a life-cycle net energy model and a life-cycle financial model for assessing the life-cycle performance of solar kilns, and to illustrate how closely these two perspectives are aligned for the present case and how they can lead to significantly different conclusions for some other cases.

A review of different drying models (e.g. empirical, diffusion, and multiple mechanism) indicated that a diffusion model with a moisture-content driving force was an appropriate choice for describing the moisture movement during drying, and thus this drying model has been incorporated with the energy flow model in the overall simulation model.

To examine the capability and usefulness of the solar kiln model and its simulation procedure for predicting the drying behaviors for different solar kiln designs, the model was numerically solved for two typical greenhouse-type wood-drying solar kilns (Oxford and Boral). The assessment of life cycle embodied energy and embodied carbon values for the

construction and maintenance of the two solar kilns (Oxford and Boral) by developing a life cycle assessment (LCA) model in "SimaPro 7.1.8 version".

To analyse the total life-cycle energy use in solar kilns, an innovative performance evaluation methodology, which considers the total life-cycle (LC) energy effectiveness in present-value terms, together with a defined set of present value performance indicators (PVPIs), has been proposed here. In the last stage of the thesis, a life-cycle cash flow (LCCF) analysis has also been carried out to compare how closely the life-cycle net energy (LCNE) and the LCCF approaches are aligned for the present case and how they can lead to significantly different recommendations for some other scenarios.

To conclude, the LCNE approach (which is not strongly dependent on the future uncertain energy prices), together with the defined PVPIs, has been suggested to be considered as a robust and reliable method for life-cycle performance evaluation of solar kilns. This approach may have an immediate application for dryer designers and manufacturers to assess and improve the performance of solar dryers to subsequently help prospective customers.

Table of contents

List of Figures

List of Tables

Chapter 1:   Introduction

1.1   Background

Timber has been suggested by many researchers, including Awadalla et al. (2004) and Falk (2009), to continue as a primary raw material for many products, in building construction and in the furniture industry. Drying of wood is an inevitable process for reducing the moisture contents (MCs) down to a level at which the wood is immediately suitable for normal services. In modern society, due to the depletion and general awareness about the ecological consequences of burning fossil fuels, it is desirable to implement alternative energy sources, such as solar energy, for drying processes. Concerns regarding greenhouse gas (GHG) emissions (related to the rapid depletion of fossil fuels), together with drying being an energy-intensive process, has prompted the development of solar-drying systems on an industrial scale (Luna et al., 2009; Pirasteh et al., 2014; Romano et al., 2009; Sharma et al., 2009). Because of the low operating and construction costs, solar kilns for the purpose of wood drying have received special attention in recent years. In addition, there has been evidence, including Helwa et al. (2004), Chadwick and Langrish (1996), and Langrish et al. (1992) indicating that solar-assisted kiln-drying of wood improves the productivity of timber processing (when compared with open-air drying) and quality of the end-use timber. These favorable features of solar kilns for wood drying have been the key motivation for this research.

1.2   Problem statement and research gaps

Over the last three decades, many numerical and experimental studies, including Aktaş et al. (2009), Jairaj et al. (2009), Romano et al. (2009), and Smitabhindu et al. (2008), for various

solar dryers have been carried out. Most solar dryers were designed for specific drying materials or climatic conditions. The simulation studies were also either type- and site-specific or did not consider long-term performance indicators.

The overall LC energy effectiveness of a solar dryer is dependent on the on-going energy inflows and outflows that occur at different times in the past, the present, and the future and the embodied energy (EE) requirements. The total life-cycle energy use in solar kilns is the sum of the EEs (assessed through a life cycle assessment model) and the total on-going OEs (predicted through a robust simulation) consumed over the whole operational life. EE is the total amount of energy consumed during the extraction of raw materials, the transport, manufacturing, construction, use (maintenance and renovation) and disposal phases. By contrast, OE is the energy required to operate (or generated by operating) the built facility in terms of processes, such as space conditioning, lighting and operating other appliances. Assessing the OE flows means assessing the annual, on-going operating energy (costs) throughputs, while the EE assessment means assessing the capital energy (cost) requirements. There is a key need to combine the EE (capital cost) with the annual, on-going operating energy (costs) for wood-drying solar kilns in order to evaluate the overall energy effectiveness and hence develop a sustainable methodology to compare the performance of kiln designs.

Literature reviews (Altobelli et al., 2014; Bucki and Perre, 2003; Romano et al., 2009; Singh and Kumar, 2012) of existing performance evaluations for solar dryers reveal that, despite several simulation and experimental studies being carried out, no or little attempt has been

made to develop a standard and robust LC performance evaluation method, so that it can be utilized for performance comparison between the kiln designs in present value terms.

Traditionally, manufacturers, investors, economists and decision makers choose projects based on their life cycle economic return, which is determined by the principle that governs the "time value of money". This approach may need development when analyzing energy-intensive technologies/utilities, such as solar dryers, because it measures cash flow, an indirect and often inaccurate measure of energy flow. Furthermore, the monetary value of energy does not always represent its true value to society because of subsidies, inaccurate pricing techniques and policies, and accounting confusion caused by inflation. As a result, the current methods for performance evaluation of solar kilns are unlikely to be able to address some key questions: (a) What is the certainty that the approach gives a robust framework for selecting an optimum design? (b) Does the decision for the optimum design change if a narrow or wide range of kiln designs is considered? (c) If a narrow or wide range of economic or environmental impact indicators is considered, what is the value for the stakeholders? (d) What is the most useful methodology for optimization model to identify the best design? These key questions and developing a sustainable methodology for life-cycle performance evaluation of solar kilns have been addressed in this thesis.

1.3   Significance of the study

The drying operation for wood processing is typically an energy-intensive process, as evaporation of moisture requires significant amounts of energy (Bentayeb et al., 2008). Thus, utilization of direct solar energy through the best possible solar dryer design can greatly improve the overall sustainability and profitability of the wood-processing industry.

However, the development of solar-drying technology, such as large-scale solar drying facilities, must be based on sound knowledge of the energy resource and the anticipated performance of the associated dryer (i.e. kiln) designs over the expected service life (Singh and Kumar, 2012). In this research, a sustainable method for evaluating the performance of solar dryers over an expected service life of 20 years has been developed in the context of hardwood drying.

The key significance of this thesis is that the model proposed here for life-cycle performance evaluation of solar kilns considers the total life-cycle (LC) energy effectiveness in present-value terms, with a defined set of present value performance indicators (PVPIs). In addition, a life-cycle cash flow (LCCF) analysis has been carried out in this thesis to compare how closely the life-cycle net energy (LCNE) and the LCCF approaches are aligned and how they can be significantly different for decision making processes. Thus, the findings of this thesis may facilitate to bring technology innovations for solar kiln designer/manufacturers, and help them to restructure their research and development activities in order to improve and analyse the design/performance of solar kilns. Moreover, it may encourage the agricultural and forest products processing industries to utilise the great potential of solar dryers for reducing the operational costs and greenhouse gas (GHG) emissions.

1.4   Objectives of the thesis

The main aim of this thesis was to develop a sustainable methodology to compare and make sound judgement on the relative performance of different solar dryer designs. However, the specific objectives of this thesis are mentioned as follows:

- To identify and discuss the future opportunities of solar kilns in the Australian context

- To develop a robust mathematical model, together with a simulation procedure, that is capable of predicting the operational performance of solar kilns in different geographical and climatic conditions.

- To implement a simulation procedure for predicting and comparing the operational performance between different solar kiln designs

- To construct a life cycle assessment (LCA) model in order to assess the embodied energy (EE) and the embodied carbon (EC) of solar kilns.

- To develop a sustainable methodology, in terms of life-cycle net energy analysis, for the life-cycle performance evaluation of solar dryers for wood drying.

- To carry out a life-cycle financial analysis for solar dryers and to illustrate its alignment with the life-cycle net energy analysis.

One of the key limitations of this research was that the proposed model was applied and analysed for only two case-study solar kiln designs. A good level of detail regarding solar kiln designs, dimensions, construction materials, and operating principles is required for the overall model and they are not generally available in the literature. This situation restricted the number of reference case kiln designs to be studied in a pre-defined time frame. However, further works on other designs of kilns (e.g. Gough design) can be undertaken to develop more reference case studies, which will increase the confidence of the kiln manufacturers/designers for making more informed design decisions for solar kilns.

1.5 Layout of this thesis

This thesis is divided into nine chapters.

Chapter 1 introduces the background to this research, the research questions and research gaps, the problem statement, the significance of the study, and the objectives. In addition, it outlines the thesis layout, with a brief introduction to each chapter.

Chapter 2 provides information about the significance and the scope of solar drying for agricultural and forest industries in the Australian context.

Chapter 3 describes the key properties (e.g. physical, mechanical, and transport) of wood during drying, as required for this research. This chapter also reviews different drying models, and explains why and how an appropriate model has been selected for this thesis. In addition, this chapter describes the climatic data, together with their sources, as used for this research.

Chapter 4 focuses on the development of a robust mathematical model, together with the simulation procedure, for solar kilns. The numerical simulation for assessing the operational performance of a given solar kiln with different geographical and climatic conditions has been discussed in this chapter. This chapter also reviews the validation of the basic model that has been carried out by Haque (2002).

Chapter 5 describes the use of the simulation procedure for the performance comparison between two different solar kilns as a case study. It also describes the design and dimensional parameters of the two case-study solar kilns.

Chapter 6 presents a life cycle assessment (LCA) model for assessing the embodied energy and carbon for the two solar kilns. It also describes the scope and objectives of the LCA model in accordance of international Organization for Standardization (ISO) guidelines on LCA.

Chapter 7 proposes and describes a sustainable methodology, based on life-cycle net energy analysis, for performance evaluation of solar kilns for wood drying. In this chapter, the significance of the approach of evaluating the performance of solar kilns, in terms of present value performance indicators (PVPIs) has also been described in detail.

Chapter 8 describes a life-cycle financial analysis of solar kilns for wood drying. This chapter also describes how closely the life-cycle net energy analysis is aligned with the life-cycle financial analysis of the two solar kilns, and why and how these energy and financial comparisons between solar kilns can be significantly different for some other cases.

Chapter 9 presents the conclusions of the research and the recommendations for future works.

Chapter 2:   Opportunities for solar kilns in drying Australian agricultural and forest products

2.1   Introduction

Solar drying of agricultural products, such as fruits and vegetables and forest products, e.g. timber, has been internationally demonstrated to be a promising technology to improve the end-use quality, reduce GHG emissions from the process industry, improve the shelf life, reduce operational, storage and transportation costs and encapsulate the original flavour and nutritional value of fruits and vegetables (Janjai et al., 2011; Pirasteh et al., 2014; Prakash and Kumar, 2014). Australia has a strong primary industry sector, while its vegetable-growing industry contributed around $3.7 billion to the gross value of agricultural production in 2013-2014, which was a 12% increase from 2011-12 (Australian Bureau of Agricultural and Resource Economics and Sciences, 2014). However, higher yields during the growing seasons have traditionally caused a large influx of those fruits and vegetables into the domestic market of Australia, leading to reduced prices and large amounts of waste per year. An analysis of household food waste by Baker et al. (2009) mentioned that Australian households throw out more than $5 billion worth of food each year, of which fruits and vegetables were valued at $1.1 billion. While two million people in Australia still rely on food relief, it was mentioned, in a CSIRO magazine (ECOS), that total food wastage is currently costing Australians up to $10 billion each year. In addition to the direct financial costs of this waste, the environmental impact associated with excessive greenhouse gas emissions and water use is substantial.

Within the wider agricultural industry, the hardwood products industry is also a growing area of Australia's primary and secondary industry sectors, with hardwood plantations increasing six-fold over the period between 1994 and 2010 (Australian Bureau of Statistics, 2013). Drying of hardwood is an energy-intensive and inevitable process for reducing the moisture contents (MCs) down to a level at which the wood is immediately suitable for normal use, such as furniture, joinery and construction materials, as mentioned by Falk (2009) and Bentayeb et al. (2008). The better productivity and quality of solar-assisted kiln-dried timber [e.g. Chadwick and Langrish (1996) and Helwa et al. (2004)], together with the low operating and embodied energy costs, have motivated the application of solar kilns for wood drying to ensure that the final kiln-dried products remain competitive in the market. The strong primary industry sector, with significant spoilage of fruits and vegetables, low export volumes, and the necessity of quality timber products, together with the availability of solar radiation (Bureau of Resources and Energy Economics, 2014), is likely to make Australia a favorable place for the development of solar drying technology, especially for industries involved in timber, fruits, and vegetables processing, as evident from Fuller (2001) and Lovegrove and Dennis (2006). However, there are only two or three small companies in Australia that manufacture solar dryers for timber and fruit processing, indicating that there still exists a significant opportunity to develop this business, especially if Australia is to decarbonize its economy at the required rate and compete in ever increasing international trade, as mentioned by Odonoghue and Fuller (1999) and Fuller (2011).

2.2   Australian horticultural industry outlook

Australia's horticulture industry consists of a wide range of products, including fruits and vegetables. In 2012-2013, the production of tomatoes, bananas, and grapes increased by

23%, 16%, and 6%, respectively, since 2011-2012 (Australian Bureau of Statistics, 2013).

Australia's horticultural industry was the nation's third largest agricultural industry in 2011-12 based on the gross value of production (Horticulture Australia Limited, 2012). In order to show the overall domestic and international markets in the years of 2010-11 and 2011-12 for fruits and vegetables in Australia, the import and export values for these commodities are given in Table 2.1.

Table 2.1. Imports and exports values (millions of dollars) for horticultural commodities (Australian Bureau of Agricultural and Resource Economics and Sciences, 2012a).

Commodity	Imports		Exports	
	2010-2011	2011-2012	2010-2011	2011-2012
Fruits	1022 (56%)	1194 (57%)	651 (59%)	734 (59%)
Vegetables[1]	786 (44%)	908 (43%)	460 (41%)	505 (41%)
Total	1808	**2102**	1111	**1239**

[1] Includes fresh and processed products.

Despite strong agricultural growth in 2011-2012 (Australian Bureau of Statistics, 2013), Australia exported $1.239 billion worth of total fruits and vegetables (i.e. fresh plus processed products), while Australia imported $2.102 billion worth of these materials, resulting in an overall trade deficit of $863 million, as shown in Table 2.1. While Australia had a trade surplus (i.e. exports exceed imports values) in fresh vegetables (Horticulture Australia Limited, 2012) , the trade deficit was mainly due to high imports of processed fruits and vegetables (Australian Bureau of Agricultural and Resource Economics and Sciences, 2012a). This issue has also recently been addressed in the Australian 44th parliamentary

library briefing book by Rob Dossor (Dossor, 2013), mentioning that "the Australian processed food sector faces a difficult future, as increased imports erode the sector's domestic market share". It was mentioned in Horticulture Australia Limited (2012) that produce was imported into Australia out of season or during periods of domestic shortage due to production failures, an inability to produce the commodity "and/or" production shortfalls relative to demand.

The total amount of food wastage in Australia is valued at $10 billion each year (OzHarvest, 2014), with two million people still relying on food relief, and opportunities may be opened up for exporting processed products to new markets in Asia or the Middle East. Therefore, preservation of surplus produce during peak production periods can diversify the opportunities for generating income and employment by small and marginal farmers and small and medium-scale horticultural industries in Australia. This situation, coupled with increased fuel and labor costs, is likely to motivate the extension of solar-drying facilities for fruits and vegetables in Australia in order to ensure food security for the entire population. This preservation may maximize the potential capacity of the primary production sector, and stabilize food supplies in the domestic and international markets throughout the year at stable and reasonably remunerative prices.

2.3   Opportunity for solar dryers to process fruits in Australia

Inadequate preservation and storage facilities, and lack of marketing facilities, lead to the spoilage of large quantity of agricultural produce in Australia (Baker et al., 2009; Horticulture Australia Limited, 2012). It has been found that the post-harvest losses are in the range of 25-30% for fruits and vegetables (Aravindh and Sreekumar, 2015). Drying of

agricultural products is still the most widespread preservation technique and is becoming an increasingly popular alternative to marketing fresh fruits, since demand for high-quality dried products is continuously increasing throughout the world (Fadhel et al., 2005; Janjai et al., 2011; Romano et al., 2009). Solar drying is seen as a means of preserving product quality and providing opportunities for value addition and income from marketing food produce in local, regional and international markets. The use of solar kiln technology for the drying of different fruits, including apples (Aktaş et al., 2009; Romano et al., 2009), bananas (Janjai et al., 2011; Smitabhindu et al., 2008), and grapes (Fadhel et al., 2005; Jairaj et al., 2009; Pangavhane and Sawhney, 2002), has been investigated both at small and commercial levels. Due to a relatively high average initial MC (above 80%) of the fresh fruits, drying of fruits is an energy-intensive process, as shown in Table 2.2. The potential of solar fruit-drying operations for reducing the drying energy costs and the associated GHG emissions for the fruit-processing industries, and hence in making the industry commercially competitive both in regional and international platforms, has been summarized in Table 2.2.

While the production data for dry fruits and vegetables are not available in the website of the Australian Bureau of Statistics, an estimation (Stefan et al., 2003) indicated that about 20% of the freshly-produced fruits and vegetables in the world are dried to increase their shelf-lives and promote food security. Thus, the drying quantity for a particular fruit has been assumed to be the 20% of its total production in Australia (Australian Bureau of Statistics, 2013). Since every variety of fruits has its own initial and final safe MCs, the energy requirements for drying the selected fruits has been estimated based on these initial and final safe MCs of the fruits, which were taken from published materials (Khuntia et al., 2003; Sandra and Kim, 2011). The savings in the drying costs and the GHG emissions have been

estimated based on the local utility price of electricity (Department of Energy and Water Supply, 2015) and the National Average Carbon Emissions (NACE) data (Australian Federal Chamber of Automotive Industries, 2011), respectively.

Table 2.2. Summary of potential savings by solar dryers for drying selected fruits in Australia (base year 2011-2012).

Products	Quantity[2] (kt/year)	Initial MC^3 (%)	Final MC^3 (%)	Energy saving[4] (TJ/year)	Cost saving[5] (million AU$/year)	GHG savings[6] (kt CO_2/year)
Apples	58	80	24	43	10	9.8
Bananas	66	75-80	15	51	12	11.5
Pears	22	84	15	19	4	4.2
Grapes	353	80	15-20	227	66	63.17
Peaches	11	85	18	10	2	2.08
Total				**350**	**94**	**90.75**

[2] 20% of the total production (Australian Bureau of Statistics, 2013) has been assumed to be dried. [3] Initial and safe final MC (wet basis) has been taken from (Khuntia et al., 2003). [4] Estimated energy required to remove the moisture from the samples. [5] Based on local utility price of electricity (Department of Energy and Water Supply, 2015). [6] Based on National Average Carbon Emissions 2012 data (Australian Federal Chamber of Automotive Industries, 2011).

It is shown in Table 2.2 that the likely savings, by using solar dryers throughout Australia, in the drying costs and GHG emissions for the selected fruits can be estimated to be 350 TJ per year. This energy can be readily delivered by an appropriate application of solar kilns, as suggested in many references (Fuller, 2001; Fuller, 2011; Janjai et al., 2011; Smitabhindu et al., 2008). These energy savings for drying the selected fruits in Australia are equivalent to saving approximately AU$ 94 million and 90.75 kilotonnes per year in the drying energy costs and GHG emissions, respectively, as shown in Table 2.2.

2.4   Prospects of solar kilns for vegetable drying in Australia

Australia has a well-established primary agricultural production sector in different climatic areas over a wide spectrum of products. However, overproduction of vegetables during the seasons leads to fluctuating vegetable prices that may not be commercially sustainable, which in turn increases the wastage through unsold products. In Australia, an estimated 25% of vegetable production goes to waste each year due to the temporary oversupply of vegetable produce (AugVeg, 2014). The challenge is not only to distribute the production of the vegetable growers throughout the whole country, but also to preserve the seasonal surplus by adopting appropriate processes. Processing of vegetables into durable products during surplus production and seasonal super-abundance can go a long way to reduce the post-harvest losses. The amounts of drying costs and CO_2 emissions that could be saved by solar drying of some selected vegetables in Australia are shown in Table 2.3.

As mentioned before, the fraction of the agricultural products that are or may be dried has been assumed to be 20% of the respective freshly produced vegetables in Australia (Australian Bureau of Statistics, 2013). The approach to calculating the drying quantity and the required energy (TJ/year) for the selected vegetables was similar to that used for the fruits in Section 2.3. The potential savings in the drying costs and the GHG emissions for solar drying of vegetables were estimated, based on the local utility price of electricity (Department of Energy and Water Supply, 2015) and the National Average Carbon Emissions (NACE) data (Australian Federal Chamber of Automotive Industries, 2011), respectively. It is shown in Table 2.3 that potatoes give the maximum potential for saving in the drying costs (49 million/year) and GHG emissions (46 kt/year), by using solar dryers throughout

Australia, followed by tomatoes, representing 21 million and 20 kt savings in the energy costs and GHG emissions per year, respectively.

Table 2.3. Summary of potential savings by solar dryers for drying selected vegetables in Australia (base year 2011-2012).

Products	Quantity[2] (kt/year)	Initial MC[3] (%)	Final MC[3] (%)	Energy saving[4] (TJ/year)	Cost saving[5] (million AU$/year)	GHG savings[6] (kt CO_2/year)
Potatoes	254	75	13	204	49	46
Carrots	54	70	5	47	11	10
Tomatoes	91	96	10	90	21	20
Onions	60	80	4	58	14	13
Beans	8	70	5	7	1.5	1.45
Total	**467**			**406**	**96.5**	**90.45**

[2] 20% of the total production (Australian Bureau of Statistics, 2013) has been assumed to be dried. [3] Initial and safe final MC (wet basis) has been taken from (Khuntia et al., 2003). [4] Estimated energy required to remove the moisture from the products. [5] Based on local utility price of electricity (Department of Energy and Water Supply, 2015). [6] Based on National Average Carbon Emissions 2012 data (Australian Federal Chamber of Automotive Industries, 2011).

The total energy saving for drying the selected vegetables can be estimated to be 406 TJ per year, as shown in Table 2.3. This large quantity of energy is needed for vegetable drying due to the relatively high initial MCs in most of the vegetables, as mentioned before. However, appropriate application of solar dryers can deliver this energy for drying processes, as evident from (Fuller, 2001; Fuller, 2011; Janjai et al., 2011; Smitabhindu et al., 2008). These savings in energy for drying these selected vegetables in Australia are equivalent to saving approximately AU$ 96.5 million and 90.45 kilo tonnes per year in drying energy costs and GHG emissions, respectively, as shown in Table 2.3.

2.5   Solar drying - hardwood industry perspective

Every year in Australia, thousands of tonnes of wood are harvested for use in construction, flooring and furniture (Burke, 2015b). The timber used for all these products must be dried to a certain moisture content (MC) to prevent it warping and deforming in service. Solar drying of hardwood timber reduces the drying costs and improves the quality of the end-use products, as evident from Langrish et al. (1992), Chadwick and Langrish (1996), and Helwa et al. (2004). Due to the significant production of native and plantation hardwood sawlogs across many Australian states and territories, there is a substantial potential for solar kilns in hardwood-drying processes in Australia. Table 2.4 summarises the production of sawn hardwoods, by state and territory, throughout Australia and the potential for solar kilns to reduce the processing costs and GHG emissions associated with the value-addition processes (drying) for these logs.

The total production of sawn hardwoods has been collected and extracted from Australian forest and wood products statistics. In Table 2.4, the estimated drying energy has been calculated as the minimum energy required for drying hardwood from an average initial MC of 50% to an average final MC of 15%. The approach for estimating the drying costs and the GHG emissions associated with hardwood-drying processes was similar to that used for fruits and vegetables in Sections 2.3 and 2.4, respectively. Table 2.4 shows that the production of sawn hardwood in NSW (including ACT) was 324 kilotonnes (kt) in 2012-2013, representing the highest sawn hardwood production (31% of the total) among the states/territories in Australia. In the same period of time, approximately 25%, 18%, 15%, and 11% of the total sawn hardwood production in Australia were generated in the states of Victoria, Tasmania, Western Australia, and Queensland, respectively, as shown in Table 2.4.

Table 2.4. Production of sawn hardwood, by states/territories, in Australia, and the potential savings in drying costs and GHG emissions (base year 2012-2013).

States	Quantity[8] (kt/year)	Energy saving[4] (TJ/year)	Cost saving[5] (million AU$/year)		GHG savings[6] (kt CO_2 /year)	
			Electricity	Gas	Electricity	Gas
NSW[7]	324 (31%)	171	41	10	39	24
VIC	260 (25%)	136	32	8	31	19
Tasmania	185 (18%)	97	23	6	22	14
WA	141 (15%)	74	17	4	17	10
QLD	119 (11%)	62	15	3	14	9
Total	**1030**	**540**	**128**	**31**	**123**	**76**

[7] Includes Australian Capital Territory (ACT). [8] Quantities are based on ABARES survey data [(Burns and Burke, 2012) and (Australian Bureau of Agricultural and Resource Economics and Sciences, 2012b)]. [4] Estimated energy required to dry from an average initial moisture content (MC) of 50% to an average final MC of 15%. [5] Based on local utility price of electricity and gas [(Department of Energy and Water Supply, 2015) and (Origin Energy, 2015)]. [6] Based on Australian National Greenhouse Accounts (Department of the Environment, 2014).

A total of 1030 kt sawn hardwood was produced in Australia over the period 2012-2013. Table 2.4 shows that, if all of this hardwood is processed using solar kilns, an approximate saving, compared with electrically-heated kilns, of AU$ 128 million and 123 kt in processing costs and GHG emissions, respectively, per year could be obtained. These values of the savings in the processing costs and GHG emissions were likely to be AU$ 31 million and 76 kt, respectively, when compared with gas-fired solar kilns, as shown in Table 2.4. The potential savings in these parameters are even more significant when the solar drying of softwood, especially radiata pine, is taken into consideration.

2.6   Overall opportunity for the selected agricultural and forest products

Table 2.5 shows the overall potential of solar kilns in reducing the operating costs and GHG emissions, in terms of the selected commodities, for the agricultural and forest industry in

Australia. It is estimated that the selected fruits and vegetables have the potential of contributing 60% (30% by each) to the overall savings, while this estimate was 40% for the timber, as shown in Table 2.5. This situation is interesting because kiln manufacturers have been traditionally focused on hardwood timber drying throughout the world, including Australia (Burke, 2015b; Solar Kilns, 2014).

A relatively high initial MC for fruits (81%) and vegetables (78%) compared with hardwood (50%) contributed to the greater energy requirements for drying these food products. This situation led to the difference in the estimated dryings costs and GHG emissions savings between the selected fruits and vegetables (AU$ 191 million and 181 kt per year, respectively) and hardwood timber (AU$ 128 million and 123 kt per year, respectively). These differences in the estimated drying costs and GHG emissions savings between the agricultural and timber industries indicate that a promising field exists for solar kilns in the Australian agricultural industry.

Table 2.5. Potential costs and GHG emissions savings by using solar kilns for drying selected agricultural and forest products.

Products	Average initial MC (%)	Cost saving[5] (million AU$/year)	GHG savings[6] (kt CO_2/year)	% contributions
Fruits	81	94	91	30
Vegetables	78	97	90	30
Timber	50	128	123	40
Total		**319**	**304**	**100**

[5] Based on local utility price of electricity and gas [(Department of Energy and Water Supply, 2015) and (Origin Energy, 2015)] . [6] Based on Australian National Greenhouse Accounts (Department of the Environment, 2014).

The total saving in the GHG emissions (i.e. 304 kt/year) due to the solar drying of hardwoods, fruits, and vegetables, as shown in Table 2.5, are equivalent to taking 105186 passenger cars off the Australian roads per year. In calculating the number of cars, the average distance travelled by a passenger car per year in Australia (i.e. 14, 000 km) has been collected from the Survey of Motor Vehicle Use (Australian Bureau of Statistics, 2012b), which was carried out by the Australian Bureau of Statistics over the period 1 July, 2011 to 30 June, 2012.

It should be noted here that, for indicative purposes, only a few of the potential agricultural products that can be dried using solar kilns have been included in this report, while there are other agricultural commodities, such as wheat, rice, maize that can also be dried by solar kilns, as mentioned by Pirasteh et al. (2014). If the processing requirements for all these agricultural products were taken into consideration, the solar dryers would provide even greater opportunities to save in terms of drying costs and CO_2 emissions from the food-processing industry. Moreover, research, innovation, and investment in the development of solar kiln technology are necessary in order to secure a smooth food supply system throughout Australia, increase the profitability for the food processing industry both in the domestic as well as international markets, increase access to export markets, decrease existing imports for processed food products in Australia.

2.7   Conclusions

Future opportunities of solar dryers for reducing the operating costs and GHG emissions in the context of Australian agricultural and timber industries have been identified and discussed in this chapter. It has been estimated that a group of ten selected fruits and

vegetables have the potential of contributing 64% to the overall savings (i.e. drying costs and GHG emission savings for drying of fruits, vegetables, and timber), while this estimate was 36% for the total timber that are likely to be processed in Australia. A relatively high average initial MC for fruits ($\sim$ 81%) and vegetables ($\sim$ 78%) compared with hardwood ($\sim$50%) contributed to the greater energy requirements for drying these food products. These differences in the estimated drying costs and GHG emissions savings between the agricultural and timber industries indicate that, along with the timber industry, a promising field for solar kilns also exists in the Australian agricultural industry. It has been concluded in Chapter 2 that research, innovation, and investment in the development of solar kiln technology are necessary in order to secure a smooth food supply system throughout Australia, increase the profitability for the food processing industry both in the domestic as well as international markets, increase access to export markets, decrease existing imports for processed food products in Australia.

Chapter 3: Review of timber properties, drying models, and climatic data description

3.1 Introduction

Timber possess high degree of variability, and it undergoes dimensional variations in changing humidity conditions. It is an anisotropic material, both in terms of strength and moisture movement, and thus the consideration of timber properties along with an appropriate direction is an important aspect for modelling timber drying processes. Due to the complex structure of timber material, the variations in the permeability and the strength of timber occur both within and between timber boards. However, when a particular species of timber is considered, the variation of properties along the three axes becomes most significant. These variations in timber properties have been studied by many workers, including Lazarescu et al. (2009), where a set of drying experiments, from green condition to 12% final moisture content, on the variations in degree of shrinkage between and within different timbers was conducted. It was found that the longitudinal shrinkage was always an order of magnitude less than it was in the transverse direction, while in the transverse plane, the tangential shrinkage was 30-40% higher of the corresponding radial component. The permeability and the strength of timber likewise are significantly axis-dependent. It was experimentally found by Desch and Dinwoodie (1996) and Green et al. (1999) that, for small clear test pieces of Sitka spruce at 12% moisture content, the degree of anisotropy in tension is higher (i.e. about 53:1, considering 139 MPa along the grain and 2.6 MPa across the grain) than that in compression (i.e. 9:1, considering 39.2 MPa along the grain and 4.25 MPa across the grain). Similarly, the moisture transport along the grain is much faster than across it

(Keey et al., 2000; Walker, 2006). However, since the cross-sectional area for moisture movement is much greater in the cross-grain direction than that in the longitudinal direction, the moisture-content gradients become largest in the cross-grain direction during wood drying (Haque, 2002; Keey et al., 2000; Perré and Turner, 2002). As a result, the properties in the cross-grain direction have most significant effects on timber drying processes. Thus, this chapter addresses the moisture transport and stress-strain properties of timber in the cross-grain direction.

During the drying of timber, differential shrinkage across the thickness of a lumber board creates stresses, the magnitude of which depend on the physical properties of the wood, the drying conditions, and the time of exposure to these conditions. As wood relieves itself of these stresses, the material may take on several forms of degrade, including warpage (e.g. bow, crook, cup, and twist), case hardening, surface checks, end checks, and collapse. Wood warping is a deviation from flatness in timber as a result of stresses and uneven shrinkage. Common types of wood warping include bow, crook, cup, and twist, as shown in Figure 3.1. Bow is a warp along the length of the lumber face. It occurs when one face of a board of lumber shrinks more longitudinally than the other. It causes the lengthwise curvature of a piece of lumber, such that it resembles a bow used in archery, as shown in Figure 3.1 (a). Crook, which is also known as wain, is a warp along the length of the edge of the wood board. It occurs when one edge shrinks more in length than the other and thus causes the edgewise curvature of a piece of lumber, as shown in Figure 3.1 (b).

(a) bow   (b) crook   (c) cup   (d) twist

Figure 3.1. Different types of wood warping due to drying (Wengert and Meyer, 1993).

A warp across the width of the face of a piece of lumber, in which the edges are higher or lower than the centre of the board is called cup. It occurs when one face shrinks more in width than the opposite face. As a result, the timber board becomes cup shaped, as shown in Figure 3.1 (c). Another degrade of timber that occurs during drying is known as twist or wind, as shown in Figure 3.1 (d), which is a distortion in which the two ends do not lie on the same plane.

Other types of physical degrade that may occur during the wood-drying process include case hardening, surface checking, and collapse, as shown in Figure 3.2.

(a) case hardening   (b) surface checking

(c) collapse
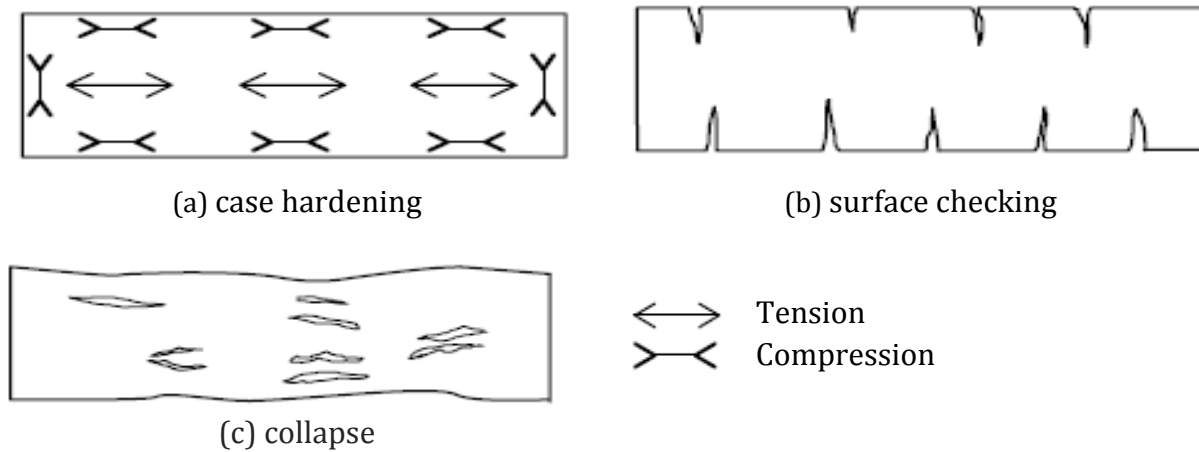
Figure 3.2. Common forms of physical degrades in wood due to drying (Nolan et al.,

2003).

Case hardening occurs in lumber or timber that has been dried too rapidly. Wood initially

dries from the shell (surface), shrinking the shell and putting the core under compression.

When this shell is at a low moisture content it will 'set' and resist shrinkage. The core of the

wood is still at a higher moisture content. This core will then begin to dry and shrink, but any

shrinkage is resisted by the already 'set' shell. This situation leads to reversed stresses;

compression stresses in the shell and tension stresses in the core [Figure 3.2 (a)], and results

in unrelieved stress called case hardening. Surface checks are failures that usually occur in

the wood rays on the flatsawn faces of boards, as shown in Figure 3.2 (b). They occur because

drying stresses exceed the tensile strength of the wood perpendicular to the grain, and they

are caused by tensile stresses that develop in the outer part, or shell, of boards as they dry.

Surface checks usually occur early in drying, but in some softwoods the danger persists

beyond the initial stages of drying. End checks, like surface checks, usually occur in the wood

rays, but on end-grain surfaces. They also occur in the early stages of drying and can be minimized by using a high relative humidity or by end coating. End checks occur because moisture moves much faster in the longitudinal direction than in either transverse or radial directions. Therefore, the ends of boards dry faster than the middle, and stresses develop at the ends. Collapse is a distortion, flattening, or crushing of wood cells [Figure 3.2 (c)]. In severe cases, collapse shows up as grooves or corrugations in the board. Slight amounts of collapse are usually difficult or impossible to detect at the board level and are not a particular problem. Sometimes collapse shows up as excessive shrinkage rather than distinct grooves or corrugations. Collapse may be caused either by (i) compressive drying stresses in the interior parts of boards that exceed the compressive strength of the wood or (ii) liquid tension in cell cavities that are completely filled with water. Both of these conditions occur early in drying, but collapse is not usually visible on the wood surface until later in the process. Collapse is generally associated with excessively high dry-bulb temperatures early in kiln drying, and thus low initial dry-bulb temperatures should be used in species susceptible to collapse. It should be noted that any of these types of degrade reduce the usefulness of the dried timber and thus decrease the market value.

It has been recognized for many years (Chadwick and Langrish, 1996; Herritsch et al., 2010; Leicester, 1971; Salin, 1992; Wu and Milota, 1995) that a key to improving the drying quality and a reduction in drying time lies in understanding and controlling internal stress development during drying. Since the cross-grain properties of timber have the most significant effects on modelling stress-induced drying processes, as mentioned before, the cross-grain mechanical properties have been used in this thesis. Since both the mechanical and drying behavior of timber are species-dependent, the relevant properties of a hardwood

species, here *Eucalyptus pilularis*, have also been used. These properties have been experimentally fitted by Haque (2002), and they have been retained in this thesis.

3.2   Shrinkage strain: mechanical property

Wood is a porous, non-homogeneous, and anisotropic material, and it undergoes dimensional variations in changing humidity conditions (i.e. gains moisture when the relative humidity of the air is high and loses the moisture when the relative humidity is low). These changes in the moisture contents cause the wood to expand and contract. However, the main concern in stress-induced drying is uneven shrinkage, which is caused by an uneven moisture distribution during drying, typically below the fibre saturation point (i.e. 30% moisture content level). In the process of drying below the fibre-saturation point, timber boards are affected due to the moisture-gradient set up between the shell and core, and in this situation, the surface fibres start shrinking first. However, the relatively wet inner layers have a tendency to restrict the shrinkage of the surface layers, resulting in uneven stress set up, which in turn may cause cracks in timber.

Stamm (1964) and Skaar (2012) found that the shrinkage strain (ε_s) was a linear function (below FSP) of moisture content and thus could be fitted to the following equation:

$$\varepsilon_s = \alpha * \left(X_{fsp} - X \right), when\ X < \ X_{fsp} \tag{3.1}$$

Here, *X* and α are the moisture content (kg kg^{-1}) and the shrinkage coefficient (m m^{-1}/kg kg^{-1}), respectively. However, for higher moisture-content levels (i.e. above FSP) and significant moisture-content gradients through the thickness of timber, this model does not follow the expected trend of overall shrinkage strain (i.e. absence of shrinkage above the FSP) (Desch

and Dinwoodie, 1996; Kollmann, 1968; Skaar, 2012; Stamm, 1964). Since the distribution of the moisture contents are likely to be non-uniform across the thickness of timber boards, a moisture-transport model (considering the moisture content distribution across the board thickness) should be used to predict the moisture-content distribution. In the following sections, examples of different drying models and the general considerations for selecting an appropriate model are described.

3.3   Examples of drying models and selection of an appropriate model

There are several models that are used to describe the water movement through the timber boards during drying. A detailed and useful review of different drying models for wood has been carried out by Rosen (1987), who divided the models into three groups, namely empirical models, multi-mechanism models, and diffusion models. In the following sections, some examples of these models, together with the general considerations in selecting an appropriate model for wood drying, are discussed.

3.3.1 Empirical models

Due to the complexity of wood structure and a wide range of natural variations in timber properties within and between species, a large number of purely empirical models have been used for describing the moisture transport through timber. For example, Bramhall (1976) presented an empirical model of the following form:

$$\frac{d\bar{X}}{dt} = \frac{p_{vd} - p_{vw}}{R} \tag{3.2}$$

where the driving force for the moisture transport was the difference between the saturation pressure of water vapour at the dry-bulb temperature *(Pvd)* and that at the wet-bulb temperature *(Pvw)*. It was experimentally found that the resistance to moisture movement (R) was a function of the average moisture content $(\bar{X})$ and was correlated by Bramhall in either of the following two forms:

$$R = c_1 * exp(-c_2 * \bar{X}) \ or \ R = c_3 * \bar{X}^{-c_4}$$

(3.3)

where c_1 to c_4 are fitted constants. As part of a model for a solar kiln, an empirical model similar to that of Bramhall (1976) was used later by Helmer et al. (1980):

$$\frac{d\bar{X}}{dt} = \frac{Y_w - Y}{R}$$

(3.4)

where the driving force for the moisture migration was the difference between the saturation humidity at the dry-bulb temperature *(Yw)* and the bulk-air humidity *(Y)*. The resistance to moisture movement *(R)* was suggested to be a function of the average moisture content $(\bar{X})$ and the dry-bulb temperature (T_d), as follows:

$$R = \bar{X}^{-2.38} * (0.298 * T_d - 4.18)$$

(3.5)

In the study of Helmer et al. (1980), although the overall predictions of the solar-kiln model were reasonable, the predictions of the drying model were not tested explicitly. Another

empirical model for the drying of boards of angelica *(Dicorynia paraensis)* within a solar kiln was used by Pallet (1988):

$$\frac{d\bar{X}}{dt} = -(a + b\bar{X} + c\bar{X}^2)(d + el) * exp(f + g/\bar{T})(\bar{X} + X_e)$$

(3.6)

where *l*, $\bar{X}$, *T* are the board thickness (m), the average moisture content of the timber board (kg kg^{-1}), the average temperature of the timber board in degrees Celsius, respectively, and the subscript *e* refers to the equilibrium moisture content. The fitted coefficients in Equation (*3.6*) were given as *a = 5.24, b = 22, c = 31, d = 3, e = -83, f = 0.84,* and *g = -47.45*. These coefficients were fitted to the data obtained for temperatures between 20 and 65°C, board thicknesses between 0.012m and 0.032m, and moisture contents between 0.2 and 0.6kg kg^{-1}. In this case also, the overall predictions of the solar-kiln model were reasonable, but the use of the drying model for extrapolation to other drying conditions is questionable, as the model has no capability for predicting the moisture-content profiles and the stress levels developed in the timber during the intermittent-drying process involved in solar kilns (Keey et al., 2000).

3.3.2 Moisture diffusion models

It is necessary to discuss a diffusion model for moisture movement in wood during drying for several reasons. Fick's second law, which states that diffusion rate is proportional to the concentration gradient, has been frequently used for describing the drying phenomena of solid and porous materials (Doe et al., 1994; Haque and Langrish, 2003; Langrish et al., 1997; Simpson, 1993; Söderström; Wu, 1989). The process of wood drying was first described by

Sherwood (1929), who adopted a diffusion approach as the main moisture transport mechanism. The diffusion approach is based on the assumption that a single transport mechanism, diffusion, acts during the wood-drying process. Since timber samples are much longer and wider than they are thick, the moisture transport within hardwood may be adequately described by Fick's law in one dimension (Doe et al., 1994; Wan and Langrish, 1995). More accurately, the diffusion model may be generally described by Fick's Second Law in one dimensional form as follows (Keey et al., 2000):

$$\frac{\partial X}{\partial t} = \frac{\partial}{\partial z}\left(D\frac{\partial(driving\ force)}{\partial z}\right)$$

(3.7)

In using Equation (*3.7*), various workers have used different driving forces, including the chemical potential, the moisture-content gradient, and the vapor pressure potential.

3.3.2.1 Chemical-potential driving force

Stanish et al. (1986) developed an effective mathematical model to simulate the drying of hygroscopic porous media, and of wood, in particular. In the model, an independent migration mechanism was used for each of three states of moisture, namely free water, bound water, and water vapor. It was considered that the free water flows in bulk form driven by a pressure-gradient within the liquid phase, whereas the bound-water migration was considered to be a diffusion process that was driven by a chemical potential $(\partial\mu/\partial Z)$ of adsorbed water molecules. Consequently, the flux of bound water, j_{wb}, was assumed to be proportional to the gradient in the chemical potential of the bound molecules, $(\partial\mu/\partial Z)$, and to the volume fraction occupied by the solid cells, $(1 - \varepsilon_d)$, as follows:

$$j_{wb} = D_b * (1 - \varepsilon_d) * \frac{\partial \mu}{\partial Z}$$

(3.8)

where D_b is a proportionality constant and represents the diffusion coefficient for bound water. In the model proposed by Stanish et al. (1986), it was also assumed that local thermal and phase equilibria were always obeyed, which meant that heat and mass-transfer relationships were coupled by the requirement that all phases of moisture remain in thermodynamic equilibrium at the local temperature.

The concept of water potential was later extended by Cloutier and Fortin (1994) to suggest that, for an isothermal drying model, the gradient in water potential can be used as the driving force for moisture movement in wood. They established the moisture content - water potential relationships experimentally for aspen (*Populus tremuloides*) sapwood in desorption, with two specimen orientations, over a range of moisture contents from 0.05 to 1.8 kg kg^{-1} and temperatures from 20 to 50°C. This situation means that they also considered the effect of temperature and specimen orientation on the moisture content - water potential relationships. However, the relationship between the water potential and the moisture content was found to be very non-linear, with values of the water potential ranging from - 10^{-6} J kg^{-1} for ultimately dry wood to -10^{-1} J kg^{-1} at a moisture content of 1.8 kg kg^{-1}. It should be noted here that this concept of the gradient in water potential as the moisture-content driving force over the entire moisture-content range was also applied in various drying models (Cloutier and Fortin, 1993; Cloutier and Fortin, 1994; Cloutier et al., 1992). For example, Cloutier and Fortin (1993) measured the diffusion coefficients from nearly

saturated to dry conditions over a range of dry-bulb temperatures from 20-50°C, a range of relative humidities from 29-69%, and air velocities from 0.3-0.5m s^{-1} on 45-mm cubes of aspen (Populus sp.). However, the reported coefficients varied by over six orders of magnitude for a range of moisture contents from 0.1 to 1.4 kg kg^{-1}. This situation suggests that considerable experimental work would be required to measure the coefficients for other species, as these coefficients would be expected to be species dependent (Keey et al., 2000). From the foregoing discussion, it appears that, although the gradient in the chemical potential can be used as the driving force for the movement of the bound-water component in wood (Stanish et al., 1986), it may have limited applicability as a driving force over the entire moisture-content range from green to dry.

3.3.2.2 Moisture-content driving force

The underlying assumption in the model based on a moisture-content driving force is that moisture migrates by diffusion, driven by a gradient in moisture content. The length and width of a timber board are normally far greater than the thickness, and thus the moisture transport within hardwood may be adequately described by a one-dimensional version of Fick's second law of diffusion, as follows (Doe et al., 1994; Wan and Langrish, 1995):

$$\frac{\partial X}{\partial t} = \frac{\partial}{\partial z}\left(D\frac{\partial X}{\partial z}\right)$$

(3.9)

where *X* is the difference between the actual moisture content and the equilibrium moisture content, *t* is the time, *z* is the distance from the core perpendicular to the airflow, and *D* is the diffusion coefficient. This form of the diffusion model, with a moisture-content driving

force, has been successfully validated by Wu (1989) and Doe et al. (1994) for describing the

moisture movement in Australian hardwood. Figure 3.3 shows the agreement between the

experimental moisture-content profiles and the moisture-content profiles predicted by the

diffusion model based on moisture-content gradients through Tasmanian eucalyptus during

drying, as studied by Wu (1989).
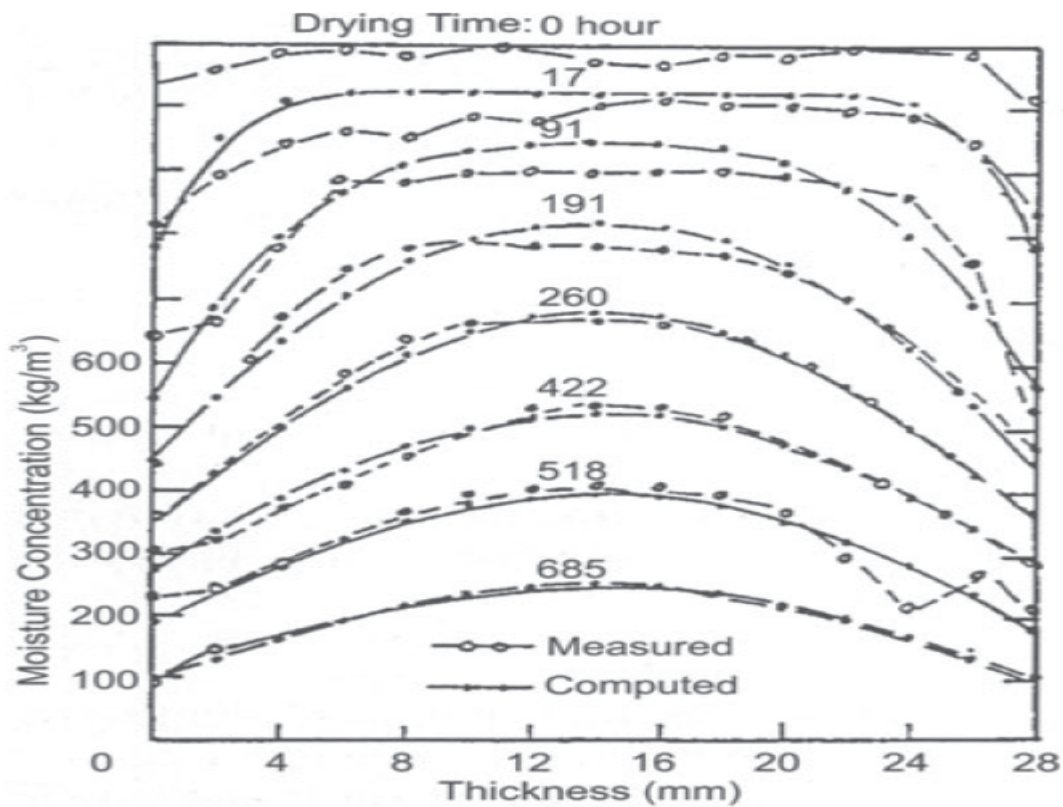
Figure 3.3. Moisture-content profiles through Tasmanian eucalyptus during drying (Wu,

1989; Haque, 2002).

It can be seen from Figure 3.3 that there is good agreement between the measured and

predicted parabolic moisture-content profiles both at high and low average moisture

contents. This situation indicates that the diffusion model based on the moisture-content

gradients can reasonably describe the moisture movements both above and below the fibre-saturation point.

It was mentioned by Keey et al. (2000) and Walker (2006) that, during drying of hardwood timber, the absorbed water is relatively hard to remove, as the mass flow of the water is blocked by the aspirated pits. In such species of wood (i.e. hardwoods), the movement of water during drying is likely to be principally by diffusion, as mentioned by many workers, including Shmulsky and Jones (2011), Walker (2006), and Mujumdar (2007). In hardwood drying, the water molecules migrate from a region of high moisture concentration to a region of low moisture concentration as a function of the moisture gradient between the wet interior and the drier surface (Walker, 2006). This situation results in parabolic moisture-content profiles (diffusion-like moisture-content profiles) during wood drying, the existence of which can also be mathematically shown by solving the one dimensional form of Fick's Second Law under unsteady-state conditions for a constant diffusion coefficient as follows:

Fick's Second Law in one dimensional form can be recalled as:

$$
\frac{\partial X}{\partial t} = -\frac{\partial}{\partial z}\left(D\frac{\partial X}{\partial z}\right)
$$

(3.10)

Partial integration of Equation (3.10) with respect to time, at each point in time, yields:

$$
-\frac{\partial}{\partial z}\left(D\frac{\partial X}{\partial z}\right) = constant = \alpha
$$

(3.11)

34

It should be noted here that, comparing Equations (3.10) and (3.11), although it appears that $\frac{\partial X}{\partial t}$ = constant, this is not the same as saying that the drying rate is always constant. This assumption is only requiring that the drying rate is fixed at one point in time

Integrating Equation (3.11) once with respect to Z to give:

$$-\left(D\frac{\partial X}{\partial z}\right) = \alpha z \tag{3.12}$$

Assuming that D is constant and not a function of z and that the moisture content, $X = X_{actual} - X_e$, where X_{actual} and X_e are the actual and equilibrium moisture contents, respectively. Then the moisture content, X, at any distance, z, from the centre of the timber board can be expressed in the following integral form:

$$-D\int_0^X \partial X = \alpha \int_Z^0 z\partial z \tag{3.13}$$

So,

$$-D(X - 0) = \alpha \left(\frac{0^2}{2} - \frac{Z^2}{2}\right) \tag{3.14}$$

Or,

$$X = \frac{\alpha}{2D}(Z)^2 \tag{3.15}$$

From Equation (3.15), it is seen that, under unsteady-state conditions and with constant D, the moisture-content profiles are likely to be parabolic in shape.

An experimental validation of the diffusion model for predicting the moisture content profiles in potato samples during drying was carried out by Srikiatden and Roberts (2008) through several experimental tests, and the results of a typical test are shown in Figure 3.4. This test was done for drying 2.8 cm diameter potato samples (with four concentric shells that were cut by a cylindrical cutter) at 70⁰C and with an air velocity of 1.5 m/s. Figure 3.4 shows that the moisture contents of Shell 1 (closest to the centre) and 2 did not decrease until towards the middle stage of drying. This situation led to the parabolic-like moisture-content profiles, as shown in Figure 3.5, indicating that diffusion is likely to be the controlling mechanism for this drying process (Gekas, 1992).
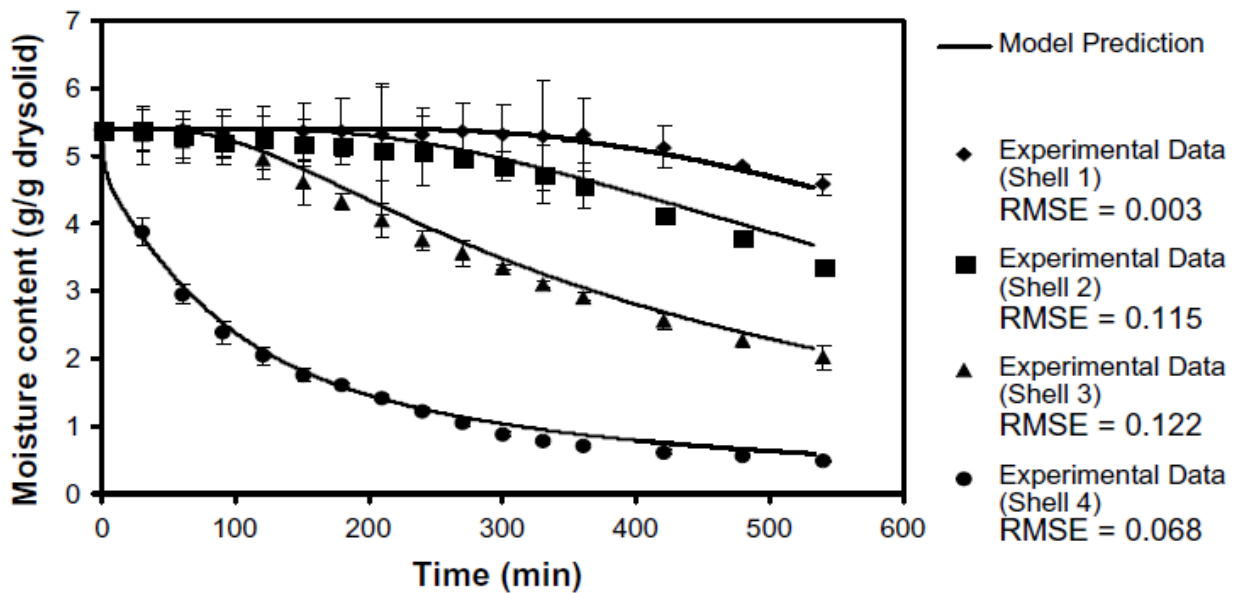
Figure 3.4. Experimental and predicted moisture-content profiles during potato drying (Srikiatden and Roberts, 2008) using a diffusion model.
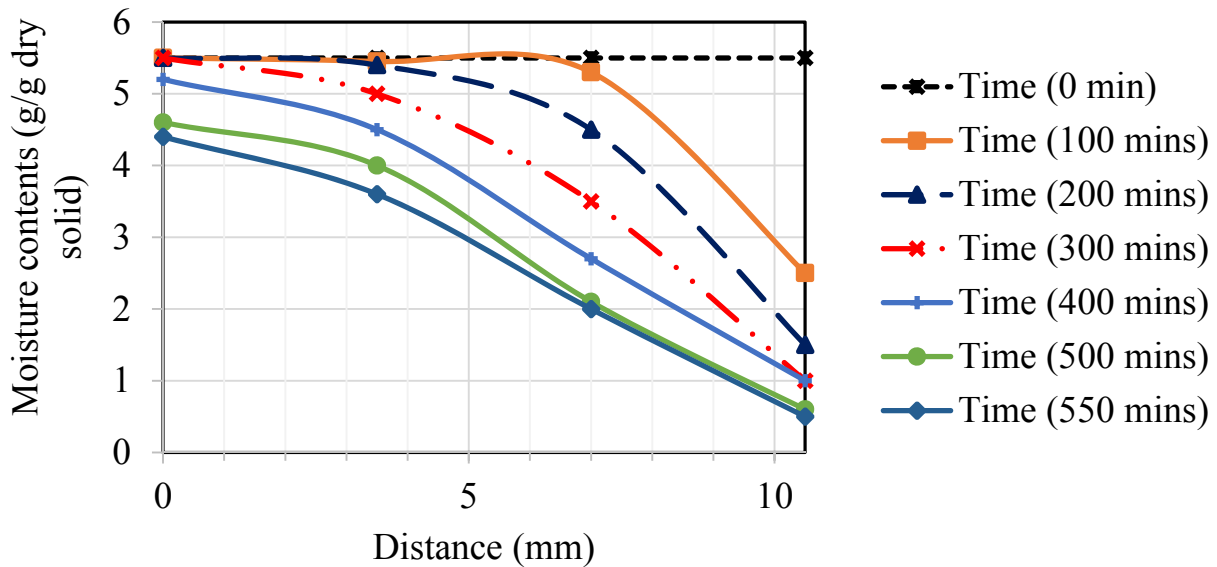
Figure 3.5. Moisture-content variations as a function of time and distance during potato drying [adapted from Srikiatden and Roberts (2008)].

It is also shown in Figure 3.4 that the diffusion model was found to accurately predict the moisture profiles of potato samples during drying, as there was a good agreement between the experimental and the model-predicted moisture contents. This favorable feature of the diffusion model for describing the moisture-content profiles is also reflected in the values of the root mean squared error (RMSE), which is an indicator for the goodness of the fit. Since all the RMSE values are close to zero, as shown in Figure 3.4, the diffusion model is likely to be an appropriate choice for predicting the moisture contents during a drying process.

3.3.2.3 Vapor-pressure driving force

It was suggested by Bramhall (1976, 1995) that the driving force for moisture transport within wood during drying is the gradient of the partial pressure for water vapor, and thus Fick's Second Law was modified as follows:

$$\frac{\partial X}{\partial t} = \frac{\partial}{\partial Z}\left(D\frac{\partial P_v}{\partial Z}\right)$$

(3.16)

where p_v is the partial pressure of water vapor at the local temperature and moisture content. Bramhall claimed that, when the temperature-dependent component of the diffusion coefficient is combined with the concentration gradient of diffusing molecules, the resulting driving force is proportional to the vapor pressure, and the diffusion coefficient is independent of the temperature. Biggerstaff (1965) and Choong (1965) carried out experimental studies at the experimental conditions of 42°C to 98°C and 40°C to 60°C, respectively, to obtain the diffusion coefficients. Biggerstaff conducted experiments on flat-sawn eastern hemlock (*T. canadensis*), with a sample thickness of 3.1 mm, whereas the species and the thickness of the sample used by Choong were western fir (*A. grandis*) and 5 mm, respectively. By dividing the obtained diffusion coefficients by the vapour pressure of water at the given temperatures, Bramhall found that the diffusion coefficients obtained by both workers were independent of temperature over the range of experimental conditions used. While it is true that the vapor pressure is proportional to the moisture content for the range of moisture contents chosen by Biggerstaff (1965) and Choong (1965), the vapour pressure is dependent on the temperature alone above the fibre-saturation point, which occurs at a moisture content of just below 0.30 kg kg^{-1} at normal kiln temperatures (Keey et al., 2000).

The practical observations of the diffusion-like (i.e. parabolic) moisture-content profiles using the diffusion model with a moisture-content driving force (as discussed before) in the work of Wu (1989) and Doe et al. (1994) may indicate that a diffusion model using the vapor-

pressure gradient as the main driving force (Bramhall, 1995) is not appropriate. The use of a vapor-pressure driving force in the work of Biggerstaff (1965) and Choong (1965) to explain the effects of temperature on the diffusion coefficient was limited to moisture contents below the fibre-saturation point (FSP). An approach using vapor-pressure as the transport potential for the moisture movement fails to relate the temperature to the diffusion coefficient at moisture contents above the FSP, which was done in the work of Wu (1989) and Doe et al. (1994). Also, since the lumber was essentially isothermal for the drying conditions used by Biggerstaff (1965) and Choong (1965) and since Rosen (1987) mentioned that no significant temperature profile exists across the thickness of the board in these isothermal conditions, the justification of the diffusion model driven by a gradient of the vapor-pressure may need further explanation. This situation and the existence of a perceptible moisture-content gradient at high moisture contents, together with the simplicity of the mathematical treatment with a diffusion model based on moisture-content driving forces, indicates that the diffusion model with a moisture-content driving force is an appropriate choice for describing the moisture movement during drying.

3.3.3   Multiple-mechanism models

Although describing moisture movement in terms of diffusion model (as will be described in next section) has been satisfactory in many practical cases, more attention has been paid by some workers to the modelling of moisture movement by including several transport mechanisms. The first attempts to use a transport-based model for the drying of wood were based on the equations developed by Luikov (1966) for heat and mass-transfer processes in capillary-porous bodies. Many other drying studies, including Turner et al. (1998), Pandey et al. (1999), and Larbi (2014), have described the drying process in porous solids by

considering different transport mechanisms for bound water, free water, and water vapour. The detailed model equations used by them are nonlinear in nature and have the same form as the equations of Luikov. In their models, they considered a large number of transport parameters, which may be complex functions of the temperature, the moisture content, the location within the log, the site, and the species (Keey et al., 2000). Hence, in order to determine the most appropriate functional relationships between transport parameters, such a transport-based model is likely to be dependent on experimental data that are required for each species and for lumber of the same species taken from different places. The resultant complexity of these models and the computing power needed to solve them reduce the utility of these ideas and limit their range of application in analyzing the timber drying process (Kayihan, 1993).

3.3.4   Selection of the drying model for this thesis

In addition to the discussion above, Langrish and Bohm (1997) have analyzed drying data for three species of Australian eucalypts, yellow stringybark (*E. muelleriana*), spotted gum (*E. maculata*) and ironbark (*E. paniculata*), in terms of both moisture-content and vapor-pressure gradients. Moisture-content gradients were found to fit the drying data for all species and drying schedules better than vapor-pressure gradients, and the diffusion coefficients based on moisture-content gradients also extrapolated one set of drying data (moisture contents against time) better than coefficients based on vapor-pressure gradients. From the foregoing discussion, it appears that the diffusion model with a moisture-content driving force is the best choice for describing moisture transport within hardwoods. This approach of using a diffusion mechanism to describe and model the process of wood drying has also widely been used by a number of workers, including Wu (1989), Simpson (1993),

Bramhall (1995), Langrish et al. (1997), Musch et al. (1998), and Haque and Langrish (2003). One of the reasons for its widespread use in describing wood drying is its relative simplicity compared with other complex models, such as multiple-mechanism models. This approach of modelling the moisture transport within the timber during drying involves relatively simple calculations, which are particularly useful when the wide variabilities in diffusion coefficients and permeabilities both within and between species are considered.

The simplicity of this approach is also beneficial for optimizing kiln-drying schedules, where the number and length of calculations, even with modern computing power, are considerable. In addition, this diffusion approach has been found to be satisfactory for predicting both average moisture contents and moisture-content profiles for some hardwood species - a feature that is important for predicting stress levels in timber during drying. In the following, the diffusion model and the stress-strain model, as used in this thesis, are described.

3.3.5 The diffusion model

Since the length and width of a timber board are normally far greater than its thickness, the moisture transport within hardwood may be adequately described by Fick's law in one dimension as follows (Doe et al., 1994; Wan and Langrish, 1995):

$$\frac{\partial X}{\partial t} = \frac{\partial}{\partial z}\left(D\frac{\partial X}{\partial z}\right) \qquad (3.17)$$

Here X is the moisture content (kg kg^{-1}), z is the distance through the timber thickness (m), and D represents the temperature-dependent diffusion coefficient,

$$D = D_r exp^{-\left(\frac{D_E}{T}\right)}$$ (3.18)

while D_r is the reference diffusion coefficient (m² s⁻¹), and D_E is the activation energy (K). Likewise, heat transport with the timber can be described by the second partial differential form of Fourier's law, as follows (Langrish et al., 1997):

$$\frac{\partial T}{\partial t} = \frac{\partial}{\partial z}\left(\frac{k}{\rho_t C_{pt}}\frac{\partial T}{\partial z}\right)$$ (3.19)

In Equation (3.19), k, ρ_t, C_{pt} are the thermal conductivity (W m⁻¹ K⁻¹), density (kg m⁻³), and specific heat capacity (J kg⁻¹ K⁻¹) of the timber, respectively, and are functions of the moisture content. As a result, Equations (3.17) and (3.19) form a coupled system of ordinary differential equations (ODEs), which can be solved simultaneously to predict the temperatures and moisture contents of the timber. A detailed description of this diffusion model are given in the next chapter. It is to be mentioned here that Equation (3.19) indicates that there is no moisture evaporation within the wood, and all moisture is assumed to be evaporated from the board surface. This situation would induce a sharp temperature gradient at the surface. However, solar drying is a low temperature drying process (maximum inside temperature 50-80⁰C), and the drying rate is relatively slow for the materials with low permeability, such as hardwoods. Since this thesis was focused on hardwood drying, the assumption that all the moisture is evaporated through the surface of the timber boards is appropriate, as the temperature gradient at the surface is unlikely to be very steep in this case.

3.3.6 Stress-strain model

The general concept of how stresses develop inside wood as it dries is well-documented in the literature (Langrish et al., 1997; Ormarsson et al., 2000; Salin, 1992; Zhan et al., 2009). Under normal drying conditions, the surface of sawn boards tend to approach the equilibrium moisture content of the prevailing conditions, and the outer zones of the wood dry below the FSP. Thus, the fibres at the surface tend to shrink, but are restrained by the fibres at the inner zones, which are in a relatively green condition and have not begun to shrink significantly. Because of this restraint, the outer layers are stressed in tension, and as a reaction, the interior layers are in compression, as shown in Figure 3.6.
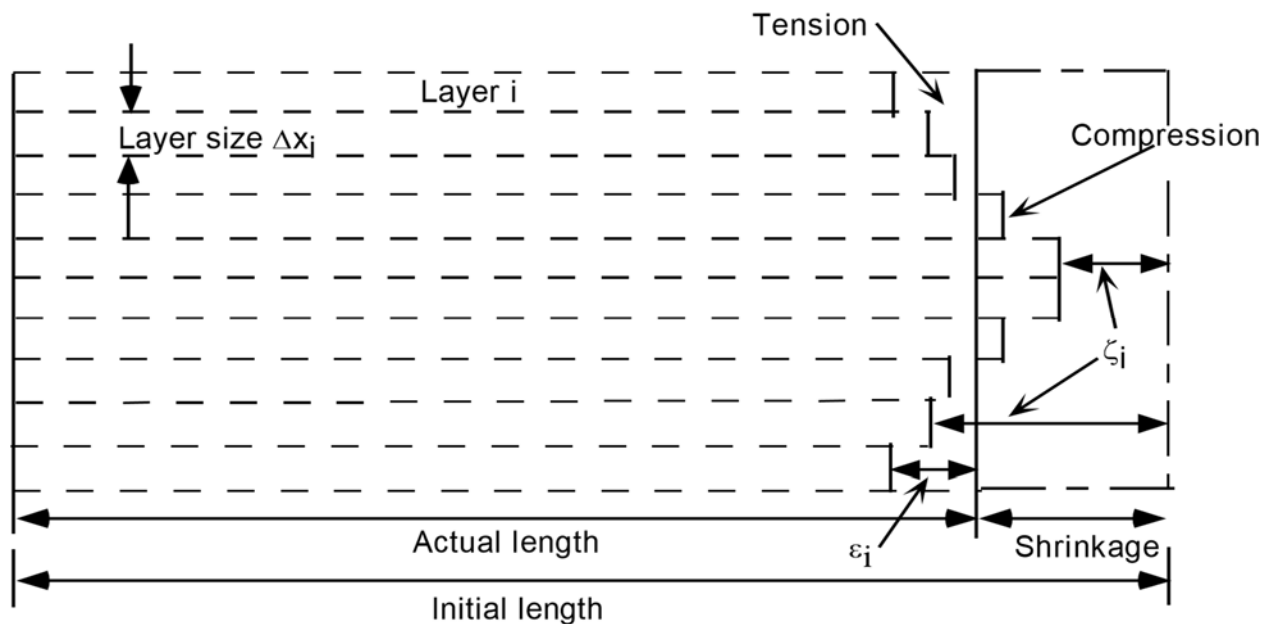
Figure 3.6. Stress development in timber during drying (Langrish et al., 1997).

If there is no restraint in the free movement of ith layer, its free shrinkage (ζ_i) may be approximated by a linear relation as follows (Johnson, 1989):

$$\zeta_i = \alpha * M_i \tag{3.20}$$

where, α is the shrinkage coefficient, and the moisture content (M_i) is given by:

$$M_i = X_{FSP} - min(X_i - X_{FSP}) \tag{3.21}$$

Here, X_{FSP} and X_i are the moisture content at FSP and the moisture content of the ith layer, respectively. The stress, σ induced due to the shrinkage strain can be related to the modulus of elasticity (E), which is dependent on the temperature and moisture content, through Hooke's law as below:

$$\sigma = E_i * \alpha * M_i \tag{3.22}$$

In reality, however, the free movement of the layers is restricted due to the presence of restraints between successive layers of wood in order to satisfy material continuity requirements (i.e. general shape of the board), and thus the successive layers can develop different stresses. As a result, the sum of internal forces can be expressed in finite element form as follows:

$$\sum E_i * (\bar{\zeta} - \alpha * M_i) * \Delta x_i = 0 \tag{3.23}$$

Rearranging Equation (*3.23*), the average shrinkage of the timber board, $\bar{\zeta}$ can be calculated as:

$$\bar{\zeta} = \frac{\sum E_i * \alpha * M_i * \Delta x_i}{\sum E_i * \Delta x_i} \tag{3.24}$$

Once the average shrinkage of a timber board, $\bar{\zeta}$ has been calculated, the individual instantaneous strain of the ith layer (ε_i) may be approximated by:

$$\varepsilon_i = \bar{\zeta} - \alpha * M_i \qquad\qquad (3.25)$$

The predicted shrinkage strains can be fitted to the experimentally obtained shrinkage strains by adjusting the shrinkage coefficient with a view to minimizing the sum of squares for the differences between the predicted and experimental shrinkage strains. Haque (2002) experimentally fitted the shrinkage strain parameters using a combined diffusion model and stress-strain model, which have been described above. Since this approach of fitting the shrinkage coefficient considered the uneven moisture-content gradients across the timber board thickness, and since data on the relevant timber properties for the model are available in the literature, the cross-grain shrinkage coefficient of 0.348 (m/m per kg/kg), as experimentally fitted by Haque (2002), for blackbutt timber has been used in this thesis.

3.4   Instantaneous stress and strain: mechanical properties

During timber drying, it is commonly understood that the strength increases as the moisture content decreases. A model (Bodig and Jayne, 1982) formulating the stress-strain relationship for timber consists of two parts, namely, the linear and nonlinear portions. Since the timber properties depend on both the temperature and moisture content of the material, the direct application of the model proposed by Bodig and Jayne (1982) is inappropriate for wood drying where simultaneous changes in stress and moisture content are involved. In this situation, the linear and the non-linear parts can be conveniently replaced by a curve consisting of a set of straight line segments. In this approach, within each line segment, the

change in instantaneous strain is considered to vary linearly with the change in stress. The

local modulus of elasticity (i.e. the proportionality) is considered to vary with the local values

of temperature, moisture content, and/or stress. As a result, the stress-strain relationships

can be expressed in the following form:

$$\Delta\varepsilon_I = C_I * \Delta\sigma$$

(3.26)

In Equation (3.26), the stress (MPa) and strain (m m^{-1}) are denoted by σ and ε_I, respectively.

It should be noted here that, in the linear part of the stress-strain relationship, the

instantaneous compliance, C_I (MPa^{-1}), is the reciprocal of the modulus of elasticity (E), which

are described in the next section.

3.5   Modulus of elasticity (E)

The modulus of elasticity, E measures the stiffness of wood. Technically, it is a measurement

of the ratio of the stress placed upon the wood compared with the strain (deformation) that

the wood shows along its length. It is normally expressed in Pascals (Pa, N m-2), and the

number is given for wood that has been dried to a 12% moisture content, unless otherwise

stated. Mathematically, the modulus of elasticity, E (Pa N m^{-2}) is the ratio of the applied

stress, σ (MPa) to the instantaneous strain, ε_I (mm^{-1}), and can be expressed as follows:

$$\varepsilon_I = \frac{\sigma}{E}$$

(3.27)

However, the approach in which the stress-strain relationships can be used to describe the

modulus of elasticity beyond the proportional limit (i.e. within the nonlinear part of the

stress-strain curve) and under varying moisture and stress conditions is not straight forward. As a result, different approaches (e.g. tangent and secant moduli) have been proposed previously for determining the modulus of elasticity in the nonlinear region of the stress-strain curve, as shown in Figure 3.7, which has been originally adapted from Dinwoodie (2000) by Haque (2002).

The tangent modulus is the slope of the tangent line drawn at any point of the stress-strain curve, whereas the secant modulus is the slope of the line from the origin to a given point in the stress-strain diagram. While the tangent modulus is appropriate when looking at the effects of changing the stress by a small amount, the secant modulus is used when studying the effects of changing the stress by an amount that cannot be considered as small.
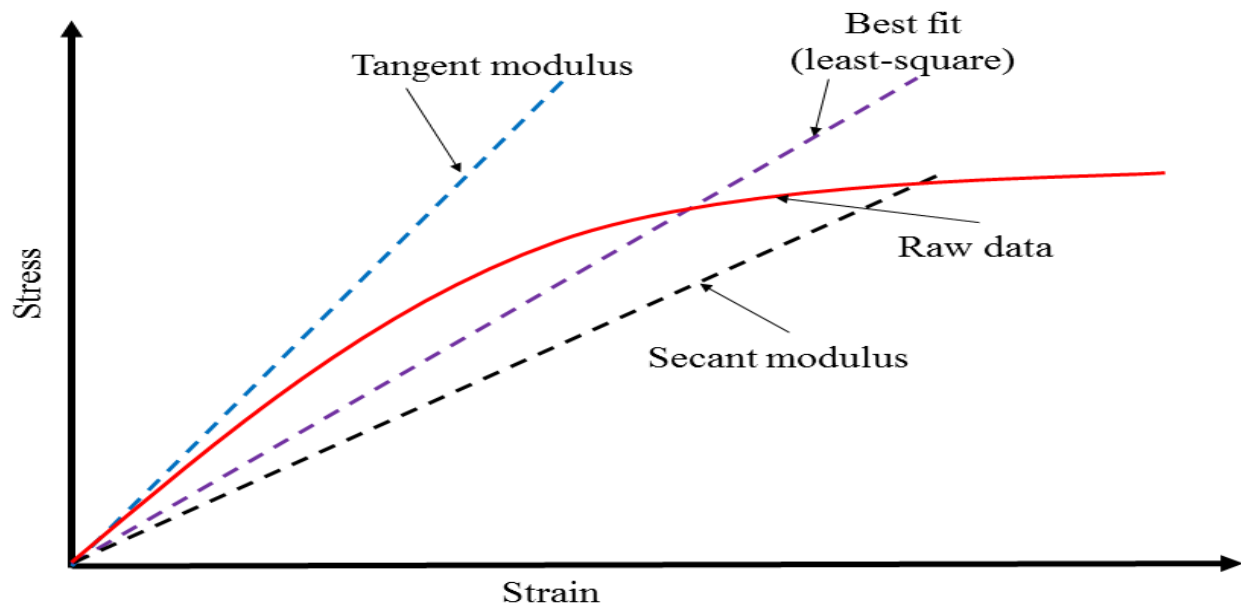
Figure 3.7. Typical stress-strain curve for rapid loading of timber (Haque, 2002 and Dinwoodie, 2000).

Since both the linear and nonlinear regions of the stress-strain curve cannot be described by a single modulus of elasticity, Haque (2002) applied a least squares technique to fit the modulus of elasticity in order to represent the overall behavior of stress-strain curve by a single straight line, as shown in Figure 3.7. Thus, the interpretation used by Haque (2002) for modulus of elasticity has been used in this thesis.

3.5.7 Temperature and modulus of elasticity

In order to have an improved understanding of the conditions at which checking (either exterior or interior) may occur during timber drying, it is important to understand the effect of the temperature and moisture content on the stress-strain relationship. Several workers, including Oliver et al. (1991), Ellwood (1954), Greenhill (1936), and Youngs (1957), have investigated the stress-strain relationship with different temperature and moisture content levels. Both Greenhill (1936) and Ellwood (1954) conducted experiments on American beach with a wide range of temperature and moisture content, and it was found that the modulus of elasticity decreased with increasing temperature and moisture content. While it is difficult to establish functional relationships between the timber strength properties, temperature, and moisture content, Ellwood (1954) proposed an empirical relationship between the temperature (T) and Youngs modulus for bone-dry timber (E_0) and green modulus of elasticity (E_g) as follows:

$$E_g = E_o * (0.475 - 0.0038 * T)$$
(3.28)

3.5.8 Moisture content and modulus of elasticity

The changes in stress-strain ratio with the change in temperature and moisture content at different regions (e.g. linear and nonlinear) of the stress-strain curve have been investigated by several workers (Greenhill, 1936; Ellwood, 1954; Dinwoodie, 2000; Oliver et al., 1991). While Greenhill (1936) investigated the tensile strength and elastic properties in the tangential direction for American beach, Ellwood (1954) tested the same species of wood in both tension and compression. The overall results indicated that, with the increase in temperature and moisture content, all the elastic modulus, the stress at the proportional limit, and the maximum tensile stress decreased. However, in these tests, no significant change in the strain at the proportional limit was observed with the change in temperature, moisture content, and loading condition. Another study conducted by Youngs (1957) demonstrated that, the cross-grain properties of Northern red oak, including the strength and modulus of elasticity in tension, compression, and shear, varied significantly with the temperature and moisture content. Oliver (1991) indicated that, for the linear part of the stress-strain curve, the relationships between the initial slope of the instantaneous stress-strain curve (Youngs modulus) and the temperature were almost linear. The influence of moisture content on the modulus of elasticity becomes significant when the wood moisture content falls below the fibre saturation point (i.e. 0.3 kg kg^{-1}), as mentioned by many workers, including Carrington (1996) and Keep (1998). While both Dinwoodie (2000) and Oliver et al. (1991) illustrated that a nearly linear relation existed between the moisture content and the modulus at a given temperature below the fibre saturation point. A linear relationship incorporating the moisture content (X), the green modulus of elasticity (E_g), and

the bone dry modulus of elasticity (E_o) for Australian eucalypts was given by Oliver as follow:

$$E = E_O - 5 * (E_O - E_g) * X * 100 \qquad (3.29)$$

A correlation for the simultaneous effects of the temperature and the moisture content on the longitudinal modulus (E) for eucalypts has also been proposed by Oliver et al. (1991) as follows:

$$(E - E_g)[E - E_O + 5 * (E - E_g) * X] = \frac{E_g^2}{1000} \qquad (3.30)$$

For the modulus of elasticity (E) appearing in Equation (3.30), Oliver et al. (1991) indicated that the tangential and radial moduli of elasticity were 5% and 10%, respectively, of the longitudinal modulus. Reviewing Equations (3.28) to (3.30), the combined effects of the temperature (T) and the moisture content (X) lead to the following empirical relations for the modulus of elasticity (E) (Oliver et al., 1991):

$$E = D + \sqrt{D^2 - (A * B) + C} \qquad (3.31)$$

Here,

$$A = E * (0.475 - 0.0038T) \qquad (3.32)$$

$$B = E - 5 * E * (0.525 + 0.0038T) * X \qquad (3.33)$$

$$C = \frac{[E * (0.475 - 0.0038T)^2]}{1000} \tag{3.34}$$

$$D = \frac{(A + B)}{2} \tag{3.35}$$

Since the effects of temperature and moisture content changes on the modulus of elasticity, E, have been included in Equations (3.31) to (3.34), it has been used for estimating the modulus of elasticity, E in the simulation of the model, as carried out in this thesis.

3.6   Diffusion coefficient: transport property

In this thesis, the cross-grain diffusion coefficient for bluckbutt has been taken from experimentally-fitted data, as found by Haque (2002). The experimental apparatus was a pilot-scale tunnel dryer, with steam-heated air circulation. In the fitting program of Haque (2002), a simple diffusion model (which are described in Chapter 4) was used with a regression analysis (least squares method) to generate moisture profiles which matched measured moisture data points by adjusting the value of the diffusion coefficient, D. The diffusion coefficient (D) is correlated with the reference diffusion coefficient (D_r), the activation energy (D_E) and the temperature (T) as follows (Doe et al., 1994):

$$D = D_r * exp^{\frac{-D_E}{T}} \tag{3.36}$$

It can be seen from Equation (3.36) that the activation energy (D_E) corresponds to the temperature dependence of the diffusion coefficient (D). The input value used in the simulation of this thesis for the activation energy was taken to be 3800 K, as this value for Eucalypts was consistent with the findings of other workers, including Schaffner (1981), Wu (1989), and Haque (2002). The key properties used in the simulation for *Eucalyptus pilularis* are summarized in Table 3.1.

Table 3.1. Timber properties for drying simulations, as used in this thesis (Schaffner, 1981; Wu, 1989; Haque, 2002).

Properties	Values	Units
Green modulus of elasticity (cross-grain) (E_g)	4.04×10^8	Pa
Free shrinkage coefficient (cross-grain) (α)	0.35	m m^{-1}/ kg kg^{-1}
Fibre saturation point (FSP)	$FSP = 0.3 - .001 * T$	kg kg^{-1}
Green density (ρ_t)	1150	kg m^{-3}
Reference diffusion coefficient (D_r)	2.0506×10^{-5} (cross grain)	m^2 s^{-1}
Activation energy (D$_E$)	3800	K

3.7   Climatic and geographical data description

One of the key problems in assessing the performance of solar dryers is that this performance is affected by the surrounding conditions. The environment varies with time significantly. Consequently, weather variations, both daily and annually, result in significantly varying ambient

temperatures, ambient humidities, wind speeds, and amounts of incident solar radiation. Thus, transient external effects have been accommodated within the program developed here. In this simulation, realistic geographical locations and climatic conditions for three places in Australia (Sydney, Melbourne, and Brisbane) have been used for a base year of 2013 as the external boundary conditions. For the estimation of the available solar energy input, a function was coded in the 'Matlab R2012b' version, where formulae and constants were used according to the approach described in Duffie and Beckman (2006), as will be described later. The climatic raw data were collected from the Australian Bureau of Meteorology's "real time" system (Meteorology, 2013), which were then processed to calculate the daily average climatic data as inputs to the simulation program. These daily average climatic data, for a representative season of the year 2013 in Australia: spring (September and October), have been given in Appendix 3A.

3.8   Conclusions

This chapter has aimed at reviewing the standard timber properties and the various drying models that can be used for a computer model to describe the drying behavior of timber in a greenhouse-type solar kiln. This chapter has focused on the properties of Eucalyptus pilularis, which has been taken to be the reference drying material for the simulation. The understanding of the significance of the cross-grain timber properties during drying has been the key aspect of reviewing the timber properties in this chapter. Different models used for describing the moisture migration within the timber boards during drying have also been described in this chapter. Among the models, the diffusion model with the moisture-content driving force has been recognized to be the most appropriate model for describing the moisture transport within hardwood. The climatic and geographical conditions used for the overall study have been discussed here, and representative climatic data have been

included in Appendix 3A. A detailed description of the drying, energy flow, and stress-strain

models and their simulation techniques, as used in this thesis, are given in the next chapter.

Chapter 4:   Model development and its numerical simulation

4.1   Introduction

In order to improve the end-use product quality and the sustainability of drying systems using the renewable energy source provided by the sun, solar drying technology has been globally recognized to be an attractive technology to dry plants, seeds, fruits, meat, fish, wood, and other agricultural and forest products (Janjai and Bala, 2011; Khater et al., 2004; Langrish et al., 1992; Pirasteh et al., 2014; Prakash and Kumar, 2014). In addition, for many rural locations in most developing countries, grid-connected electricity and supplies of other non-renewable sources of energy are still either unavailable, unreliable or too expensive (Visavale, 2012). In such conditions, solar dryers appear to be increasingly attractive, from the economic point of view, for drying a range of agricultural and forest products (Mekhilef et al., 2011; Zhang et al., 2012). Improving drying operations to save energy to improve product quality and to reduce the environmental impact have been the key objectives of many research and development works on solar drying systems (Fadhel et al., 2011). However, the technical development of solar drying systems may proceed in two directions (Othman et al., 2006): (a) the simple, low power, short life, and comparatively low efficiency-drying systems, and (b) the sophisticated, high efficiency, high power, long life, and expensive solar drying systems.

Since the overall performance of a solar dryer relies on the climatic and geographical conditions, assessing the performance of solar dryers using an experimental procedure poses practical difficulties due to the very large number of variables that must be considered, in

addition to the large time involved and the cost (Langrish et al., 1992; Thibeault et al., 2010). As a result, the modeling and simulation of solar kilns for drying products (hardwood timber for this thesis) has been the subject of numerous works, including Khater et al. (2004), Haque and Langrish (2003), Bucki and Perre (2003), Perré and Turner (2002), Wan and Langrish (1995), and Winter and Viskanta (1998). For example, in the simulation of Wan and Langrish (1995), the finite-volume method was applied for solving the diffusion equations for hardwood timber drying.

Most of the previous simulation works, including Khater et al. (2004) and Langrish et al. (1992), implemented finite-difference techniques, including the finite-volume method and backward-difference methods (i.e. Gear's method) to solve the differential equations that are associated with the mathematical modeling of solar kilns. Haque (2002) developed a mathematical model for solar kilns that predicted the air temperature, relative humidity, and moisture content in solar kilns as a function of time and weather conditions of a particular location in Australia. This model was solved by using a FORTRAN program, which was later validated experimentally by Haque and Langrish (2003). The key results of their validation study are highlighted in Figure 4.1, which shows that a good agreement between the experimental and predicted results was obtained. It can be seen from Figure 4.1 that the maximum difference between the actual and predicted moisture contents was 0.05 kg/kg. It should be noted here that the operational policy for the kiln venting (i.e. status and rate) for this validation study was controlled by an electronic digital output. Whenever the output was "on" status, the vents opened up and the air flow rate was measured directly by a handheld anemometer. Since the measurement position for the venting rate was awkward,

there was a possibility of errors in the venting rate measurement, and thus several measurements of the venting rate were made (Haque, 2002).
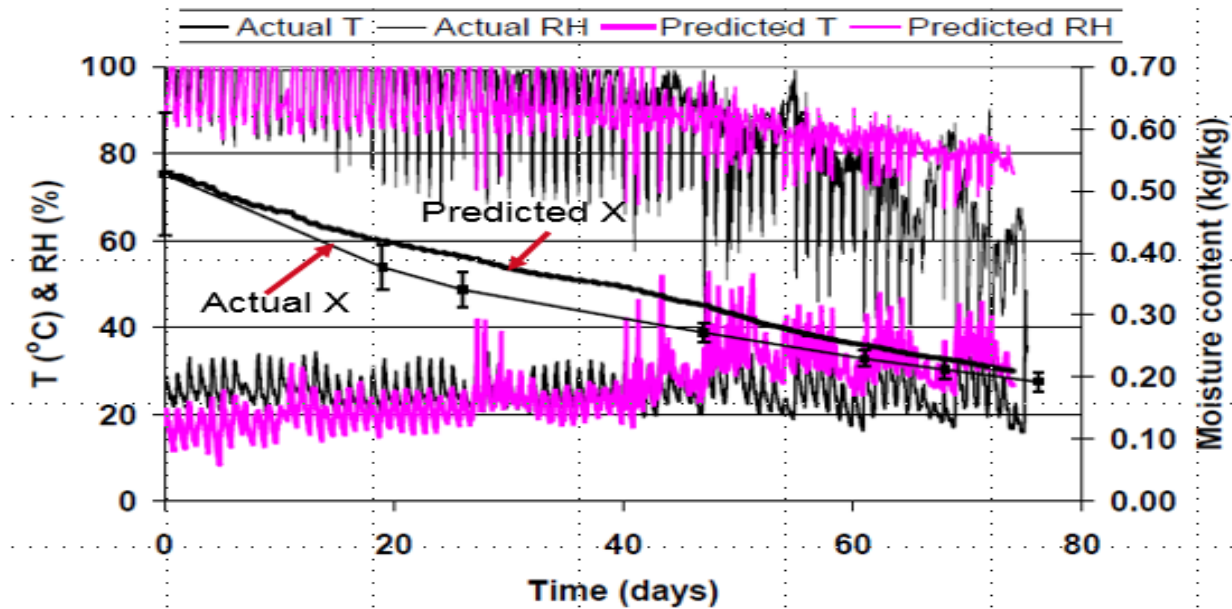
Figure 4.1. Comparison between the actual and simulated internal air temperatures, relative humidities, and timber moisture contents (Haque and Langrish, 2003).

The matches between the predicted and measured values for both the temperatures and the RHs of the internal air were also reasonable, and in each case, they showed a similar cyclic pattern. In such a situation, although the model was found to be basically sound, the approach used by them to solve the model by Fortran programming was limited in its capacity to robustly solve the model equations. Thus, the objectives of this chapter are to: (a) identify the stability issues of the basic model, (b) develop a robust model and an appropriate simulation technique, and (c) solve the model for predicting the performance of a given solar kiln design with different geographical and climatic conditions in Australia.

4.2   Stability issues and overcoming them

One of the challenges in solving the system of ODEs (as given later), which describe the physical variables as a function of time, is the stiffness of the system. Stiffness occurs when the solution components evolve on very different timescales. In the wood-drying process, the mass-transfer process is extremely slow due to the typically low moisture diffusion coefficient, while the heat-transfer process is very much faster than the mass-transfer process (Pordage and Langrish, 1999), which causes the system of ordinary differential equations to be stiff. In stiff physical systems, the step size is restricted both due to accuracy requirements and for stability, as illustrated by Kushnir and Rokhlin (2012). These features complicate the numerical work, where small time steps introduce round-off errors and cause numerical instabilities. To improve numerical stability, and hence to widen its capability for handling transient boundary conditions, the Matlab ODE solver "ode15s" has been suggested and used in this simulation by adjusting the solver algorithm and parameters. For example, the Numerical Differentiation Formulae (NDFs) with a maximum order of "two" have been used as the solver (ode15s) algorithm through "odeset" function in Matlab suite. This procedure has been followed because several researchers, including Lepik (2009) and Shampine and Reichelt (1997), reported that this method appeared to give the most stable (i.e. A-stable) solutions for the stiff problems. A numerical method is said to be A-stable if its region of absolute stability contains the entire left half-plane.

Even after using this simulation technique, there were still stability issues with respect to the energy flow model due to the high flows of heat into relatively small thermal masses. In the energy flow model, the overall kiln has been grouped, as will be described later, into several aggregate components, such as the walls, the roof, and the absorber. The model

describes the energy and mass transfers between each of them and the timber stack. Since the thermal units are considered to be interconnected when constructing the model, most of the heat-flow terms become a function of the temperature difference between the components, thus each unknown parameter (temperature) is a function of itself and the other (mostly unknown) temperatures. In such situation, if one of the thermal units grossly overshoots, then the heat flow to another unit becomes excessively large, leading to an overshoot in the next unit as well, thus rapidly spreading out the instability. This spreading of instability was stopped by limiting the temperatures of some thermal units to between $+5^{\circ}C$ and $+ 95^{\circ}C$. This procedure was done without affecting the integration stage of the calculation, but preventing the resulting temperatures from becoming unreasonably large.

4.3   Materials and methods

This simulation has been done for a greenhouse-type solar kiln design (e.g. Oxford design), as shown in Figure 4.2. The overall model consists of three main sub-models - the energy flow model, the drying model, and the stress/strain model, as are described in the following sections.

4.3.1   Basic description of the Oxford kiln

The schematic diagram and the dimensions of the Oxford solar kiln, which has an overall size of 5.51 m long, 5 m wide, and 3.05 m high, is shown in

Figure *4.2*. However, the load capacity of this kiln is 10 cubic metres of timber, with the size of the drying chamber being 4.88m x 2m x 1.83m. Two painted matt-black corrugated-iron solar absorbers, resting on wooden frames, are attached to the equipment and used to capture solar energy in order to provide heat to dry the timber in the stack. Two axial fans

driven by 0.25 hp electric motors are used to circulate air over the absorber surfaces and through the stack of timber.
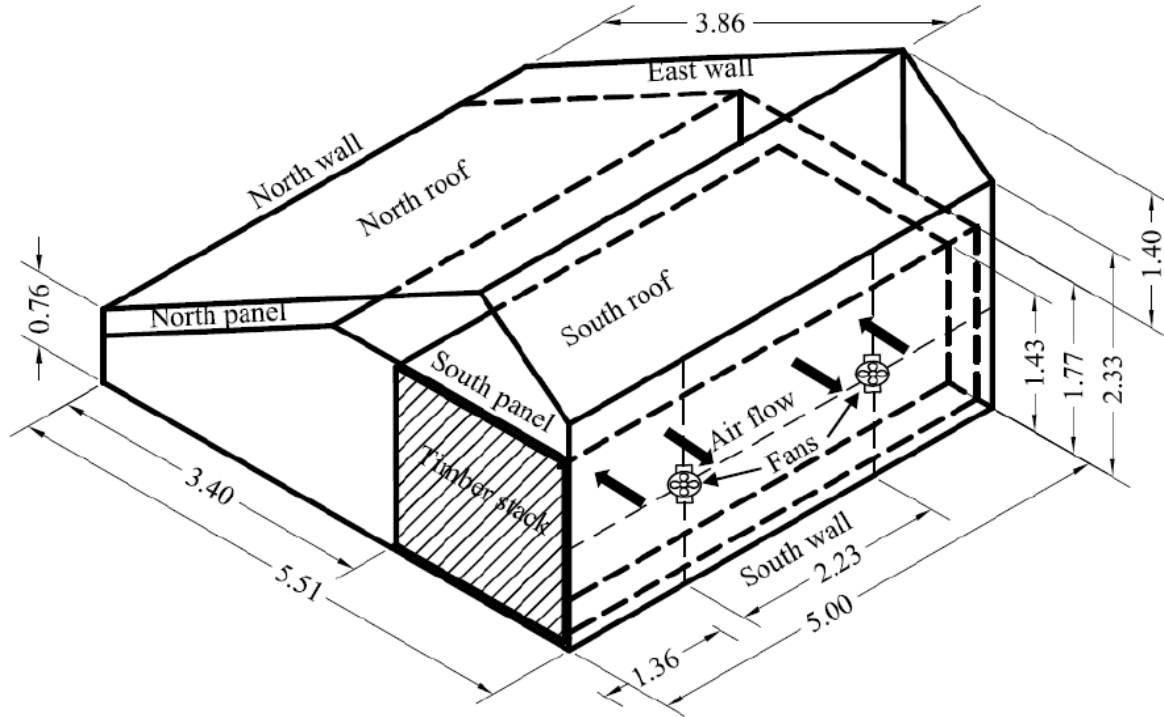
Figure 4.2. Fan and loading arrangements for the Oxford solar kiln (dimensions are in metres).

The circulating air loses sensible heat and gains moisture (from drying the timber) on its passage through the stack, and leaves through an exhaust vent. The north absorber is placed parallel to the inclined north roof, while the south panel is horizontal. The side covers and the roof of the dryer are constructed of transparent materials and let solar radiation through.

4.3.2 The energy flow model

The energy flow model, as carried out in this thesis, was based on the unsteady state analysis of the energy and mass-transfer mechanisms in the solar kiln. In order to construct the model, an aggregate or lumped parameter approach in dealing with the components or

entities involved in the heat-transfer processes has been used. Each aggregate part or component has been assumed to be uniform in temperature and has been represented as a single temperature value. Furthermore, it has been assumed that there is negligible conduction heat transfer between the aggregate parts. The overall kiln has been grouped into several aggregate components, such as the walls, the roof, the absorber, and the model describes the energy and mass transfers between each of them and the timber stack, as shown in Figure 4.3.
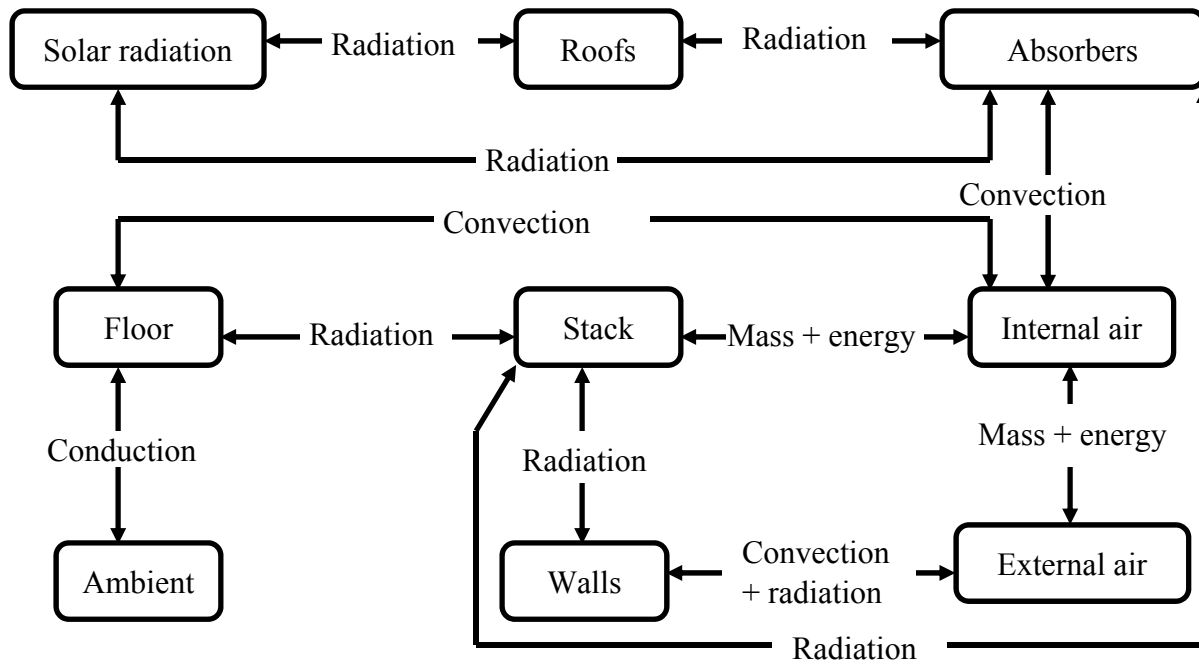
Figure 4.3. The model aggregate components and the key mass/energy flow pathways between them.

A key parameter of these components is known as the thermal mass, M (J K^{-1}), which gives the degree of temperature change associated with a specific energy input and can be defined as follows:

$$M = m * C_p \tag{4.1}$$

where m and C_p are the mass (kg) and the specific heat capacity (J kg^{-1} K^{-1}) of the particular component, respectively.

The model determines the temperature/humidity change of each component based on its thermal mass and the associated energy/mass flows. This energy-flow model has been described by the state variables that include the temperatures of different components, and the humidity of the drying air. The values of these state variables were determined by solving a system of ODEs, which was obtained through the consideration of unsteady-state energy and mass balances to be described in the following sections.

4.3.3 Energy and mass balances

While considering the unsteady-state balances: rate of accumulation = flow rate in – flow rate out = net energy/mass flow rate, the net energy/mass flows can be related to the state variables as shown in the following generic forms:

Energy balance for the kiln aggregate components:

$$\frac{dT}{dt} = \left(\frac{1}{m * C_p}\right) * E_n \tag{4.2}$$

Mass balance for the drying air:

$$\frac{dY}{dt} = \left(\frac{1}{m}\right) * W_n \tag{4.3}$$

Here, T is the temperature of the component under consideration (K), and Y is the inside air humidity (kg kg^{-1}). E_n is the net energy flow rate (W) and W_n is the net water flow rate

(kg s^{-1}) into the air.

4.3.4 Energy balances for different kiln components

Energy balance for the walls:

In this research, using the aggregated-parameter approach, all the four walls have been lumped into one parameter, the walls. The rate of change of the wall temperature can be expressed, using Equation (4.2) and the thermal pathways shown in Figure 4.3, by a differential equation as follows:

$$\frac{dT_w}{dt} = \frac{1}{M_w}\left(-C_{w-air} - C_{w-a} + TR_{stk-w} + TR_{sky-w} + TR_{a-w} + SR_w \right.$$
$$\left. + (Cond_{intw} + Cond_{intw}) * H_{vap}\right) \tag{4.4}$$

Similarly, energy balances for other components can be expressed as follows:

Energy balance for the floor:

$$\frac{dT_f}{dt} = \frac{1}{M_f}\left(-C_{f-air} - TR_{f-na} + SR_f + Cond_{intf} * H_{vap} - Evap_{intf} * H_{vap}\right) \tag{4.5}$$

Energy balance for the circulating air:

$$\frac{dT_{air}}{dt} = \frac{1}{M_{air}}\left(-C_{air-stk} + C_{w-a} + C_{f-a} + C_{nr-a} + C_{sr-a} + C_{na-a} + C_{sa-a} + WS\right.$$

$$* H_{vap} - LR * C_p(T_{air} - T_a) - VR * C_p(T_{air} - T_a) - Cond_{int} * H_{vap} \qquad (4.6)$$

$$\left. + Evap_{intf} * H_{vap}\right)$$

Energy balance for the south roof:

$$\frac{dT_{sr}}{dt} = \frac{1}{M_{sr}}\left(-C_{sr-air} - C_{sr-a} + TR_{sky-sr} + TR_{sa-sr} + SR_{sr} + (Cond_{extsr}\right.$$

$$\left. + Cond_{intsr}) * H_{vap}\right) \qquad (4.7)$$

Energy balance for the north roof:

$$\frac{dT_{nr}}{dt} = \frac{1}{M_{nr}}\left(-C_{nr-air} - C_{nr-a} + TR_{sky-nr} + TR_{na-nr} + SR_{nr} + (Cond_{extnr}\right.$$

$$\left. + Cond_{intnr})H_{vap}\right) \qquad (4.8)$$

Energy balance for the south absorber:

$$\frac{dT_{sa}}{dt} = \frac{1}{M_{sa}}\left(-C_{sa-air} + TR_{stk-sa} - TR_{sa-sky} - TR_{sa-sr} + SR_{sa} + Cond_{intsa}\right.$$

$$\left. * H_{vap}\right) \qquad (4.9)$$

Energy balance for the north absorber:

$$\frac{dT_{na}}{dt} = \frac{1}{M_{na}}\big(-C_{na-air} + TR_{stk-na} - TR_{na-sky} - TR_{na-nr} + SR_{na} + Cond_{intna}$$
$$* H_{vap}\big)$$

(4.10)

In Equations (4.4) to (4.10), the symbols *C, TR, SR, Cond, Evap,* and *Hvap* represent the convective heat transfer rate (W), the thermal radiative heat transfer rate (W), the solar radiative heat transfer rate (W), the condensation rate (kg s⁻¹), the evaporation rate (kg s⁻¹), and the latent heat of vaporization for water (J kg⁻¹), respectively. The subscripts *w, f, air, sr, nr, sa, and na,* denote the walls, the floor, the internal air, the south roof, the north roof, the south absorber, and the north absorber, respectively. The heat transfers between the aggregated components have been represented by hyphenation in the subscripts. For example, *w-air, w-a,* and *stk-w* represent the heat transfers between the walls and the circulating air, between the walls and the ambient air, and between the timber stack and the walls, respectively. Other subscripts denote similar heat-transfer nomenclature, and a full list of symbols, subscripts, and superscripts used in the model has been given in the nomenclature list of this thesis.

4.3.5 Mass balance for internal circulating air

The rate of change of the kiln air humidity, dY_{air}/dt can be described by performing a mass balance on the air in the kiln using Equation (4.3), as follows:

$$\frac{dY_{air}}{dt} = \frac{1}{m_{air}}\big(MF_{stk-air} + WS - Cond_{int} + \mathrm{LR}(Y_a - Y_{air}) + VR(Y_a - Y_{air})\big)$$

(4.11)

Here, *Y, MF, WS, LR, VR* are the humidity (kg kg^{-1}), the mass flow rate (kg s^{-1}), the water spray rate (kg s^{-1}), the leakage rate (kg s^{-1}), and the venting rate (kg s^{-1}), respectively. The subscripts *stack-air* and *int* denote the transfers from the stack to the circulating air and the internal condensation process, respectively. In Equation (4.11), *Ya* represents the ambient humidity (kg kg^{-1}).

4.3.6 Major thermal energy flows

The major thermal energy flows include the solar gains (SG), the convection losses (CL), and the radiation losses (RL), as mentioned before. While the heat-transfer terms in the calculation of these energy flows have been determined by solving the model described by the previous energy and mass balances, the energy flows were evaluated using the following equations:

$$SG = S_{na} + S_{sa} + S_{nr} + S_{sr} + S_{w} \tag{4.12}$$

$$CL = C_{w-a} - C_{nr-a} - C_{sr-a} \tag{4.13}$$

$$RL = -TR_{sky-nr} - TR_{sky-sr} - TR_{sky-w} + TR_{stk-a} + TR_{sa-sky} + TR_{na-sky} \\ - TR_{f-na} \tag{4.14}$$

In Equations (4.12) to (4.14), the *SG*, the *CL*, and the *RL* are the rate of solar gain (W), the convection losses (W), and the radiation losses (W), respectively.

4.3.7 Heat transfer calculations for the simulation

A review of Equations (4.4) to (4.10) indicates that the relationships describing the rate of heat transfer via solar radiation, thermal radiation, and convection heat-transfer processes have been used to calculate the rates of the temperature changes involved in the energy-balance equations of the model. In the following description, the procedures and the equations used for these heat-transfer calculations within the model studied in this thesis have been described.

4.3.8 Solar radiation heat transfer

To determine the radiant energy incident on a surface, a solar input function, as a function of time, azimuth angle, and tilt angle, has been coded in MATLAB 2014b. The formulae and constants used in the function were based on the isotropic diffuse model, which is an improved model for the estimation of solar radiation at a point of time, as described by Duffie and Beckman (2006). This model determines the total irradiance as the sum of the three components: beam radiation, isotropic diffuse radiation (from the sky), and solar radiation reflected diffusely from the ground. Thus, the total flux of solar radiation on a tilted surface, I_T can be expressed as follows (Duffie and Beckman, 2006):

$$I_T = G_{cb}R_b + G_{cd}\frac{(1+cos\gamma)}{2} + (G_{cb} + G_{cd})\rho_g\frac{(1-cos\gamma)}{2} \tag{4.15}$$

where, G_{cb}, R_b, $G_{cd,}$, γ, and ρ_g are the beam radiation flux on a flat surface, the ratio of the beam radiation on a tilted surface to that on a horizontal surface, the diffuse radiation flux on a flat surface, the slope angle between the surface and the horizontal plane, and the reflectance of

the ground, respectively. Since the actual incident solar energy on a surface is affected by the absorptivity of the surface and whether or not the radiation has passed through another solar energy absorbing surface, the solar radiation obtained by Equation (4.15) has been adjusted in the calculation of this model depending on the absorptivity, transmissivity, and emissivity of the surfaces associated with the calculation of a reference component, as will now be described.

4.3.9 Thermal radiation heat transfer

Heat is transferred between two bodies/surfaces through thermal radiation by three forms, namely direct radiation, radiation through a partially transparent cover, and radiation between an object and a partially transparent cover. Each of these thermal radiation pathways has been estimated using the appropriate correlations, as follows:

Direct radiation (Shires et al., 1994):

$$Q = A\sigma(T_{s1}^4 - T_{s2}^4) \tag{4.16}$$

Radiation through a partially transparent cover (Duffie and Beckman, 2006):

$$Q = A\frac{\sigma\tau_c\varepsilon_p}{(1 - \beta_p\beta_c)}\left(T_p^4 - T_s^4\right) \tag{4.17}$$

Radiation between an absorber/sky/stack and a partially transparent cover (Duffie and Beckman, 2006):

$$Q = A \frac{\sigma \tau_c \varepsilon_p \varepsilon_c}{(1 - \beta_p \beta_c)} \left(T_p^4 - T_s^4 \right) \tag{4.18}$$

In Equations (4.16) to (4.18), Q is the radiation energy flow rate (W), σ is the Stefan-Boltzmann constant (W m^{-2} K^{-4}), A is the area of the reference surface, $\boldsymbol{\varepsilon_p}$ is the emissivity of the absorber panel, τ is the transmissivity of cover for thermal radiation, and β_p and β_c are the reflectivities of the absorber panel and the plastic cover, respectively. T_p and T_s are the temperatures in Kelvin for the absorbers/sky and the particular surface, respectively.

4.3.10 Convective heat transfer

The convective heat transfer terms have been calculated in this model using the following equation:

$$Q = hA(T - T_s) \tag{4.19}$$

where, h is the heat-transfer coefficient between the air and the particular surface (W m^{-2} K^{-1}), T is the temperature of the drying/ambient air (K). The value of h depends on whether convection is natural or forced, whether the flow is laminar or turbulent, the orientation of the surface, and whether or not there is any condensation occurring on the relevant surface. Taking all these factors into consideration, in this thesis, several user-defined sub-functions for the calculation of h were coded in the Matlab environment. While different flow situations involve different empirical relations for the Nusselt number, Nu_l and it is not the purpose of this thesis to present them all here (all the correlations have been listed in Appendix 4A), the

heat-transfer coefficients, *h*, are generally correlated with the Nusselt number, Nu_l, in the following form:

$$Nu_l = f(R_{el}, R_{al}, P_r) \tag{4.20}$$

where,

$$Nu_l = \frac{hl}{k_G}, R_{el} = \frac{\rho_G U l}{\mu_G}, R_{al} = \frac{g.\beta.\Delta T.l^3.\rho_G^2.C_{pG}}{k_G.\mu_G}, P_r = \frac{C_{pG}.\mu_G}{k_G} \tag{4.21}$$

In Equations (4.20)-(4.21), $R_{el}, R_{al}, and\ P_r$ are the Reynolds, the Raleigh, and the Prandtl numbers, respectively. The physical properties of the air, namely the thermal conductivity (W m^{-1} K^{-1}), the density (kg m^{-3}), the dynamic viscosity (kg m^{-1} s^{-1}), the thermal expansion coefficient (m m^{-1} K^{-1}), and the specific heat capacity (J kg^{-1} K^{-1}) have been represented by the symbols $k_G, \rho_G, \mu_G, \beta, and\ C_{pG}$, respectively. The acceleration due to gravity (m s^{-2}) and the characteristic length of the surface (m) are represented by *g* and *l*, respectively. It should be noted here that, while the formulae and the empirical relations for the calculation of *h* have been taken from different sources, including Duffie and Beckman (2006), Kakaç et al. (1987), and Shires et al. (1994), the physical properties of the air were evaluated at the film temperature, the average temperature of the surface and the flowing air.

4.3.11 Drying model

The drying model describing the rates of changes of moisture contents (MCs) and temperature of the drying material (i.e. timber) is based on Fick's law of diffusion for mass transfer and Fourier's law for heat transfer, and is linked to the energy flow model through

the mass and energy exchanges between the circulating air and the timber stack. Since the description of these fundamental equations in the drying model has been given in many previous papers, including Bentayeb et al. (2008), Cabardo et al. (2006), and Haque and Langrish (2001), only the governing equations related to the drying model are presented here.

The moisture transport within hardwood may be adequately described by Fick's law in one dimensions as follows (Wan and Langrish, 1995):

$$\frac{\partial X}{\partial t} = \frac{\partial}{\partial Z}\left(D\frac{\partial X}{\partial Z}\right)$$
(4.22)

Here X is the MC (kg kg^{-1}), Z is the distance through the timber thickness (m), and D represents the temperature-dependent diffusion coefficient,

$$D = D_r exp^{-\left(\frac{D_E}{T}\right)}$$
(4.23)

while D_r is the reference diffusion coefficient (m^2 s^{-1}), and D_E is the activation energy (K). Likewise, heat transport with the timber can be described by the second partial differential form of Fourier's law, as follows (Langrish et al., 1997):

$$\frac{\partial T}{\partial t} = \frac{\partial}{\partial Z}\left(\frac{k}{\rho_t C_{pt}}\frac{\partial T}{\partial Z}\right)$$
(4.24)

In Equation (4.24), k, ρ_t, C_{pt} are the thermal conductivity (W m^{-1} K^{-1}), the density (kg m^{-3}), and the specific heat capacity (J kg^{-1} K^{-1}) of the timber, respectively, and are functions of the moisture content. As a result, Equations (4.22) and (4.24) form a coupled system of ordinary differential equations (ODEs). It should be noted here that, in a moderately humid condition (as in this case), the flux of moisture from the timber board, J, can be considered to be proportional to the difference in the humidities between the timber surface, Y_{ts} and that in the bulk air stream, Y_{air}, which leads to an expression for the flux of moisture from the board, *J* as follows (Keey, 1978):

$$J = \beta * (Y_{ts} - Y_{air}) \qquad (4.25)$$

The mass-transfer coefficient (kg m^{-2}s^{-1}) is denoted by β in Equation (4.25). The bulk air humidity (Y_{air}) can be obtained from the dry and wet-bulb temperatures in the kiln, and Y_{ts} is a function of the moisture content and temperature at the timber surface (Langrish et al., 1997).

Similarly, both convective heat transport and heat transfer associated with the evaporation of moisture at the timber surface must be considered for the drying model. Thus, the total rate of heat transfer (Q) may be expressed in terms of the heat-transfer coefficient (h), the dry-bulb temperature (T_{db}), the surface temperature (T_{ts},), the latent heat of vaporization (λ_w), and the heat of sorption (λ_s) to give the following expression (Langrish et al., 1997; Haque, 2002):

$$Q = h * (T_{db} - T_{ts}) - J * (\lambda_w + \lambda_s) \qquad (4.26)$$

Since the parameters appearing in the above equation represent the heat-transport phenomena at the timber surface during drying (assuming that the evaporation of moisture occurs adjacent to the board surface), Equation (4.26) becomes a boundary condition, when solving the drying model numerically, for Equation (4.24). Reviewing Equations (4.22) to (4.26) indicates that the drying model involves simultaneous heat and mass transfer processes. This situation, together with the presence of considerable mass transfer rates in drying process, makes the Chilton-Colburn analogy between heat and mass transfer an appropriate choice for determining the unknown transfer coefficient when the other coefficient is known (Tsilingiris, 2010). It should be noted here that the validation study of the overall drying model, as used in this thesis, with both the experimental and analytical results have been carried out by several workers, including Wu (1989) and Brooke (1999).

The energy flow model, combined with the drying model, resulted in a stiff system of ODEs, which was solved in this thesis by a built-in ODE solver in Matlab, namely "ode15s", with adjusted parameters and an algorithm for stiff systems of ODEs, as described in Section 4.2. The next section describes the overall simulation method for predicting the thermal energy flows around a solar kiln.

4.3.12 Data description of the thermal energy simulation program

The overall thermal energy flow model is composed of various differential equations that describe the rates of change of moisture contents in the timber, X, the humidity of the drying air, Y, and the temperatures of the kiln components, T. To solve this model, the overall program required a number of inputs for material properties (e.g D_r, D_E, ρ_t) and design

variables (e.g. areas, angles, and M) depending on the drying material and geometry of the kiln, respectively. These input parameters, together with the variables predicted by solving these models, for the drying and energy flow models, have been given in Table 4.1.

Table 4.1. Materials properties and design variables for the solar-kiln simulation.

Drying model		Energy flow (equipment) model	
Input parameters	Predictions	Input parameters	Predictions
Timber properties • Reference diffusion coefficient, D_r • Activation energy, D_E • Timber density, ρ_t • Modulus of elasticity, E • Shrinkage coefficient, β_s Stack properties • Board dimension (thickness, width, and length) • Sticker thickness Initial guesses • MCs • Timber temperature	• Moisture content of the timber as functions of time • Temperature of the timber as functions of time	Design variables • Areas for heat transfer calculations • Characteristic lengths. • Circulating air velocity • Angles • Thermal masses, M • Thermal and solar radiation properties. Process variables • Venting, leakage, and water spray rates. Initial guesses • Initial values for all the model state variables and for the ambient conditions.	• Temperature of the kiln components, such as the walls, absorbers, drying air, and the humidity of the circulating air as functions of time. • Energy flows e.g. convection losses, radiation losses, and incoming solar energy as functions of time.

Table 4.1 shows that the input parameters for the drying model included the material properties (e.g. D_r, D_E, and ρ_t) and stack properties (e.g. board dimensions and sticker thickness), while the energy flow model included the design variables (e.g. areas, angles, M) and process variables (e.g. venting rate, water spray rate, and leakage rate). Since "ode15s"

is an initial-value ODE solver, the program required initial guesses for all the state variables present in the system of ODEs, such as the moisture contents, the temperatures, and the humidity of the drying air. The program also required the external ambient conditions as boundary conditions for the model. As the performance of a solar kiln relies heavily on variable external conditions, such as solar irradiation, ambient humidity, ambient temperature, and wind speed, their transient effects have been included, by using user-defined functions, within the Matlab program used in this chapter.

In the simulation, the year 2013 was considered as the base year for the climatic conditions, while using the geographical location of Brisbane in Australia. All of the values for the input parameters required for the simulation program have been given in Appendix 4B. It should be noted here that the drying model was used to predict the moisture content and temperature of the timber, while the energy flow model predicted the thermal energy flows, such as the solar gain, SG, the energy losses from the kiln, EL, as shown in Table 4.1.

4.3.13 Simulation techniques

To numerically solve the solar kiln model, a number of functions were coded in the Matlab (version 2012a) programming environment, which were linked with a main program. The drying model was described by a stiff system of ODEs, implying (as illustrated by Suleiman, Musa, Ismail, and Senu, 2013) that the solver was limited by stability rather than accuracy, so the variable step-size Matlab ode solver "ode15s" has been used in this simulation. To improve the numerical stability of the solver, within the solver (ode15s), Numerical Differentiation Formulae (NDFs) with a maximum order of "two" have been used by adjusting the solver parameters. This procedure has been followed because several researchers, including Lepik (2009) and Shampine and Reichelt (1997), reported that this

method appeared to give the most stable (i.e. A-stable) solutions for the stiff problems. Since the performance of the solar kiln heavily relies on variable boundary conditions, such as solar irradiation, ambient humidity, ambient temperature, and wind speed, their transient effects have been accommodated within the program developed here. In this simulation, realistic geographical locations and climatic conditions of the year 2013 for three representative places (i.e. Sydney, Melbourne, and Brisbane) in Australia have been used, with the base season being the spring (i.e. September and October). The climatic raw data (e.g. ambient humidity, ambient temperature, and wind speed) were collected from the Australian Bureau of Meteorology (Meteorology, 2013), which were then processed to calculate the daily average climatic data as inputs to the simulation program. All the climatic data were also coded as a function of time, and thus the transient variations in boundary conditions have been included appropriately in the simulation program. The simulation was run over a drying period of 50 days (real time).

It should be noted here that the available solar energy inputs (i.e. sunlight hours) for the solar kilns vary with the declination angle of the sun, which is dependent on the day of the year. This variation in the sunlight hours (and hence in the available solar energy for drying process) with the seasons has been included, following the approach described in Duffie and Beckman (2006), within the solar input function. The solar input function is one of the user-defined functions coded in the 'Matlab R2012b' version as part of the overall simulation scheme and calculates the energy input from the sun as a function of time and the orientation of the absorbers with respect to the sun.

4.4   Results and Discussion

The results and discussion of this simulation study are given in the following sections.

4.4.1   The timber moisture contents and level of strains

Figure 4.4 Figure 4.4. Predicted timber MCs during solar kiln drying, as a function of time.shows the numerical prediction of the predicted change in the average MC for the hardwood timber boards during the drying period in the solar kilns (assuming they are located in the three different regions of Australia), while Figure 4.5 shows the maximum strain developed in the boards, as functions of time, over a drying period of 50 days.
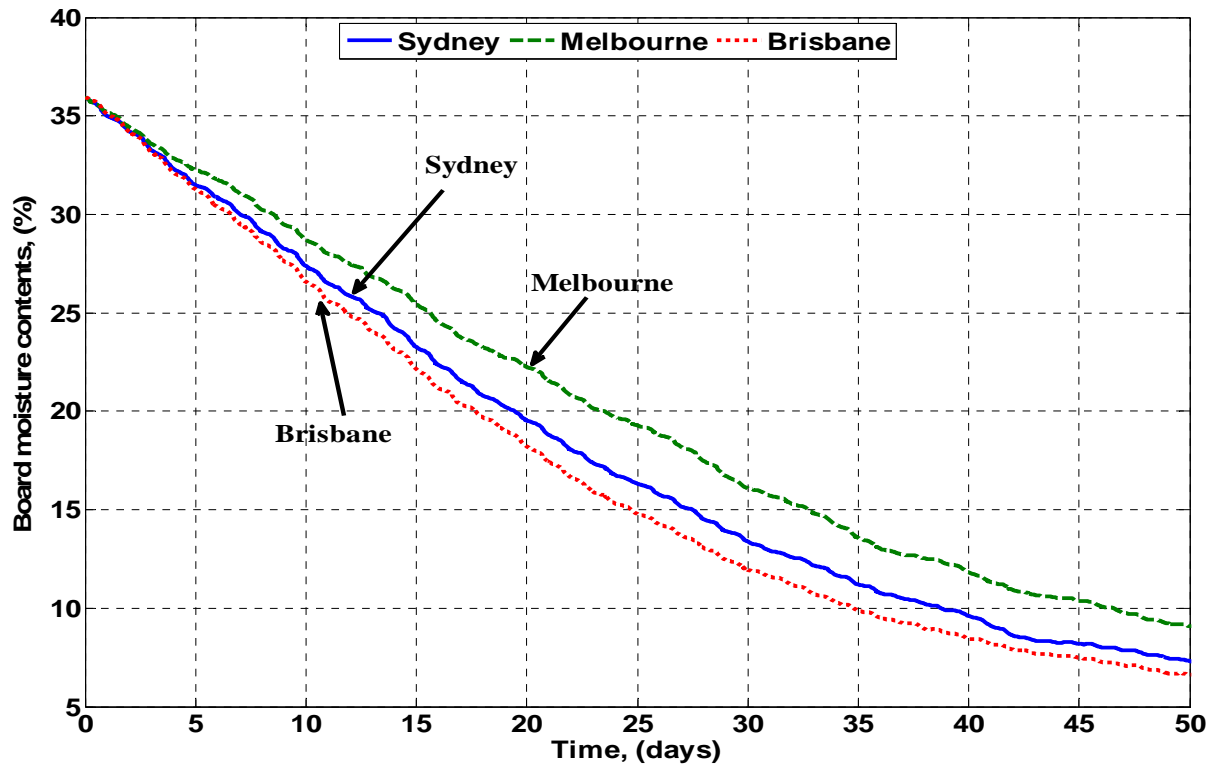
Figure 4.4. Predicted timber MCs during solar kiln drying, as a function of time.

For all the locations included in Figure 4.4, the drying rate was faster in the earlier part of the drying process (for example, in Brisbane, the reduction in MC is 0.84% per day for the first 25 days) than it was in the later stage (0.36% per day for the last 25 days). This result was due to the greater hindrance to moisture transport within the timber boards at lower moisture contents, leading to slower drying rates. Out of the three regions, the minimum

final average MC was achieved in Brisbane (6%), while this value was 7% and 9% for Sydney

and Melbourne, respectively, as shown in Figure 4.4. This variation arises from the difference

in the boundary conditions for the solar kilns, which include the geographical locations and

the climatic conditions around the kilns. From a geographical point of view, Brisbane is

situated at 27.46^0 S while Sydney and Melbourne are located at latitudes of 33.86^0S and

37.81^0S, respectively. This lower latitude of Brisbane causes greater solar radiation to be

incident on the absorbers of the kilns, which increases the kiln air temperature and hence

causes higher diffusion coefficients in the timber.
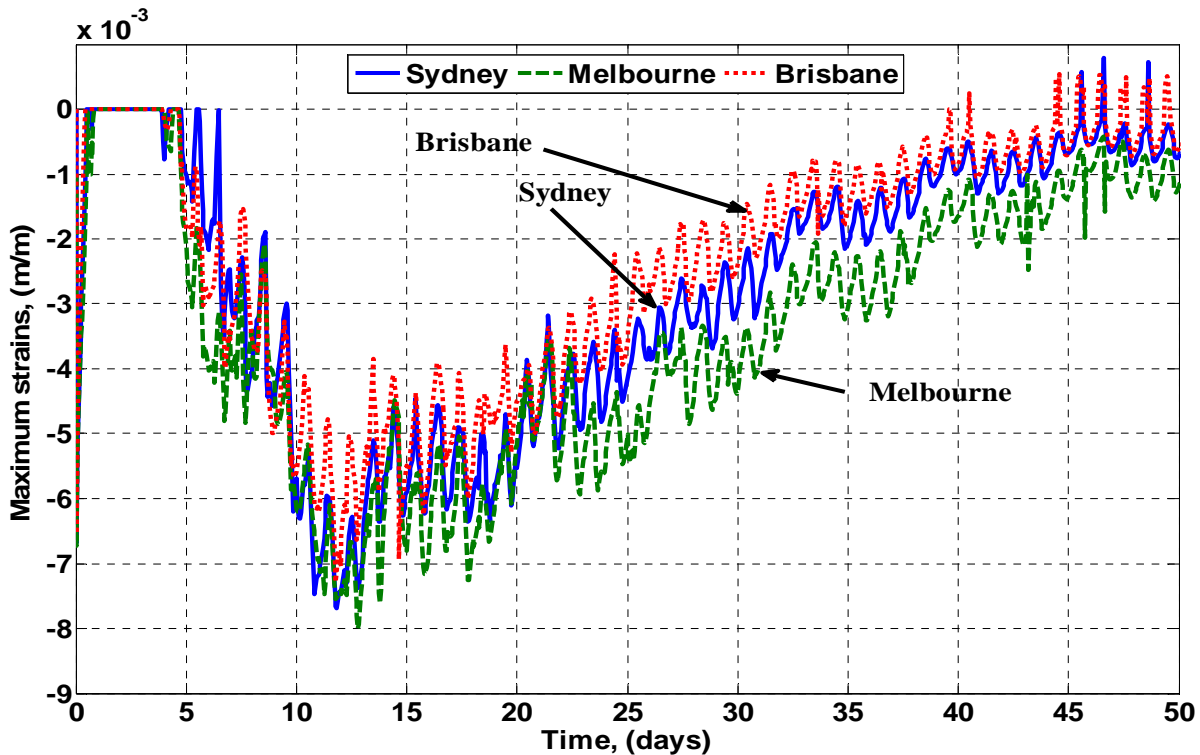
Figure 4.5. The predicted maximum instantaneous strains experienced by the timber

during drying, as a function of time.

This situation in turn allows faster moisture movement within the boards. However, faster

drying rates sometimes may result in higher strain levels within the timber. In this context,

the strain level was also predicted, and the highest strain value for Brisbane was predicted to be 0.0075 m/m, which is less than the maximum allowable value of 0.02 m/m suggested by Doe et al. (1994), a feature which is likely to make the end product of very good quality. Initially there was assumed to be no strain within the timber, as shown in Figure 4.5. As drying continued, the strain began to develop and reached a maximum value, which was followed by a decline in the strain level towards the end of the drying period. Hence considering the drying rate and the level of strains experienced by the timber during drying, Brisbane is likely to be the most suitable location for the drying of hardwood timber by solar kilns in order to minimize the drying time while maintaining good timber quality. This phenomenon is also consistent with the work of Gough (1981), which was carried out near Brisbane, possibly supporting the use of solar kilns in this region of Australia.

4.4.2 Convection and radiation losses

The convection and radiation losses (as functions of time) from the kilns, if they were located in the three different cities considered in this simulation, are shown in Figure 4.6 and 4.7, respectively.

It was predicted that the radiation losses are substantially greater than the convection losses throughout the drying period, which is consistent with the experimental study of Langrish et al. (1993), where the radiation losses from the walls and the roof of the kiln were (experimentally) reported to be about 59% of the incoming total solar energy, while the convection losses were only 32% of the total.
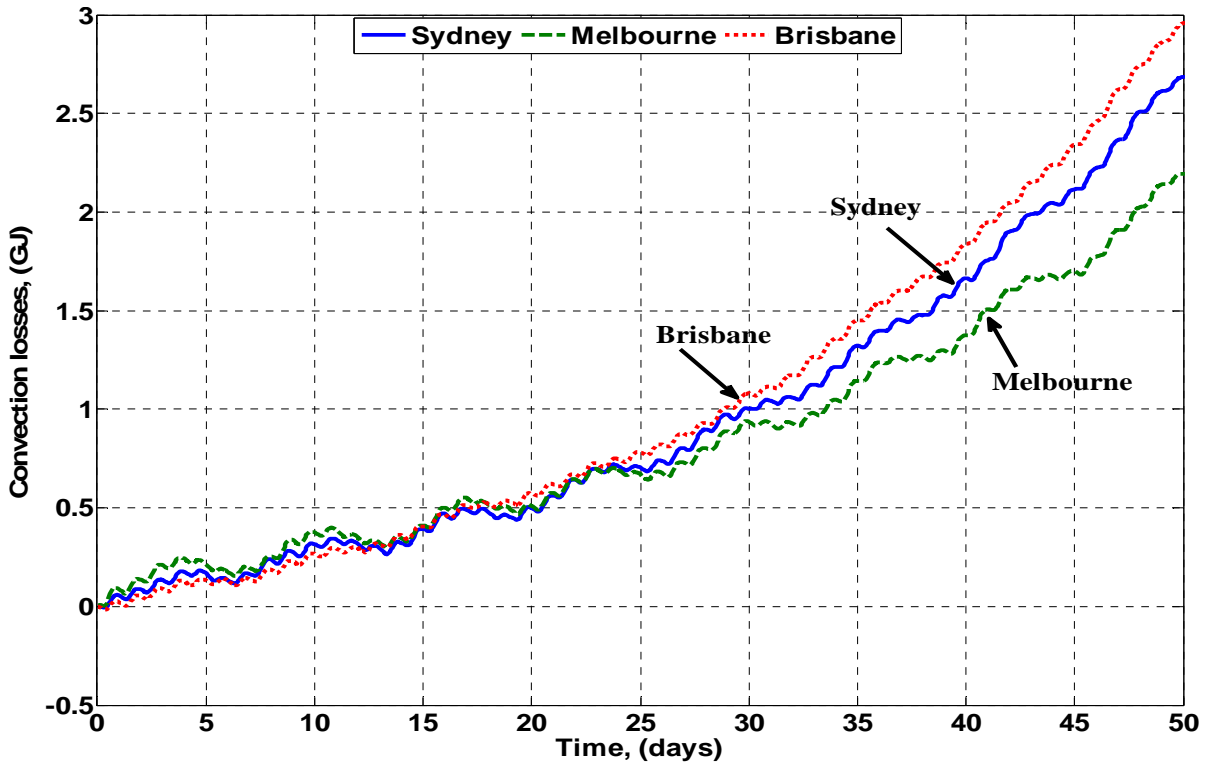
Figure 4.6. Convection losses from the kiln as functions of time for Sydney, Melbourne

and Brisbane locations.

From Figures 4.6 and 4.7, it is noticeable that the radiation losses are very similar, irrespective of locations. However, the location affects the convective energy losses more significantly. One of the reasons for this variation is that the dominant convection loss terms (convection walls to ambient, convection north roof to ambient, and convection south roof to ambient) are more dependent on the climatic boundary conditions, since these terms involve the wind speed, ambient temperature, and the ambient humidity (if condensation occurs). By contrast, the radiation loss terms are mainly linked to the sky temperature that was calculated, in this model, by using the correlation proposed by Swinbank (1964). In order to accurately predict the losses from the kilns, it is important to calculate the sky

temperature with a reasonable accuracy since the sky temperature affects both the radiation (directly) and convection (indirectly) losses.
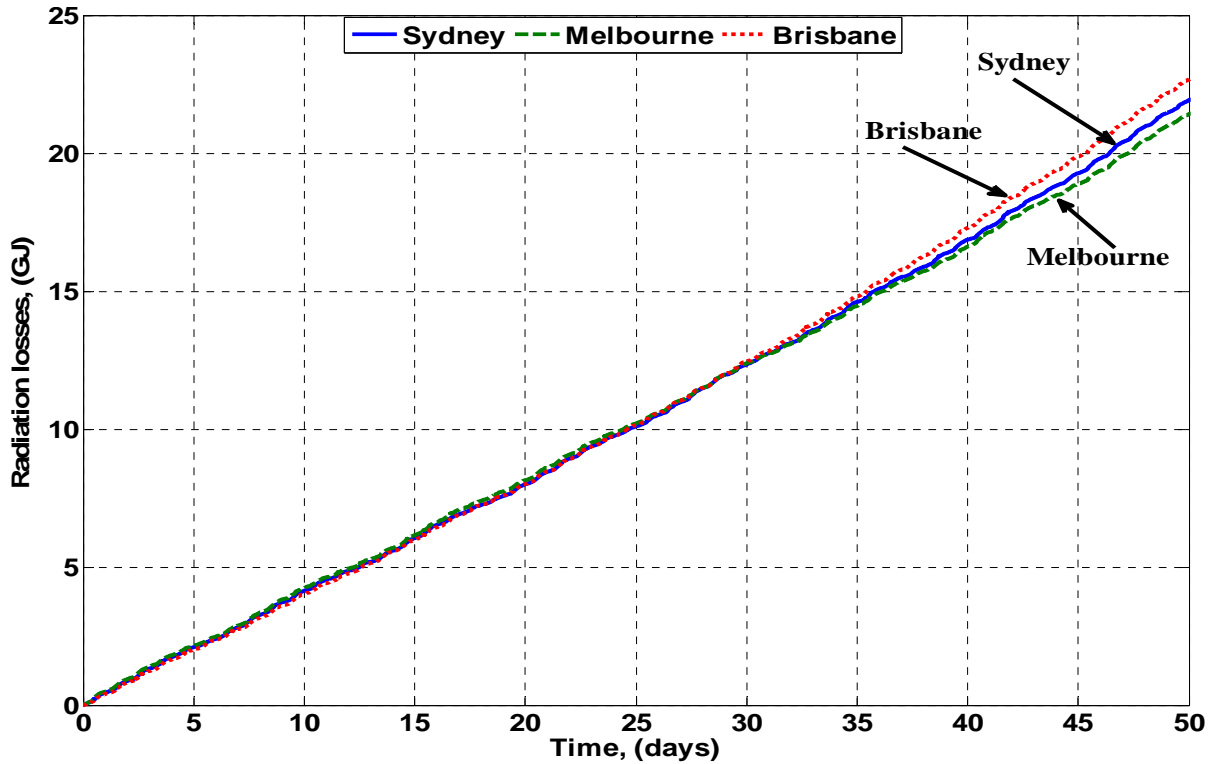
Figure 4.7. Radiation losses from the kiln as functions of time for Sydney, Melbourne and Brisbane locations.

Table 4.2 compares the variation in the predicted convection and radiation energy losses from the solar kilns (corresponding to different correlations for the sky temperature) in different locations of Australia. Table 4.2 indicates that the predicted sky temperatures affect both the convective and radiation losses more than the kiln locations do. As a comparison between the correlation proposed by Swinbank (1964), as used here, and that used by Adelard et al. (1998), for Brisbane, a 3.4 % change (11^0C to 21^0C, increase) in the sky temperature causes 50% (3.0 GJ to 6.0 GJ, increase) and 20% (22.5 GJ to 18.0 GJ, decrease)

changes in total convection and radiation losses, respectively, over the entire drying period (50 days).

Table 4.2. Comparison of predicted convection and radiation losses corresponding to different correlations for the sky temperature between Sydney, Melbourne, and Brisbane locations (total over the full 50-day drying period).

Correlations for T_{sky}	$(T_{amb}-T_{sky})$ (^{0}C)	Total convection losses (GJ)			Total radiation losses (GJ)		
		Sydney	Melbourne	Brisbane	Sydney	Melbourne	Brisbane
Berger et al. (1984)	11.5	2.70	3.10	3.00	21.0	20.0	22.5
Martin and Berdahl (1984)	17	1.10	1.50	1.90	23.0	22.0	24.0
Adelard et al. (1998)	6	6.50	6.80	6.00	16.0	15.0	18.0
Bliss (1961)	11	3.90	4.00	3.95	20.0	18.0	21.0
Swinbank (1964)	16	2.80	2.10	3.00	22.0	21.5	22.5

The internal temperatures (both the air and the internal surfaces) corresponding to the reduced radiation losses (increased predicted sky temperature) were predicted using the sky-temperature correlation of Adelard et al. (1998) to be higher than those predicted using the correlation of Swinbank (1964), which in turn gave increased convection losses from the kiln, as shown in Table 4.2. The effect of different correlations for the sky temperature was, however, predicted to be small in terms of the average board final moisture contents (5.26% change due to a 3.4% change in the predicted sky temperature), as shown in Table 4.3.

Table 4.3. Effects of the predicted sky temperature on the final moisture contents for three different cities in Australia.

Correlations for T_{sky}	Average difference between T_{amb} and T_{sky} (^{0}C)	Final moisture contents, (%)		
		Sydney	Melbourne	Brisbane
Berger et al. (1984)	11.5	7.16	8.65	6.42
Martin and Berdahl (1984)	17	7.72	9.16	6.65
Adelard et al. (1998)	6	6.38	7.90	5.70
Bliss (1961)	11	7.06	8.45	6.24
Swinbank (1964)	16	7.22	9.03	6.44

In summary, the prediction of a reliable sky temperature is likely to mean better prediction of the convection and radiation losses from the kilns. The next section will discuss the effects of the kiln air temperature and humidity on the timber drying performance.

4.4.3 Temperature and humidity of the internal air

The predicted temperature and humidity of the air inside the solar kilns for all three locations considered in this work are shown (as functions of time) in Figure 4.8 and 4.9, respectively.
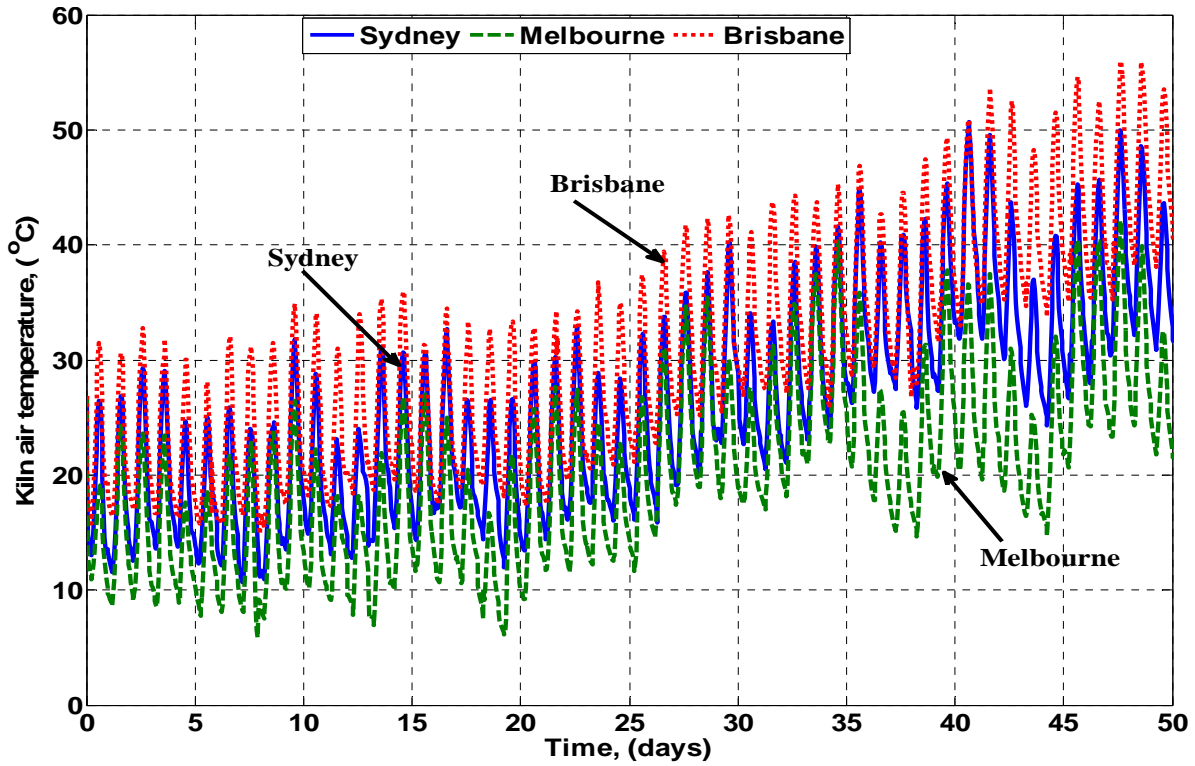
Figure 4.8. Internal air temperatures as a function of time for Sydney, Melbourne and

Brisbane locations.

The diurnal variations of the boundary conditions result in variations of drying conditions (temperature and humidity of the internal air) at different sites, as illustrated in Figure 4.8 and 4.9. The drying air temperature and humidity (Figures 4.8 and 4.9, respectively) for Brisbane were predicted to be higher than those at the other two locations (Sydney and Melbourne).
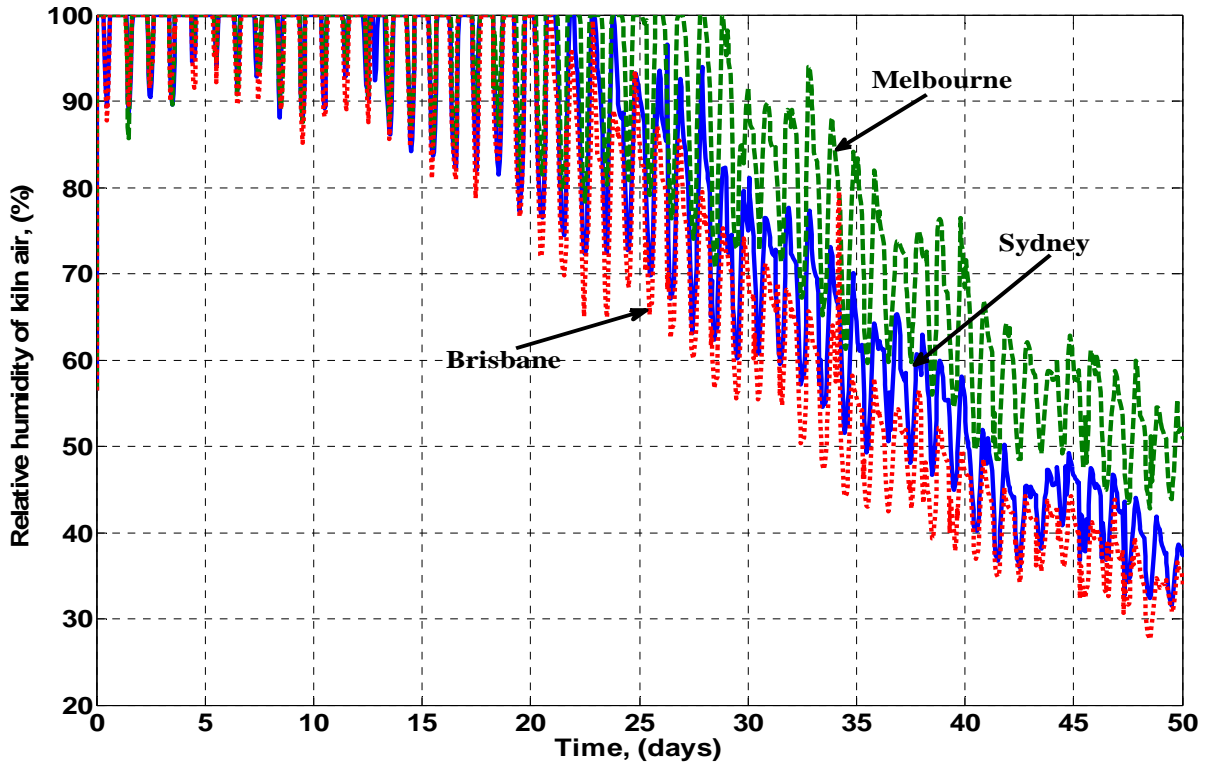
Figure 4.9. Internal air humidities as a function of time for Sydney, Melbourne and

Brisbane locations.

One important factor is that higher air temperatures mean higher moisture-holding

capacities in the air. Note that, in this simulation, venting was only allowed if the ambient air

humidity was less than the internal air humidity, in order to avoid ineffective venting. Since

the diffusion coefficient is a temperature-dependent parameter, the diffusion coefficients

and hence the drying rates increase with the increase in air temperature, which is also

reflected in Figure 4.4. These favorable drying conditions, together with the lower strain

levels, make Brisbane a better predicted choice of solar kiln location for wood drying.

4.4.4   Moisture-content distributions

To produce a good-quality wood product, it is desirable to obtain as uniform a moisture distribution as possible throughout the board thickness, as suggested by Khater et al. (2004), and Wan and Langrish (1995). This simulation also predicted the moisture profiles at different stages of the drying time, as shown in Figure 4.10.
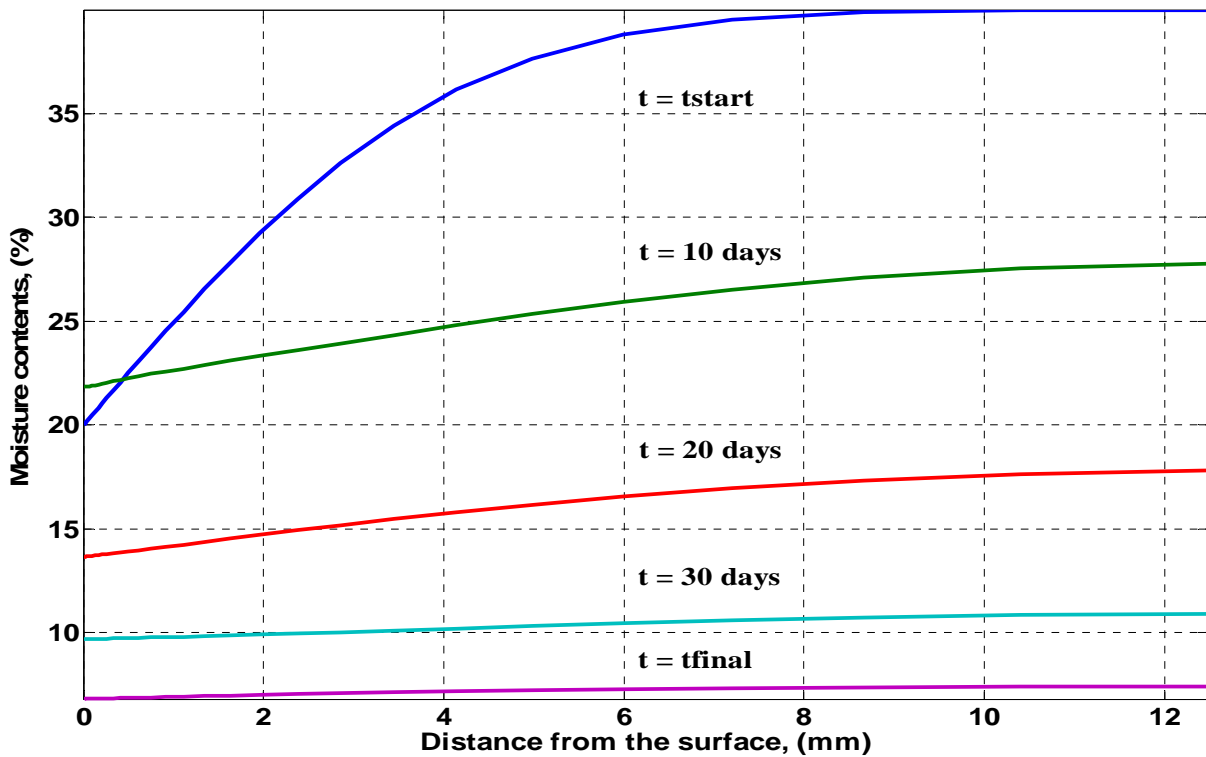
Figure 4.10. Moisture content distribution in a typical board at different stages of the total drying time.

From Figure 4.10, it can be seen that the differences between the surface and the centre moisture contents are highest at the start of the drying process. As the drying progresses, the moisture concentration profile becomes flatter, finally showing a profile that is almost horizontal, indicating a uniform moisture-content distribution within the dried boards. This is achieved because, in cyclic drying, the movement of moisture continues through the

boards during the relaxation time, which causes less degrade in the timber, as mentioned in Wan and Langrish (1995). It should be noted here that, while the overall moisture content reduced after 10 days, the surface moisture content increased from 20% at the start of drying to around 22% during this time, as shown in Figure 4.10. This happened due to the factor that moisture evaporated from the surface of the timber board first, which caused the moisture movement (relatively high in early stage of drying) from the centre (high moisture content region) to the surface (low moisture content region). However, as drying continued, the moisture-content level decreased both at the centre and surface of the boards, resulting in an overall reduction of the average moisture content, as shown in Figure 4.10.

4.5   Conclusions

A robust numerical simulation based on the Oxford solar kiln design has been developed in order to predict the behavior of this design for drying hardwood timber in different geographical and climatic conditions for Australia. For hardwood timber, the prospect of better productivity and quality in the end product have been predicted to be higher if the kiln could be located in Brisbane, Queensland, Australia. The maximum strain level has been predicted to be 0.0075 m/m (significantly less than the failure value of 0.02 m/m) in this location. It is predicted to be desirable to increase the air temperature in order to increase the drying rate by reducing the radiation losses from the kiln. The effects of the predicted sky temperatures (corresponding to different correlations) on the radiation and convection losses have been analyzed and predicted to have a significant impact on the convection and radiation losses. The correlation for the sky temperature, as used by Adelard et al. (1998), has been found to give the lowest predicted radiation losses from the kilns for all three climatic conditions. The moisture-content distribution profiles at different stages of drying

were also predicted and found to be consistent with those suggested earlier by other researchers to give low timber degrade. The internal drying conditions for the selected sites were also found to be acceptable for drying hardwood timber. Finally, this simulation may be used as a tool to anticipate the performance of different solar kiln designs for a range of varying geographical and climatic conditions. In the next chapter, application of the model and its simulation procedure, as developed in this chapter, are demonstrated for comparing the performance between solar kiln designs.

Chapter 5:   Performance comparisons between solar kiln designs

5.1   Introduction

Kiln drying of wood has been an attractive process for reducing the moisture contents (MCs) of the timber down to a level at which it is immediately suitable for normal services, for example, for the furniture, joinery and construction industries (Falk, 2009; Haque et al., 2014; Keey et al., 2000; Pirasteh et al., 2014). However, drying is a complex heat and mass-transfer process and the performance of dryers depends on a large number of internal (e.g. design) and external (ambient) variables (Keey et al., 2000; Langrish et al., 1992; Thibeault et al., 2010). This situation makes it challenging to compare the performance of different kiln designs. Literature reviews (Guzman et al., 1987; Herritsch et al., 2010; Hossain et al., 2005; Ong, 1997) of existing simulation and experimental studies show that very few studies have been carried out to compare the relative performances of different solar kiln designs for wood drying. Guzman et al. (1985) experimentally compared solar kilns (with box type collectors) with open-air drying. Later, they developed a model through a heat and mass-transfer analysis, as discussed in Guzman et al. (1987), to compare the relative performance of these different kiln designs. In the model, the rate at which water was evaporated during drying was determined through an inside air circulation parameter (*R*) as follows:

$$G_r = G * (R - 1) \tag{5.1}$$

where, G_r and G are the recirculating air mass flow (kg h^{-1}) and the air mass flow (kg h^{-1}) rates, respectively. However, according to the definition of the recirculation parameter, R, as given in Equation (5.1), a less-than-unity value of R leads to a negative value of G_r, which is unlikely to have any physical meaning (as the air flow rate cannot be negative). Since in the study of Guzman et al. (1985) and Guzman et al. (1987), the value of R was found to be less than unity for both falling and constant drying rate periods, and since no explanation on the negative value of R was present in their work, the value and the contribution of the works appear to be unclear in terms of comparing the performance of different kiln designs. Another comparative study was carried out experimentally by Ong (1997), where a solar dryer was compared with an electrically-heated kiln. The solar dryer gave slower drying rates than the electrically-heated kiln but also gave a lower final moisture content than open-air drying. The relative difference between the intermittent and continuous drying of red beech timber was discussed by Herritsch et al. (2010), where intermittent drying (a feature of solar kiln drying) was found to be superior to continuous drying. In general, with few exceptions, a number of research solar kilns have been documented in the literature over the last few decades, and a summary of them has been mentioned in Haque (2002). Most of the solar kilns reported have been of a greenhouse-type, or a modification of a greenhouse-type structure, but they have varied significantly both in size and design. As mentioned in Chapter 4, Haque (2002) developed a model for solar kilns, which was later validated experimentally by Haque and Langrish (2003). When solving the model by Fortran programming, however, the approach used by them was limited in its capacity to robustly solve the model equations. In Chapter 4, an improved numerical procedure has been developed by using Matlab (R2012 version) in order to predict the solar kiln behavior for the Oxford design with the

geographical and climatic conditions of three representative cities (Sydney, Melbourne, and Brisbane) in Australia. Among the three locations, the simulation results indicated that Brisbane was likely to give the most favorable drying conditions (faster drying times consistent with acceptable timber qualities) for the Oxford design. However, no attempt was made to apply the simulation technique for different kiln designs, which has been done in this chapter. Also, no discussion was included regarding the seasonal effects on the kiln performances in the previous chapter. Taking these aspects into consideration, the aim of this chapter may be broken up into three main objectives: - (i) to apply the previously developed simulation procedure for different solar-heated timber drying kiln designs, (ii) to carry out a comparative analysis (based on a reference functional unit) between the Oxford and Boral designs, and (iii) to analyze whether and to what extent the seasonal boundary conditions affect the kiln performance and the relative performance. Since a high level of detail regarding solar kiln designs and dimensions for hardwood drying is not generally available in the literature, this comparative study has been carried out only for the Oxford and the Boral kiln designs.

5.2   Materials and methods for the comparisons of the kiln performances

The materials and methods for this comparative study are explained in the following sections.

5.2.1   Climatic and geographical data description

The performance of the two solar kiln designs (Oxford and Boral kilns) has been compared, in this chapter, for the climatic situations and geographical location of Brisbane (latitude 27.46^0S) in Australia. This particular location was chosen for the current study because in

Chapter 4, it was found that Brisbane was the most favorable location for solar wood drying out of the three representative cities (Sydney, Melbourne, and Brisbane) in Australia. The climatic raw data for the chosen location were collected from the Australian Bureau of Meteorology (Meteorology, 2013), which were then processed to calculate the daily average climatic data as input to the simulation program. The simulation was carried out for three representative seasons of the year 2013 in Australia: summer (January and February), spring (September and October), and winter (June, July, and August). These daily average climatic data for the year 2013 have been included in Appendix 5A.

5.2.2   Basis of comparison

While different designs of the solar kilns have different dimensions and layouts, it is necessary to have a common "functional unit" for the designs being compared, in order to compare the relative performance between them through a simulation. This functional unit quantifies the function/performance of the two designs as a reference basis. There is strong evidence, including Cabardo et al. (2006) and Khater et al. (2004), indicating that the timber species, the stack velocity (velocity across the timber stack), the board thickness, and the thicknesses of the stickers may affect the drying behavior significantly. Taking these features and the dimensions of the two kilns into consideration, in this study, the reference functional unit was defined as the drying of 10 m^3 of hardwood timber of a specific species, board and sticker thicknesses (as listed in Table 5.1) to the final moisture content of 15% (dry basis) – a typical final MC level for hardwood (10% to 20%). Since the original Boral kiln, as studied by Haque (2002) and shown in Figure 5.1, has a load capacity of over 90 m^3, its dimensions have been scaled down to give the same timber load capacity (i.e. 10 m^3) as the Oxford kiln

while not affecting the basic kiln design and shape. This scaling method may be given in the following mathematical form:

$$(SLD)_{Boral} = k * (OLD)_{Boral} \tag{5.2}$$

$$(SSA)_{Boral} = k^2 * (OSA)_{Boral} \tag{5.3}$$

$$(SV)_{Boral} = k^3 * (OV)_{Boral} \tag{5.4}$$

$$Scale\ factor, k = \left[\frac{(OSV)_{Oxford}}{(OSV)_{Boral}}\right]^{\frac{1}{3}} \tag{5.5}$$

Here, *SLD, OLD, SSA, OSA, SV, OV,* and *OSV* are the scaled linear dimension (m), the original linear dimension (m), the scaled surface area (m²), the original surface area (m²), the scaled volume (m³), the original volume (m³), and the original stack volume (m³), respectively. The subscripts *Oxford* and *Boral* represent the corresponding kiln designs. It should be noted that the kiln volumetric scaling factor has been the same as the stack volume scaling factor, meaning that the degree of scaling in all three dimensions is consistent, which further helps to keep the basic kiln design undistorted.
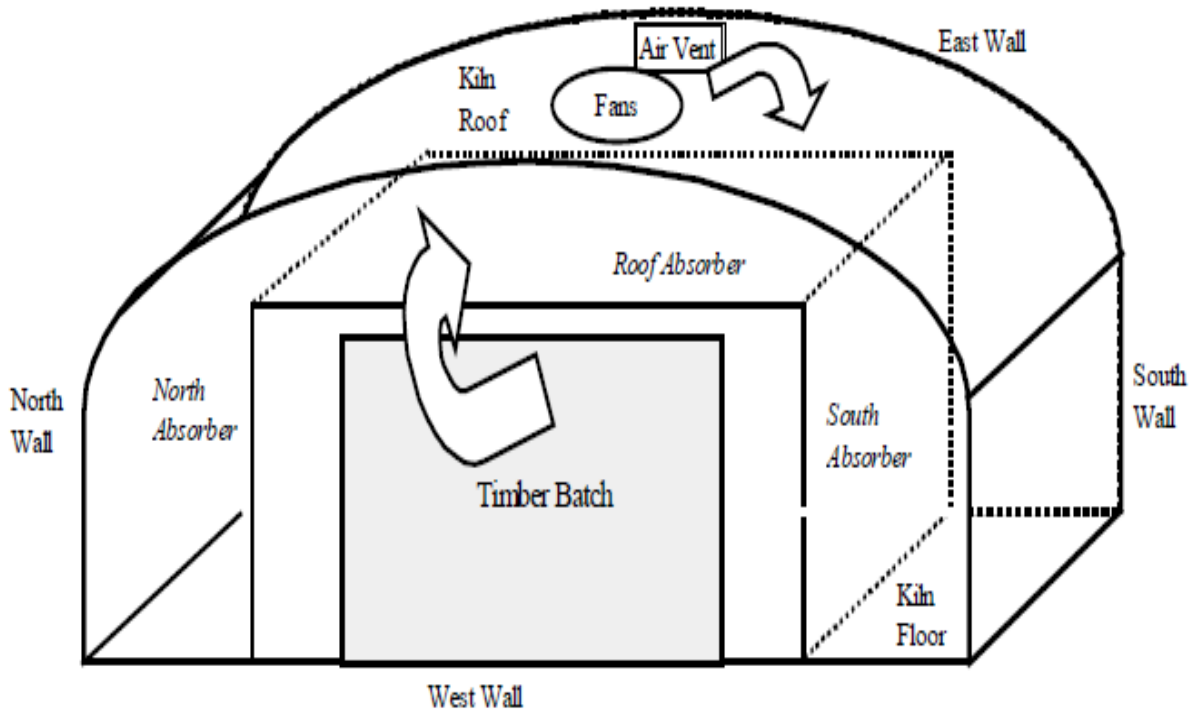
Figure 5.1. Schematic view of the Boral kiln (Haque and Langrish, 2003).

It should be noted from Figure 5.1 that the large curved roof (actual kiln view) of the Boral kiln creates some complexity in the analysis. Thus, adjusted dimensions for the Boral kiln were used in the simulation, assuming that the kiln could be fairly represented by a rectangular prism of identical volume. This assumption of treating the Boral kiln design as a rectangular prism of identical volume was tested and validated successfully in Haque (2002) and Haque and Langrish (2003). The resulting adjusted dimensions are shown in Figure 5.2.

East-west elevation

North-south elevation
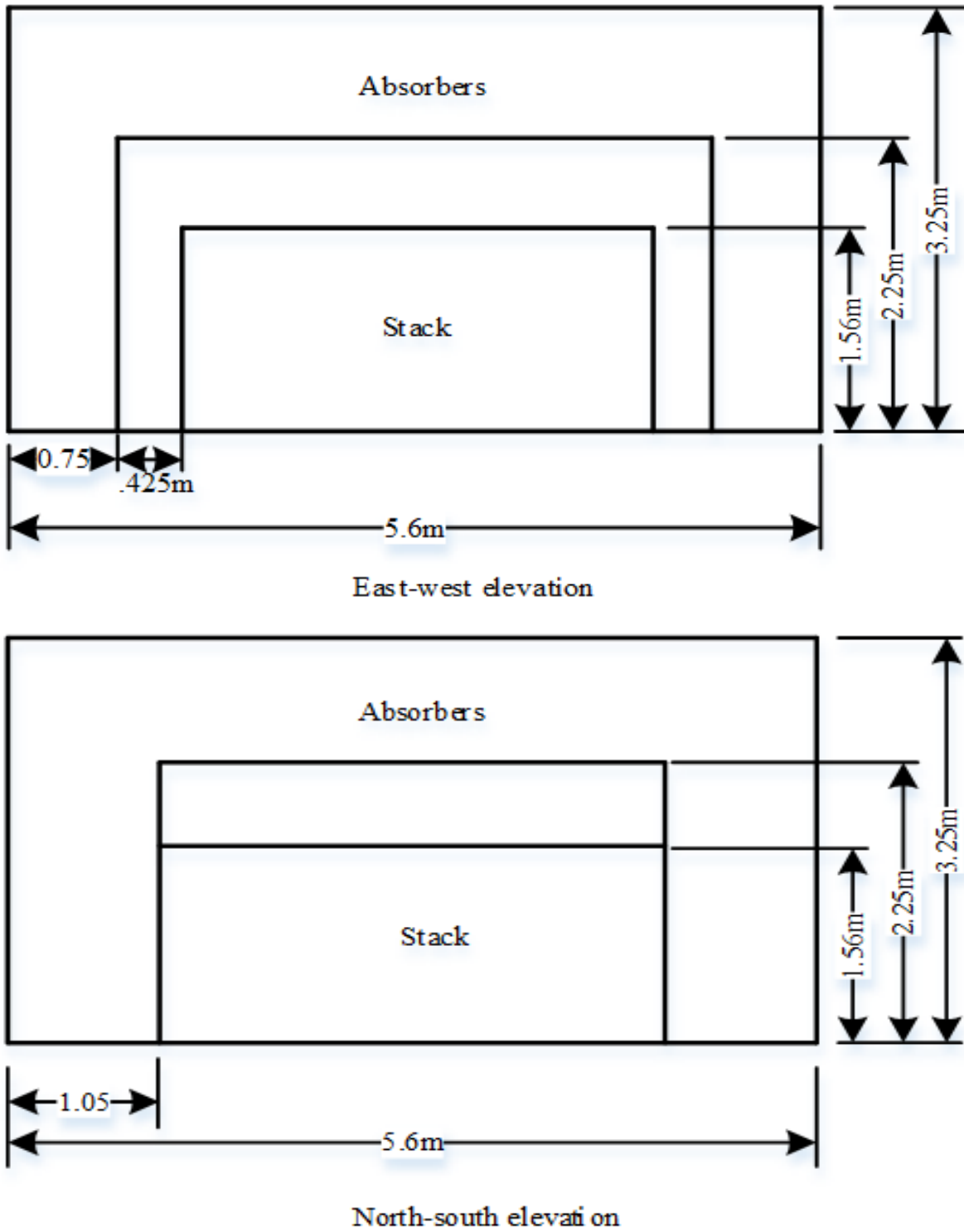
Figure 5.2. The scaled-down dimensions of the Boral kiln.

5.2.3 Key features used in the simulation

The key features for the Oxford and the scaled-down Boral kilns used in the simulation for this comparative study are given in Table 5.1.

Table 5.1. Key features used in the simulations for the Oxford and Boral kilns.

Parameters	Oxford design	Boral design (scaled-down)
Timber species	Blackbutt (*Eucalyptus pilularis*)	Blackbutt (*Eucalyptus pilularis*)
Board thickness (m)	0.025	0.025
Sticker thickness (m)	0.02	0.02
Board length (m)	4.88	3.5
Total width of boards (m)	2	3.25
Number of board layers	41	35
U_{stack} (during active/natural drying) (m/s)	0.50/0.05	1/0.05
h_f (during active/natural drying) (W/m^2/K)	4.80/2.40	5.40/2.40

Table 5.1 shows the major stack dimensions used in this study, including the lengths and total width of the boards, thicknesses of the boards and stickers, and the total number of board layers for the two designs being studied here. The stack velocities (U_{stack}) during the active (day) and natural (night) drying periods, together with the corresponding heat transfer coefficients (h_f) between the circulating air and timber boards are also shown in Table 5.1. It is apparent from Table 5.1 that, while the board and sticker thicknesses are the same for the two designs, the length and width of the stack, together with the number of board layers are different. This difference in the stack dimensions between the kiln designs

is unavoidable as long as the kilns are of different designs – a point where the reference functional unit becomes relevant. It should be noted here that, as the circulating air travels across the stack of timber, it becomes gradually more humid and cooler. These variations in the temperature and moisture content have been accommodated in the main model through a stack-wide model, which predicts the temperature and moisture content at different positions across the timber stack. This stack-wide model was constructed based on the unsteady-state mass (for humidity variation) and energy (for temperature variation) balances. The study was carried out with the scaled-down Boral kiln, and the actual stack velocity (1 m/s) for the Boral kiln was used in the simulation. Thus, the stack velocities during the active drying periods were 0.5 m/s and 1 m/s for the Oxford and Boral kilns, respectively, and the corresponding heat transfer coefficients (h_f) were 4.80 W/m²/K and 5.40 W/m²/K, respectively. During the relaxation drying periods (natural drying), the stack velocity for both the kilns was 0.05 m/s while the corresponding heat transfer coefficient (h_f) was 2.40 W/m²/K. The heat transfer coefficients, as given in Table 5.1, are generally correlated with the Nusselt number, Nu_l, in the following form:

$$Nu_l = f(R_{el}, R_{al}, P_r) \qquad (5.6)$$

where,

$$Nu_l = \frac{hl}{k_G}, R_{el} = \frac{\rho_G U l}{\mu_G}, R_{al} = \frac{g.\beta.\Delta T.l^3.\rho_{G.}^2 C_{pG}}{k_G.\mu_G}, P_r = \frac{C_{pG.}.\mu_G}{k_G} \qquad (5.7)$$

In Equations (5.6)-(5.7), $R_{el}, R_{al}, and\ P_r$ are the Reynolds, the Rayleigh, and the Prandtl numbers, respectively. The physical properties of the air, namely the thermal conductivity

(W m^{-1} K^{-1}), the density (kg m^{-3}), the dynamic viscosity (kg m^{-1} s^{-1}), the thermal expansion coefficient (m m^{-1} K^{-1}), and the specific heat capacity (J kg^{-1} K^{-1}) have been represented by the symbols $k_G, \rho_G, \mu_G, \beta,$ and C_{pG}, respectively. The acceleration due to gravity (m s^{-2}) and the characteristic length of the surface (m) are represented by g and l, respectively. The three different heat transfer coefficients, as included in in Table 5.1, corresponding to the three different stack velocities have been calculated using Equations (5.6)-(5.7). As an example, a sample calculation for determining the heat-transfer coefficient corresponding to the stack velocity of 0.05 m s^{-1} is given as follows:

The first dimensionless number to be determined for calculating the heat-transfer coefficient is the Reynolds number, which involves the characteristic length of the timber board (l) = 0.2 m (the board was assumed to be a flat board of width 200 mm), the standard air density (ρ_G) = 1.2 kg m^{-3}, and the standard dynamic viscosity (μ_G) = 1.8 x 10^{-5} kg m^{-1} s^{-1}.

Using these dimension and standard air properties, the Reynolds number for a stack velocity of 0.05 m s^{-1} can be calculated as follows:

$$R_{el} = \frac{\rho_G U l}{\mu_G} = \frac{1.2 * 0.05 * 0.2}{1.8 * 10^{-5}} = 667 \tag{5.8}$$

Since the correlations for the Nusselt number depend on whether the heat transfer is occurring by natural convection or by forced convection, it is necessary to identify the mode of convection heat transfer first. The relative magnitudes of dimensionless groups, called the Grashof number (G_r), and the Reynolds number (R_{el}) can be used to determine whether the heat transfer is occurring by forced convection or by natural convection (Incropera and

DeWitt, 2002; Shires et al., 1994). In general, free (or natural) convection may be negligible if the square of the Reynolds number is significantly larger than the Grashof number (i.e. $G_r/R_{el}^2 \ll 1$) and, conversely, forced convection may be negligible if the square of the Reynolds number is significantly smaller than the Grashof number (i.e. $G_r/R_{el}^2 \gg 1$). When the numbers are of similar magnitude (i.e. $G_r/R_{el}^2 \sim= 1$), combined effects of forced and the natural convection have to be taken into consideration (Bejan, 2004; Incropera and DeWitt, 2002). The Grashof number can be calculated as follows (Incropera and DeWitt, 2002; Shires et al., 1994):

$$G_r = \frac{g * \beta * \Delta T * l^3 * \rho_G^2}{\mu_G{}^2} = \frac{9.8 * 3.2 * 10 * 0.2^3 * 1.2^2}{(1.8 * 10^{-5})^2} = 5.5 * 10^6 \qquad (5.9)$$

Since $G_r/R_{el}^2 = (5.5*10^6)/ (667)^2 = 12.5 \gg 1$, the heat transfer is occurring by natural convection. The correlation for the Nusselt number also depends on whether the flow is laminar or turbulent. For natural convection, as in this case, the Rayleigh number, which is the product of Grashop and Prandtl number, is a good indication of whether the natural convection boundary layer is laminar or turbulent, with the transition from laminar to turbulent taking place at $R_{al} \sim 10^9$ (Incropera and DeWitt, 2002; Shires et al., 1994). The Rayleigh number can be calculated as follows:

$$R_{al} = G_r * P_r = (5.5 * 10^6) * \frac{1.005 * 10^3 * 1.8 * 10^{-5}}{.0285} = 3.49 * 10^6 \qquad (5.10)$$

Since R_{al} is less than 10^9, the flow is laminar, and thus the corresponding Nusselt number correlation for the upper surface of the board or the lower surface can be given as (Bejan, 2004; Incropera and DeWitt, 2002):

$$Nu_l = 0.54 * R_{al}^{\frac{1}{4}} = 16.85 \qquad\qquad (10^4 \leq R_{al} \leq 10^7) \qquad\qquad (5.11)$$

From Equation (5.11), the heat-transfer coefficient can be calculated as follows:

$$h = \frac{Nu_l * k_G}{l} = 2.40 \ W/m^2/K \tag{5.12}$$

It should be noted here that, in Equations (*5.8*)-(*5.12*), the physical properties of the air, namely the thermal conductivity (k_G), the density (ρ_G), the dynamic viscosity (μ_G), the thermal expansion coefficient (β), and the specific heat capacity (C_{pG}) have been evaluated at the film temperature, which is taken to be equal to the the average of the surface temperature and the bulk air temperature. All the correlations used for calculating the other heat-transfer coefficients have been given in Appendix 5A.

The main goal of this chapter was the implementation of the simulation processes for the two different kiln designs, so an analysis of other parameters associated with the drying processes, such as the humidity and venting control strategies, has been excluded in this study. The description of these processes was fully given in Chapter 4 and have been maintained in this chapter. Two four bladed axial fans powered by 0.25 hp electric motors were used for both the kilns, which was sufficient to provide a stack velocity of up to 1 m/s during the active drying (day time) period. A detailed discussion regarding the fans used for

the kilns has not been done, because the simulation was done for the same stack velocity with both the kilns, as shown in Table 5.1. Also the thermal and solar radiation properties used in the simulation, as shown in Table 5.2, for different components of the two kilns were assumed to be the same, so that the relative performance could be predicted, even though they used materials with the same heat-transfer properties.

Table 5.2. Thermal and radiation properties used in the simulation for different elements of the kilns (Haque, 2002).

Components	Properties	Solar radiation properties (solar radiation)	Thermal radiation properties (infrared radiation)
Walls and roofs	Absorptivity	0.08	-
Walls and roofs	Transmissivity	0.84	0.06
Walls and roofs	Emissivity	-	0.91
Walls and roofs	Reflectivity	-	0.03
Absorbers	Absorptivity	1	-
Absorbers	Emissivity	-	1
Absorbers	Reflectivity	0	0
Stack	Absorptivity	1	-

5.2.4 Drying and energy flow models

The drying model for the stack timber was based on Fick's law of diffusion for mass transfer, and Fourier's law for heat transfer. These heat and mass transport equations were solved simultaneously in the simulation program, as they formed a coupled system of differential equations within the drying model. Since the description of these fundamental equations for drying model has been given in Chapter 4, they will not be repeated here again. Thus, the discussion in connection with the basic drying equations has been excluded from this chapter. For the energy flow model, the mass and energy balances for the circulating air and the kiln components, respectively, were performed by applying unsteady-state balances:

rate of accumulation = flow rate in - flow rate out = net energy/mass flow rate. A detailed

description of these rate equations, as used in this comparative simulation study, has been

given in Chapter 4.

5.3   Results and Discussion

The results and discussion of this comparative study are given in the following sections.

5.3.5 Comparative drying time and timber quality

The numerical prediction of the drying rates for the hardwood timber and the corresponding

timber qualities for the Oxford and Boral kiln designs are shown in Figure 5.3 and 5.4,

respectively.
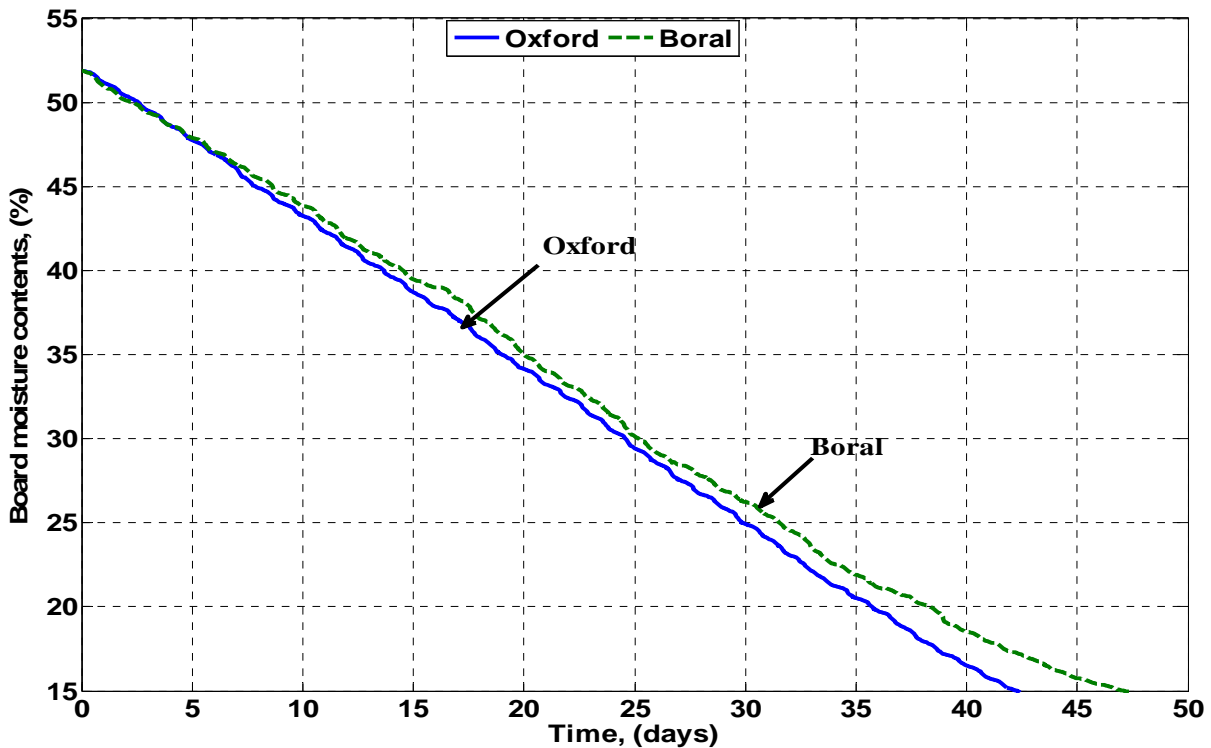
Figure 5.3. The predicted drying rates for the Oxford and the scaled Boral kilns during

drying to the final MCs of 15% by using the climatic conditions of spring season, 2013.

Figure 5.3 shows the predicted drying times (days) for the Oxford and Boral kilns in the season of spring, 2013, in Brisbane, Australia for drying timber to the same final MC of 15% (dry basis) in both kilns. The drying times for the Oxford and Boral kilns have been predicted to be approximately 42 days and 47 days, respectively, as shown in Figure 5.3. This shorter predicted drying time for the Oxford kiln is probably mainly due to the differences in the collected heat between the kilns, which were likely due to the differences in the solar collector areas and their orientations with respect to the sun. The scaled Boral kiln has 11 m² of absorber (horizontal) facing the sky and a combined area of 14 m² of absorbers (perpendicular) facing to the north and south. By contrast, the Oxford kiln has 25.7 m² of absorbers facing the sky (either horizontal or slightly inclined, Figure 5.1). Due to the vertical orientation of the north and south absorbers in the Boral kiln, the areas of the absorbers seem to be used less effectively to collect the solar radiation. This situation is reflected in the results given in Table 5.4, where the predicted solar gain over 42 days for the Oxford kiln and 47 days for the Boral kilns were 28 GJ (0.67 GJ/day) and 26 GJ (0.55 GJ/day), respectively. It is noticed from Figure 5.3 that the moisture removal rate in the Boral kiln decreases more significantly than in the Oxford kiln towards the later stage of the drying period, especially when the moisture content falls below the FSP. This situation further indicates the drying process is less effective in the Boral kiln compared with the Oxford kiln. The key reason for this is that, with lower and lower level of moisture content, more and more energy is required to evaporate per unit mass of water from the timber during drying. The Boral kiln appears to have difficulty in providing this energy at lower moisture-content level, as shown in Figure 5.3.
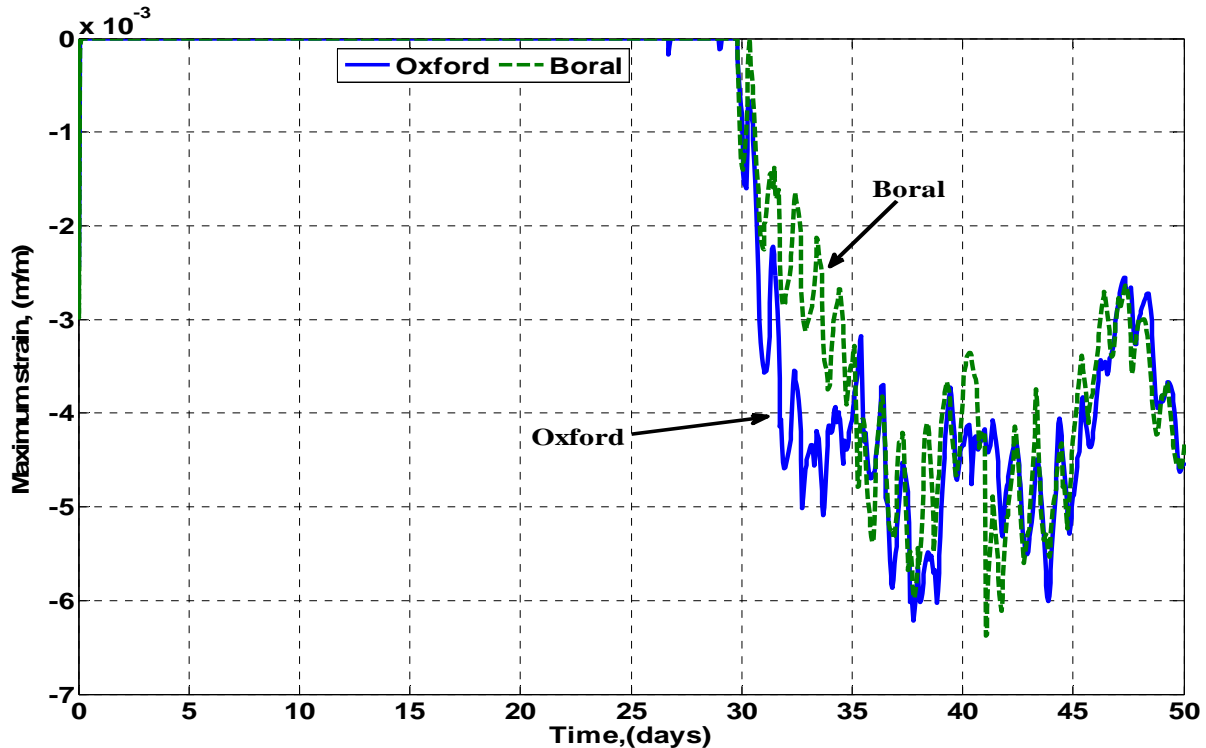
Figure 5.4. The predicted maximum strains developed within the boards during drying, as functions of time, for the Oxford and the scaled Boral kilns.

Moreover, the total calculated volume of the scaled Boral kiln (101 m^3) was greater than that of the Oxford kiln (58 m^3). The larger dimensions of the Boral kiln appeared to result in larger thermal masses of both the internal air (for the same load capacity) and the kiln structures in the Boral kiln, which further means that more energy would be required to raise the temperature of the kiln internal conditions by 1K. This condition is likely to lower the kiln air temperature "and/or" the board temperature (Table 5.3), which in turn would decrease the diffusion coefficient for the moisture transport within the boards. This situation in the Boral kiln (lower diffusion coefficient within the boards) has led to slower drying rates in this Boral design.

It is interesting to note that the difference in the drying times (days) between the two kilns has been predicted to be negligible (0.2% or less) on or before the fibre saturation point (FSP), which is approximately 30% moisture content (dry basis), while this difference was predicted to be approximately 10% towards the end of the drying period, as shown in Figure 5.3. This situation probably occurred because additional heat is required in order to remove the moisture from the wood while drying below the FSP. However, the difference in the final drying times (10%) between the two designs is not very large, especially in the drying time range of (0 – 47) days. This relatively small difference in the drying rates, in part, corresponds to the thermal masses of the kiln air and the kiln structure being significantly less than the thermal masses of the wood stack. The thermal mass ($m*C_p$) measures the amount of energy (J K^{-1}) stored in a particular component if its temperature is raised by 1K. Since the thermal mass of the wood stack (corresponding to 10 m^3 of wood) is expected to be significantly higher (usually by 2 or more order of magnitudes) than those for the other kiln components, most of the heat entering into the kilns is stored by the timber stack itself. This situation implies that the contribution of the differences in thermal masses due to dimensions and/or construction materials between kiln designs to the difference in the drying times is not significant as long as the load volume is the same. Different kiln designs, as here, cause differences in energy flows. These differences in energy flows cause the observed differences in drying times, and this work has quantified these differences in drying times.

Regarding the quality of the timber, no significant difference has been predicted in terms of the developed strains during the drying of hardwood timber between these two different designs, as shown in Figure 5.4. In both cases, no strains experienced by the boards were

105

predicted on or before 30 days of drying, as can be seen from Figure 5.4. This situation was the case mainly because, before 30 days, the MCs within the boards were above the FSP (approximately 30% MCs, dry basis) during which only free water was removed from the wood cell cavities.

5.3.6 Energy losses through convection and radiation

The predicted convection and radiation losses from the two different solar kilns (Oxford and Boral), if they were used in the spring season, 2013, in Brisbane, Australia, are shown in Figure 5.5 and 5.6, respectively.
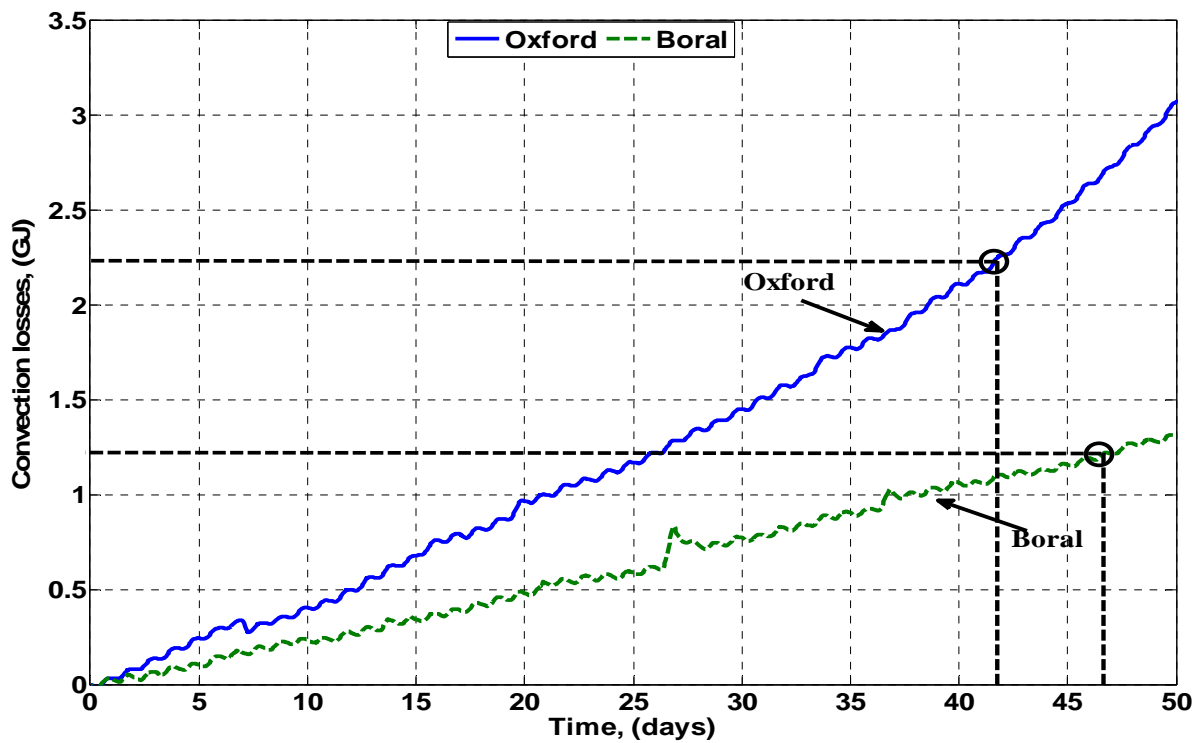
Figure 5.5. The predicted convection losses, as functions of time, for the Oxford and Boral solar kilns.

For the scaled-down Boral kiln, the total surface areas involved in the convection losses were calculated to be 99 m² (areas of the roof and the walls), which are greater than those for the Oxford kiln, where this value was 70 m² (the area of the roofs and the walls). Higher convection losses from the scaled-down Boral kiln were thus expected. However, this was not the case predicted here, as shown in Figure 5.5, even though the Boral kiln was predicted to take five days more than the Oxford kiln in order to achieve the final MC of 15% (dry basis).
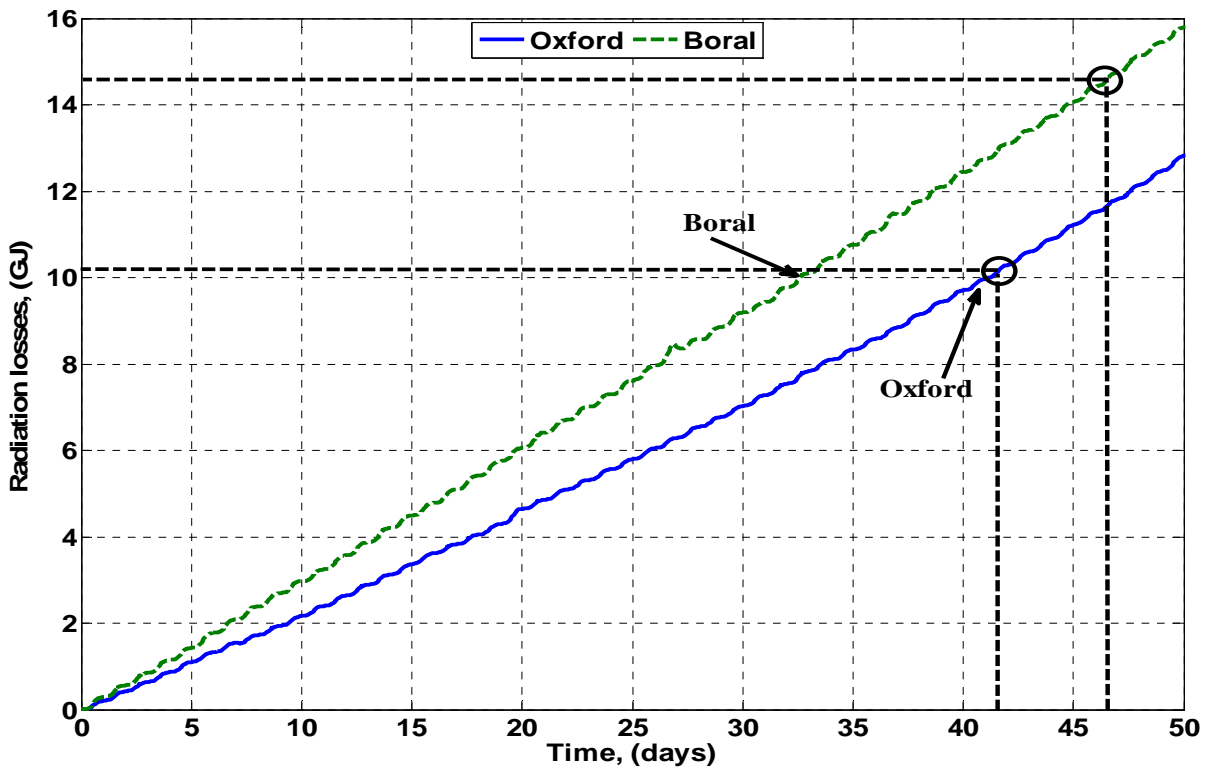
Figure 5.6. The predicted radiation losses, as functions of time, for the Oxford and Boral solar kilns.

This result may have occurred because the predicted average temperatures of the Boral kiln components (roof and walls) were lower than those of the Oxford kiln, as shown in Table 5.3.

Table 5.3. The predicted average temperatures of important kiln components.

Design	*Tboard*	*Tair*	*Twalls*	*Tna*	*Tsa*	*Tnr*	*Tsr*	*Tr*	*Tra*
	(K)	(K)	(K)	(K)	(K)	(K)	(K)	(K)	(K)
Oxford	298	297	295	299	307	298	302	-	-
Boral	297	296	294	296	294	-	-	296	303

As a result, the temperature difference terms ($Ts - Ta$) in the calculation of the convection losses became smaller (fraction or negative during the night) for the Boral kiln than for the Oxford kiln, resulting in lower convection losses in the former kiln despite a larger surface area participating in the energy transfers. By contrast, the sizes of the radiation losses for the Boral kiln were predicted to be larger than those for the Oxford kiln, as shown in Figure 5.6. One of the reasons for this result may be that most of the kiln surfaces radiate energy to an effective sky temperature that is always less than the ambient temperature, making the outward radiation energy transfers positive (losses). This situation is different to the calculation of the convective heat losses, where the pairs of temperatures are the kiln surfaces and the ambient temperatures. The total thermal radiation areas involved in the long-wave radiation energy transfers, corresponding to radiation losses, are greater in the scaled-down Boral kiln (approx. 169 m^2) than those in the Oxford kiln (approx. 102 m^2), which further causes greater radiation losses in the Boral kiln design. The differences between the convection and thermal radiation surfaces (70 and 102 m^2 for the Oxford, and 99 and 169 m^2 for the Boral kilns, respectively) were mainly due to the differences in the

thermal pathways between the convection and radiation heat flows. The equation for the energy flow rates of each component was formulated according to the thermal pathways [see Figures 4.9 to 4.11 in Haque (2002)] for the convection and radiation heat flows of the particular component. For the convection heat transfers, only the roof and wall surfaces of the kilns were involved (the surfaces in contact with the ambient conditions) while the thermal radiation heat transfers (long-wave/ infrared radiation) occurred between other surfaces, such as, stack to absorber, absorbers to sky, absorbers to ambient, absorbers to walls, absorbers to roofs, roofs to sky [depending upon the thermal pathways, Figures 4.9 to 4.11 in Haque (2002)]. In the calculation of radiation surface areas, view factors were considered for the surfaces that were not oriented parallel to each other.

In addition to the greater thermal radiation areas, as mentioned before, the larger thermal masses of the internal air and the kiln structures for the Boral kiln (for the same load capacity) may cause more energy to be stored during the sunlight hours (day time), which is later (during night time) released as long-wave radiation through the kiln surfaces, whose temperatures are mostly above both the ambient and the effective sky temperatures.

From Table 5.3, it also should be noted that, for the Oxford kiln, the predicted average temperature of the south absorber is higher than that predicted for the north absorber. This result is interesting because the total solar gain through the north absorber was predicted to be greater (11.4 GJ) than that predicted for the south absorber (10.2 GJ), as shown in Table 5.4. A possible reason for this situation is that the design of the Oxford kiln resulted in a higher velocity (1.61 m/s) over the sloping panel (north absorber) than the velocity (0.56 m/s) used for the horizontal panel (south absorber). This greater velocity appeared to cause

a correspondingly larger heat-transfer coefficient for the north absorber (greater amount of heat transferred from the north absorber to the circulating air), which in turn lowered the north panel temperature. This finding is comparable with the earlier experimental study of Langrish et al. (1993), which was carried out in the northern hemisphere.

Table 5.4. Major energy gains and losses over 42 days for the Oxford and 47 days for the Boral kilns (based on climatic data of spring season, 2013 in Brisbane and for drying from initial MC of 53% (dry basis) to the final MC of 15% (dry basis) in both kilns).

Parameters	Oxford kiln	Boral kiln
Solar gain (north absorber) (GJ)	11.4	2.1
Solar gain (south absorber) (GJ)	10.2	0.70
Solar gains (roof absorber) (GJ)	-	13.50
Total solar gain (including the energy transferred into the kiln through the other surfaces of the kilns) (GJ)	28	26
Convection losses (GJ)	2.7	1.10
Radiation losses (GJ)	10.10	14.50
Convection and radiation losses (% of the incoming solar energy)	45	60
Approximate energy consumed to evaporate water (% of the incoming solar energy)	30	25

Table 5.4 summarizes the important energy gains and the shares of the different losses in terms of the percentages of the total incoming solar energy. The results show that the total solar gain for the Oxford kiln is about 7% higher than that for the Boral kiln. Possible reasons

for this difference were discussed before. However, the contribution to the energy losses (as a percentage of the incoming solar energy) by convection and the radiation was found to be 25% higher for the Boral kiln than that for the Oxford kiln, as shown in Table 5.4. This situation may indicate that much of the input energy for the Boral kiln leaves without effectively drying the wood stack, resulting in slower drying in this kiln. One of the reasons for this may be that, while the same stack velocities (across the stack) were used in the simulation for both the kilns, the velocity distribution outside the timber stack for the two different designs resulted in different velocities in different sections (sections between roof and absorbers, and between walls and absorbers etc.) based on the different cross-sectional areas. Most of these cross-sectional areas for the Boral kiln were appeared to be larger than those for the Oxford kiln, as also appeared from Figure 5.1 and 5.2. These greater cross-sectional areas for the Boral kiln resulted in lower circulating air velocities over the different surfaces (hotter surfaces) in the Boral kiln, as shown in Table 5.5. This condition may have caused a lower heat-transfer coefficient between the air and the kiln surfaces.

Table 5.5. The velocities (m/s) used in the simulation for different components of the two kilns.

Components	Oxford kiln	Boral kiln
Walls	0.38	0.4
Floor	0.30	0.25
North absorber	1.61	0.28
South absorber	0.56	0.28
North roof/ roof absorber	1.61	0.56
South roof/ Roof	0.56	0.56

In summary, the total predicted losses (convection and radiation) for the Boral kiln were 15.6 GJ, which are greater than the losses predicted for the Oxford kiln (12.8 GJ). It should be noted that the total predicted losses for both the kilns included in this study are of same order of magnitude. This is probably again due to the insignificant amount of energy stored in the kiln air and in the kiln external structure, hence leading to the small differences in the energy losses between the two designs while the load volume was kept constant. Therefore, comparing the performance of different kiln designs for the drying of hardwood, on the basis of the reference functional unit used in this study, may be a reasonable method for a wide range of weather conditions and geographical locations.

5.3.7 Important kiln features with different seasonal conditions

In order to assess the kiln performance with varying seasonal conditions for Brisbane in Australia, some of the important parameters from the simulation have been summarized in Table 5.6.

Table 5.6 summarizes the effects of seasonal varying climatic conditions on the performances of the two kilns in terms of the predicted differences within and between the kiln designs. It is shown in Table 5.6 that the predicted drying periods in summer for the Oxford and Boral kilns were 38 and 46 days (Oxford kiln 21% faster), respectively, and in winter these drying periods were 55 and 73 days (Oxford kiln 32% faster), respectively. The differences in the predicted drying times between these seasons (summer and winter) were found to be 44% and 58% (Table 5.6, difference within designs) for the Oxford and the Boral kilns, respectively. However, the drying-time variations between the designs were found to be 21% and 32% in summer and winter, respectively, as shown in Figure 5.6.

Table 5.6. Summary of the kiln performances with different seasonal conditions of Brisbane in the year of 2013 (drying for the final MC of 15%, dry basis).

Parameters	Summer		Spring		Winter		Difference within design[9] (%)		Difference between designs[10] (%)	
	Oxford	Boral	Oxford	Boral	Oxford	Boral	Oxford	Boral	Summer	Winter
Drying time (days)	38	46	42	47	55	73	+ 44	+ 58	+ 21	+ 32
Solar gain (GJ)	27	24.6	21.6	20	16.6	17.3	- 38	- 29	- 8	+ 4
Total losses (% of solar gain)	47	67	59	74	68	81	+ 44	+ 20	+ 42	+ 19
Ratio of radiation to convection losses	3.92	8.94	3.74	13.18	8.46	20	+ 115	+ 123	+ 128	+ 136
Energy consumed to evaporate water (% of solar gain)	32	29	30	23	27	12	- 15	- 58	- 9	- 55
Total heat (losses + evaporation) (% of solar gain)	79	96	89	97	95	93	+ 20	-3	+ 21	-2

[9] % difference within design = [(winter – summer)/(summer)]*100.
[10] % difference between designs = [(Boral – Oxford)/(Oxford)]*100.

This larger difference in the required time for drying timber to a certain MC (15%, dry basis) between designs, together with the absorber temperatures being appreciably higher than the temperatures of other surfaces (when compared with the corresponding temperatures for the Boral kiln) within the Oxford kiln (Table 5.3), may indicate that heat is transferred from the air to the timber stack more quickly in the Oxford kiln than in the Boral kiln. This

situation is likely to make the performance of Oxford design more sensitive to the varying boundary conditions (mainly input solar energy) than the Boral kiln.

Table 5.6 also shows that the difference in the predicted solar gains (through the collectors) between the summer and the winter for the Oxford design is 38% (greater in summer) while this difference was 29% (greater in summer) for the Boral kiln. It is interesting to note that in summer, despite 21% shorter drying time for the Oxford kiln, the predicted solar gain (over drying period of 38 days) for the Oxford design is 8% higher than that for the Boral kiln (over drying period of 46 days). This result indicates that it is necessary to improve the Boral kiln design in order to increase the solar gain. During winter, however, the total solar gain for the Boral kiln was predicted to be 4% higher than that for the Oxford kiln. This increase of total solar gain for the Boral kiln was partly due to an increased drying time (32% greater than Oxford kiln) for the Boral kiln during the winter season, as shown in Table 5.6. The differences in total losses (convection and radiation) between the seasons, when calculated as a percentage of the total incoming solar radiation, were predicted to be 44% and 20% for the Oxford and Boral kilns, respectively. However, for the Boral kiln, larger portions (67% and 81% in summer and winter, respectively) of the incoming solar energy were predicted to be lost by convection and radiation than those (47% and 68% in summer and winter, respectively) predicted for the Oxford kiln. This prediction is consistent with the earlier discussion included in the convection and the radiation losses section of this work.

It is also apparent from Table 5.6 that, in spring, heat losses by convection and radiation, together with the heat used for the evaporation of water (latent heat and the heat of sorption), accounted for about 89% of the total incoming solar energy for the Oxford kiln while their share for the Boral kiln was about 97%. These shares of losses are consistent with

those mentioned by Langrish et al. (1993), who experimentally found that the radiation and convection losses accounted for 91% (59% and 32%, respectively) of the total incoming solar energy, while Prins found (as mentioned by Langrish et al. (1993)) this value to be 78%. For the Oxford kiln, in summer, the ratio of the radiation to convection losses predicted here (approximately 4:1) is greater than that found by Langrish et al. (1993), where it was approximately 2:1. It was previously discussed in Chapter 4 that the difference in the radiation losses resulted from the use of different correlations for the calculation of the sky temperature. For the Boral kiln, this ratio of radiation to convection losses was increased from summer (9:1) to winter (20:1). Convection energy transfer through individual pathways (roofs and the walls), as predicted by this model, indicated that this increase (from summer to winter) in the ratio of radiation to convection losses is probably due to the very low convection heat losses (resulting from lower surface temperatures) from the Boral kiln during winter. The earlier study of Haque (2002) mentioned this ratio to be 20:1 for the full-scale Boral kiln (approximately double the dimensions used here), which is comparable with the current study (with scaled-down dimensions) except for the greater increase in winter.

5.4   Conclusions

A comparison of the predicted performance between the Oxford and Boral kilns has been made on the basis of a defined reference functional unit. The results have shown that the Oxford design is likely to produce faster drying rates (lower drying times required) and relatively smaller energy losses (by radiation and convection) than those for the Boral kiln. There were no significant differences predicted in the timber quality between the two designs. The Oxford design was also predicted to receive a relatively larger amount of solar energy (compared with the Boral kiln) for a given geographical location (here Brisbane in

Australia). In the spring season, the heat used for the evaporation of moisture was predicted to be about 25% of the incoming solar energy for the Boral kiln while this heat use for the Oxford kiln accounted for 30% of the input solar energy. The capability of the model of accommodating the seasonally varying boundary conditions has also been discussed. The predicted results for the different seasons of the year (summer, spring, and winter, 2013) have shown that the Oxford kiln is consistently better than the Boral kiln throughout the year in terms of the drying times, solar gains, and the major energy losses (convection and radiation). The individual performances of the solar kilns (Oxford and Boral) were predicted to vary with the seasons. The drying times were predicted to be the lowest in the summer and highest in the winter for both the kilns. Significant differences in the total energy losses (when calculated as percentages of incoming solar energy) between seasons have also been predicted for a given kiln design. From the overall discussion, it is clear that, for a given set of conditions (climatic, geographical, and operating), the Oxford kiln is likely to be better for the purpose of wood drying than the Boral kiln irrespective of the seasons. However, it is still necessary to carry out a more focused and detailed life cycle energy analysis by considering the embodied energy requirements for both the solar kilns (Oxford and Boral) in order to compare their life cycle benefits for the purpose of drying. In the next chapter, a detailed embodied energy and embodied carbon analysis of these two solar kilns are described.

Chapter 6   Embodied energy and embodied carbon analysis

6.1   Introduction

Building materials and components of any built facilities consume a large amount of energy during their life cycle stages of construction, use, and demolition. The total life-cycle energy use in a built facility consists of two components, namely the embodied energy (EE) and the operational energy (OE). Embodied energy is usually defined (Alwan and Jones, 2014; Sartori and Hestnes, 2007; Zaid and Paul, 2014) as the total amount of energy expended during the extraction of raw materials, the transport, manufacturing, construction, use (maintenance and renovation) and disposal phases, whereas operational energy is the energy required to operate (or generated by operating) the built facility in terms of processes such as space conditioning, lighting and operating other building appliances. Generally, OE has been found to make up a larger proportion of a building's total life-cycle energy compared with EE (Hegner, 2007). However, several studies, including Plank (2005), Sartori and Hestnes (2007), and Yung et al. (2013) have indicated that, with a growing number of energy efficient buildings, the fraction of the embodied energy forms an increasingly high proportion of the total life-cycle energy consumption in built facilities.

Over the past decade, there has been rising interest in reducing the total energy (EE and OE) consumption in built facilities in order to decrease the burdens on global climate change. In 2007, the United Nations Environment Program (UNEP) reported that, as mentioned by Ximenes and Grant (2013), the construction, operation, maintenance and demolition of the buildings sector worldwide contributed 40% of global GHG emissions. Zaid and Paul (2014)

mentioned that, in European Union (EU) countries, the building sector accounted for approximately 40-50% of the total energy consumption in 2001. They also highlighted a number of measures and targets that have been introduced globally, including various fiscal and regulatory instruments to tackle climate change and move towards low and zero carbon buildings.

However, these approaches have largely focused on the operational energy consumption of built facilities, particularly heating, lighting and services. As mentioned before, the relative proportion of EE in the total life-cycle energy is increasing, because more energy-efficient buildings are being built. Furthermore, a relationship between the energy use in built facilities and greenhouse gas emissions was pointed out by Dixit et al. (2010), where the environmental significance of embodied energy was highlighted. This situation implies that it is important to assess the EE of a facility, which is either an energy-efficient utility or mostly dependent on renewable energy sources, so that it can be evaluated in environmental quality terms. A solar dryer for wood drying is one such type of facility, where most of the energy used for drying the wood is captured from the sun. Thus, the relative importance of embodied energy analysis for solar kilns may be compared with the operational energy requirement in a way that is consistent with other energy-efficient building facilities, mainly because the majority of the operational energy (i.e. energy required for timber drying) for solar kilns comes from a renewable source (e.g. the sun). The description of the operational performance for the two kilns (Oxford and Boral) by numerical simulation has been given in Chapter 5. The assessment of EE and EC is an important part of the total energy consumption and GHG emissions for an overall processing unit with dried timber. In order to assess the life cycle embodied impacts (i.e. EEs and ECs), it is necessary to calculate the energy

consumption and carbon emissions associated with the extraction and production of raw materials, the transportation of materials to the construction site, the transportation of the wastes to the waste-disposal points, and the waste-treatment plants. In order to assess all these components of EEs and ECs, and since there seems to be no or little information in the literature regarding the assessment of embodied impacts (i.e. EEs and ECs) for solar kilns, a life cycle assessment (LCA) model for the materials used in the construction and maintenance of the two kilns was built in this chapter by using "SimaPro" software, which was one of the major aims of this chapter.

However, the overall objective of this chapter was to define and build a LCA model, and consequently to use this model to assess the EEs and ECs for the construction and maintenance of the two solar kilns. It should be noted that, in the assessment of EE and EC by a life cycle assessment (LCA) study, it is rare that one single value for a particular product/facility can be universally agreed upon by researchers. Due to the large variations in the specified system boundaries from study to study, and the economy and technology variations from country to country, the results from a LCA study are not usually designed for comparison with other studies, as mentioned by Hammond and Jones (2008). It was also stated in Dixit et al. (2012) that most of the currently used methods for assessing the EE differ in their collection of material and energy input data, thus resulting in a considerable variation in the EE values. Thus, the assessment of the EE and EC have been carried out in this chapter with a defined system boundary (Section 6.3.3), which is also a requirement for any LCA study in accordance of ISO 14044 guidelines.

6.2   Construction details of the two kilns

The basic descriptions of the Oxford and Boral kilns have been given in Chapters 4 and 5, respectively. Since the embodied energy analysis of the kilns involves the quantity surveying of the equipment, the construction details of the kilns have been described in the following sections while the detailed breakdowns of the components have been given in appendices 6A and 6B.
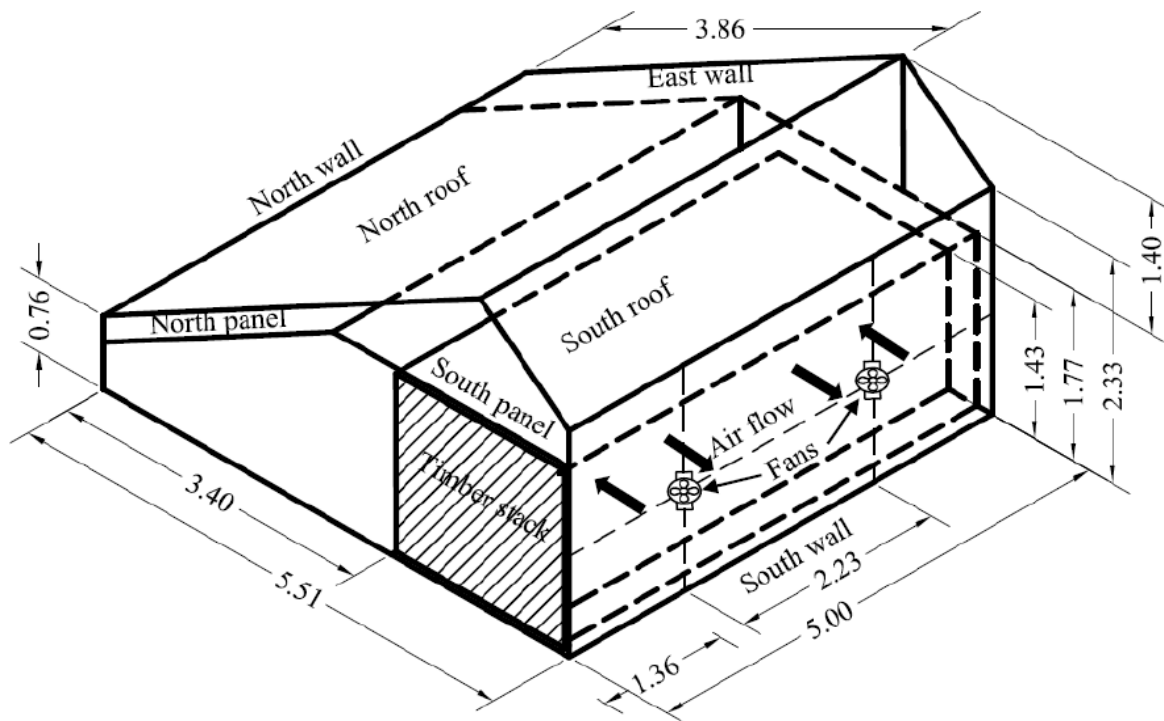
Figure 6.1. Fan and loading arrangements for the Oxford solar kiln [dimensions are in metres and extracted from Haque (2002)].

The key difference between the two kilns is that the Oxford kiln has two absorbers, with one being horizontal (the south panel) and the other one being inclined (the north panel), whereas the Boral kiln has three absorbers, with two being vertically orientated (the north

and south panels) and the other one being horizontal, as shown in Figures 6.1 and 6.2. Furthermore, the Oxford kiln is a wooden- framed structure, while the Boral kiln is a tunnel-like aluminium structure.
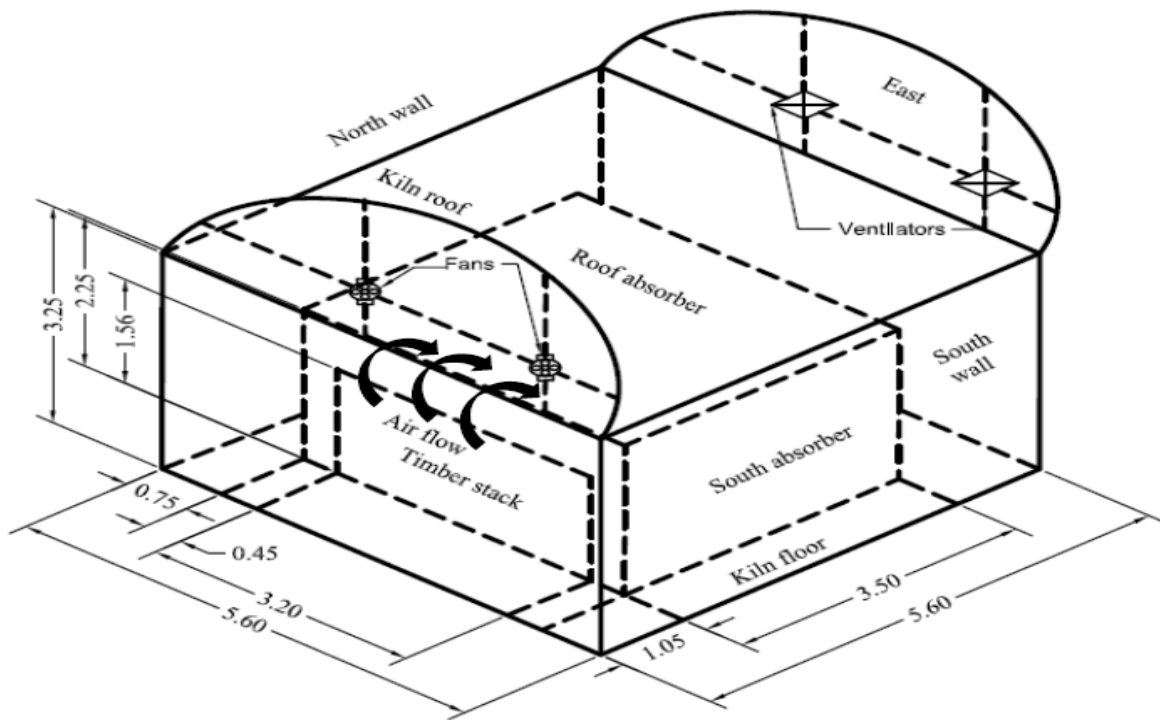
Figure 6.2. Fan and loading arrangements for the scaled-down Boral solar kiln

[dimensions are in metres and extracted from Haque (2002)].

For both the kilns, two fans driven by 0.25 hp electric motors were assumed to be installed in the positions shown in Figures 6.1 and 6.2 in order to circulate the drying air. Due to the variation of the fan locations between the two kilns, the directions of the circulating air were

also different between the two kilns – north/south in the Oxford kiln and east/west in the Boral kiln.

The Boral kiln was manufactured in Western Australia by Advanced Environmental Structures Pty Ltd. and supplied by Australian Design Hardwoods Pty Ltd, as mentioned by Haque (2002). LCA guidelines set out in ISO 14044 state that, for any comparative study, it is necessary to define a reference functional unit for the systems being compared. The reference functional unit for this study has been defined and presented in Section 6.3.2. Based on the defined reference unit, the original dimensions for the Boral kiln have been scaled down to give the same timber load capacity (i.e. 10 m³) as the Oxford kiln while not affecting the basic kiln design. The scaling procedure used for this study may be given in the following mathematical forms:

$$(Scaled\ linear\ dimension)_{Boral} = k * (Original\ linear\ dimension)_{Boral} \qquad (6.1)$$

$$(Scaled\ surface\ area)_{Boral} = k^2 * (Original\ surface\ area)_{Boral} \qquad (6.2)$$

$$(Scaled\ volume)_{Boral} = k^3 * (Original\ volume)_{Boral} \qquad (6.3)$$

$$Here, scale\ factor, k = \left[\frac{(Original\ stack\ volume)_{Oxford}}{(Original\ stack\ volume)_{Boral}}\right]^{\frac{1}{3}} \qquad (6.4)$$

Reviewing Equations (6.1) to (6.4) indicates that linear dimensions have been multiplied by the scale factor, k, while the areas and the volumes have been multiplied by k^2 and k^3, respectively. It should be noted that the kiln volumetric scaling factor has been the same as the stack volume scaling factor, meaning that the degree of scaling in all three dimensions has been consistent, which further helps to keep the original kiln design undistorted. This scaling method has also been described in Chapter 5. The resultant scaled-down dimensions, which have been used in this chapter, are shown in Figure 6.2. It shows that the stack-dimensions for the Boral kiln have been assumed to be 3.5 m long, 3.25 m wide and 1.56 m high, which also gave a stack capacity of 10 m^3 of timber, and this volume has been the same as the Oxford kiln with the same boards and sticker thicknesses. In this kiln, the glazing material (polycarbonate sheets) has been used for the walls and roofs, and has been supported by aluminium frames. The absorbers for the Boral kiln have been constructed from corrugated iron sheets (zinc coated), which have been painted matt black. The floors for both the kilns have been made of concrete.

6.3   Materials and methods

The materials and methods used in this chapter for the assessment of life cycle EE and EC of the solar kilns are described in the following sections.

6.3.1   Data sources and assessment software

The assessment of life cycle embodied energy (LCEE) and life cycle embodied carbon (LCEC) associated with the construction and maintenance for the two solar kilns has been carried out in this chapter by using the software "SimaPro 7.1.8 version" in accordance with ISO 14040/14044 guidelines on LCA. Since different geographical locations of the kilns can cause

considerable variations in the values of EE and other environmental impacts due to differences between various countries, this study has been carried out, as far as possible, from an Australian perspective. Two major data libraries, namely the Australian Life Cycle Inventory (AusLCI) library and the eco-invent library have been used, while the models have been analyzed by using the Australian Impact Method with Normalization including Cumulative Energy Demand (AIM-CED). AusLCI and AIM-CED have been chosen for this study because they are complimentary and include Australian region specific data, as mentioned in Australian Life Cycle Assessment Society (2009), Tharumaharajah and Grant (2006), and Newton et al. (2009). When data have not been available in AusLCI, the eco-invent database (developed by the Swiss Centre for Life Cycle Inventories) has been used after being adjusted for Australian electricity and transportation costs. This procedure has been followed in some previous studies, including Islam et al. (2014), Tharumaharajah and Grant (2006), and Henriksen (2006).

6.3.2   Functional units

The overall functional unit of this study has been to construct the two different solar kilns (Oxford and Boral) for wood drying with the same timber load capacity of 10 m³ and subsequent maintenance over an   assumed 20-year service life.

6.3.3   System boundaries

The system boundaries, i.e. what stages, processes, inputs and outputs have been included within the assessment, and what have been omitted, are given in Table 6.1.

Table 6.1 shows that the excluded elements from the system are the production of capital equipment, human labor, employee transport and food. Usually, these parameters are

excluded from the system boundary in life cycle assessment (LCA) study, mainly because they are assumed to contribute only a minor proportion to the total impact, as mentioned by PE International (2012). Since the final kiln-dried wood products are used in a broad range of applications (e.g. furniture, joinery, construction), it is difficult to specify their individual use and subsequently model their end of life (EoL) scenarios. Thus, the operational and EoL phases for the kiln-dried wood products have been excluded from this study. These phases would be added in design specific and end-use product specific studies so that a complete life cycle assessment can be done. However, the EoL phase for the kiln-construction materials, wherever applicable, has been included in the study.

Table 6.1. System boundaries for both the Oxford and Boral kilns – inclusions and exclusions.

Inclusions	Exclusions
Extraction and production of raw materials (including the associated emissions).	Construction of capital equipment.
Transportation of materials to the construction site.	Human labor, employee transport, and production of food for employees.
Transportation of the wastes (produced on site due to replacements and EoL) to the waste disposal point, and subsequently to the waste treatment plant.	The operational phase for the kilns.
Waste scenario (including the environmental benefits resulting from recycling and landfill processes).	EoL phase of the dried wood products.

6.3.4   Key impact indicators

The main goal of this chapter has been to assess the LCEE and the LCEC of the building materials for the solar kilns. Thus, the results have been discussed in terms of the LCEE (GJ) and GHG (t-CO_2-e), which are also indicators of primary interest for many sustainable systems in Australia (Grant and Peters, 2008). Other impact indicators, such as water usage, solid wastes, biodiversity, and land use, have not been discussed here, either because they are not very relevant to the context of the goal of this chapter or there is no agreed method of analyzing these indicators in quantitative terms (Bayart et al., 2010; Berger and Finkbeiner, 2013; Ximenes and Grant, 2013). For example, Berger and Finkbeiner (2013) mentioned that there is no agreed standard so far and even less consistency available in the LCA community on how to assess the impact of water use in a LCA framework. Similarly, the assessment of the biodiversity impact still requires a common metric that can be generally applied in LCA studies (Penman et al., 2010), and there is no mature technology available to assess the impact of industrial activity on biodiversity (PE International, 2012). Thus, these impact indicators have been excluded from the analysis of this study.

6.3.5   Key materials, their replacement schedules and EoL scenarios

While detailed material quantifications and descriptions have been given in appendices 6A and 6B, Table 6.2 contains the key materials used for the two kilns, the sources of data, the replacement schedules, the total quantities, and the Eol scenarios. The key materials used for the two kilns, as included in Table 6.2, were sourced from either the AusLCI database or the ecoinvent database available in the 7.1.8 version of SimaPro. Normally, copper chromium arsenic (CCA) treatment, a widely used wood treatment process in Australia, increases the service life of *Pinus radiata* for outdoor applications (e.g. posts) up to 30 years or more

(Forest & Wood Products, 2004). Since the treated structural timber (*Pinus radiata*) used in the frames for the Oxford kiln was exposed to a relatively aggressive environment (i.e. high heat and humid conditions) inside the kiln compared with many outdoor applications, the expected service life for the framing material was assumed to be 20 years or more.

Table 6.2. Summary of the key materials, their maintenance schedules, and EoL treatments for the two solar kilns (Oxford and Boral) with 10 m^3 of load capacity each over a service life of 20 years.

Kilns	Materials	Data source	Kiln components	Replacement schedules	Total amount (kg)	EoL treatment
Oxford	Timber	AusLCI data base	Frames	20 years plus	690	80% landfill, 20% incineration.
	Aluminium	AusLCI data base	Absorbers	20 years plus	500	n/a
	Poly-carbonate	Ecoinvent data base	Walls and roofs	10 years	1211	Landfill
	Concrete	AusLCI data base	Floor	Unlimited	6612	n/a
Boral	Aluminium	AusLCI data base	Frames	20 years plus	263	n/a
	Iron (tin-coated)	AusLCI data base	Absorbers	20 years plus	1537	n/a
	Poly-carbonate	Ecoinvent data base	Walls and roofs	10 years	2123	Landfill
	Concrete	AusLCI data base	Floor	Unlimited	7526	n/a

Thus, the framing materials were quantified without replacing them over the kiln service life of 20 years, as shown in Table 6.2. Because the manufacturers or the distributors normally give a 10-year limited written warranty for polycarbonate sheets (Sabic Innovative Plastics, 2008), they were assumed to be replaced every ten years. Mr. R. Burke (Director, Solar Dryers Australia) mentioned in an email (personal communication) on November 3, 2014 that, in constructing solar kilns, aluminium iron sheets (zinc coated) and concrete are normally assumed to have an unlimited life, or (at least) over twenty years. Thus, these materials were not assumed to be replaced over the kiln service life of twenty years, as shown in Table 6.2. The landfill process was modelled as the EoL scenario for the polycarbonate sheets. About 80% of the timber waste was assumed to be landfilled, while the remaining 20% was assumed to be incinerated. It should be note here that there are some environmental issues associated with the incineration and landfilling of chromated copper arsenate (CCA)-treated wood wastes. For example, Jambeck (2004) found that CCA-treated wood, when co-disposed with municipal solid waste, increased the arsenic and chromium concentrations in leachate. In addition, incineration of CCA-treated wood causes emissions of arsenic, and the resulting ash becomes concentrated with arsenic, copper and chromium, as mentioned by Solo-Gabriele et al. (2002). Another study (Song et al., 2006) found that, when CCA-treated wood was incinerated, the chromium can be oxidized into the more toxic and mobile form of chromium. However, assessing these environmental impacts associated with CCA-treated wood is a complex procedure and subject matter of an independent research. Thus, these issues have not been considered in the LCA model presented in this thesis.

In all of the EoL scenarios, the benefits either due to the avoidance of material production from the virgin feedstock, or due to energy generation (i.e. energy produced from methane (CH_4) in landfills reducing the electricity use generated from black coal), were included in the model. It should be noted that the materials used for the auxiliary components (i.e. for small fittings, fans, sprayers) were not included in this study, as they were not expected to give a significant difference between the designs.

6.4   Results and Discussion

The results for the Oxford and Boral kilns in terms of the LCEE and LCEC are discussed in the following sections.

6.4.1   Embodied energy share for the solar kilns

Figures 6.3 and 6.4 show the breakdowns, by components, of the total embodied energy over a service life of 20 years for the Oxford and Boral kilns, respectively.

Since the polycarbonate sheets used for the walls and roofs have been assumed to be replaced every ten years, this material was consumed in significant quantities for both the kilns (Table 6.2) over their entire service lives. As a result, the greatest share of the embodied energy (EE) came from the walls and roofs over a 20-year service life for both the Oxford and Boral kilns (51% and 65%, respectively), as shown in Figures 6.3 and 6.4.
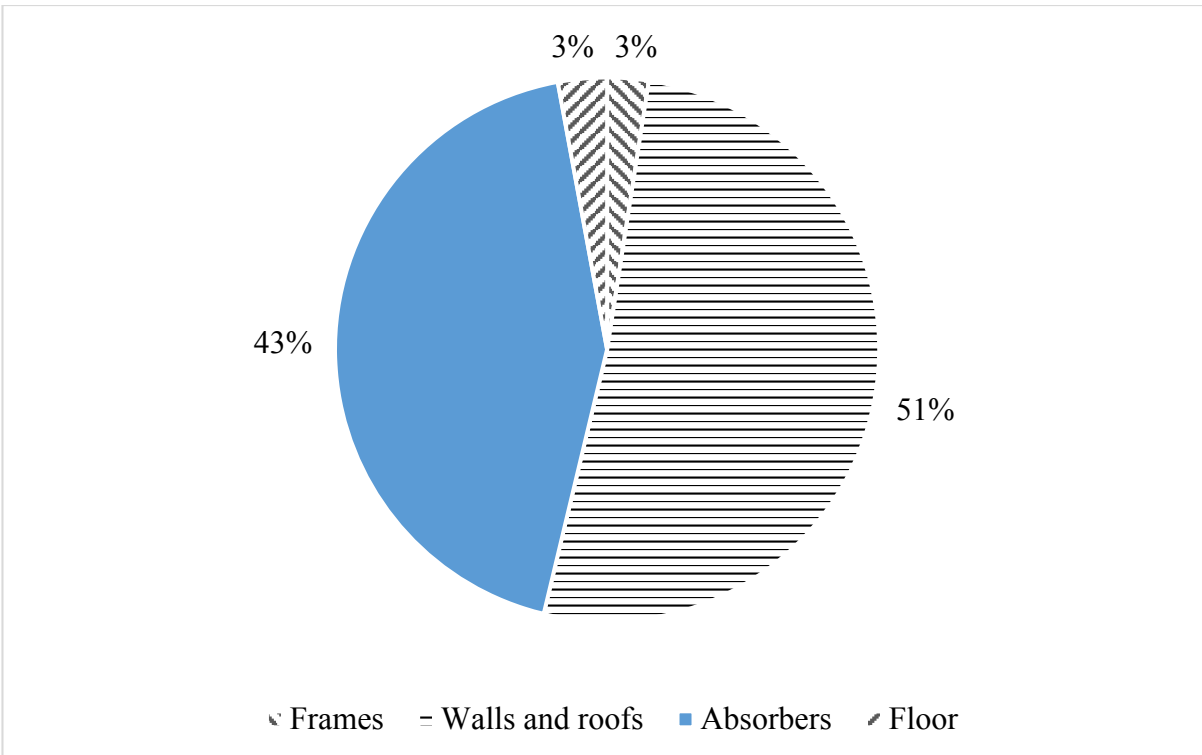
Figure 6.3. Embodied energy share, by component category, for the Oxford kiln, base case.

One of the possible reasons for the higher share from the walls and roofs for the Boral kiln than the Oxford kiln may include the relatively increased amounts of polycarbonate materials used and their subsequent replacements (at year 10) over the entire service life, which was likely to increase the EE share for the Boral kiln. It should be noted here that the embodied impacts (i.e. EE and EC) are quite sensitive to variations in the assumptions about replacing the polycarbonate walls and roofs. Thus, a sensitivity analysis, using different replacement schedules and different materials, has been included in this chapter (please see Section 6.4.6). The amounts of energy embodied in the absorbers for the Oxford and Boral kilns contributed 43% and 16%, respectively, to the corresponding total EE. These values indicate that the absorber material (aluminium) for the Oxford kiln has a higher embodied

energy than that (iron sheet) for the Boral kiln. This result is consistent with many other studies, including Falk (2009), Milne and Reardon (2013), and Hammond and Jones (2008), where aluminium was found to be the material with a higher embodied energy relative to other construction materials. A relatively large difference was found in this study between the percentages (for each kiln) of the total EE that came from the framing material (3% for the Oxford kiln, 17% for the Boral kiln).
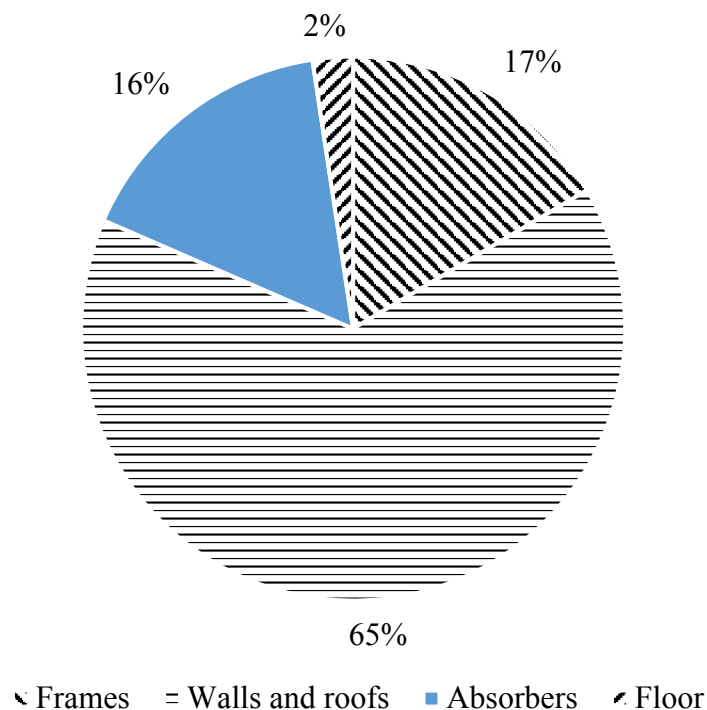
Figure 6.4. Embodied energy share, by component category, for the Boral kiln, base case.

This difference was due to the comparatively clean and low-energy manufacturing processes involved for wood manufacturing (Falk, 2009), which makes wood a very low embodied-energy material. An area of design improvement, in terms of EE for the Boral kiln, would therefore be the replacement of the aluminium frames with their wooden counterparts (timber frames). Because concrete is a low-embodied energy material and has a relatively

longer service life (no replacement requirement for this study), floors for both the kilns shared the smallest EE (less than or equal to 3% in each design).

6.4.2 Embodied energy and carbon by life cycle stages

The embodied energy and embodied carbon values for the two solar kilns (Oxford and Boral), by life-cycle stages, and their corresponding percentage contributions to the total impact values, are given in Table 6.3.

Table 6.3. Embodied energy and embodied carbon values for different life-cycle stages.

Kilns		Initial stage (Year 0)		Maintenance stage (Year 1-20)		Disposal stage (Year 20)	
		EE (GJ)	EC (t CO_2-e)	EE (GJ)	EC (t CO_2-e)	EE (GJ)	EC (t CO_2-e)
Oxford	Impact	180	14.2	62	3.65	1.71	-1.09
	% of total	73	79	25	20	2	-6
Boral	Impact	317	21.8	216	12.85	1.45	0.10
	% of total	59	62	40	36	0.27	0.29

Table 6.3 shows that the greatest energy consumption and carbon emission occurred during the initial phase for both the Oxford (with 73% of total EE and 79% of total EC) and Boral (with 59% of total EE and 62% of total EC) kilns. These larger energy consumptions and carbon emissions for the initial stage were mainly due to the majority of materials used in constructing the solar kilns not needing to be replaced over a typical 20-year service life (Table 6.2). As mentioned before, since there is little documentation in the literature

regarding the building materials for solar kilns and their service lives, the replacement schedules have been assessed for different kiln materials based on the information obtained from material datasheets, product guides, and personal communications with kiln manufacturers. This situation gives rise to an uncertainty associated with the actual material quantification for the kilns, and thus the effects of replacement schedules on the EE and EC have been discussed in the sensitivity analysis of this chapter. The percentage contributions of EE and EC from the maintenance stage to their corresponding total values were 25% and 20%, respectively, for the Oxford kiln, whereas these values were 40% and 36%, respectively, for the Boral kiln.

A relatively low contribution from the disposal phases to the total impacts was found in this study. This low share of EE and EC for the EoL phases was mainly because only the timber and the polycarbonate sheets needed to be landfilled after the end of kiln's useful life, while other materials were not sent to the disposal sites due to their longer expected service lives. It should be noted that there was a GWP benefit (i.e. negative carbon impact) from the EoL phase for the Oxford kiln, as shown in Table 6.3. This negative GWP impact for the Oxford kiln was mainly due to the benefits obtained from the waste treatment process for the wood (i.e. landfill). The landfill of wood, as used in this study, was modeled in such a way that the methane part (about 55%) was assumed to be captured and used as fuel, which was further treated as a lower amount of natural gas being needed to be produced elsewhere. This avoidance of this natural gas production caused the GWP impact to be offset (i.e. negative GWP) for the Oxford kiln. However, this situation of the embodied impacts (i.e. EE and EC) in the disposal phase for the Oxford kiln would be significantly different if the methane part was not assumed to be captured and used as fuel. Since approximately half of the total GHG

emissions from wood products in landfills are in the form of CO_2 and half are in the form of

methane (Lippke et al., 2011), and since methane has an estimated GWP of approximately

23 times greater than CO_2 (Ximenes et al., 2008), landfill sites without a methane-collection

system can significantly increase the GWP due to the decomposition of wood waste. In such

a situation, the EC associated with the disposal phase for the Oxford kiln would be 0.545 t

CO_2-e higher (when the methane-collection efficiency is assumed to be 50%) than they are

shown in Table 6.3, and this change in the EC for the Oxford kiln would result in a 118%

difference (Oxford higher) in the EC for the disposal phase between the Oxford and Boral

kilns. It should be noted here that the state of the art in methane-collection systems is an

evolving field, and the recovery efficiency has increased from 20% in 1990 to 50% in 2006

(United States Environmental Protection Agency, 2014). However, where there is no

methane-collection system at the landfill sites, recycling the wood-based products would

still be a better practice than putting them in landfills (Lippke et al., 2011).

6.4.3   Comparative life-cycle embodied energy

Figure 6.5 shows the life-cycle cumulative embodied energies for the Oxford and Boral kilns

over a service life of 20 years.

Figure 6.5 shows that the difference in the initial EEs between the two kilns was 45 GJ, and

after ten years, this difference became larger (92 GJ). One of the reasons for this increase in

the EE difference between the kilns was the subsequent EE associated with the

polycarbonate sheets that were replaced after ten years. Since the amount of the materials

replaced in the tenth year was higher for the Boral kiln (1061 kg polycarbonate) than that

for the Oxford kiln (605 kg polycarbonate), the contribution to the increase in the EE was

larger for the Boral kiln after ten years through the life times of the kilns, as shown in Figure

6.5. It should be noted that the energy embodied in the walls and roofs for the Boral kiln is higher than the summation of the energies embodied in the walls, roofs, and frames for the Oxford kiln.
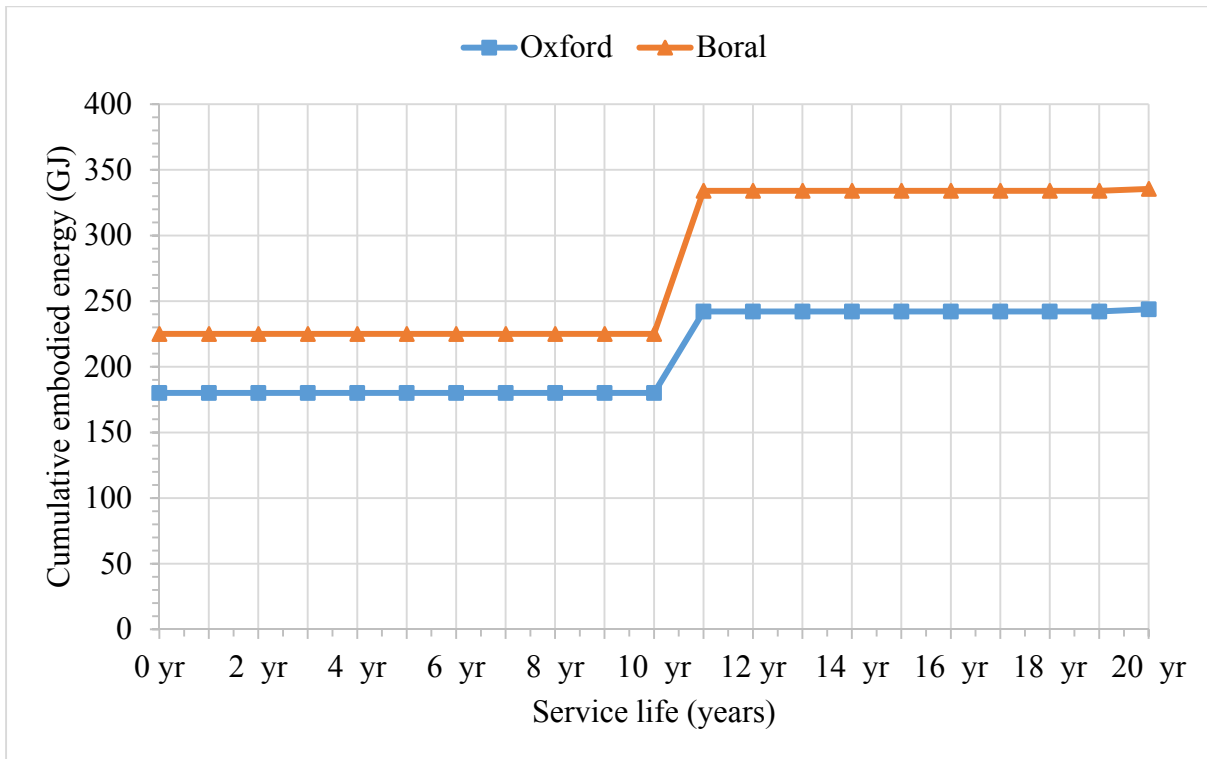
Figure 6.5. Cumulative life-cycle embodied energies for the Oxford and Boral kilns, as functions of kiln service lives.

This feature can also be seen from Figures 6.3 and 6.4, where the walls and roofs (51%), together with the frames (3%) for the Oxford kiln, contributed to 54% of the total EE, whereas this value was 65% for the walls and roofs of the Boral kiln due to the low EE of the wood. Due to the subsequent replacement of the materials (particularly polycarbonate) throughout the kilns' useful life, the difference in the EE between the kilns was predicted to become higher with increasing service life.

6.4.4 Embodied carbon shares for the kilns

Figures 6.6 and 6.7 show the breakdowns, by kiln components, of the embodied global warming potentials (GWP) over a service life of 20 years for the Oxford and Boral kilns, respectively.
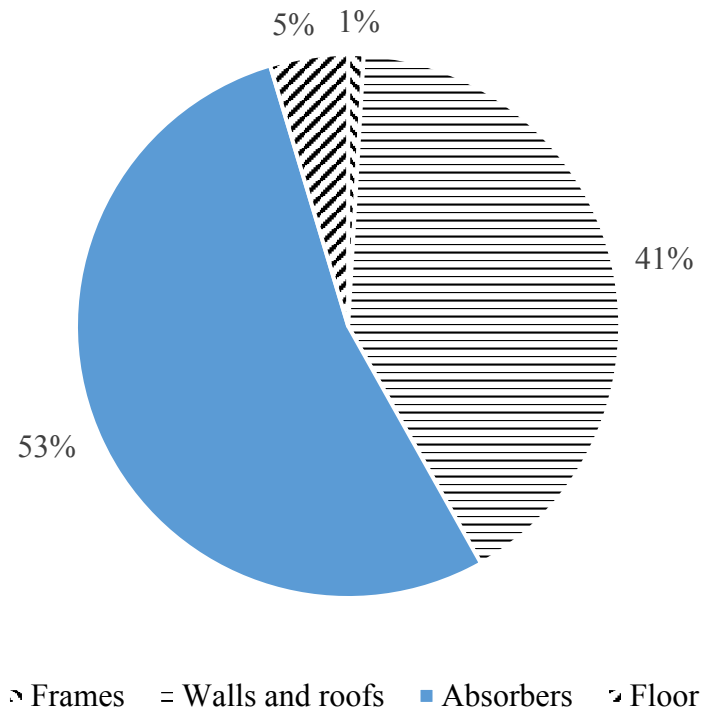
Figure 6.6. Shares of global warming impact, by component category, for the Oxford kiln.

Figures 6.6 and 6.7 show that the absorbers for the Oxford kiln, and the walls, along with the roofs, for the Boral kiln had the highest GWP impact. The highest GWP impact for the Oxford kiln was followed by the impact made by the walls and roofs (41%), with the frames and floor contributing 1% and 5%, respectively, to the total GWP impact. Reviewing Figures 6.3 and 6.6 indicates that, for the Oxford kiln, the materials used for the walls, roofs, and absorbers were found to have a significant impact, both in terms of EE and GWP. By contrast, for the Boral kiln, polycarbonate sheets used for the walls and roofs had the highest GWP

impact (55%) while other components, namely frames, absorbers, and floor, contributed 22%, 19%, and 4%, respectively to the GWP impact. A review of Figures 6.3 to 6.7 indicates that, for the Oxford kiln, the materials used in the absorber, walls, and roofs have significant impacts in terms of EE and GWP, whereas for the Boral kiln, the walls and the roofs had the greatest impacts in these two impact categories.
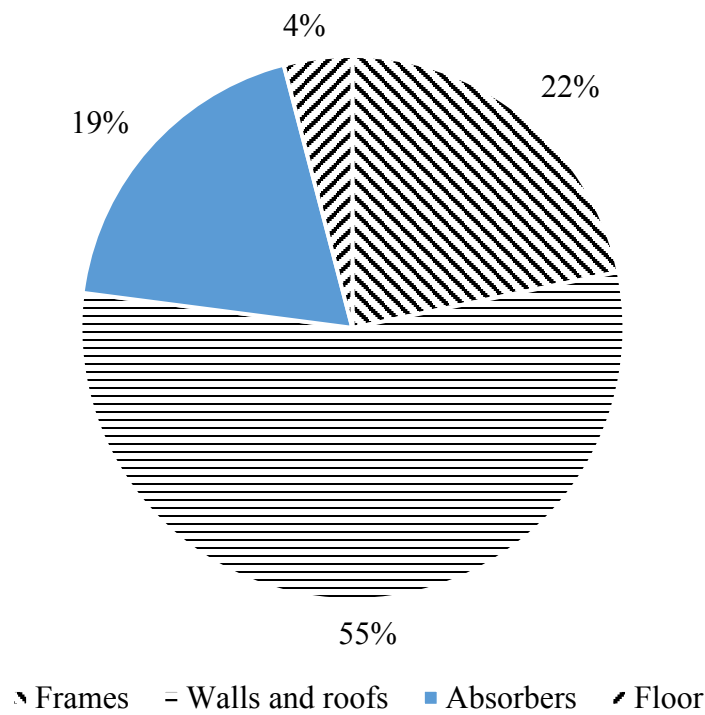
Figure 6.7. Shares of global warming impact, by component category, for the Boral kiln.

However, the absorbers (aluminium) for the Oxford kiln had the higher GWP share (53%) compared with the absorbers (zinc-coated iron) for the Boral kiln, where this value was only 19%. There is considerable evidence, including Hammond and Jones (2008) and McDougall and White (2001), that the energy consumption in manufacturing aluminium is higher than that for iron (zinc-coated). This situation caused the higher EE and the associated GHG emission (t CO_2-e) for the Oxford kiln's absorber. The lower GWP impact of the absorbers

(zinc-coated iron) for the Boral kiln, together with the lower energy (when compared with the aluminium) embodied in the iron (zinc-coated), Figure 6.4 suggests that aluminium could be replaced reasonably by the iron (zinc-coated) for the Oxford kiln. The aluminium frames for the Boral kiln caused a higher environmental impact (22%) compared with the wooden frames (1%) for the Oxford kiln. This result of lower embodied energy and GWP impact for timber, compared with the aluminium, is consistent with several other works, including Ximenes and Grant (2013) and Falk (2009).

6.4.5 Comparative life cycle embodied carbon

The life cycle cumulative ECs for the Oxford and Boral kilns over a service life of 20 years are shown in Figure 6.8.
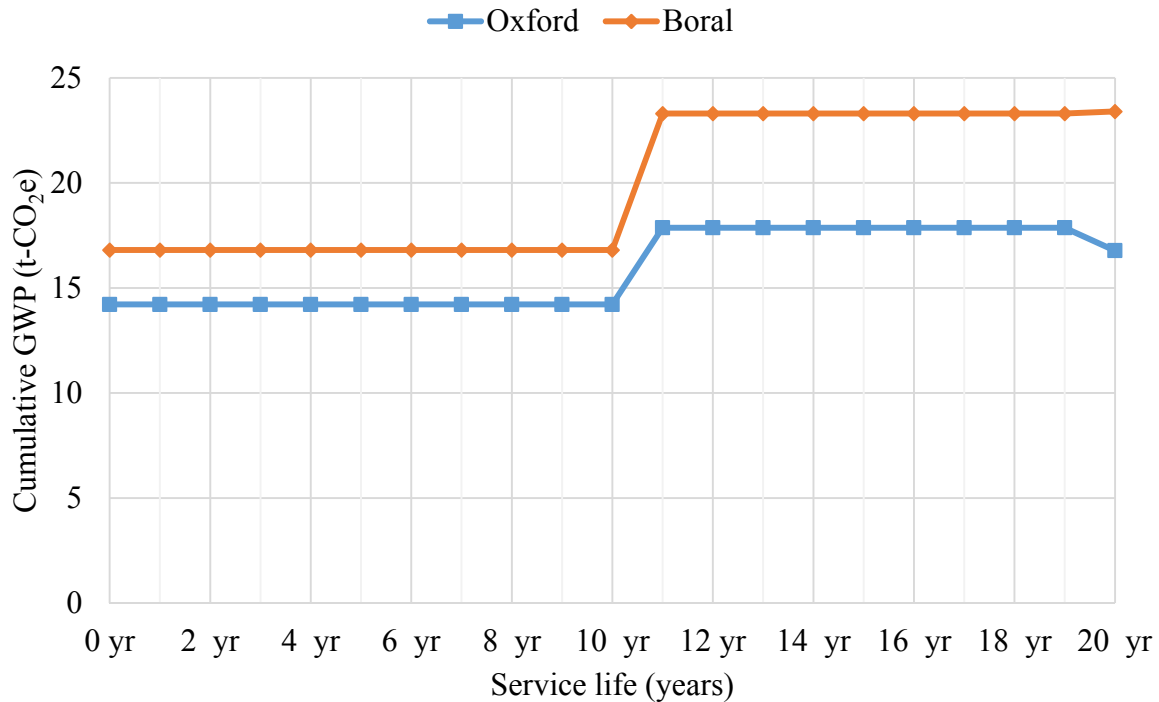
Figure 6.8. Cumulative life-cycle embodied GWPs for the Oxford and Boral kilns, as

functions of kiln service lives.

Figure 6.8 shows that the Boral kiln resulted in a consistently higher EC than the Oxford kiln

throughout its entire service life. The EC associated with the walls and the roofs for the Boral

kiln (55%) was higher than that associated with the walls and the roofs, together with the

frames for the Oxford kiln (42%), as shown in Figures 6.6 and 6.7. This situation indicates

that the consistently higher EC for the Boral kiln, as shown in Figure 6.8, was mainly due to

the increased use of polycarbonate sheets in the walls and roofs for the Boral kiln. It should

be noted here that there was a decline in the EC for the Oxford kiln towards the end of its

service life, as shown in Figure 6.8. This decrease in EC for the Oxford kiln was mainly due to

the benefits obtained from the waste treatment process for the wood (i.e. landfill), as

mentioned before in Section 6.4.2.

Although the results of this chapter were not designed to compare with other studies, it is

suggested that, for the set goal of this chapter, the comparison of the coefficients for the EE

and EC found in this study with a widely-cited existing database (with the same boundary

specification) was meaningful in order to ensure the credibility of the results found here. One

such highly-cited inventory database is the ICE (Inventory of Carbon and Energy) database

compiled by the Sustainable Energy Research Team of University of Bath in UK, which has

been cited over 250 times (as of 31st of August, 2014). The coefficients, as found in this study,

for the EE and EC of the key materials associated with this study have been found to be very

similar to the ICE database (Hammond and Jones, 2008), and they are given in Table 6.4.

Since the ICE database was based on the "Cradle to Gate" boundary conditions, only the

upstream values (excluding the impacts from the disposal phase, thus creating the same boundary conditions) for the EE and EC of this study were used for this comparison.

Table 6.4. Comparison of EE and EC coefficients with ICE database.

Materials	EE coefficients (MJ/kg)			EC coefficients (kg CO_2-e/kg)		
	This study	ICE	Difference (%)	This study	ICE	Difference (%)
Aluminium	208	218	4.5	16.5	11.46	-43
Polycarbonate	102	112	8.9	5.94	6	1
Concrete	1.05	.95	-10.5	.125	.13	3.8
Timber	5.50	7.80	19	.49	.47	4

Table 6.4 shows that the differences in the values for the EE and EC coefficients between this study and the ICE database are within ±20%, except for the EC coefficient of the aluminium, which is 43% lower in the ICE database compared with this study. The differences in the EC coefficients for the aluminium between the studies are not surprising, because aluminium is an energy and process-intensive material, which is likely to lead to a significant difference in the embodied impact (EC to a greater extent and EE to a lesser extent) between different technologies and country energy mixes in the two studies. For example, two given factories could produce the same product, resulting in the same EE per kilogram of product produced, but the total carbon emitted by the two facilities (e.g. factories) could vary significantly, depending on the mix of fuels consumed by the factories. This situation is shown in Table 6.4, where the difference in the EE coefficients for the aluminium between this study and ICE database is 4.5 %, whereas the difference in the EC is 43%. Moreover, Hammond and Jones

(2008) mentioned that ICE contains both EE and EC data, but EE coefficients are more accurate, because the majority of the collected data for ICE was for EE, and not EC, thereby giving rise to greater uncertainty in the ICE values for the EC coefficients. With this in mind, the results of the embodied impacts (i.e. EE and EC) for the two solar kilns, as found in this study, can be considered to be reliable.

6.4.6   Sensitivity analysis

Since there were some assumptions made in this analysis, a sensitivity analysis has been carried out in order to assess the robustness of the results by altering the model assumptions. The effects of the use of alternative materials have also been analyzed in the later part of this sensitivity analysis. The scenarios are given in Table 6.5 with respect to the changes in replacement schedules for the polycarbonate sheet (a major contributor to the overall impact), the changes in the transport distances, and the changes in useful service lives for the kilns, together with the corresponding results.

The effects of different replacement schedules for the polycarbonate sheets on the final EE and EC were assessed, and significant impacts were found for both the kilns when compared with the base case scenario, as shown in Table 6.5. The results show that, for more frequent replacement schedules, the EE and EC increased by 50% and 43%, respectively, for the Oxford kiln, and by 64% and 53%, respectively, for the Boral kiln. When the glazing sheets were replaced every fifteen years, these values of the EE and EC decreased by 25% in both cases for the Oxford kiln, and by 32% and 31%, respectively, for the Boral kiln. This variation in the embodied impacts is expected because more frequent material replacements resulted in larger amounts of overall building materials for the solar kilns (thereby increasing the

recurrent EE and EC), which in turn increased the total embodied impacts (i.e. EE and EC).

Similar results were obtained for the variations in the lifetimes of the kilns, as shown in Table 6.5.

Table 6.5. Scenarios and results of the sensitivity analysis for the EEs and ECs.

Impact	Replacement schedules (years)			Transport distances (t-km)			Service lives (years)		
	5	10	15	100	150	200	10	20	30
EE (Oxford) (GJ)	368	244	182	244	244	244	169	244	318
% change in EE (Oxford)	50	base	-25	- 0.3	base	0.3	-30	base	30
EC (Oxford) (t CO_2-e)	23	16	12	16	16	16	13	16	18
% change in EC (Oxford)	43	Base	-25	0	base	0	-16	base	12.5
EE (Boral) (GJ)	552	335	227	335	335		227	535	
% change in EE (Boral)	64	base	-32	0	base	0	-32	base	32
EC (Boral) (t CO_2-e)	36	23.40	16	23.3	23.40	23.3	16.8	23.4	29.7
% change in EC (Boral)	53	base	-31	0	base	0	-28	base	26

The base case transport distance was assumed to be 150 tkm, which is the average freight haulage distance (tonnes-kilometres) for Australia, as reported by the Department of Infrastructure and Transport (2011). No significant impact, either on EE or EC, was found due to the changes in transportation distances from the base scenario. The key point here is to assess if, for the same case scenario, there is an increase in the EE or EC for the Oxford kiln but a decrease in the EE or EC for the Boral kiln or vice versa. Reviewing Table 6.5 shows

that, for any variation made in the assumptions, the increases or decreases in the EE and EC are similar for the two kilns - as the Oxford kiln changes, so goes the Boral kiln, and vice-versa. This situation implies that the results of this study appear to be robust. Table 6.6 shows the effects of the alternative material selections on the overall embodied impacts for the two solar kilns.

Table 6.6. Effects of the alternative material uses on the EEs and ECs for the Oxford and Boral kilns.

Scenarios	EE (GJ)				EC (t CO_2-e)			
	Oxford	% change	Boral	% change	Oxford	% change	Boral	% change
Scenario 1 (Glazing material – general polyethylene).	651	+148	1018	+203	25	+56	39	+66
Scenario 2 (Oxford frames – aluminium, Boral frames - timber).	265	+10	209	-37	20	+25	9	-61
Scenario 3 (Oxford absorbers – iron, Boral absorbers - aluminium).	174	-33	494	+47	7	-56	41	+75

 In Scenario 1, polythene sheets instead of polycarbonate sheets were assumed to be used as the glazing material with a useful service life of two years, as mentioned by Haque (2002) and Giacomelli and Roberts (1993). The polythene sheets have a limited service life (typically two years) mainly due to the degradation of their physical and optical properties, particularly under conditions of direct sun and rain- a typical situation for the solar kilns. Even though polythene is a lower-embodied energy material than polycarbonate, Table 6.6 shows that higher replacement rates for the polythene coverings caused the EE and the EC to be increased from the base scenario by 148% and 56%, respectively, for the Oxford kiln, and by 203% and 66%, respectively, for the Boral kiln. Thus, the polycarbonate sheet was likely to be a better choice of greenhouse covering, when compared with the polythene coverings, for the solar kilns. If the framing material was assumed to be swapped between the kilns (Scenario 2), an increase in both the EE and the EC for the Oxford kiln, but a significant decrease for the Boral kiln, was found. It is interesting to note here that, under Scenario 2, both the EE (209 GJ) and the EC (9 tons) for the Boral kiln were lower than those for the Oxford kiln.   This reduction in the overall embodied impacts (i.e. EE and EC) for the Boral kiln is not too surprising because timber is a very low-embodied energy material compared with aluminium. When corrugated iron (zinc-coated) instead of aluminium was used in the absorbers for the Oxford kiln (Scenario 3), the EE and EC decreased by 33% and 56%, respectively. The overall results suggest that, in order to reduce the embodied impacts (i.e. EE and EC) for the two kilns, the frames for the Boral kiln should be constructed with timber while corrugated iron (zinc-coated) should be used as the absorber material for the Oxford kiln, because selecting these materials decreased the embodied impacts (i.e. EE and EC) for both the kilns significantly, as shown in Table 6.6. The effects of the alternative

material use, as discussed here, are all found to be consistent with the results shown in Figures 6.3, 6.4, 6.6, and 6.7 of this chapter.

6.5   Conclusions

In this chapter, a LCA model was constructed and used to analyze the EE and EC for the two different solar kiln designs. The general results indicated that both the life cycle EE and EC associated with the Oxford kiln were lower than those associated with the Boral kiln. For both the kilns, the polycarbonate sheets contributed significantly to the EE and EC, mainly due to their increased use over the kilns' service lives. Overall, the walls, the roofs, and the absorbers for the Oxford kiln were found to be the main contributors (above 90%) to both the EE and EC associated with the Oxford kiln, with the frames and floor having individually small effects (less than 20%) on the overall value. However, the frames for the Boral kiln contributed more than 17% to both the EE and the EC. The coefficients of the EE and the EC for the key materials related to this study were found to be consistent with a widely-acknowledged inventory database. Finally, a sensitivity analysis was carried out, which showed that the main trends in the results obtained from this study were relatively insensitive to various uncertainties in the inputs. The assessment of the use of alternative materials for the two solar kilns suggested that, in order to reduce the embodied impacts (i.e. EE and EC) for the two kilns, the frames for the Boral kiln should be constructed with timber while corrugated iron (zinc-coated) should be used as the absorber material for the Oxford kiln. Overall, the Oxford kiln was found to have 37% and 43% lower life cycle embodied energy and embodied carbon values, respectively, than the corresponding values for the Boral kiln. In the next chapter, a life-cycle net energy analysis of solar dryers are described.

Chapter 7 Proposed life-cycle net energy analysis

7.1 Introduction

The use of solar energy for low-temperature commercial and industrial applications is increasing worldwide and being considered as one of the most promising areas for the utilization of solar energy (Janjai et al., 2011; Prakash and Kumar, 2014). Concerns regarding greenhouse gas (GHG) emissions (related to the rapid depletion of fossil fuels), together with drying being an energy-intensive process (Bentayeb et al., 2008), have prompted the development of solar-drying systems on an industrial scale (Luna et al., 2009; Pirasteh et al., 2014; Romano et al., 2009; Sharma et al., 2009). The diversity of drying operations, particularly in chemical engineering, has been discussed in Islam et al. (2014). They mentioned that typical features of drying operations include variations in the material size and shape, the variety of drying media used, and the wide range of materials to be dried, each of them having different drying characteristics (i.e. drying rates). This diverse nature of drying operations has caused solar dryers to evolve into a wide range of designs, sizes, and shapes over the last three decades. However, the development of solar-drying technology, such as large-scale solar drying facilities, must be based on sound knowledge of the energy resource and the anticipated performance of the associated dryer (i.e. kiln) designs over the expected service life (Singh and Kumar, 2012).

A comprehensive review of the various designs, details of construction and operational principles of the wide variety of practically-realized designs of solar-energy drying systems has been presented by Sharma et al. (2009). In modern society, due to the depletion and general awareness about the ecological consequences of burning fossil fuels, it is desirable

to implement alternative energy sources, such as solar energy. Solar drying of timber is not only an energy-intensive process that is carried out by the use of solar energy, but also a process for reducing the overall timber-processing time (increasing the productivity) and improving the quality of the end-use timber, as mentioned in many studies, including Chadwick and Langrish (1996) and Langrish et al. (1992). Traditionally, designing and choosing a particular solar kiln is based on small-scale testing to assess the kiln performance (Langrish et al., 1997). One of the main difficulties for this experimental approach is the involvement of a large number of variables that vary in time and with the geographic location, as mentioned by Langrish et al. (1992) and Thibeault et al. (2010). Moreover, different drying materials have different drying properties (e.g. drying rates) even with the same environmental conditions. This situation makes it problematic to compare the performances between solar dryers of different designs based purely on experimental studies.

There is no or little information in the literature about the life cycle energy requirements of solar kilns for wood drying. Several experimental and modeling approaches have been reported in the literature to assess the timber properties during solar drying and the performance of the kiln itself. For example, a simulation study (Khater et al., 2004) investigated the effect of several design parameters (e.g. drying air velocity, timber thickness, and volume to absorber ratio) on the drying rate and described the optimization of a solar kiln design through a parametric study. A mathematical model of solar kilns was solved and experimentally validated by Haque and Langrish (2003). The predicted parameters (e.g. timber moisture contents, timber temperature, and the drying air humidity) were found to be in good agreement with the experimental data. Another example is a

comparative study (Helwa et al., 2004) between solar wood drying and traditional air drying, where only the results for a single drying cycle were discussed. These studies have been limited in their capacity to consider the variability of the ambient conditions and the likely change in the performance of the kiln over the life time of the drying system. Moreover, most of them have been either type- or site- specific approaches or did not consider long-term costs or energy-use sustainability. The energy effectiveness of solar dryers is greatly affected by the energy flows associated with a particular kiln design. The future is likely to be described by increasing use of renewable energy sources, conventional oil production constraints, and varying energy prices, so it is necessary to develop a robust methodology/tool that is capable of predicting and comparing the performances between the kiln designs with a range of drying materials, climatic conditions, and geographical locations. This approach may assist kiln manufacturers/designers in improving solar kiln designs and users in selecting appropriate dryers.

The total life-cycle energy use in solar kilns is the sum of the EEs and the total on-going OEs consumed over the whole operational life. EE is the total amount of energy consumed during the extraction of raw materials, the transport, manufacturing, construction, use (maintenance and renovation) and disposal phases. By contrast, OE is the energy required to operate (or generated by operating) the built facility in terms of processes, such as air conditioning, lighting and operating other appliances. For the two solar kiln designs, the simulation procedure for estimating the OE requirements has been given in Chapter 5, while the model for assessing the EE has been presented in Chapter 6. Assessing the OE flows means assessing the annual, on-going operating energy (costs) throughputs, while the EE assessment means assessing the capital energy (cost) requirements. There is a key need to

combine the EE (capital cost) with the annual, on-going operating energy (costs) for wood-drying solar kilns in order to evaluate the overall energy effectiveness. Addressing this key requirement to combine a single capital-cost equivalent with an on-going operating-cost equivalent is one of the contributions of this chapter.

Since the primary purpose of a solar kiln is to produce a net positive quantity of energy and consequently use this energy for drying timber as efficiently as possible, a direct net energy analysis should be used to achieve that goal. In this chapter, two overall kiln designs are compared as part of an "option" analysis of two significantly different kiln designs. The key contribution of the chapter is the time-valued net energy analysis in order to assess and compare the overall energy efficiency of the solar kilns in terms of their life-cycle performance. The value of a technology (a particular design of solar kiln) also depends on whether the ratio of the desired output to the input energy flows is growing, steady, or falling over the entire service life. Literature reviews of existing performance evaluations for solar dryers reveal that, despite several simulation and experimental studies being carried out, no attempt has been made to develop a standard and robust LC performance evaluation method, so that it can be utilized for performance comparison between the kiln designs in present value terms.

In this situation, three questions set the key objectives of the current chapter: (1) Does a particular solar kiln design utilize the incoming solar energy more or less effectively compared with other designs, considering the energy losses compared with the energy used for drying? (2) Does this utilization of solar energy rise, fall, or remain steady over a long period of time? (3) How does the amount of EE compare with the operating energy, both used for drying timber and lost from the kiln, for different kiln designs, considering the

operating lives of the kilns? While the first question assesses the feasibility of using different solar kiln designs, the second question assesses the desirability of using that particular kiln over the specified operational life. The third question addresses the relative proportion of EEs needed for the different solar kiln designs in order to provide the target services. These three questions together form a set of necessary conditions for a comprehensive energy evaluation of a given solar kiln design for wood drying. This chapter first describes the state of the art for evaluating the performance of solar dryers. Based on the shortcomings and inadequacies of the prevailing procedures, a novel method for LC performance analysis of solar dryers has been presented in this chapter.

7.2   State of the art

To assess the performance of different solar dryers, several methods and procedures, including Bucki and Perre (2003), Perré and Turner (2002), Romano et al. (2009), Smitabhindu et al. (2008), and Wan and Langrish (1995), have been reported in the literature. It was found by Chadwick and Langrish (1996) that cyclic drying (solar drying) of wood gave better quality products with a comparatively shorter drying period than continuous drying. Theoretical and experimental studies on the performance of solar kilns for wood drying have been carried out by Khater et al. (2004) and Helwa et al. (2004), respectively. However, these studies were limited in their capacity to consider the variability of the ambient conditions and the likely change in the performance of the kiln over the system life time. Various testing methods and procedures, including the National Bureau of Standards (NBS) in United States, American Society of Heating, Refrigeration and Air Conditioning Engineers (ASHRAE), and Federal Association for Solar Energy in Germany, for evaluating the comparative and absolute thermal performance of solar collectors have been

reviewed in Sodha and Chandra (1994). In these methods, the dryers were evaluated by measuring and comparing certain selected parameters, but no specific systematic procedure was followed in these assessments.

In most of the recently-proposed methodologies for characterizing the performance of solar dryers (Altobelli et al., 2014; López-Vidaña et al., 2013; Singh and Kumar, 2012), parameters, such as the pick-up efficiency (η_p), the drying efficiency (η_d), and the first-day drying efficiency (η_{d1}), have been used as performance indicators. While the pick-up efficiency measures how efficiently the circulating air is used to pick up the moisture from the drying material, the drying efficiency is a measure of how effectively the input energy into the dryer is used for drying the materials. When the drying efficiency is determined based on data obtained during the first day of the drying process, it is called the first-day drying efficiency. A laboratory-scale mixed-mode solar dryer model has been designed to perform indoor drying experiments with cylindrical potato samples in order to develop a test procedure for performance comparison between solar dryer designs (Singh and Kumar, 2012). In Altobelli et al. (2014), a model of free water evaporation in a forced solar dryer was described, where the total solar radiation and the saturation deficit of ambient air were considered as the driving force for drying processes.

The key shortcomings of the proposed methods for evaluating the performance of solar dryers to date are: (1) none of the methods determined the performance parameters based on the overall energy requirements (they considered only the thermal energy requirement while ignoring the EE requirement), and (2) none of the methodologies considered the future energy flows or took the time value of energy into consideration (ignored the performance evaluation over the whole service life in present value terms). Some recent studies (Dixit et

al., 2014; Dixit et al., 2012; Yung et al., 2013; Zaid and Paul, 2014) have indicated that, with a growing number of energy-efficient processes, the EE forms an increasingly high proportion of the total LC energy consumption in built facilities. In the case of solar dryers, where the majority of the operational energy (OE) comes from renewable sources (e.g. the sun), considering the EE requirement in evaluating the performance parameters is very important. Moreover, the performance of a solar dryer (kiln) is heavily influenced by the future thermal energy flows (inflows and outflows) around the kiln, and these energy gains/losses are spread over the entire service life of the system. Thus, there is a key need to develop a methodology that can address these issues and assess life-cycle (LC) performance parameters in present value terms, which in turn can then facilitate performance comparisons between different solar dryer designs. Taking all these shortcomings of the existing methods for evaluating the performance of solar dryers into consideration, a novel methodology has been proposed in this chapter, as will now be described.

7.3   Proposed methodological framework

The overall LC energy effectiveness of a solar dryer is dependent on the on-going energy inflows and outflows that occur at different times in the past, the present, and the future and the embodied energy (EE) requirements. This fundamental characteristic of solar dryers may cause misleading choices if a particular dryer is selected without considering the incoming and outgoing energy streams at different times and the EE requirements – a sophisticated design may have a higher initial EE but lower on-going operational energy (OE) requirements. Thus, the proposed method should assess all the initial and future energy flows occurring over the expected service life of the kiln being considered.

In this chapter, a methodological framework to assess the performances of solar dryers, while considering all the future energy flows associated with the dryer operation, is presented. The proposed method is capable of evaluating the performance of a given dryer in terms of a set of performance indicators, called present value performance indicators (PVPIs). This method of performance evaluation for solar kilns is likely to facilitate the robustness of the decision-making processes, which is important for any energy-intensive system in order to achieve its large-scale and wide-spread industrial and commercial growth. The block diagram of the overall methodology proposed in this chapter is shown in Figure 7.1.
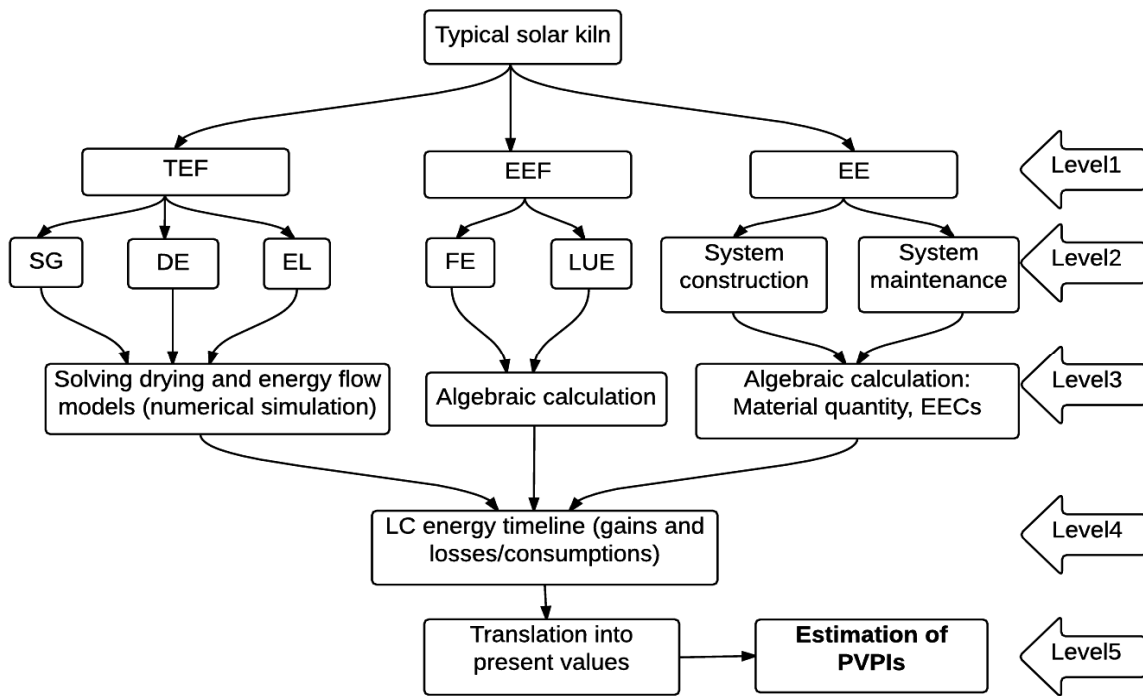
Figure 7.1. Block diagram of the proposed methodology.

In this chapter, the proposed methodology has been illustrated with the design dimensions of the two greenhouse-type solar kilns (i.e. Oxford and Boral) in the context of hardwood (i.e.

E. pilularis) drying. The estimation of the overall energy flows associated with this solar kiln includes the estimation of the thermal energy flows (TEFs), the electrical energy flows (EEFs), and the embodied energy (EE), as shown in Level 1 of Figure 7.1. It can be seen from the left side of Level 2 in Figure 7.1 that the TEFs consist of three energy flows, namely the solar gain (SG) (incoming solar energy), the drying energy (DE) (energy used for drying the material), and the energy losses from the kiln (EL). The EEFs are connected with the fan energy (FE) (energy consumed for operating the fans) and the loading/unloading energy (LUE) (energy consumed for loading/unloading system). No auxiliary energy source, apart from the electrical energy for the fans, has been considered in this analysis. The procedures for assessing the energy flows associated with the solar kiln are presented at Level 3 of Figure 7.1. In order to predict the TEFs associated with the drying of a hardwood species (*E. pilularis*), two models (the drying and the energy flow models), to be described later, were solved numerically in the Matlab (2014b version) environment. The EEFs were estimated algebraically depending on the fan capacity and the loading/unloading requirements for the drying system. The assessment of EE required the quantification of the materials used for the construction and the subsequent maintenance (material replacements) of the kiln over the whole service life. The calculated mass values of the different materials were then multiplied by the embodied energy coefficients (EECs) of the corresponding materials to give the total EE for the overall equipment. As the next step, a LC energy timeline (annual energy benefits and losses over the entire service life) was constructed, as shown in Level 4, from all the energy streams associated with the solar kiln studied here. Finally, as shown in Level 5 of Figure 7.1, all the future energy benefits/losses have been translated into their

respective present values by adopting an appropriate method, and the present values for each year in turn have been used for estimating the PVPIs, as will be described later.

7.4   Overview and significance of the approach

Traditionally, manufacturers, investors, economists and decision makers choose projects based on their life cycle economic return, which is determined by the principle of the "time value of money". This approach may need development when analyzing energy-intensive technologies/utilities, such as solar dryers, because it measures cash flow, an indirect and often inaccurate measure of energy flow, as mentioned by Rock (2006). Furthermore, the monetary value of energy does not always represent its true value to society because of subsidies, inaccurate pricing techniques and policies, and accounting confusion caused by inflation, as mentioned by Cleveland (2013) and Hannon (1982).

There are a few studies in the literature regarding the overall energy benefits and energy costs associated with a particular process/system/built-facility. A benefit-cost analysis for renovation of existing residential buildings was carried out by Wang et al. (2015). The study considered a set of benefit-cost ratios calculated on annual basis in order to rank some alternative retrofit plans. The energy and economic analysis of a tri-generation plant (for electricity, thermal, and cooling energy production) (Buonomano et al., 2015), powered by solar and geothermal energies, was also carried out through a one-year performance simulation. In the literature, there are also many optimization models/methods proposed for heat-transfer problems. For instance, the models proposed by Dolan et al. (1989) and Yee and Grossmann (1991) considered both the operating costs (analogous to the OE flows of this chapter) and the capital costs (analogous to the EE assessment of this chapter) simultaneously to determine a heat-exchanger network with the minimum total cost. In

Dolan et al. (1989), the method of simulated annealing was proposed as a synthetic technique, while in Yee and Grossmann (1991), a mixed integer nonlinear programming (MINLP) model was formulated for a retrofit heat-exchanger network design. Since both of these methods accounted for the trade-offs between the operating and the capital costs, they were computationally expensive. A more computationally efficient model to obtain a cost-optimal heat-exchanger network was proposed by Yee and Grossmann (1990), while accounting for all the associated costs in the objective function. A stage-wise superstructure representation for heat integration, as developed in Yee et al. (1990), was applied to the model. This superstructure approach, together with the simplified assumptions for isothermal mixing of streams, created an optimization model with linear constraints, and hence a computationally- efficient solution scheme was developed. While these methods/models have been useful for the optimization of a process or system as a preliminary choice, they have been carried out either on a financial basis or did not account for the time value of energy when energy gains or losses occurred at different times in the future. Also, some of the workers used a direct payback approach [e.g. Wang et al. (2015)], which did not discount future energy flows compared with current energy use. This discounted energy flow analysis is a key contribution of this chapter.

The technique of discounted net energy analysis (DNEA) has been used in this chapter in order to assess and evaluate the relative life-cycle energy effectiveness for the two different solar kilns over a service period of 20 years. This approach provides decision-makers with quantitative information about whether or not the discounted net present value of the kilns is positive, and the relative desirability of the alternative kilns, especially when inflows (benefits) and outflows (costs) of energy occur at different times and over long periods.

Within the topic of DNEA, decision-making parameters, such as the net present energy value (*NPEV*), the net benefit to loss ratio (*NBLR*), the internal rate of return (*IRR*), and the discounted energy payback period (*DEPP*) are all linked with each other. Definitions of these decision-making parameters are given in Sections 7.5.7 and 7.6.5, and they are immediately relevant to this context.

Several other energy analysts and ecologists have also emphasized the use of a NEA-approach in their respective studies. For example, it was stated in a recent study (Carbajales-Dale et al., 2014) that "*The true value of energy is the net energy*". It was also mentioned in Hannon (1982) that the pervasiveness of energy, along with its uniqueness, makes energy the ideal commodity for a standard and measure of value. Participants in the workshop of International Federation of Institutes for Advanced Study (IFIAS) on Energy Analysis and Economics concluded that (International Federation of Institutes for Advanced Study, 1975):

"The principal goal of energy analysis is the development of a portion of the precise physical description of the operation of real-world processes. This description does not supplant that of economic analysis, but supports and complements it and may provide new perspectives."

From the foregoing discussion, it seems that the technique of DNEA is a significant development of conventional economic analysis, and as such can be an important tool for policymakers/investors/companies in their decision-making process when choosing a particular project. Thus, a DNEA method appears to be appropriate for a reliable assessment and evaluation of solar kilns, which has been done in this chapter.

7.5   Materials and methods

To carry out a net discounted energy flow analysis for solar kilns, it was necessary to calculate all the energy streams (direct or indirect) used to construct, operate, and maintain

the wood-drying solar kilns over the whole analysis period. The process of assessing and estimating these energy flows is valuable in itself, and is one of the key challenges for carrying out a life-cycle net energy (LCNE) analysis for solar kilns. Obtaining appropriate estimates for these energy flows required using a mathematical model for solar kilns (as described in Chapter 4), a life cycle assessment (LCA) model (as described in Chapter 6) for the kiln construction materials, and a manual calculation in an Excel spreadsheet, depending upon the component of energy being calculated. While the detailed constructional description of the two kilns has been given in Chapters 5 and 6, the procedures and approaches for estimating the above mentioned components of energy flows have been described in the following sections.

7.5.1 Basic flow system of a solar kiln for wood drying

The key components of the overall energy flows around a solar kiln for wood drying are shown in Figure 7.2. The areas of energy consumption in a solar kiln include the energy for the fan motors, the energy for the loading and unloading system, and the energy embodied in the kiln structure. Solar energy, which is captured by the kiln absorbers, is partly used for drying the timber, while the rest is lost through conduction, convection and radiation heat-transfer processes. The relative proportions of the energy used for drying and the ratio of the energy losses to the incoming solar energy depend upon the energy effectiveness associated with the particular kiln design. The better the kiln design, the larger the proportion of energy used for drying and the lower the energy losses from the kiln.
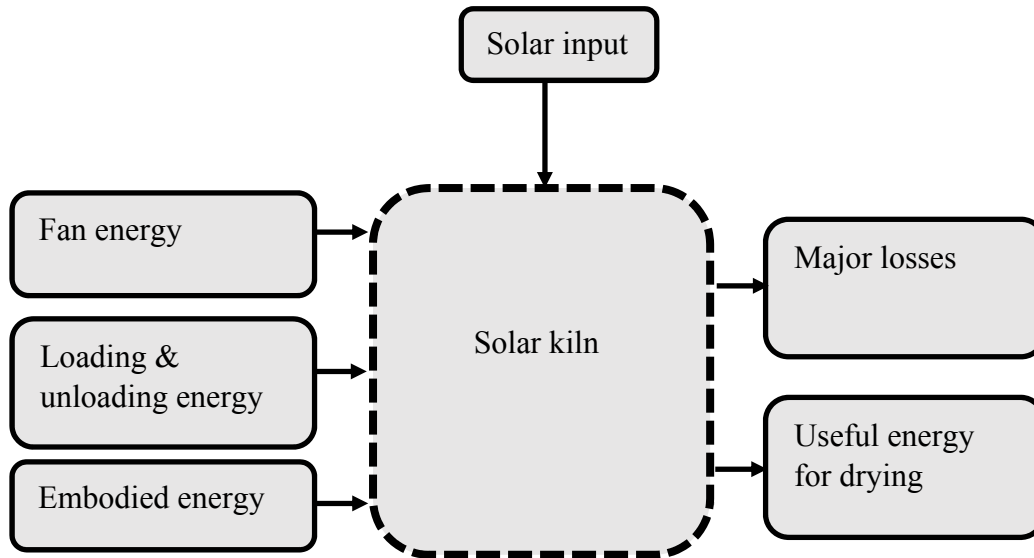
Figure 7.2. Basic energy streams around a solar kiln.

7.5.2 Operational energy analysis method

The energy use for drying timber (i.e. drying energy), the energy losses from the kiln, and

the solar input into the kiln have been predicted in this chapter by using the previously-

developed numerical simulation for a solar-kiln model, as described in Chapter 4. This

particular model has been chosen mainly due to two reasons: (a) the basic solar kiln model

was experimentally validated by Haque and Langrish (2003) for a specific design, site and

climatic conditions, and (b) the modified simulation procedure for the model, as described

in Chapter 4, is capable not only of robustly solving the model equations, and accommodating

a wide range of climatic and geographical conditions, but also simulating kilns with different

designs. The latter feature of the model has been tested in Chapter 5 by predicting several

performance parameters for the two different kiln designs (Oxford and Boral), including the

timber drying times, the timber quality, the solar energy captured by the kiln, and the major

energy losses from the kilns. A detailed description of these operational parameters for the

two kilns, combined with the explanation of why those results were obtained, was given in Chapter 5. While it is not the purpose of this chapter to repeat them here, the energy-flow terms, such as the drying energy and the energy losses from the kilns that are related to the purpose of the current analysis, have been predicted using the same numerical procedure. The key features of the model used for predicting the OE in this chapter and the data used for the model are described in the following sections.

7.5.3   Data description and functional unit for the OE analysis

The year 2013 has been considered as the base year for this study, and the OE requirements for the two kilns have been predicted by using the climatic situations and geographical location of Brisbane (latitude 27.46^0S) in Australia. This particular location has been chosen for the current study because, in Chapter 4, it was found that Brisbane was the most favorable location for solar wood drying out of three representative locations (Sydney, Melbourne, and Brisbane) in Australia. There is strong evidence, including Khater et al. (2004) and Helwa et al. (2004), indicating that the timber species, the stack velocity (velocity across the timber stack), the board thickness, and the thicknesses of the stickers may affect the drying behavior of timber significantly. Taking these features into consideration, the reference functional unit for the assessment of OE has been defined as the drying of 10 m^3 of hardwood timber for a specific species (Eucalyptus pilularis), and typical board and sticker thicknesses (0.025m and 0.02m, respectively) from an average initial MC of 53% to the final average MC of 15% (dry basis) – a typical final MC level for hardwood (10% to 20%). Since the stack velocity is associated with a particular kiln design, the original stack velocities for the two kilns (0.5 m/s and 1 m/s for the Oxford and Boral kilns, respectively) have been used in the simulation here.

7.5.4   Drying and energy flow model description

The overall drying model (Chapter 4) was based on a coupled system of heat and mass transport equations, and the system of equations was solved simultaneously in the simulation program. The drying times of each timber load (i.e. 10 m^3) for the two kilns have been predicted by solving this model numerically. For the purpose of energy flow analysis, the components of the overall kiln being analyzed have been grouped into several thermal units (walls, floor, north roof, south roof, north absorber, south absorber, circulating air, roof absorbers, roof, and the stack). These thermal units are linked to each other and to the external conditions (ambient temperature, velocity, humidity, and the solar radiation) by different thermal pathways (Haque, 2002; Haque and Langrish, 2003). The mass and energy balances for the circulating air and the kiln components, respectively, have been performed by applying unsteady-state balances: rate of accumulation = flow rate in - flow rate out = net energy/mass flow rate. The energy and mass transfers through venting and leakage have been appropriately considered in the model. By solving this energy-flow model, together with the drying model, the solar input to the kilns, the major energy losses from the kilns, and the energy used for the drying processes have been predicted over the analysis period for the two kilns. A detail description of these rate equations, and the numerical approaches to solve the resulting set of differential equations, together with the governing equations used for the calculation of convection and radiation heat transfers, have been given in Chapter 4**.**

7.5.5   Fan and loading /unloading energy analysis method

Two 0.25 hp electric fans were used to circulate the internal air through and around the timber stack. Since the fans are normally turned off during the night in wood-drying solar

kilns, the electrical energy requirements for operating the fans have been calculated by assuming that the fans were run for 12 hours per day.

The energy consumption of the loading and unloading system has been estimated for a typical electric powered fork-lift (4 wheel, 2 – 3.5 tonnes capacity). This calculation of energy consumption has been done based on the average motor power (drive motor and lift motor) of 7.25 kW for a fork-lift of capacity 2-3.5 tonnes, as mentioned in Trucks (2008). The average time for loading and unloading the kiln has been assumed to be an hour, as mentioned in Solar Kilns (2014).

7.5.6 Embodied energy analysis method

The EEs associated with the construction and maintenance periods for the two solar kilns have been calculated by using a life cycle assessment (LCA) model, which has been constructed in "SimaPro" software in accordance with International Organization for Standardization (ISO) 14044 guidelines on LCA (ISO, 2006). The data description and the system boundary of the EE analysis model have been given in Chapter 6, and the key features of the model are given in the following sections.

7.5.6.1 Data description and system boundary for the EE analysis

Since the different geographical locations of the kilns can cause considerable variations in the values of EE due to the differences in economy and technology, and since the OEs for the two kilns have been estimated with respect to the geographical location of Brisbane in Australia, the EE assessment has been done from an Australian perspective, as far as possible. The inventory data have been sourced either from the Australian Life Cycle Inventory (AusLCI) library or the European eco-invent library, while the model has been

analyzed by using the Australian Impact Method with Normalization including Cumulative

Energy Demand (AIM-CED). AusLCI and AIM-CED have been chosen for the purpose of EE

assessment because they are complimentary and include Australian region-specific data

(Australian Life Cycle Assessment Society, 2009; Newton et al., 2009; Tharumaharajah and

Grant, 2006). The functional unit for assessing the EE was to assess the two different solar

kilns (Oxford and Boral) for wood drying with the same timber load capacity of 10 m^3 and

subsequent use over a 20-year service life. Since the EE assessment has been carried out in

this chapter as a part of LCA study, and since it is necessary to specify the system boundary

for any LCA study (ISO 14044 guidelines on LCA (ISO, 2006)), the system boundary for the

model used for estimating the EE in this chapter is shown in Figure 7.3.
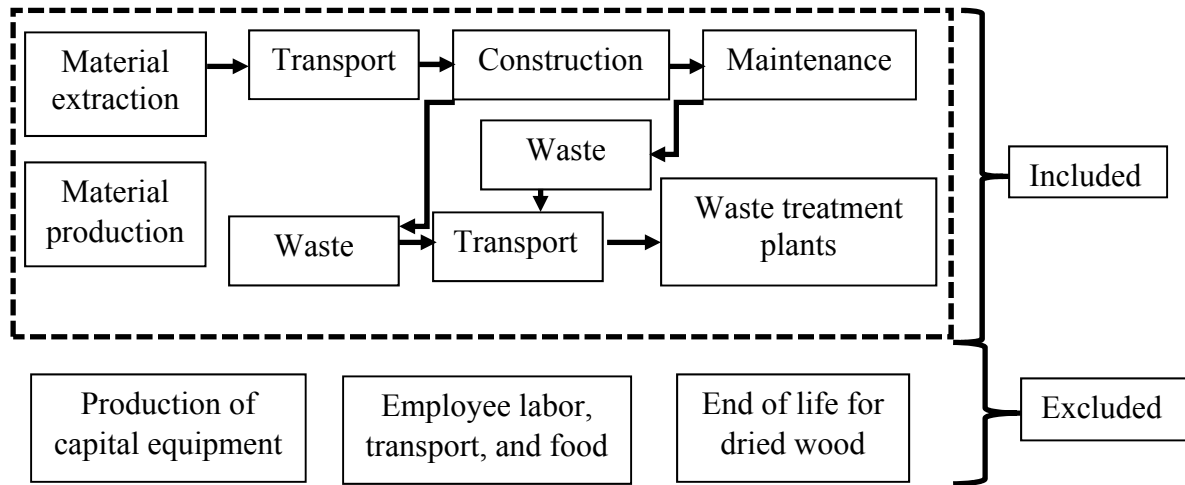
Figure 7.3. System boundary for EE assessment.

The system boundary specifies which components of processes, inputs, and outputs have

been taken into consideration for the EE assessment and which have been excluded. The

energy components that have been included in this EE analysis have been shown inside the

dotted box in Figure 7.3, whereas the excluded elements have been placed outside the dotted

box. It is shown in Figure 7.3 that this EE assessment included the energy consumption associated with the extraction and production of raw materials, the transportation of materials to the construction site, and the transportation of the wastes to the waste treatment plants. Thus, this assessment of EE included a significant number of energy streams that were directly or indirectly committed to the processes associated with the kiln construction, maintenance, and waste handling systems. However, the energy associated with the production of capital equipment, and the labor, the transport, and food for the employees have been excluded from this analysis, as shown in Figure 7.3 (outside the dotted box). These components are traditionally excluded from the system boundary in life cycle assessment (LCA) studies, mainly because they are assumed to contribute to only a minor proportion of the total energy requirements, as mentioned by PE International (2012). Since it is difficult to specify the individual use, and subsequently to model the end of life (EoL) scenarios, for the final kiln-dried wood products, as they are used in a broad range of applications (e.g. furniture, joinery, construction), the final disposal phases for the kiln-dried wood products have not been included in this analysis. However, the final disposal phase for the materials used in the construction of the solar kiln has been included in this EE assessment.

7.5.6.2   Materials and building components for the two solar kilns

While a detailed description of the key materials used for the two solar kilns, their maintenance requirements, and final disposal scenarios, together with the justification of assumptions associated with the material quantification, has been given in Chapter 6, a brief summary of the materials and components for the two kilns as relevant to this study is given in Table 7.1.

Table 7.1. Summary of construction materials and their respective quantities for the two kilns.

Kiln components	Component materials		Quantity (kg)	
	Oxford	Boral	Oxford	Boral
Frames	Timber	Aluminium	690	263
Absorbers	Aluminium	Corrugated iron	500	1537
Walls and roofs	Polycarbonate sheets	Polycarbonate sheets	1211	2123
Floor	Concrete	Concrete	6612	7526

Table 7.1 shows that the key constructional difference between the two kilns is in the materials used for the frames and the absorbers. Timber was used as the framing material for the Oxford kiln, whereas this material was aluminium for the Boral kiln. Aluminum and corrugated iron (zinc-coated) were the absorber materials for the Oxford and Boral kilns, respectively. These differences in the building materials between the kilns are reflected in the material requirements for the two kilns (690 kg and 500 kg in the frames and absorbers, respectively, for the Oxford kiln, whereas these values were 263 kg and 1537 kg, respectively, for the Boral kiln), as shown in Table 7.1. However, a significant difference has been identified in the material requirements for the walls and roofs, and for the floor between the two kilns (1211 kg and 6612 kg, respectively, for the Oxford kiln, and 2123 kg and 7526 kg, respectively, for the Boral kiln) despite using the same material for these components in both the kilns. One of the reasons for the higher material requirements in the walls, the roofs, and the floor for the Boral kiln than the Oxford kiln was the relatively increased use of polycarbonate sheets and concrete (due to increased area) and the corresponding replacements of the polycarbonate sheets at year 10 into the kiln operational life. This situation has increased the material requirements for the Boral kiln.

7.5.7 Proposed methodology for life-cycle performance evaluation

The total LC energy use in solar kilns is the sum of the EEs and the on-going OEs consumed over the whole operational life, as mentioned before. The assessment of the OE for solar kilns over the whole life involves simulation of the future heat energy flows around the kiln, as described before, and a spreadsheet calculation for the estimation of the FE and LUE.   The FE has been estimated on the basis of 12 hours per day operation for two 0.25 hp electric fans, as mentioned by Langrish et al. (1993). The energy consumption of the loading and unloading system has been estimated for a typical electrically-powered fork-lift on the basis of an average motor power of 7.25 kW (Trucks, 2008) and an estimated loading and unloading time (Solar Kilns, 2014). In the following sections, the methods and equations for calculating the life-cycle net present values of all the energy flows around the solar kilns are discussed.

7.5.7.1 Calculation procedure and governing equations

Since there are several energy flows associated with the solar kilns that occur in the future over the kiln service life, and since every year further into the future that energy is produced, the less valuable it may be considered to the society today, all the performance parameters have been determined based on their present-value terms. This basic principle of valuing energy over time can be expressed by the following mathematical expression:

$$PEV = \frac{FEV}{(1+d)^n}$$ (7.1)

Here, *FEV* is the future energy value, *PEV* is the present energy value, *d* is the minimum attractive rate of return (MARR), n is the time (years) into the kiln service life when the *FEV* is produced or consumed. The value of *"d"* adjusts the future energy value to its respective present value.

To carry out a life-cycle net energy (LCNE) analysis for the solar kilns, it was necessary to construct an energy time line containing all the future annual energy inflows and outflows associated with the construction, operation, and maintenance of wood-drying kilns over the entire service life. All these future energy production values (*FEPV*) or future energy consumption values (*FECV*) have been adjusted to their relative present values by using Equation (7.1), and then added up using Equations (7.2) and (7.3).

$$TPEPV = \sum_{n=0}^{N} \frac{(FEPV)_n}{(1+d)^n} \qquad\qquad (7.2)$$

$$TPECV = \sum_{n=0}^{N} \frac{(FECV)_n}{(1+d)^n} \qquad\qquad (7.3)$$

Here, *TPEPV* and *TPECV* are the total present energy production and consumption values, respectively. Similarly, *FEPV* and *FECV* are the future energy production and consumption values, respectively. These net present energy values have been used to compare different solar kilns. Unlike a life cycle analysis based around costs, the focus here is on producing the greatest net energy rather than the most net cash flow. The kiln that produces the higher net energy, or achieves the most energy utilized while consuming the least energy or losing the least incoming energy, has been considered to be the better or more energy efficient kiln.

Once the basic parameters have been defined and estimated using Equations (7.1) to (7.3), the determination of the performance indicators for the solar kilns can be carried out using the following equations:

$$NPEV = TPEPV - TPECV = \sum_{n=0}^{N} \frac{(FEPV)_n}{(1+d)^n} - \sum_{n=0}^{N} \frac{(FECV)_n}{(1+d)^n} \qquad (7.4)$$

$$NBLR = \frac{\sum_{n=0}^{N} FEPV_n * (1+d)^{-n} - \sum_{n=0}^{N} FECV_n * (1+d)^{-n}}{\sum_{n=0}^{N} FECV_n * (1+d)^{-n}} \qquad (7.5)$$

$$\eta_{pd} = \frac{TPEPV - TPELV}{TPEPV} = \frac{\sum_{n=0}^{N} \frac{(FEPV)_n}{(1+d)^n} - \sum_{n=0}^{N} \frac{(CL+RL)_n}{(1+d)^n}}{\sum_{n=0}^{N} \frac{(FEPV)_n}{(1+d)^n}} \qquad (7.6)$$

Here, the three PVPIs are the net present energy value, *NPEV*, the net benefit to loss ratio, *NBLR*, and the present drying efficiency, η_{pd}. The drying efficiency here has been calculated in present-value terms, while considering the LC energy streams, and thus is denoted by η_{pd} in order to differentiate it from η_d, as used in other studies, where the calculations of η_d were based either on a single experimental datum or simulation results for a single drying cycle rather than for the whole life cycle of the dryer. In equation (7.6), *TPELV*, *CL*, and *RL* are the total present energy loss value, the convection loss, and the radiation loss, respectively. It should be noted here that the values of *CL* and *RL* have been obtained from the simulation described in Chapter 4 (please see Equations 4.12 to 4.14 in Chapter 4).

The proposed model of evaluating the performance indicators for solar dryers focusses on producing the greatest net present energy allowing for the time value of energy. The kiln that

produces the higher value of the net present energy, or achieves the most energy utilized while consuming the least energy or losing the least incoming energy, has been considered to be the better or the more energy-efficient kiln. The *NPEV* is the difference between the *TPEPV* and *TPECV* (Equation 7.4), which gives the amount of presently-valued energy available for the drying process during the kiln's service life. Another important factor that can be used to determine the relative value of a kiln is the *NBLR*, which can be used to determine the relative value of a kiln and describes how much presently-valued energy is produced relative to the energy consumed over the lifetime of the kiln. A kiln that returns a *NBLR* equal to or greater than unity means that, over its lifetime, it produces not only more energy than it consumes, but also at a rate at or above the minimum attractive rate of return (MARR), which is the lowest rate of return that investors are willing to accept before they invest. The present drying efficiency of a solar dryer, η_{pd} , which can be expressed by Equation (7.6) while taking the time value of energy into consideration, describes the ratio of the presently-valued energy available to evaporate moisture from drying the material (timber) to the input energy supplied to the dryer. In summary, the overall program associated with the proposed methodology for estimating the PVPIs for the solar kilns may be illustrated by the following flowchart.
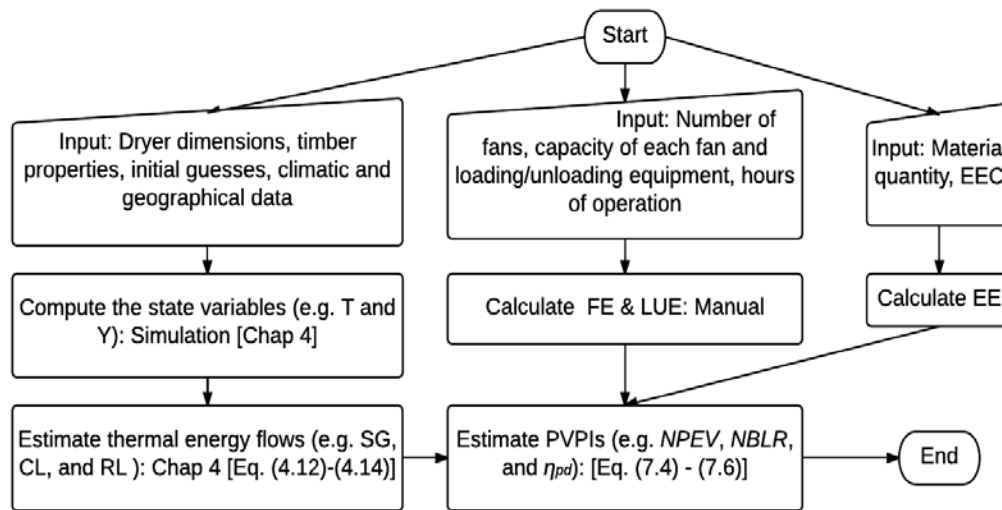
Figure 7.4. Program flowchart to evaluate the PVPIs for the Oxford kiln.

7.5.7.2   Discount rate (*d*)

There is a widespread debate about choosing the value of the discount rate (*d*) for discounting the distant time outputs, as mentioned by Kelleher (2012) and Harrison (2010). However, in Australia, some agencies (including the Commonwealth's Office of Best Practice Regulation) recommend real rates around 7 per cent. For example, the NSW Treasury recommends using a real rate of 7 per cent (with sensitivity tests using 4 and 10 per cent), as mentioned by Harrison (2010). The Office of Best Practice Regulation of Australian government (Department of the Prime Minister and Cabinet, 2014) has used a 7 per cent discount rate in its cost-benefit analysis. Infrastructure Australia (2008) recommended that the cost-benefit studies submitted to it should use 'real risk free' discount rates of 4, 7 and 10 per cent. Reviewing all these recommendations, it is clear that there is no professional consensus on what discount rate should be used. As mentioned before, *d* in Equation (7.1) is the MARR, which is the minimum rate of return that companies/clients are willing to accept

on their investment. This MARR is normally considered to be the rate for government bonds, because buying government bonds is a secured (relatively risk free) investment. Thus, the recommendation made by the NSW Treasury to use a discount rate of 7% has been adopted in this chapter. This approach of using the Treasury rate in energy analysis is also consistent with the study of Rock (2006). However, an appropriate response to the uncertainty around the discount rate is to conduct a sensitivity analysis. If the sensitivity analysis shows that the choice of discount rate changes the ranking against the alternative projects, then more consideration should be given to the choice of the appropriate discount rate. From this perspective, a sensitivity analysis with discount rates of 4% and 10%, as recommended by the NSW Treasury, has been carried out in this chapter to assess if the choice of discount rates changes the ranking of the kilns in terms of the *NPEV*-rule or other decision rules.

7.6   Results and Discussion

The following sections describe the results and discussion of this chapter.

7.6.1 Annual operational energy results

The OE results included the incoming flows of solar energy, heat energy used for drying, energy losses from the kilns through the heat-transfer processes, and the electrical energy uses for the fans and loading/unloading system. As mentioned before, the geographical location (solar radiation) and the climatic data (i.e. ambient temperature, ambient humidity, and wind speed) of Brisbane, with the base year being 2013, have been used in this analysis. These climatic data have been collected from the Australian Bureau of Meteorology's "real time" system (Meteorology, 2013). While the future heat energy flows (i.e. incoming solar energy, energy losses from the kilns, and the useful drying energy) have been predicted using the simulation procedure described in Chapter 4 for a solar kiln model, the uses of electrical

energy for the fans and loading/unloading system have been estimated by spreadsheet calculation. The annual quantities of all these numerically-predicted and estimated streams of energy are given in Table 7.2. It shows that the predicted annual quantities of the incoming solar energy and the drying energy are larger for the Oxford kiln (244 GJ and 94 GJ, respectively) than those for the Boral kiln (202 GJ and 70 GJ, respectively), while the sizes of the annual energy losses for the Oxford kiln (110 GJ) are smaller than those for the Boral kiln (121 GJ). Consequently, a greater proportion of the incoming solar energy was utilized in the drying process for the Oxford kiln (39%) than that for the Boral kiln (34%), as shown in the bottom row of Table 7.2. These results indicate that the Oxford kiln is not only capable of capturing larger amount of solar energy than the Boral kiln but using a larger amount of energy for drying purposes as well.

Table 7.2. Operational energy flows (annual) for the Oxford and Boral kilns.

Energy components	Oxford kiln	Boral kiln
Incoming solar energy (GJ/year)	244	202
Fan energy (GJ/year)	5.8	5.9
Loading/unloading energy (GJ/year)	0.55	0.5
Energy losses (convection and radiation) (GJ/year)	110	121
Drying energy (GJ/year)	94	70
% of input solar energy used for drying (%)[11]	39	34

[11] % calculation = [(drying energy)/ (incoming solar energy)*100].

One of the reasons for the greater energy capture in the Oxford kiln is probably due to the differences in the solar collector areas and their orientations with respect to the sun, as will

be discussed in the following section. There have been relatively insignificant differences in the annual consumption of electrical energy for the fan and the loading/unloading system between the two kilns, as shown in Table 7.2. This result arises because there has been a small difference, depending on the time required for a drying cycle, both in the operating hours for the fans and the requirements of loading/unloading activities between the two kilns. These results imply that there is scope for the Boral kiln to improve its capacity in capturing the incoming solar energy.

7.6.2 Life- cycle operational energy results

The undiscounted life-cycle OE components for the two kilns over the lifetime of 20 years are shown in Figure 7.5. It is shown in Figure 7.5 that the total life-cycle energy values of the fans and loading/unloading system have been very small compared with the sizes of the other energy streams (i.e. solar input, drying energy, and energy losses) for both the designs. It should be noted here that, in the overall analysis, the electrical energy required for the fans and loading/unloading systems has been given in delivered energy rather than primary energy units. The primary energy can be many times higher than the delivered energy due to the heat losses in the power plant and transmission losses in the electricity grid. In addition, the conversion efficiency may change from time to time. In such a situation, consideration of the net (end-use) energy requirements is more appropriate for a life-cycle net energy analysis, which has been done in this thesis. Figure 7.5 also shows that the size of the life-cycle useful energy (drying energy) for the Oxford kiln (1888 GJ) was larger than that for the Boral kiln (1408 GJ).

By contrast, the size of the energy losses is smaller for the Oxford kiln than that for the Boral kiln. The differences in these life-cycle energy flows between the kilns were due to

differences in the design features of the kilns. The key features of the designs that cause these differences may include the differences in the solar collector areas and their orientation with respect to the sun, and the difference in the total volume for the same load capacity between the two kilns. As mentioned before, the scaled Boral kiln has 11 m² of absorber (horizontal) facing the sky and a combined area of 14 m² of absorbers (perpendicular) facing to the north and south. By contrast, the Oxford kiln has 25.7 m² of absorbers facing the sky (either horizontal or slightly inclined). Due to the vertical orientation of the north and south absorbers in the Boral kiln, the areas of the absorbers seem to be used less effectively to collect the solar radiation, resulting in a lower solar energy input for the Boral kiln than that for the Oxford kiln, as shown in Figure 7.5.
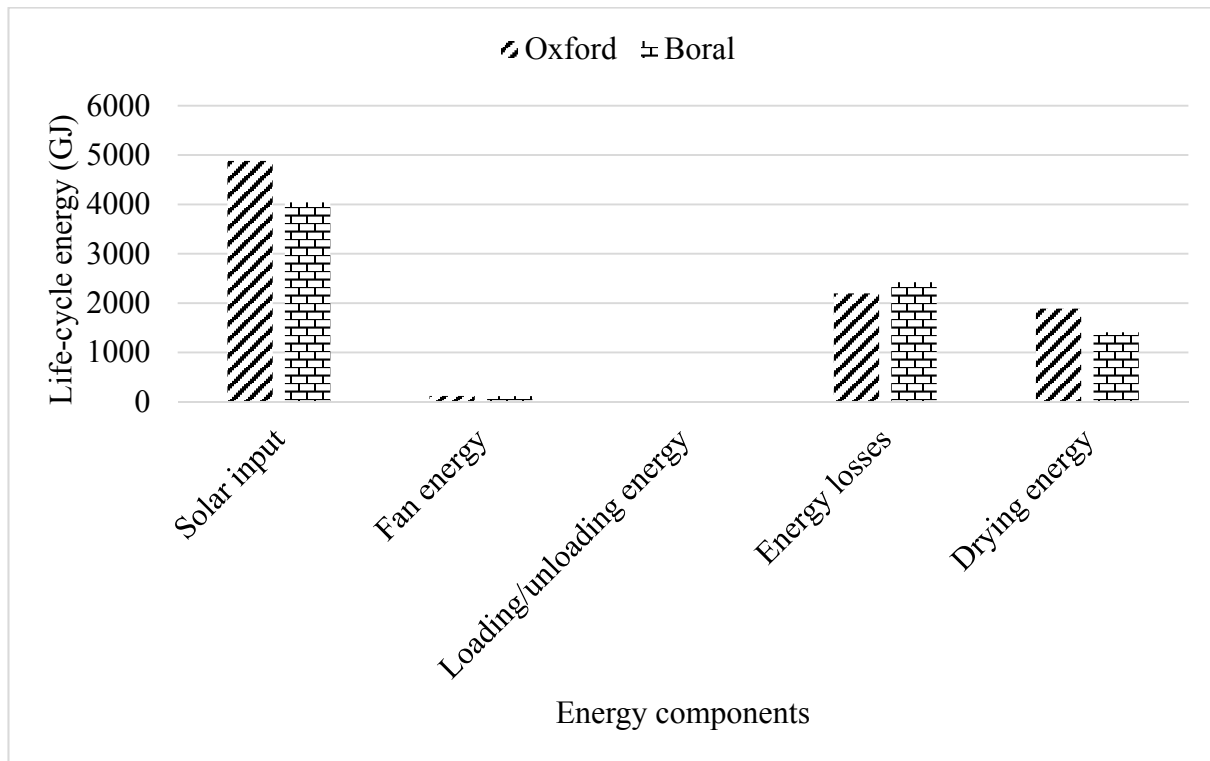
Figure 7.5. Total life-cycle undiscounted OE components for the Oxford and Boral kilns.

Another design feature that may affect the heat-transfer rates between the internal air and the timber stack is the total volume of the kiln for a given load capacity. For the timber load capacity of 10 m^3, the total volume for the scaled Boral kiln has been calculated to be 101 m^3, which was significantly greater (possibly due to the large curved shape of the roof) than that for the Oxford kiln (58 m^3). The larger dimensions of the Boral kiln appeared to result in larger thermal masses of both the internal air (for the same load capacity) and the kiln structures in the Boral kiln, which further means that more energy would be required to raise the temperature of the kiln internal conditions by 1K. This condition is likely to lower the kiln air temperature and the board temperature (please see Table 5.3 in Chapter 5), which in turn would decrease the diffusion coefficient for the moisture transport within the boards. This situation in the Boral kiln (lower diffusion coefficient within the boards) has led to slower drying rates in Boral kiln and smaller amounts of useful energy used for drying purposes, as shown in Figure 7.5. Reviewing the results in Table 7.2 and Figure 7.5, the Oxford kiln appears to be superior to the Boral kiln on the basis of operating energy.

7.6.3 Embodied energy results

The assessment of the EEs has been carried out using a LCA model, which has been constructed in "SimaPro" software in accordance with ISO 14044 guidelines on LCA, as mentioned before. The data and the system boundary used for this analysis have been described in Section 7.5.6.1 of this chapter. The EE values for the two solar kilns (Oxford and Boral) are given, by life cycle stages, in Table 7.3. Table 7.3 shows that the greatest amount of energy was expended during the initial construction for both the Oxford (with 180 GJ) and Boral (with 225 GJ) kilns. This larger energy consumption for the initial stage has been

mainly due to the requirements of the majority of the kiln materials used in the construction phase.

Table 7.3. Embodied energy values for the Oxford and Boral kilns.

Kiln designs	Initial (GJ)	Maintenance (GJ)	Disposal (GJ)	Total (GJ)
Oxford	180	61.8	2.28	244
Boral	225	109	1.44	335

The EEs associated with the maintenance phases were 61.8 GJ and 109 GJ for the Oxford and Boral kilns, respectively. This consumption of energy for the maintenance stage has been mainly due to the replacement works associated with the polycarbonate sheets (replaced every ten years) used for the kilns. It should be noted here that, due to the energy consumption associated with the waste treatment processes, there were energy embodiments during the waste disposal phase. The energy embodiments during the waste disposal phases were found to be 2.28 GJ and 1.44 GJ for the Oxford and Boral kilns, respectively. In summary, the overall energy embodied in the Boral kiln (335 GJ) has been higher than that in the Oxford kiln (244 GJ), as shown in Table 7.3.

7.6.4 Embodied energy shares for kiln components

The percentage contributions by different kiln-components to the total life-cycle EE, as calculated by a LCA model constructed in "SimaPro", for the two kilns are shown in Figure 7.6 and 7.7.
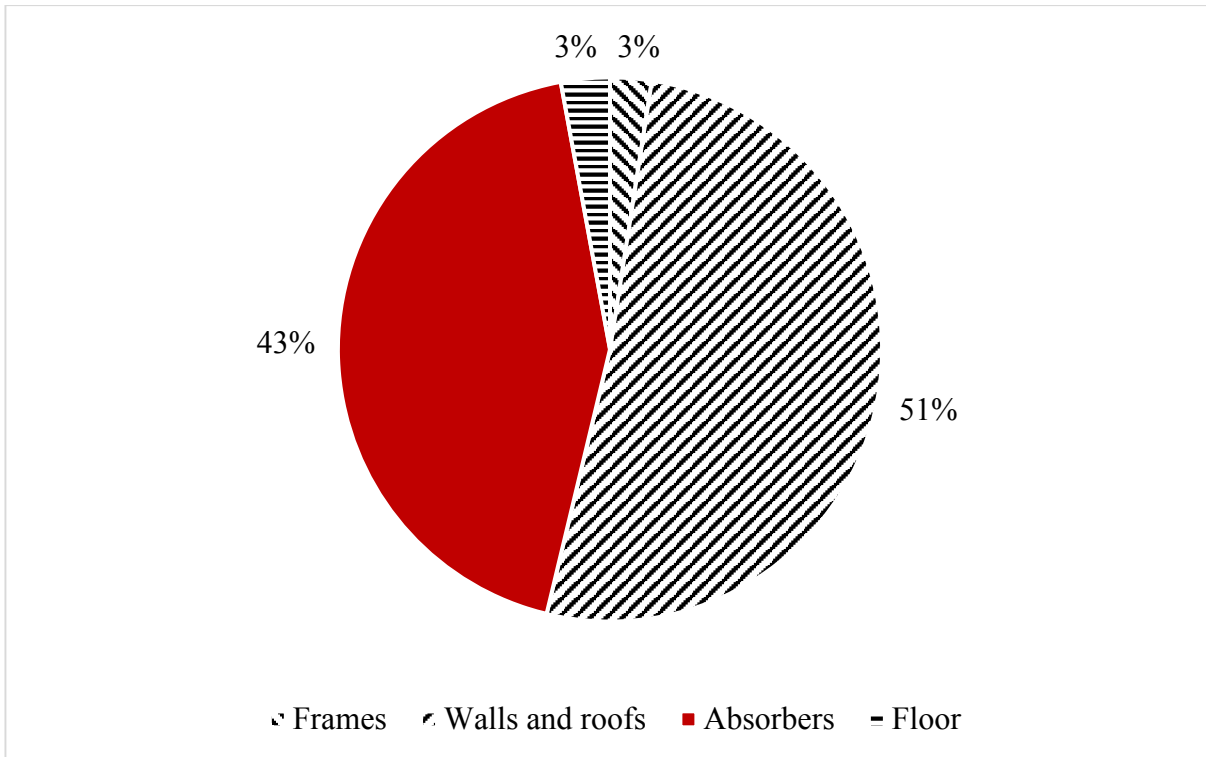
Figure 7.6. Embodied energy shares for the Oxford kiln.

Figures 7.6 and 7.7 show that the greatest share of the EE came from the walls and roofs over the whole analysis period (20 years) for both the Oxford and Boral kilns (51% and 65%, respectively). One of the possible reasons for the higher share from the walls and roofs for the Boral kiln than the Oxford kiln may include the relatively increased amount of polycarbonate materials used for the Boral kiln (Table 7.1) over the entire service life, which was likely to increase the EE share for the Boral kiln. The energy embodied in the absorbers for the Oxford and Boral kilns contributed 43% and 16%, respectively, to the corresponding total EE.
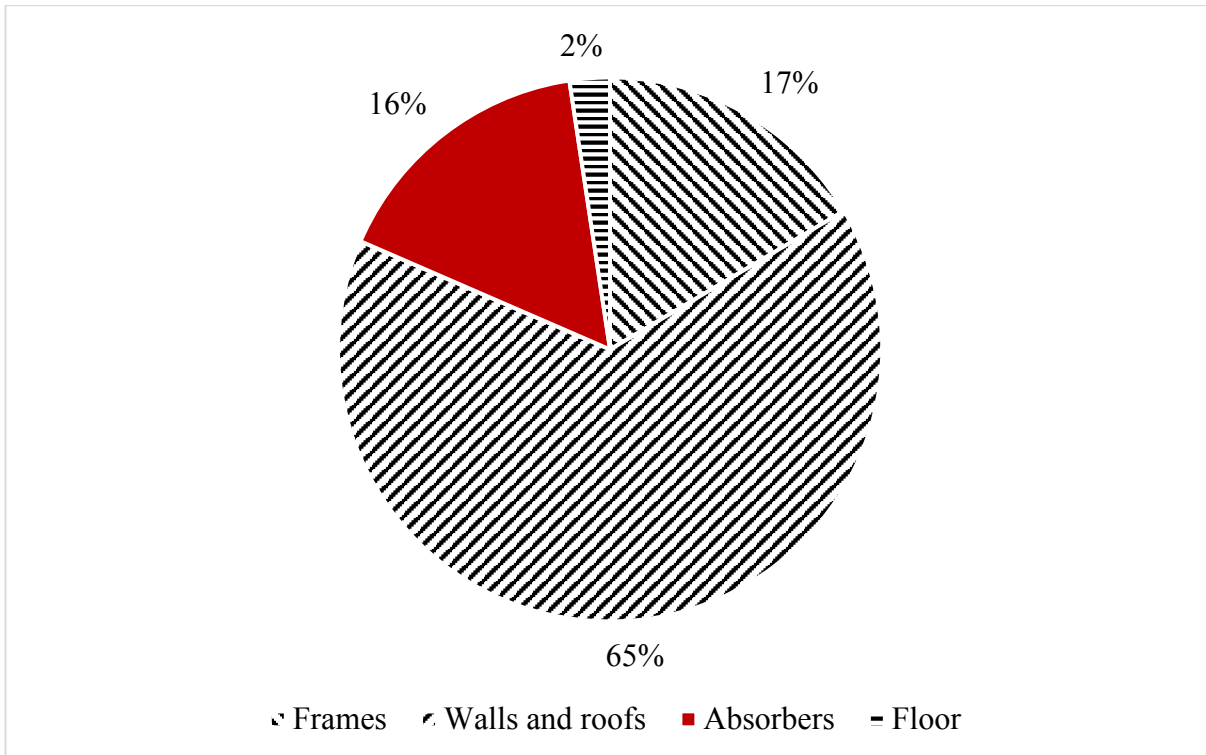
Figure 7.7. Embodied energy shares for the Boral kiln.

These values indicate that the absorber material (aluminium) for the Oxford kiln has a higher EE than that (iron sheet) for the Boral kiln. This result is consistent with many other studies, including (Falk, 2009; Hammond and Jones, 2008; Milne and Reardon, 2013), where aluminium was found to be the material with a higher EE relative to other construction materials. A significant difference between the percentages (for each kiln) of the total EE that comes from the framing material (3% for the Oxford kiln, 17% for the Boral kiln) has been found in this study. This difference was due to the comparatively clean and low-energy manufacturing processes involved for wood manufacturing (Falk, 2009), which makes wood a very low embodied-energy material. Because concrete has a relatively longer life and can be recycled efficiently, as has been assumed in this study, floors for both the kilns shared the smallest EE (less than 5% in each design).

7.6.5 Life-cycle net energy (LCNE) analysis results

The LCNE of a particular solar kiln involves both the present value of all the future OE flows (predicted by an appropriate numerical simulation) and the present value of the life-cycle EE (calculated by an appropriate LCA model) associated with the particular solar kiln. All the future energy streams have been discounted to their present values by adopting the methodology described in Section 7.5.7. The LCNE results may be discussed in terms of several present value performance indicators (PVPIs), as given in Table 7.4.

Table 7.4. Present values of the key energy flows per cubic metre of dried timber for the Oxford and Boral kilns over a service life of 20 years.

Parameters	Oxford	Boral	% difference[12]
Net present energy value (NPEV) (MJ)/ m3 of dried timber	657	408	+37
Present value of energy losses (PVEL)(MJ)/m3 of dried timber	668	828	-24
Net benefit to loss ratio (NBLR)	4.12	1.84	+55
Present drying efficiency (η_{pd})	55	40	+27
Present drying energy value (PDEV)(MJ)/m3 of dried timber	575	481	+16
Present value of fan energy (PVFE) (MJ)/ m3 of dried timber	36.2	40	-11
Present value of loading/unloading energy (PVLE) (MJ)/ m3 of dried timber	3.45	3.25	+5
Present value of embodied energy (PVEE) (MJ)/ m3 of dried timber	121	179	-47

[12] % change = [(Oxford – Boral)/Oxford*100].

Table 7.4 shows that the NPEVs per m^3 of dried timber were positive for both the Oxford and Boral kilns, which imply that both the kilns were feasible for drying purposes in energy terms. These parameters indicate the net energy savings for drying one cubic metre of timber. However, the NPEV for the Oxford kiln (657 MJ) has been larger (37%) than that for the Boral kiln (408 MJ). The net energy values have been calculated by subtracting the energy consumption values (EEs, fan energies, loading/unloading energies), together with the energy-loss values, from the energy benefits (input solar energy).

This chapter proposes that, when mutually exclusive projects are considered, the project which maximizes the NPEV should be chosen. This statement has also been supported by many other energy and economic analysis guidebooks and studies, including Commonwealth of Australia (2006), Carbajales-Dale et al. (2014), and Heun and de Wit (2012). Thus, the larger NPEV for the Oxford kiln indicates that the Oxford kiln is more desirable than the Boral kiln over the analysis period of 20 years. This favorable feature of the Oxford kiln is also reflected in the individual present values, as given in Table 7.4, for the fan energy, the loading/unloading energy, the drying energy, the EE, and the energy losses through the heat-transfer processes. While the present values of EE (major initial energy investment) and energy losses (major losses) were smaller for the Oxford kiln (124 MJ and 786 MJ, respectively) than those for the Boral kiln (186 MJ and 974 MJ, respectively), the present value of the energy used for drying purposes has been larger for the Oxford kiln (667 MJ) than that for Boral kiln (566 MJ).

In this chapter, the *NBLR* has been calculated as the ratio of the net present energy value (net energy benefits) to the total present energy consumption value [Equation (7.5)]. Generally, it is required that, for a project to be acceptable, the NEPR must have a value greater than

unity – a condition for the *NPEV* to be positive. Table 7.4 shows that *NBLR* for the Oxford kiln is 55% larger than that for the Boral kiln. However, the *NPEV* and *NBLR* rules may rank alternative solar kilns differently because, in some cases, projects with higher *NPEV* may yield smaller *NBLR* or vice versa (Commonwealth of Australia, 2006). In this situation, the decision should be made depending on the *NPEV*, because the *NBLR* does not displace the objective of maximizing *NPEV*. From Table 7.4 it is seen that both the *NPEV* and *NBLR* are larger for the Oxford kiln than those for the Boral kiln, which further indicates the superiority of the Oxford kiln over the Boral kiln. The present drying efficiency, η_{pd} for the Oxford kiln has been found to be 27% larger that for the Boral kiln, which implies that Oxford kiln is 27% more efficient than the Boral kiln in using the input solar energy for drying purposes. Unlike other studies, where the drying efficiency, η_d was calculated without considering the future energy flows, the drying efficiency of the kiln has been determined in this chapter based on the presently-valued energy terms i.e. η_{pd}, as mentioned in Section 7.5.7. Since various kiln designs have different patterns of energy flows that occur in the future at various time intervals, η_d and η_{pd} may rank alternative solar kiln designs differently. This difference arises because, in some cases, projects with higher initial energy input may require lower on-going energy requirements, and thus give different choices according to the parameters η_d and η_{pd}. Thus, the determination of the η_d based on the *NPEV* (i.e. η_{pd}) is suggested to be a robust approach for evaluating the performance of different designs for solar dryers. The 16% higher value of the present drying energy for the Oxford kiln than that for the Boral kiln, as shown in Table 7.4, implies that a greater amount of input solar energy is used for drying purposes in the Oxford kiln. These results address the first two questions (Questions 1 and 2) that have been set as part of the objectives for this chapter.

In addition to the *PVPI*s listed in Table 7.4, there are a few other decision parameters that may be used for assessing the performance of a particular drying system relative to the other available alternative systems. These decision parameters may include the internal rate of return (*IRR*), the discounted energy payback period (*DEPP*), the net present energy to EE ratio, and the present drying energy to EE ratio, as shown in Table 7.5.

Table 7.5. Supplementary decision-making parameters for evaluating the solar kilns.

Items	Oxford	Boral	% difference[13]
Internal rate of return (IRR) (%)	71	37	+47
Discounted energy payback period (years)	2	3.5	-85
Net present energy to EE ratio	5.44	2.28	+58
Present drying energy to EE ratio	4.76	2.70	+43

[13] % change = [(Oxford – Boral)/Oxford*100].

An alternative decision rule commonly used for project evaluation is the IRR, which is the discount rate that produces a *NPEV* of zero. Thus, it is the rate that equates the discounted consumption of energy flows (energy costs) and the discounted production of energy flows (energy benefits). In this analysis, the IRR has been calculated to be 47% higher for the Oxford kiln than that for the Boral kiln, as shown in Table 7.5. In general, if the IRR of a project exceeds the selected discount rate for estimating the present values of future energy streams, the project gives a positive *NPEV* and is considered to be acceptable. Like *NBLR*, a decision based only on the IRR may be misleading when ranking alternative projects that differ in scale. However, since the nature and timing of the energy inflows and outflows are similar for the two kilns considered in this study, the IRR-decision rule is consistent with the *NPEV*-decision rule, as both of these values are larger for the Oxford kiln than those for the Boral kiln.

The energy payback period is defined as the time necessary (usually in years) for a solar kiln to collect the energy equivalent to that used to produce it. Table 7.5 shows that the payback period for the Oxford kiln is 85% lower than that for the Boral kiln. The values of the net energy to EE and the drying energy to EE ratios were also larger for the Oxford kiln (58% and 43%, respectively) than those for the Boral kiln, as shown in Table 7.5. These ratios imply that not only was the Oxford kiln likely to produce a greater positive quantity of net energy over the entire service life while consuming less energy in its construction and maintenance (EE) than the Boral kiln, but also that the Oxford kiln used a larger proportion of the incoming energy for the drying process. This result directly addresses the third question set in the introduction of this chapter.

In summary, the net *NPEV* should be used as the primary basis for recommendation and decision-making in many project evaluations. Other alternative decision rules may provide supplementary information or reduce the frequency of inferior choices, but should be employed only when they do not imply misleading recommendations. Reviewing the results given in Tables 7.4 and 7.5 shows that the PVPIs (i.e. *NPEV*, *NBLR*, and η_{pd}) are the most reliable parameters in the decision-making process for solar dryers, and the Oxford kiln is likely to be better than the Boral kiln in terms of feasibility, desirability, and energy effectiveness.

7.6.6 Sensitivity analysis

In this analysis, the effect of discount rate on the decision-making parameters for the two kilns has been analyzed. The results for the sensitivity analysis with respect to three different discount rates (4%, base case, and 10%) are given in Table 7.6. It shows that the *NPEV* has been affected significantly by the choices of discount rates. The *NPEV* increased and

decreased when the discount rate decreased and increased, respectively. These changes in *NPEV* were expected, as the future energy streams increased in value with reduced discount rate and vice versa.

It should be noted that all the other parameters (mostly related to the ratio of energy benefits to energy costs) have been negligibly affected by the discount rate. One of the main reasons for this is both the energy inflows (benefits) and outflows (costs) have been adjusted to their respective present values with the same discount rate.

Table 7.6. Influences of discount rate on decision-making parameters.

Parameters	Discount rate (4%)		Discount rate (7%) (base case)		Discount rate (10%)	
	Oxford	Boral	Oxford	Boral	Oxford	Boral
NPEV (GJ)	1515	870	1414	633	885	468
NBLR	4.9	2.27	4.12	1.84	3.44	1.48
IRR (%)	71	37	71	37	71	37
DEPP (years)	2	3.43	2	3.6	2.19	3.78

Thus, the *NBLR*, *IRR*, and *DEPP* have not been changed significantly with respect to the discount rate. It should be noted here that any variation made in the discount rate did not alter the ranking of the kilns - the Oxford kiln is better than the Boral kiln, as shown in Table 7.6. Since the replacement schedule for the polycarbonate sheets has a direct impact on the embodied impacts (i.e. EE and EC) for the two kilns, the effects of the uncertainties around the replacement schedule have been discussed in the sensitivity analysis of Chapter 6 (please see Section 6.4.6). The results showed that the replacement schedule for the walls/roofs material had a significant impact on the EE and the EC for both the kilns, but were unlikely

to change the relative embodied impacts (i.e. EE and EC) of the two kilns. Thus, the general conclusion of this chapter is relatively insensitive to the uncertainty associated with the discount rate and the replacement schedule for the polycarbonate sheets.

7.7   Conclusions

As different solar dryers have energy streams that are spread out differently over their entire service life, an innovative approach has been proposed here to assess the PVPIs of the solar dryers in the context of hardwood drying in Australia. The estimated OE, in combination with the EE, has been used in order to carry out a LCNE for the two solar kilns over a service life of 20 years. This analysis involved the use of a combined drying and energy flow model for solar kilns to predict the future flows of operating energy, and a LCA model to assess the EE over the entire life cycle of the kilns. The undiscounted values for all these streams of energy have been discussed either in the form of annual energy flows, or different life cycle stages, or total life-cycle energy flows, depending upon the types of energy flows. All of these undiscounted energy flows have then been translated to their corresponding present values as part of the LCNE, which has been carried out to assess and evaluate the relative energy effectiveness for the two solar kilns over the service life of 20 years. A simplified flowchart of the overall methodology has been presented. The general results indicated that the *NPEV*, the *NBLR*, and the *IRR* were larger for the Oxford kiln than those for the Boral kiln, by approximately 37%, 55%, and 47%, respectively. However, the *DEPP* and the present value of energy losses (*PVEL*) were smaller for the Oxford kiln by 85% and 24%, respectively, than those for the Boral kiln. The sensitivity analysis showed that, although the *NPEV* was significantly sensitive to the discount rates, the ranking of the kilns (Oxford is superior to Boral) has been relatively insensitive to the uncertainty associated with the discount rate

not only in terms of the *NPEV*, but also other decision-making parameters, such as the *NBLR*, IRR, and the DEPP. The overall LCNE results indicated that the Oxford kiln design was likely to be more productive and energy efficient than the Boral kiln design for the purpose of solar-assisted hardwood-drying processes. The key design features that have made the Oxford kiln the better choice for hardwood drying were likely to be the more effective orientation of the absorbers with respect to the sun and the lower total volume requirements for a given load capacity than the Boral kiln. The proposed method, together with the defined PVPIs, has been appeared to be a robust and reliable technique to assess the relative performance of different kiln designs. In the next chapter, a discounted cash flow analysis for the two solar kilns will be described.

Chapter 8   Discounted cash flow analysis

8.1   Introduction

A few studies about the life-cycle economic return associated with solar kilns for wood drying applications are available in the literature. An economic analysis of solar drying systems for seaweed was carried out by Fudholi and Ruslan (2011). A similar study analyzing the relations between the technical solutions and the economy of solar dryers was carried out by Imre (1986). However, most of them were either type or site-specific approaches or did not consider the long-term costs or savings in their calculations.

The total life cycle financial and environmental performance evaluation of solar kilns includes the material costs, the labor costs, the maintenance costs, the on-going operational energy costs/savings, and the GHG emissions savings over the whole operational life of the kilns. One of the key challenges in carrying out the economic analysis of solar kilns is the projection of future on-going energy flow profiles over the kiln's service life. A relatively robust simulation procedure for predicting these future energy flows around solar kilns with varying climatic and geographical conditions has been presented in Chapter 4. This computer simulation technique of estimating the future energy flows for the solar kilns has been adopted in this chapter in order to estimate the corresponding future cash flows associated with the solar kilns. In order to evaluate the overall life cycle economic and the environmental performance of the solar kilns, there is a key need to analyze the total energy costs/gains (the capital energy and the annual, on-going operating energy costs/savings), together with the GHG emissions savings, associated with solar-kiln operations for drying processes. These economic and environmental aspects of solar kilns for wood drying can be

addressed by carrying out a discounted cash flow (DCF) analysis. However, it should be noted here that, although in a process of project investment decision making, economists, governments, and other financial organizations use the DCF approach, this methodology cannot fully quantify the risks and uncertainties (as also discussed in Chapter 7) that arise from changing energy price in competitive energy markets, the uncertain future carbon price, uncertain government policy on climate change, and uncertain international regimes for accounting for climate change (Blyth et al., 2007; Fernandes et al., 2011; Reuter et al., 2012). This situation arises the question that is the life-cycle performance ranking of the two kilns on the basis of energy the same as the ranking on the basis of cost? Thus, the key objectives of this chapter have been set to carry out a life-cycle cash flow (LCCF) analysis of solar kilns over an expected service life of 20 years, to illustrate the alignment of this financial analysis with the net energy analysis (Chapter 7), and to describe how these energy (Chapter 7) and financial (Chapter 8) comparisons differ for other cases.

8.2 Materials and methods

The materials and methods of this study are described in the following sections.

8.2.1 General overview of the life-cycle cash flow (LCCF) analysis

Life-cycle cash flow (LCCF) analysis, as carried out in this chapter, considers costs and benefits, in terms of both initial costs/benefits and future ongoing costs/benefits over a specified period of time. In the LCCF analysis, the time value of money has been taken into consideration for calculating the future ongoing expenses/benefits. This value of money decreases every year further into the future due to the return that is expected on investments. Future cash inflows and outflows have been estimated based on the current energy price with an appropriate estimate of future cost increases, and then discounted to

the present value by adopting an appropriate discount rate, as will be explained later in this chapter.

8.2.2   Initial cost estimation approach

The key initial costs of solar kilns are split into the materials costs and the labor costs in constructing the kilns. While the information on LCCF analysis for solar kilns is scarce in the literature, two commonly used life-cycle cost (LCC) approaches for built facilities (e.g. residential buildings) are RS Mean and Dodge Unit Cost Guide (Islam et al., 2015). However, these approaches are useful only in the North American regions (Ontario Construction Secretariat, 2001; Zachariah, 2003). In Australia, Rawlinsons Construction Cost Guides provide costs based on local average cost data. Quantity surveyors and construction cost consultants have been using this guide, especially for residential, small commercial and industrial projects, throughout Australia (Rawlinsons Group, 2014). Thus, the relevant cost factors have been collected, wherever appropriate, from this guide. The labor costs have been calculated based on the 2015 average labor pay rates in the building and construction industry from the Fair Work Ombudsman (2015). The material purchase prices have been collected from the relevant company websites, and then translated to their respective full costs by including the appropriate delivery and installation costs (please see Section 8.3.4).

8.2.3   Ongoing cash flows estimation approach

The ongoing cash flows of the solar kilns include the costs/benefits associated with the maintenance (e.g. material replacement costs, repainting costs of the absorbers, fan energy costs, and loading/unloading energy costs), the solar energy input, the useful energy for drying, and the energy losses from the kilns through conduction, convection, and radiation heat-transfer processes. By solving the drying and energy flow models, as described in

Chapter 4, the solar input to the kilns, the major energy losses from the kilns, and the energy used for the drying processes have been predicted over the analysis period of 20 yeras for the two kilns. These energy flows have been translated to their respective cash-flow values by using the current energy prices, and adopting an appropriate LCCF model, as will be described in Section 8.3. The electrical energy costs associated with the fan, and loading/unloading systems have also been estimated based on the local electricity utility rates from the Department of Energy and Water Supply (2015).

8.2.4 Key cash flow components for the solar kilns

Table 8.1 shows the key components of the overall cash flows around the solar kilns used in this study.

Table 8.1. Cash flows associated with the solar kilns.

Key cash-flow components	Sub cash flow components	Cash inflows/outflows
Initial costs	Material costs	- cash flows
	Labor costs	
Maintenance costs	Replacement costs	- cash flows
	Repainting the absorbers	
Thermal energy costs/benefits	Solar input	+ cash flows
	Energy losses	- cash flows
	Drying energy	+ cash flows
Electrical energy costs	Fan energy costs	- cash flows
	Loading/unloading energy costs	

The key cash outflows for the solar kilns included the costs associated with the requirements for the fan energy, the loading and unloading systems, the materials and maintenance, and the labor, as shown in Table 8.1. The initial costs were split into the material costs and the labor costs in constructing the kilns. The maintenance costs included the material replacement costs and the repainting of the absorbers over the kiln's service life of 20 years. The main energy inflow was the input solar energy, which was partly used for drying the timber (the useful energy), while the rest was lost (cash outflow) through conduction, convection and radiation heat-transfer processes. The benefit-cost ratio (*BCR*) of a solar kiln depends upon the cost effectiveness of the particular kiln design. The better the kiln design, the larger the proportion of energy used for drying (cash inflow) and the lower the energy losses (cash outflow) from the kiln.

8.3   Modelling and assumptions of the life cycle cash flow (LCCF) model

In the following sections, the life-cycle cash flow (LCCF) model, as used in this study, are described in detail.

8.3.1   LCCF model description: discounted cash flow (DCF) analysis

To construct and analyze a LCCF model for the solar kilns, a discounted cash flow (DCF) approach of valuing the future cash flows has been used in this chapter. In the model, all the relevant costs/benefits associated with the solar kilns have been calculated throughout the expected service life of 20 years. As mentioned before, the cash flows can broadly be categorized into two components, namely the materials and maintenance costs, and the energy costs/benefits. The drying energy, the energy losses from the kiln, and the solar input into the kiln have been predicted in this chapter by using a previously developed numerical simulation (Chapter 4) for a solar-kiln model. In this study, all these future energy quantities

have been translated to their respective monetary values by using the current energy prices, while the corresponding future cash flows (costs/benefits) have been calculated using Equation (8.1), with an appropriate inflation rate. After that, those future cash flows have been discounted using Equation (8.2) to their respective present values with a suitable discount rate, and then added up using Equations (8.3) and (8.4).

$$FC \; (FB) = PC(PB) * (1+i)^n \tag{8.1}$$

$$DPC \; (DPB) = \frac{FC \; (FB)}{(1+d)^n} \tag{8.2}$$

$$TPB = \sum_{n=0}^{N} \frac{FB_n}{(1+d)^n} \tag{8.3}$$

$$TPC = \sum_{n=0}^{N} \frac{FC_n}{(1+d)^n} \tag{8.4}$$

In equations (8.1) – (8.4), *FC* is the future cost, *FB* is the future benefit, *PC* is the present cost, *PB* is the present benefit, *i* is the inflation rate, *n* is the number of years into the project life, *DPC* is the discounted present cost, *DPB* is the discounted present benefit, *d* is the discount rate, *TPB* is the total present benefit, *TPC* is the total present cost, and *N* is the total analysis period (service life of the kiln in years). The inflation rate (*i*) used in this study was 3%, which was the average of the Australian inflation rate over the past 10 years (Inflation Rate, 2015). Following the recommendations made by Harrison (2010), the Australian Department of Infrastructure (Infrastructure Australia, 2008), and the Office of Best Practice Regulation of

Australian Government (Department of the Prime Minister and Cabinet, 2014), the discount rate (*d*) used in this study was 7, which was also used in Chapter 7. However, a sensitivity analysis with respect to the discount rates has been carried in this chapter, as there were some uncertainty associated with the discount rate. The key predicted thermal energy costs/benefits (i.e. drying energy, energy losses) were calculated both based on the local electricity (Department of Energy and Water Supply, 2015) and gas (Origin Energy, 2015) utility rates, assuming that the required energy for drying would be provided by either electricity or gas heating. These costs of electricity and gas included the unit prices and the daily service charges. For the simplicity and the scope of the study, the initial settlement costs (i.e. land, property taxes, and other fees), the plumbing costs, electrical wiring, were not included in this study, as they were assumed to be nearly similar for the solar kilns of the same load capacity. All the costs/benefits were calculated in Australian dollars.

8.3.2 Fan energy, loading/unloading energy, and labor costs

Two 0.25 hp electric fans were used to circulate the internal air through and around the timber stack. Since the fans are normally turned off during the night in wood-drying solar kilns, the electrical energy requirements for operating the fans were calculated by assuming that the fans were run for 12 hours per day.

The energy consumption of the loading and unloading system has been estimated for a typical electric powered fork-lift (4 wheel, 2 – 3.5 tonnes capacity). This calculation of energy was based on the average motor power (drive motor and lift motor) of 7.25 kW for a fork-lift of capacity 2-3.5 tonnes, as mentioned in Specifications of CAT Lift Trucks (Trucks, 2008). The average time for loading and unloading the kiln was assumed to be an hour, as mentioned in Solar Kilns (2014). Both the fan and loading/unloading energy costs were

calculated based on the current utility electrical energy prices from the Department of Energy and Water Supply (2015).

For the construction phase of the kilns, the approximate time to build, insulate, paint, and wire the solar kiln was assumed to be 60 hours, as mentioned by Bergman (2008). The total labor costs were calculated based on the average labor pay rates in the building and construction industries from the Fair Work Ombudsman (2015).

8.3.3 Material and equipment costs

A summary of the major materials and equipments required for the two kilns, together with their estimated basic costs, is given in Table 8.2.

Table 8.2 shows that the key construction difference between the two kilns is the materials used for the frames and the absorbers. Timber was used as the framing material for the Oxford kiln, whereas this material was aluminium for the Boral kiln. Aluminum and corrugated iron (zinc-coated) were the absorber materials for the Oxford and Boral kilns, respectively. These differences in the building materials between the kilns are reflected in the basic material costs for the two kilns (AU$ 890 and AU$ 1166 in the frames and absorbers, respectively, for the Oxford kiln, whereas these values were AU$ 613 kg and AU$ 2315, respectively, for the Boral kiln), as shown in Table 8.2. It should be noted here that the basic costs included only the purchase prices of the materials. However, in the life cycle cost analysis of this chapter, these basic costs were translated to their respective realistic costs by including appropriate delivery and installation costs. The delivery and the installation costs were assumed to be 10% of the purchase price and 40% of the delivered purchase price, respectively, as mentioned by Peters et al. (2003). A significant difference was identified in the material costs for the walls and roofs, and the floor between the two kilns

(AU\$ 1815 and AU\$ 705, respectively, for the Oxford kiln, and AU\$ 3183 and AU\$ 802, respectively, for the Boral kiln), despite using the same material for these components in both the kilns.

Table 8.2. Summary of the estimated materials and equipment costs for the two kilns.

Materials (components)	Quantity (kg)		Basic costs (AU\$)		References
	Oxford	Boral	Oxford	Boral	
Timber (lm)	146	-	890	-	(Barrenjoey, 2015)
Aluminium (kg)	500	263	1166	613	(Mundi, 2015)
Corrugated iron (kg)	-	1537	-	2315	(Metalroofing, 2015)
Polycarbonate sheets (kg)	1211	2123	1815	3183	(Construction & Real Estate, 2015)
Concrete (kg)	6612	7526	705	802	(Hanson Heidelberg Cement Group, 2015)
Painting material (litre)	2	3	110	165	(Masters Home Improvement, 2015)
Fans (number)	2	2	240	240	(Atwork Supplies, 2015)

One of the reasons for the higher material costs in the walls, the roofs, and the floor for the Boral kiln than in the Oxford kiln was the relatively increased use of polycarbonate sheets and concrete (due to the increased size/volume of Boral kiln) and the corresponding replacements of the polycarbonate sheets at year 10 into the kiln operational life. This situation was likely to increase the material costs for the Boral kiln. Due to the larger surface areas of the absorbers for the Boral kiln than those for the Oxford kiln, the painting cost was higher for the Boral kiln, as shown in Table 8.2. However, since two fans were installed in both the kilns, this equipment cost was the same for the two kilns.

8.4   Results and Discussion

The following sections describe the results and discussion of this chapter.

8.4.1 Simulated thermal and equivalent cash flows

The annual thermal energy flows around the solar kilns included the incoming flows of solar energy, heat energy used for drying, energy losses from the kilns through the heat-transfer processes. The estimated annual quantities of all these streams of energy, together with the electrical energy use for the fans and loading/unloading systems, are given in Table 8.3. These values of cash flows have been used in constructing the timeline of the cash flows for the two solar kilns. Table 8.3 shows that the predicted equivalent annual cash flows (or equivalents) of the incoming solar energy and the drying energy are larger for the Oxford kiln (AU$ 58, 989 and AU$ 22, 931, respectively) than those for the Boral kiln (AU$ 48, 893 and AU$ 17, 162, respectively), while the size of the annual energy loss costs for the Oxford kiln (AU$ 26, 777) was smaller than that for the Boral kiln (AU$ 29, 421).

Table 8.3. Predicted annual cash flows for the Oxford and Boral kilns.

Cash flow components	Oxford kiln	Boral kiln
Incoming solar energy benefits (AU$/year)	58, 989	48, 893
Fan energy costs (AU$/year)	1, 720	1, 729
Loading/unloading energy costs (AU$/year)	467	460
Energy losses costs (convection and radiation) (AU$/year)	26, 777	29, 421
Drying energy benefits (AU$/year)	22, 931	17, 162

These results indicate that the Oxford kiln is not only capable of capturing a larger amount of solar energy than the Boral kiln but of using a greater energy for drying purposes as well. One of the reasons for the greater energy capture in the Oxford kiln is probably due to the

differences in the solar collector areas and their orientations with respect to the sun. For the Boral kiln, the area of the horizontal absorber facing to the sky was calculated to be 11 m², while the combined area of perpendicular absorbers facing to the north and south was calculated to be 14 m². By contrast, the Oxford kiln has 25.7 m² of absorbers facing the sky (either horizontal or slightly inclined). Due to the vertical orientation of the north and south absorbers in the Boral kiln, the absorbers' areas were likely to be used less effectively to collect the solar radiation. The electrical energy costs associated with the operation of the fans and the loading/unloading system were not significantly different between the two kilns, mainly due to the small difference both in the operating hours for the fans and the requirements of the loading/unloading activities between the two kilns.

8.4.2 Major undiscounted life-cycle cash flows

The major undiscounted life cycle (over 20 years) cash inflows (the red columns) and outflows (the black columns) for the two kilns are shown in Figure 8.1.

Figure 8.1 shows that the overall life-cycle cash-flow values of the materials and labor, the fans, and the loading/unloading system were very small compared with the sizes of the other cash flows (i.e. solar input, drying energy, and energy losses) for both the kilns. The size of the lifetime cash inflows (benefits) due to the useful drying energy for the Oxford kiln (AU$ 458,000) was larger than that for the Boral kiln (AU$ 343,000). By contrast, the size of the cash outflows caused by the energy losses from the kilns was smaller for the Oxford kiln (AU$ 535,000) than that for the Boral kiln (AU$ 588,000).
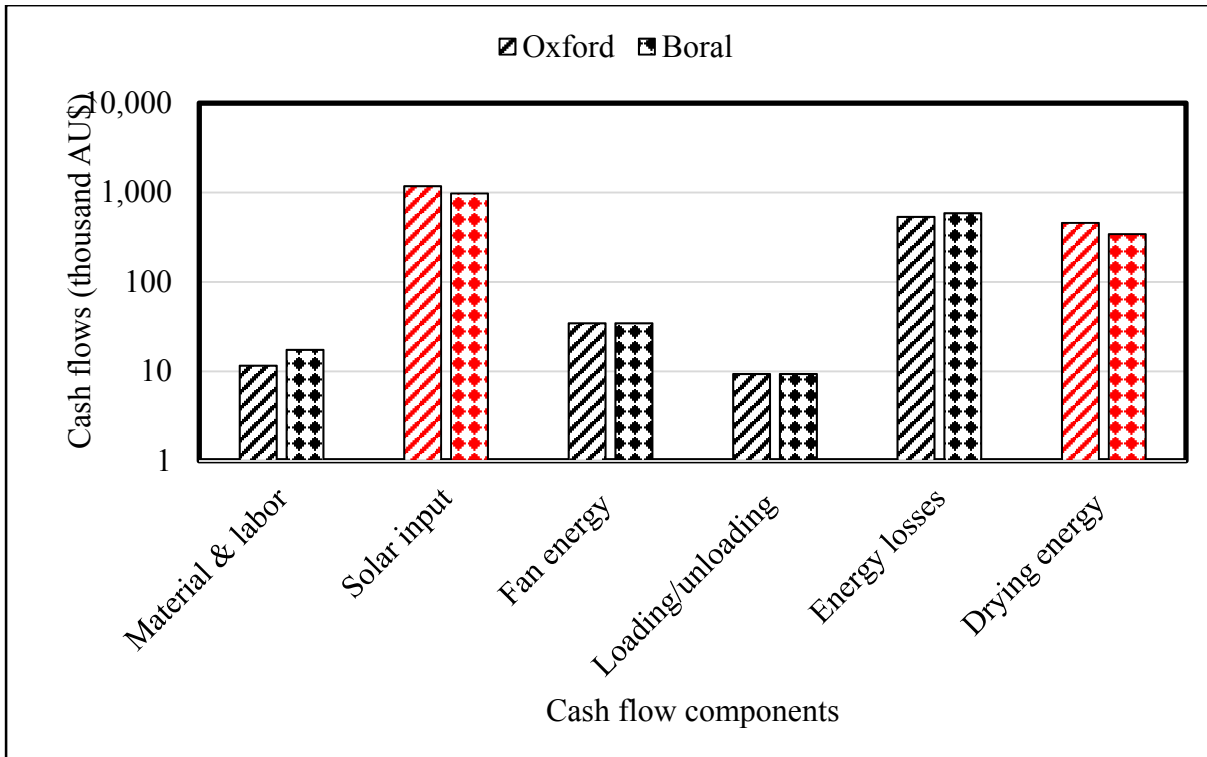
Figure 8.1. Total life cycle undiscounted cash flows for the Oxford and Boral kilns (log

scale on vertical axis).

The costs associated with the materials and labor were also lower for the Oxford kiln (AU$

11,000) than that for the Boral kiln (AU$ 17,000), as shown in Figure *8.1*. Reviewing all these

individual values, as shown in Figure 8.1, of the life cycle cash flows, the Oxford kiln was

likely to be superior to the Boral kiln on the basis of life cycle economic returns.

8.4.3 Overall LCCF analysis

The parameters considered for the LCCF analysis in this chapter and their respective values

per unit service output (i.e. m^3 dried timber) for the two solar kilns over a lifetime of 20

years, are given in Table 8.4. It shows that the net present cash benefits (*NPCB*s) per m^3 of

dried timber were positive for both the Oxford and Boral kilns, which imply that both the

kilns were feasible for drying purposes in monetary terms. However, the *NPCB* for the Oxford

kiln (AU\$ 230) was larger (38%) than that for the Boral kiln (AU\$ 142).

Table 8.4. The key LCCF analysis values per m^3 of dried timber for the Oxford and Boral kilns

over a service life of 20 years.

Parameters	Oxford	Boral	% difference[14]
Net present cash benefits (NPCB) (AU\$)/m^3 of timber	230	142	+38
Present energy losses costs (PELC) (AU\$) m3 of timber	211	260	-23
Present drying energy benefits (PDEB) (AU\$)/m3 of timber	180	152	+16
Present fan energy costs (PFEC) (AU\$)/ m3 of dried timber	13	13	0
Present loading/unloading costs (PLC) (AU\$)/ m3 of dried timber	3.7	3.68	0.55
Present material & labor costs (PMLC) (AU\$)/ m3 of dried timber	6.10	10.12	-66

[14]% change = [(Oxford – Boral)/Oxford*100]

The net cash benefits were calculated by subtracting the cash outflows (material & labor

costs, fan energy costs, loading/unloading energy costs, energy-loss costs), from the

equivalent monetary energy benefits (input solar energy). When mutually exclusive projects

have been considered, as in this work, the project that maximizes the NPCB should be chosen,

as suggested in many energy and economic analysis guidebooks/studies (Cleveland, 2013;

Commonwealth of Australia, 2006; Heun and de Wit, 2012). Thus, the larger *NPCB* for the

Oxford kiln indicates that the Oxford kiln is more desirable than the Boral kiln over the

analysis period of 20 years. This favorable feature of the Oxford kiln is also reflected in the individual present values, as given in Table 8.4, for the fan energy costs, the loading/unloading energy costs, the drying energy benefits, the material & labor costs, and the energy losses costs. While the present values of material & labor costs and energy losses costs (major losses) per m^3 of dried timber were smaller for the Oxford kiln (AU$ 6.10 and AU$ 211, respectively) than those for the Boral kiln (AU$ 10.12 and AU$ 260, respectively), the present value of drying energy was larger for the Oxford kiln (AU$ 180) than that for Boral kiln (AU$ 152). These monetary values indicate that not only is more money required for constructing and operating the Boral kiln, but the Boral design also loses more energy than the Oxford kiln, which would otherwise be used for drying timber. The 16% higher drying energy benefit for the Oxford kiln compared with the Boral kiln, as shown in Table 8.4, implies that Oxford kiln is more economical overall than the Boral kiln for hardwood timber drying.

8.4.4 Economic and environmental benefits

The economic and environmental benefits, both in terms of electricity and gas costs, for the Oxford and Boral solar kilns have been given in Table 8.5.

Table 8.5 shows that both the Oxford and Boral solar kilns represent a saving, not only in the running costs (drying energy cost) for the kilns, but also a saving in the amount of greenhouse gas (GHG) emissions from the timber-drying process. The savings in GHG emissions, compared with electrically-heated kilns, are 6.54 kg and 5.47 kg of CO_2-e per m^3 of dried timber per year for the Oxford and Boral kilns, respectively, as shown in Table 8.5. These savings in the GHG emission emissions are 3.74 kg and 3.13 kg of CO_2-e, respectively, when compared with gas-fired kilns. Timber NSW (Australian Bureau of Agricultural and

Resource Economics and Sciences, 2012b) have mentioned that the annual volume of hardwood saw logs processed by NSW sawmills was 772,000 m³

Table 8.5. Energy and GHG emissions savings in timber drying for the Oxford and Boral kilns.

Items	Oxford		Boral		%
	Electricity	Gas	Electricity	Gas	Difference[15]
Drying cost saving (AU$/ m³ year)	9	2.2	7.6	1.88	+16
CO_2 savings (kg CO_2-e/m³ year).	6.54	3.74	5.47	3.13	+17
Drying cost saving AU$/ year (NSW 2012)	2.78 million	0.68 million	2.34 million	.58 million	+13
Equivalence of GHG savings (car/year)	767	438	641	220	+16
Equivalence of GHG savings (houses/year)	386	220	323	111	+16

[15]% change = [(Oxford – Boral)/Oxford*100]

It was also mentioned that NSW accounted for 40% of the total hardwood sawlogs processed and supplied within Australia in 2012-2013. These values for hardwood timber demand in NSW indicate that, by operating solar kilns for hardwood drying, an approximate GHG emission savings of 2019 tonnes and 1689 tonnes (on the basis of electricity heating) and 1154 tonnes and 966 tonnes (on the basis of gas heating) per year for the Oxford and Boral kilns, respectively, could be obtained in NSW alone. These values of GHG emissions saving

for the Oxford and Boral kilns are equivalent to taking 767 and 641 (when compared with electrically-powered kilns) and 438 and 220 (when compared with gas-fired kilns) passenger cars, respectively, off the NSW roads per year or taking 386 and 323 (when heat is provided by electricity) and 220 and 111 (when heat is provided by gas) standard family houses off the NSW electricity grid per year for the Oxford and Boral kilns, respectively. This is a significant environmental benefit of solar kiln technology in the timber industry.

In calculating these equivalents, the CO_2 emissions from cars have been collected from the National Average Carbon Emissions (NACE) data supplied by the Australian Federal Chamber of Automotive Industries (2011). The average distance travelled by a passenger car per year in Australia has been assumed to be 14,000 km, as mentioned in the Survey of Motor Vehicle Use (SMVU) (Australian Bureau of Statistics, 2012b). This survey was carried out by the Australian Bureau of Statistics (ABS) over the period 1 July, 2011 to 30 June, 2012. The equivalent number of family houses have been calculated from the Household Energy Consumption Survey (HECS) data (Australian Bureau of Statistics, 2012a), which was 1223 kWh per week or 17.47 kWh per day. Table 8.5 also shows that solar kilns are likely to save the timber customers AU$ 9 and AU$ 7.6 per m^3 of dried timber for the Oxford and Boral kilns, respectively, in electricity costs per year. In addition to the savings in the drying energy costs and GHG emissions (environmental benefits) for the solar kilns, cyclic drying (as done in solar kilns) improves the quality (less degrade) of the end-use timber (Helwa et al., 2004; Chadwick and Langrish 1996; Langrish et al.,1992). This feature is also reflected in Figure 4.4, where the strain developed within the timber during drying is predicted to be way below the maximum permissible value of 0.02 m/m.

However, these savings become smaller (i.e. AU\$ 2.2 and AU\$ 1.88 for the Oxford and Boral kilns, respectively) when compared with the gas-fired kilns, as gas is cheaper than electricity in Australia. The equivalent savings in drying energy costs for the solar kilns have been based on the local electricity (Department of Energy and Water Supply, 2015) and gas (Origin Energy, 2015) utility rates, assuming that drying energy would be provided by either by electricity or gas heating. Both the unit prices and the daily service charges have been included in these cost calculations. The overall cost estimates represent a saving of AU\$ 2.78 and AU\$ 2.34 million (based on electricity) and AU\$ 0.68 and AU\$ 0.58 million (based on gas) per year if using the Oxford and Boral kilns, respectively, throughout NSW. While the timber industry underpins important demand and supply relationships with the Australian design, manufacturing, construction, and properties sectors, the timber export trade was relatively small compared with products imported into Australia, as mentioned in Timber NSW (2013). In this situation, there is a key need to focus attention into solar kiln deployment for timber processing in Australia.

8.5   Sensitivity analysis

In this section, the impact of the discount rate on the key financial parameters for the two kilns has been analyzed. As mentioned in Section 8.3, there are some uncertainties associated with the discount rate (d). An appropriate response to these uncertainties around the discount rate is to conduct a sensitivity analysis, which has been done in this section. A detailed discussion on the discount rates has been included in Section 7.5.7.2 of Chapter 7. In Australia, some agencies, including the Commonwealth's Office of Best Practice Regulation, recommend discount rates around 7%. For example, the NSW Treasury recommends using a real rate of 7%, with sensitivity tests using 4% and 10%, as mentioned

by Harrison (2010). A 7% discount rate has been used in the cost-benefit analysis, as carried out by the Office of Best Practice Regulation from the Department of the Prime Minister and Cabinet (2014). Infrastructure Australia (2008) recommended that any cost-benefit studies submitted to it should use 'real risk free' discount rates of 4, 7 and 10 per cent. Reviewing all these recommendations, a sensitivity analysis with discount rates of 4% and 10% around the base discount rate of 7% has been carried out in this chapter. The results for the sensitivity analysis with respect to these three different discount rates (4%, base case, and 10%) have been given in Table 8.6.

The value of the discount rate had a significant effect on the net present cash benefit (NPCB), as shown in Table 8.6. The NPCB increased (from AU$ 230 to AU$ 306 and from AU$ 142 to AU$ 190 for the Oxford and Boral kilns, respectively) and decreased (from AU$ 230 to AU$ 180 and from AU$ 142 to AU$ 110 for the Oxford and Boral kilns, respectively) when the discount rate decreased (from 7% to 4%) and increased (from 7% to 10%), respectively.

Table 8.6. Effects of discount rate on the key parameter values per m^3 of dried timber.

Parameters	Discount rate (4%)		Discount rate (7%) (base case)		Discount rate (10%)	
	Oxford	Boral	Oxford	Boral	Oxford	Boral
NPCB (AU$)	306	190	230	142	180	110
PDEB (AU$)	238	200	180	152	141	119
BCR	11.74	6.11	11.38	5.82	11	5.52

These changes in NPCB were expected, since the future cash streams increased in value when the discount rate decreased and vice versa. For the same reason, the present drying energy benefit was also significantly affected by the discount rate, as shown in Table 8.6. However, the benefit cost ratio (BCR) was only slightly affected by the discount rate. One of the reasons

for this situation is that both the cash inflows (benefits) and outflows (costs) were adjusted to their respective present values with the same discount rate. Thus, as shown in Table 8.6, the BCR was not changed significantly with the changes made in the discount rate value. It should be noted here that any variation made in the discount rate did not alter the ranking of the kilns - the Oxford kiln is more beneficial economically than the Boral kiln, as shown in Table 8.6. Hence the general conclusion of this chapter is relatively insensitive to the uncertainty associated with the discount rate.

8.6   Alignment with the life-cycle net energy (LCNE) analysis

Like most of the other renewable energy technologies, investment in solar drying systems always involves uncertainty over the future return from the investment, because both future energy and carbon prices are unpredictable, which lead to uncertain cash flows for the project return. The technique of LCCF analysis, as used here, can partially take the risks and the uncertainties associated with future currency-values into account by using different discount rates. However, it still involves at least two problems. Firstly, the forecast of future cash flows is uncertain (due to the uncertain energy and carbon prices), which has been assumed in the LCCF model. Secondly, it is difficult to determine the most appropriate discount rate or cost of capital. Users of the discounted cash flow (DCF) methodology argue that the uncertainties around the future cash flows can be addressed by raising the discount rates (Blyth et al., 2007). However, there is no clear methodology available to justify to what extent the discount rates will really incorporate all the future risks (Yang and Blyth, 2007).

The key performance parameter, the net present cash benefit (NPCB), in the LCCF model, as presented in this chapter, for energy-intensive projects is highly dependent on energy prices. If energy prices increase significantly, the NPCB of these projects will drop rapidly. However,

the project that produces the most net present energy value (Chapter 7) would still become the most profitable project, irrespective of the energy price changes. Thus, the net energy approach of evaluating the life-cycle performance for solar dryers has been suggested in this research. It should be noted here that, for the two solar kilns studied in this thesis, both the net energy (Chapter 7) and cash flow (Chapter 8) analyses are very closely aligned, as they have led to the same conclusion that the Oxford kiln is more profitable and energy-efficient than the Boral kiln. However, in some other cases, these two perspectives can be significantly different.

Generally, in designing solar kilns, the higher the complexity of the kiln, the lower the energy that is needed to operate it or the lower energy losses from the kiln. However, at the same time, manufacturing a sophisticated kiln costs more than a simple kiln. Using engineering economics based on current energy prices (i.e. LCCF model), designers/manufacturers may optimize the system to have the largest NPCB over the life of the project. As a result, they are likely to choose a simpler design with higher energy losses, but lower initial capital costs. The resulting system will consume more energy to operate, but the presently-valued cost of that energy would be less than the increased cost associated with manufacturing the sophisticated kiln. This project would be profitable only in terms of the current energy price, which has been used in the LCCF model. If the prices of energy change during the life of the project, the original calculation is likely to be incorrect. With higher energy prices, the presently-valued cost of the operating energy is likely to be greater than the initial cost of the sophisticated kiln. In such a situation, the project will end up costing more energy and money than if it was originally designed to maximize the net present energy (Chapter 7), as shown Figure 8.2.

In this example, rather than looking at the cost of the sophisticated kiln, energy engineers would study the energy invested in the kiln in order to design a system that makes the most sense from an energy point of view, and this approach is not so strongly dependent on the price of energy. This criterion is the net present energy value, not the net present economic value that should be used in choosing any long-lasting and energy-intensive project.
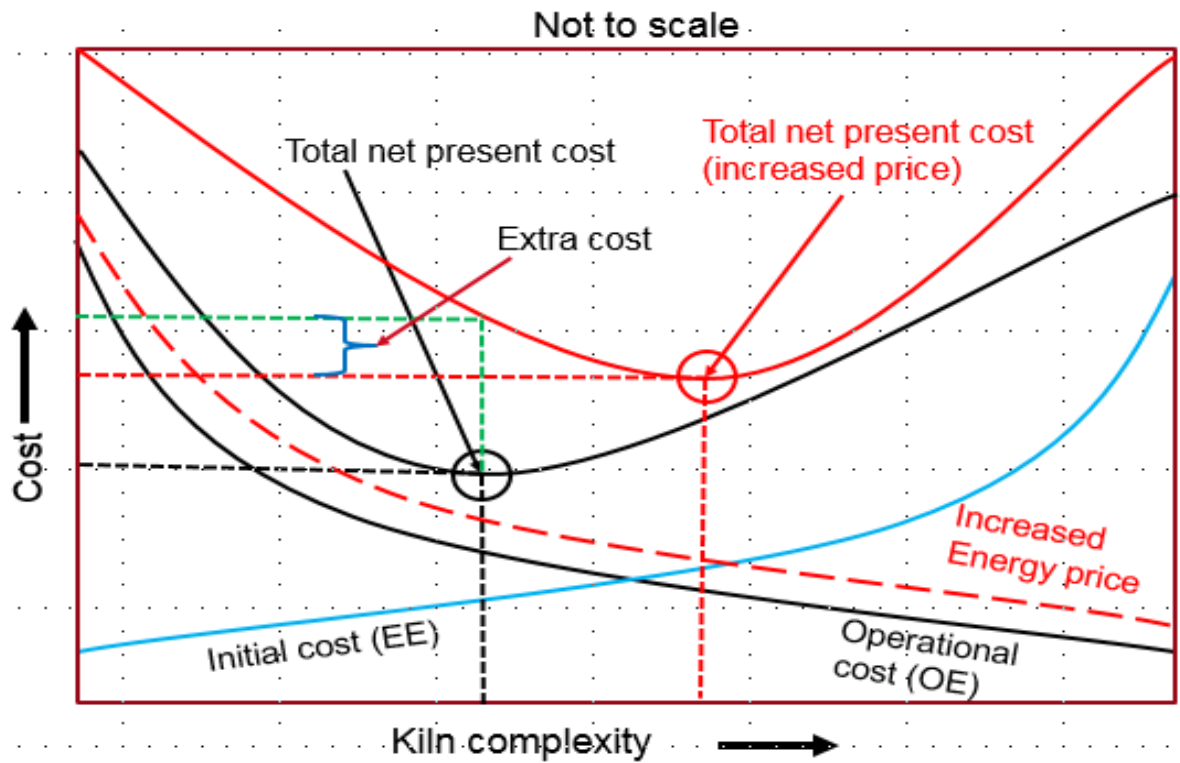
Figure 8.2. Effects of increased energy prices on the overall cost (schematic) diagram.

Thus, the general recommendation of this thesis is that, where the energy flow patterns and the design parameters of the alternative solar kilns are significantly different, the life-cycle net energy (LCNE) model (Chapter 7), instead of LCCF model (Chapter 8), should be used for choosing, decision making, and assessing the performance of solar kilns.

8.7   Conclusions

A life-cycle cash flow (LCCF) analysis has been carried out for two designs of solar kilns over a service life of 20 years by using the model-predicted future cash flows, together with the material and labor costs. The general results indicated that the presently-valued drying energy benefits and the net energy cash benefits were larger for the Oxford kiln than those for the Boral kiln, by approximately 16% and 38%, respectively. However, the present material & labor costs and the energy losses costs were smaller for the Oxford kiln by 66% and 23%, respectively, than those for the Boral kiln. It was also found that the hardwood industry could save AU$ 2.7 and AU$ 2.34 million per year (based on 2012 data) if using the Oxford and Boral kilns, respectively, throughout NSW, Australia. The GHG emissions saving for the Oxford and Boral kilns were found to be equivalent to taking 13238 and 10996 passenger cars, respectively, off the NSW road per year, or taking 5060 and 4203 standard family houses off the NSW electricity grid per year for the Oxford and Boral kilns, respectively. The sensitivity analysis showed that, although the net present cash benefits were significantly affected by the discount rates, the financial ranking of the kilns (Oxford is more cost effective than Boral) was relatively insensitive to the uncertainty associated with the discount rate. Although, for the two kilns studied in this thesis, the LCCF and the LCNE models have resulted in a similar ranking of the kilns, this assessment can be significantly different for some other cases, especially when the energy flow patterns and the design variables between the kilns vary significantly. In summary, the Oxford kiln was likely to be more productive, and economically viable, than the Boral kiln for hardwood-drying industries. In the next chapter, the overall conclusions of this thesis and the recommendations for future works are described.

Chapter 9   Conclusions and future work

9.1   Conclusions

The overall findings and conclusions of this thesis, together with the new knowledge generated by this research, are presented as follows:

- General information and opportunities of solar kilns: The background and motivation, the problem statement and research questions/gaps, and the objectives of this research have been described in Chapter 1. The first aim of the thesis was to identify and discuss the future opportunities of solar kilns for reducing the operating costs and GHG emissions in the context of Australian agricultural and forest industries, which have been the subject matter of Chapter 2. It has been estimated that a group of ten selected fruits and vegetables have the potential of contributing 64% to the overall savings (i.e. drying costs and GHG emission savings for drying of fruits, vegetables, and timber), while this estimate was 36% for the total timber in Australia that are likely to be dried. A relatively high average initial MC for fruits ($\sim$ 81%) and vegetables ($\sim$ 78%) compared with hardwood ($\sim$50%) contributed to the greater energy requirements for drying these food products. These differences in the estimated drying costs and GHG emissions savings between the agricultural and timber industries indicate that, along with the timber industry, a promising field for solar kilns also exists in the Australian agricultural industry. It has been concluded in Chapter 2 that research, innovation, and investment in the development of solar kiln technology are necessary in order to secure a smooth food supply system throughout Australia, increase the profitability for the food processing

industry both in the domestic as well as international markets, increase access to export markets, decrease existing imports for processed food products in Australia.

- Drying models and data description: One of the key objectives of this research was to develop a robust mathematical model, together with a simulation procedure, that is capable of predicting the key operational energy flows of solar kilns in a range of geographical and climatic conditions. The development of this mathematical model, together with its numerical simulation procedure, has been described in Chapter 4, while the key properties (physical, mechanical, and transport) of wood during drying have been discussed in Chapter 3. This chapter also reviews different drying models (e.g. empirical, diffusion, and multi-mechanism), and explains the general considerations in selecting an appropriate drying model. The climatic data required for the energy flow model, together with their sources, have also been described in Chapter 3.

- Prediction of performance with different geographical and climatic conditions: The numerical simulation of the kiln model has been found to be robust in predicting the behavior of a kiln design (i.e. Oxford kiln) for drying hardwood timber in different geographical and climatic conditions for Australia. For hardwood timber, the prospect of better productivity, together with an acceptable level of strain in the dried timber, has been predicted to be higher if the kiln could be located in Brisbane, Australia. The maximum strain level has been predicted to be 0.0075 m/m (significantly less than the failure value of 0.02 m/m) in this location. The effects of the predicted sky temperatures (corresponding to different correlations) on the radiation and convection losses have been analyzed and predicted to have a significant impact on the convection and radiation losses. The correlation for the sky temperature, as used by Adelard et al. (1998), has been

found to give the lowest predicted radiation losses from the kilns for the studied climatic conditions. The moisture-content distribution profiles at different stages of drying were also predicted and found to be consistent with those suggested earlier by other researchers to give low timber degrade. The internal drying conditions for the selected sites were also found to be acceptable for drying hardwood timber. The key knowledge/skill developed here was to deal with numerical stability by adjusting the algorithm and parameters of "ode" solver in Matlab environment.

- Comparison of operational performance: In Chapter 5, the model and its simulation procedure have been used as a tool to compare the operational performance between two different solar kiln designs (i.e. Oxford and Boral). This comparison has been made on the basis of the same timber load capacity of 10 cubic metres. The results have shown that the Oxford design is likely to produce faster drying rates (lower drying times required) and relatively smaller energy losses (by radiation and convection) than those for the Boral kiln. There were no significant differences predicted in the timber quality between the two designs. The Oxford design was also predicted to receive a relatively larger amount of solar energy (compared with the Boral kiln) for a given geographical location (here Brisbane in Australia). The capability of the model of accommodating the seasonally varying boundary conditions has also been discussed. The predicted results for the different seasons of the year (summer, spring, and winter, 2013) have shown that the Oxford kiln is consistently better than the Boral kiln throughout the year in terms of the drying times, solar gains, and the major energy losses (convection and radiation). However, two important embodied impacts (i.e. embodied energy and embodied carbon) of the solar kilns have not been included in the comparative study described in Chapter

5. The key contribution of this section of the thesis was to enhance the understanding of how the model can be solved for different designs of solar kilns and how to define a common basis when a comparison is made between them.

- Embodied energy and carbon analysis: The analysis of the life-cycle embodied energy (EE) and embodied carbon (EC) for the two solar kiln designs has been presented in Chapter 6. The general results indicated that both the life cycle EE and EC associated with the Oxford kiln were lower than those associated with the Boral kiln. Overall, the walls, the roofs, and the absorbers for the Oxford kiln were found to be the main contributors (above 90%) to both the EE and EC associated with the Oxford kiln, with the frames and floor having individually small effects (less than 20%) on the overall value. However, the frames for the Boral kiln contributed more than 17% to both the EE and the EC. A sensitivity analysis was carried out, which showed that the main trends in the results obtained from the EE and EC analysis were relatively insensitive to various uncertainties around the replacement schedules, the transport distances, and the kiln service lives. The assessment of the use of alternative materials for the two solar kilns suggested that, in order to reduce the embodied impacts (i.e. EE and EC) for the two kilns, the frames for the Boral kiln should be constructed with timber while corrugated iron (zinc-coated) should be used as the absorber material for the Oxford kiln. In general, the Oxford kiln was found to have 37% and 43% lower life cycle embodied energy and embodied carbon values, respectively, than the corresponding values for the Boral kiln. The realization of the importance of considering the embodied energy in a life-cycle energy assessment and the development of a LCA model for solar kilns by using "SimaPro" software have been the key knowledge/skills generated in this section of the thesis.

- Life-cycle net energy (LCNE) analysis: A novel life-cycle net energy analysis of solar kilns has been presented in Chapter 7. The general results indicated that the *NPEV*, the *NBLR*, and the *IRR* were larger for the Oxford kiln than those for the Boral kiln, by approximately 37%, 55%, and 47%, respectively. However, the *DEPP* and the present value of energy losses (*PVEL*) were smaller for the Oxford kiln by 85% and 24%, respectively, than those for the Boral kiln. The sensitivity analysis showed that, although the *NPEV* was significantly sensitive to the discount rates, the ranking of the kilns (Oxford is superior to Boral) has been relatively insensitive to the uncertainty associated with the discount rate not only in terms of the *NPEV*, but also in terms of other decision-making parameters, such as the *NBLR*, IRR, and the DEPP. The overall LCNE analysis results indicated that the Oxford kiln design was likely to be more productive and energy efficient than the Boral kiln design for the purpose of solar-assisted hardwood-drying processes. The key design features that have made the Oxford kiln the better choice for hardwood drying were likely to be the more effective orientation of the absorbers with respect to the sun and the lower total volume requirements for a given load capacity than the Boral kiln. The key knowledge generated here is that, since the total life-cycle energy use in solar kilns is the sum of the EEs and the total on-going OEs consumed over the whole operational life, and since different solar dryers have energy streams that are spread out differently over their entire service life, combining the EE (capital cost) with the annual, on-going operating energy (costs) for wood-drying solar kilns can potentially provide with a reliable and robust technique to assess the relative performance of different kiln designs.

- Life-cycle financial analysis: In order to evaluate the overall life cycle economic and the environmental performance of the solar kilns, there is a key need to analyze the total

energy costs/gains (the capital energy and the annual, on-going operating energy costs/savings), together with the GHG emissions savings, associated with solar-kiln operations for drying processes. These economic and environmental aspects of solar kilns for wood drying have been addressed by carrying out a life cycle-cash flow (LCCF) analysis in Chapter 8. The alignment of this financial analysis (Chapter 8) with the net energy analysis (Chapter 7) and how these energy (Chapter 7) and financial (Chapter 8) comparisons can vary significantly for other cases have also been described in Chapter 8. The general results indicated that the presently-valued drying energy benefits and the net energy cash benefits were larger for the Oxford kiln than those for the Boral kiln, by approximately 16% and 38%, respectively. However, the present material & labor costs and the energy losses costs were smaller for the Oxford kiln by 66% and 23%, respectively, than those for the Boral kiln. It was also found that the hardwood industry could save AU$ 2.78 and AU$ 2.34 million (based on electricity) and AU$ 0.68 and AU$ 0.58 million (based on gas) per year (based on 2012 data) if using the Oxford and Boral kilns, respectively, throughout NSW, Australia. These values of GHG emissions saving for the Oxford and Boral kilns are equivalent to taking The GHG emissions saving for the Oxford and Boral kilns were found to be equivalent to taking 767 and 641 (when compared with electrically-powered kilns) and 438 and 220 (when compared with gas-fired kilns) passenger cars, respectively, off the NSW roads per year or taking 386 and 323 (when heat is provided by electricity) and 220 and 111 (when heat is provided by gas) standard family houses off the NSW electricity grid per year for the Oxford and Boral kilns, respectively. The sensitivity analysis showed that, although the net present cash benefits were significantly affected by the discount rates, the financial ranking of the kilns

(Oxford is more cost effective than Boral) was relatively insensitive to the uncertainty associated with the discount rate. In summary, the Oxford kiln was likely to be more productive, and economically viable, than the Boral kiln for hardwood-drying industries. It was also illustrated that, although, for the two kilns studied in this thesis, the LCCF and the LCNE models have resulted in a similar ranking of the kilns, this assessment can be significantly different for some other cases, especially when the energy flow patterns and the design variables between the kilns vary significantly. Thus, the life-cycle net energy approach (which is not strongly dependent on the future uncertain energy prices, as proposed in Chapter 8), together with the defined PVPIs, has been suggested as a robust method for life-cycle performance evaluation of solar kilns. The main contribution of this section of thesis to the new knowledge is to answer the question that is only the technological innovation important or a change in the way people think can be even more important.

9.2 Recommendations for future works

For future research in this field, the following recommendations are made:

- Since a good level of detail regarding solar kiln designs, dimensions, construction materials, and operating principles is required for the life-cycle net energy, financial, and environmental analyses, as presented in this thesis, and since they are not generally available in the literature, two case-study solar kiln designs have been thoroughly analyzed in this research. Further works on other designs of kilns (e.g. Gough design) can be undertaken to develop more reference case studies, which will increase the confidence of the kiln manufacturers/designers for making more informed design

decisions for solar kilns. These works may involve the collection of the information on the design parameters (e.g. variables and dimensions), the construction materials, the operating variables, and the operating principles of the associated kilns, and the application of the models and methods proposed in this thesis for evaluating the life-cycle performance of solar kilns.

- Optimisation of kiln designs, by adjusting the design parameters (e.g. dimensions and variables), in order to maximize the life-cycle energy benefits (as described in Chapter 7) or life-cycle economic return (as described in Chapter 8) would be a promising and immediate research work.

- In this thesis, the performances of different solar kilns have been analysed in terms of the life-cycle energy benefits (Chapter 7), the life-cycle financial benefits (Chapter 8), and the life-cycle environmental benefits (Chapters 6 and 8). However, for these analyses/models to become more adaptable for the kiln manufacturers and designers, a multi-objective optimization (MOO) framework could be developed in the future for optimizing the kiln designs through a combination of the presented analyses/models (i.e. energy, economic, and environmental). In MOO, there does not normally exist a single solution that simultaneously optimizes each objective, as it is a particular challenge to minimize or maximize contradictory objective functions simultaneously. In such a situation, there exists a (possibly infinite) number of optimal solutions. To deal with such difficulties, in a MOO framework, the optimal decisions are taken in the presence of trade-offs between the conflicting objectives. In the case of solar kilns, maximizing energy benefits while minimizing costs and environmental impacts is an example of a MOO problem involving three objective functions. This approach of multiple-criteria decision-

making process would give a more useful tool for the decision makers to quantify the trade-off relationships in satisfying different objectives, and/or to predict an optimal design amongst a wide variety of designs by satisfying the subjective preferences of a human decision maker.

- A computational fluid dynamics (CFD) study may also be carried out to visually analyze the flow phenomena (e.g. distribution of the air velocities and the temperatures) inside the solar dryers. The efficiency of a solar kiln is mainly depended on the distribution of the thermal and flow fields inside the kiln. The modelling features of different softwares (e.g. Matlab for solving the ODE equations, CAD for geometry creation, and ANSYS-Fluent for simulating the velocity, humidity, and temperature distributions) can be applied for this purpose. The airflow and heat transfer distributions could be analyzed by CFD tools under different operational modes, such as varying positions of the fans in a solar kiln in order to get more uniform temperature and airflow distributions. This approach of visual simulations may give further insights into the design optimization of solar kilns, which would not otherwise be identified. For example, the presence of high temperatures in a low-velocity region or vice versa is an indication of poor design/operation. This situation can best be analyzed/identified by using a CFD simulation tool.

- Another potential work would be the consideration of scalability in the design/optimization process for solar kilns. In this process of kiln design, the key answers to be addressed may include: (a) What is the potential market size of the kilns based on a given supply and demand situation? (b) One large centralized kiln or multiple small distributed kilns? (c) What will be the load capacity strategy – lead, follow/adjustment, or lag? Lead capacity strategy is a proactive approach of adding

capacity in anticipation of an increase in demand. This is an aggressive strategy with the objective of improving the service level, decreasing the lead time, and reducing the stock-out costs. Follow/adjustment strategy refers to adding or reducing capacity in small or large amounts due to changing consumers' demand or due to major changes in the product or system architecture. Lag capacity strategy involves adding capacity only when the firm operates at full capacity or beyond due to increase in product demand. This is a reactive approach that adjusts its capacity in response to demand. Thus, a lag strategy is a conservative strategy that reduces the risk of waste, but may lead to the loss of potential buyers either by stock-out or poor service levels.

- Finally, a comparison study can be conducted to examine the difference between solar kiln drying and traditional controlled kiln drying of hardwood timber.

Appendices

5.5   Appendix 3A

The daily average climatic data for the spring season (September and October, 2013) of Brisbane in Australia [data extracted from the Australian Bureau of Meteorology (Meteorology, 2013)].

Date	September (2013)			October (2013)		
	Temperature (K)	Velocity (m/s)	Humidity (%)	Temperature (K)	Velocity (m/s)	Humidity (%)
01	296.9	2.777778	53	299.55	2.777778	61.5
02	294.55	2.361111	59	298.65	2.361111	50
03	293.9	2.916667	57.5	302	2.638889	37.5
04	294.35	2.638889	48	294.75	2.638889	34
05	294.5	1.527778	51.5	296.75	2.083333	44
06	294	1.805556	55.5	300.1	2.361111	44.5
07	294.9	1.527778	58.5	302	1.527778	41
08	295.85	1.805556	56	297.85	2.361111	55.5
09	295.9	1.527778	53.5	296.6	2.083333	47.5
10	296.05	1.805556	63	298.25	2.638889	52
11	298	1.25	51.5	301.7	2.361111	43
12	297.45	2.916667	55	298.5	3.055556	68.5
13	296.85	3.333333	59	299.8	3.055556	52
14	297.25	3.055556	71	299.75	3.055556	20
15	298.05	2.222222	50	297	2.083333	46.5
16	292.95	2.777778	80	296.75	3.055556	52.5
17	298.5	2.083333	60	298.5	3.333333	52.5
18	299.6	2.638889	31.5	294.3	1.805556	80
19	299.05	2.083333	56	297.65	3.055556	50
20	299.1	3.055556	24	297.25	3.333333	62
21	296	2.083333	37.5	298.85	2.083333	55.5
22	295.9	1.805556	57	298.5	2.5	54
23	297.65	1.805556	56	299.5	3.055556	56
24	299.8	2.361111	50.5	301.4	1.527778	45.5
25	301.65	2.361111	37	296.9	4.722222	55.5
26	299.35	1.527778	67	299.75	2.083333	52.5
27	298.55	5.416667	48	297.75	3.611111	52.5
28	295.4	1.388889	67.5	297.65	2.777778	58
29	299.15	3.194444	53.5	298.4	3.055556	65.5
30	296.9	1.805556	64.5	296.8	3.888889	59
31	-	-	-	297.05	3.333333	54.5

5.6 Appendix 4A

Drying model

$$\frac{\partial X}{\partial t} = \frac{\partial}{\partial z}\left(D\frac{\partial X}{\partial z}\right)$$ Fick's Law for mass transfer (moisture transport)

$$D = D_r exp^{-\left(\frac{D_E}{T}\right)}$$ Diffusion coefficient (temperature dependent)

$$\rho_t C_{pt}\frac{\partial T}{\partial t} = \frac{\partial}{\partial z}\left(\frac{K\partial T}{\partial z}\right)$$ Fourier's Law (thermal diffusion inside the board)

$$Q = h(T_A - T_S) - (\lambda_w + \lambda_S)J$$ Surface transport

$$J = \beta(Y_{TS} - Y_A)$$ Mass flux from the board

Energy and mass flow model

$$\frac{dT}{dt} = \left(\frac{1}{m.C_p}\right) * net\ energy\ flow\ towards\ any\ component$$ For energy balance

$$\frac{dY}{dt} = \left(\frac{1}{m}\right) * net\ mass\ flow\ towards\ any\ component$$ For mass balance

Convective mode of heat transfer

$$Q = hA(T_{air} - T_{surface})$$ General form of convective heat transfer

$$N_{uL} = f(R_{el}, R_{al}, P_r)$$ Used to estimate film heat-transfer coefficients

Dimensionless group:

$$N_{uL} = \frac{hl}{k_G},\ R_{el} = \frac{\rho_G UL}{\mu_G},\ R_{al} = \frac{g.\beta.\Delta T.L^3.\rho_G^2.C_{pG}}{k_G.\mu_G},\ P_r = \frac{C_{pG}.\mu_G}{k_G}$$

Thermal Radiation Heat Transfer

Direct radiation

$$Q = A\sigma(T_{s1}^4 - T_{s2}^4)$$ Shires et al. (1994)

Radiation through a partially transparent cover

$$Q = A\frac{\sigma\tau_c\varepsilon_p}{(1-\beta_p\beta_c)}\left(T_p^4 - T_s^4\right)$$ Duffie and Beckman (1991)

Radiation between a plate/absorber/sky/stack and a partially transparent cover

$$Q = A \frac{\sigma \tau_c \varepsilon_p \varepsilon_c}{(1 - \beta_p \beta_c)} \left(T_p^4 - T_s^4 \right)$$ Duffie and Beckman (1991)

Sky temperature

$$T_s = 0.0552 T_a^{1.5}$$ Swinbank (1964)

Solar Radiation

$$I_T = G_{cb} R_B + G_{cd} \frac{(1 + cos\gamma)}{2} + (G_{cb} + G_{cd})\rho_g \frac{(1 - cos\gamma)}{2}$$ Duffie and Beckman (1991)

5.7   Appendix 4B

Areas for convection heat-transfer processes

Component	Areas for natural convection (m²)		Areas for forced convection (m²)	
	Oxford	**Boral (scaled)**	**Oxford**	**Boral (scaled)**
Walls	38.75	67.76	38.75	67.76
Floor	17.79	16.73	17.79	16.73
North absorber	29.64	18.33	29.64	18.33
South absorber	30.55	18.33	30.55	18.33
North roof	23.22	18.33	23.22	18.33
South roof	8.18	18.33	8.18	18.33
Roof absorber		30.55		30.55
Roof		31.36		31.36

Areas for thermal radiation heat-transfer processes

Thermal radiation pathways	Thermal radian areas (m²)	
	Oxford	**Boral (scaled)**
Stack to north absorber	12.06	10.12
Stack to south absorber	-	10.12
Floor to south absorber	12.35	-
Stack to ambient	14.14	8.01
South absorber to sky	13.0	4.05
North absorber to sky	13.4	4.05
Stack to walls	19.38	20.32
Sky to walls	15.15	27.10
Ambient to walls	23.25	40.65
Sky to south roof/roof	23.22	31.36
South absorber to south roof	13.0	-
Sky to north roof/roof	8.18	31.36
North absorber to north roof/'roof absorber to roof	13.4	16.87

Areas for solar radiation heat-transfer processes

Solar radiation pathways	Solar radian areas (m²)	
	Oxford	**Boral (scaled)**
Solar to stack	17.14	14.625
Solar to walls	31.13	27.10
Solar to floor	3.56	3.13
Solar to north roof/roof	8.18	31.36
Solar to south roof	23.22	-
Solar to north absorber	13.0	5.06
Solar to south absorber	12.7	5.06
Solar to roof absorber	-	16.87

5.8   Appendix 5A

The daily average climatic data for the summer season (January and February, 2013) of Brisbane

in Australia [data extracted from the Australian Bureau of Meteorology (Meteorology, 2013)].

Date	September (2013)			October (2013)		
	Temperature (K)	Velocity (m/s)	Humidity (%)	Temperature (K)	Velocity (m/s)	Humidity (%)
01	301.15	2.361111	57	300.85	2.361111	66
02	303.9	2.361111	51.5	301.45	3.611111	45.5
03	301.35	4.722222	53.5	298.9	2.083333	45.5
04	301.05	3.611111	47.5	299.05	2.916667	54.5
05	300	2.638889	59	298.5	1.944444	60.5
06	299.8	3.611111	66.5	299	3.611111	61.5
07	300.75	3.888889	51.5	297.7	1.944444	62
08	300.95	2.083333	60	297.55	2.083333	74
09	302.85	2.916667	56.5	300.7	3.055556	60
10	303.6	3.194444	55.5	300.5	2.083333	54.5
11	303.95	3.055556	57	301	3.055556	55
12	304.95	2.361111	58	299.9	3.611111	56
13	303.8	2.083333	58.5	298.65	4.166667	59.5
14	301.75	3.333333	60	300.4	3.333333	54.5
15	299.05	4.166667	57	297.35	2.638889	77
16	300.95	2.083333	52.5	296.15	1.388889	82
17	301	2.361111	51.5	297	3.888889	71.5
18	302.25	2.5	54.5	295.5	1.25	92
19	304.15	2.361111	56.5	296.2	3.333333	88
20	302.3	2.361111	60.5	300.35	2.222222	63
21	299.6	1.527778	72.5	298.3	2.222222	73.5
22	298.2	1.388889	80	299.55	4.166667	57
23	301.4	2.361111	64	302	2.222222	55
24	298.75	1.527778	80	301.55	2.777778	71
25	297.6	3.055556	91	296.4	3.333333	95
26	298.15	4.444444	91.5	298.6	3.055556	82.5
27	297.1	6.388889	94.5	300.05	3.888889	70.5
28	299.45	6.944444	83	299.85	2.777778	63.5
29	300.85	1.805556	73.5	-	-	-
30	301.95	4.166667	69.5	-	-	--
31	299.85	1.666667	68.5	-	-	-

5.9   Appendix 5B

The daily average climatic data for the spring season (September and October, 2013) of Brisbane

in Australia [data extracted from the Australian Bureau of Meteorology (Meteorology, 2013)].

Date	September (2013)			October (2013)		
	Temperature (K)	Velocity (m/s)	Humidity (%)	Temperature (K)	Velocity (m/s)	Humidity (%)
01	296.9	2.777778	53	299.55	2.777778	61.5
02	294.55	2.361111	59	298.65	2.361111	50
03	293.9	2.916667	57.5	302	2.638889	37.5
04	294.35	2.638889	48	294.75	2.638889	34
05	294.5	1.527778	51.5	296.75	2.083333	44
06	294	1.805556	55.5	300.1	2.361111	44.5
07	294.9	1.527778	58.5	302	1.527778	41
08	295.85	1.805556	56	297.85	2.361111	55.5
09	295.9	1.527778	53.5	296.6	2.083333	47.5
10	296.05	1.805556	63	298.25	2.638889	52
11	298	1.25	51.5	301.7	2.361111	43
12	297.45	2.916667	55	298.5	3.055556	68.5
13	296.85	3.333333	59	299.8	3.055556	52
14	297.25	3.055556	71	299.75	3.055556	20
15	298.05	2.222222	50	297	2.083333	46.5
16	292.95	2.777778	80	296.75	3.055556	52.5
17	298.5	2.083333	60	298.5	3.333333	52.5
18	299.6	2.638889	31.5	294.3	1.805556	80
19	299.05	2.083333	56	297.65	3.055556	50
20	299.1	3.055556	24	297.25	3.333333	62
21	296	2.083333	37.5	298.85	2.083333	55.5
22	295.9	1.805556	57	298.5	2.5	54
23	297.65	1.805556	56	299.5	3.055556	56
24	299.8	2.361111	50.5	301.4	1.527778	45.5
25	301.65	2.361111	37	296.9	4.722222	55.5
26	299.35	1.527778	67	299.75	2.083333	52.5
27	298.55	5.416667	48	297.75	3.611111	52.5
28	295.4	1.388889	67.5	297.65	2.777778	58
29	299.15	3.194444	53.5	298.4	3.055556	65.5
30	296.9	1.805556	64.5	296.8	3.888889	59
31	-	-	-	297.05	3.333333	54.5

5.10   Appendix 5C

The daily average climatic data for the winter season (June and July, 2013) of Brisbane in Australia

[data extracted from the Australian Bureau of Meteorology (Meteorology, 2013)].

Date	June (2013)			July (2013)		
	Temperature (K)	Velocity (m/s)	Humidity (%)	Temperature (K)	Velocity (m/s)	Humidity (%)
01	292.5	1.111111	72	288.5	2.222222	91.5
02	293.55	2.916667	75.5	293.3	2.083333	70
03	293	1.944444	47.5	293.7	2.361111	65
04	292.55	1.25	51	294.45	1.388889	62.5
05	291.15	1.388889	70	293.95	1.25	74
06	292.9	0.694444	67	293.4	1.666667	56.5
07	293.7	1.111111	66.5	291.4	1.805556	62
08	290.85	1.388889	84	291.8	1.388889	58
09	292.1	2.083333	74.5	290.15	2.083333	61
10	290.15	1.111111	96	288.6	1.666667	85
11	293.45	1.666667	78.5	291.2	1.805556	66.5
12	292.75	2.361111	90	291.4	1.111111	68.5
13	293.9	1.388889	79.5	289.9	1.527778	70
14	292.25	3.611111	51.5	288.85	0.833333	83
15	290.5	4.444444	54	290.55	1.388889	77.5
16	291.55	0.833333	54	291.75	2.083333	72.5
17	290.5	3.055556	43	291.75	2.361111	73
18	289.8	2.5	42.5	292.6	1.527778	73
19	289.6	2.083333	44	292.9	1.25	80.5
20	289.95	1.388889	60.5	292.1	1.388889	84.5
21	286.2	1.111111	91	292.35	2.5	53.5
22	289.4	1.388889	68	288.05	1.111111	67.5
23	290.45	1.388889	59	290.65	2.083333	49
24	291.5	1.527778	51.5	290.3	1.527778	49
25	289.05	1.805556	47.5	291.5	2.083333	57.5
26	289.55	2.5	48	291.15	1.527778	69.5
27	289.65	1.805556	81.5	291.35	2.361111	68.5
28	291.35	2.222222	76	292.1	2.361111	65
29	290.7	1.944444	79	291	0.833333	79.5
30	288.35	1.388889	88.5	290.35	1.388889	77.5
31	-	-	-	292.7	1.666667	61.5

5.11   Appendix 5D

Heat transfer calculation

This section shows the calculation procedure for determining the heat transfer coefficients

for three different air velocities (i.e. 0.05 m/s, 0.5 m/s, and 1 m/s), as used in the simulation

of this thesis. An effective air velocity of 0.05 m/s has been assumed to calculate the heat-

transfer coefficient for natural convection.

The first dimensionless number to be determined for calculating the heat-transfer coefficient

is the Reynolds number, which involves the characteristic length of the timber board (l) =

0.2 m (the board was assumed to be a flat board of width 200 mm), the standard air density

(ρ_G) = 1.2 kg m^{-3}, and the standard dynamic viscosity (μ_G) = 1.8 x 10^{-5} kg m^{-1} s^{-1}.

Using these dimension and standard air properties, the heat-transfer coefficients for the

three velocities can be calculated in the following stages:

Stage 1: Determination of the Reynolds number

Case 1   U ~ 0.05 m/s

$$R_{el} = \frac{\rho_G U l}{\mu_G} = 667$$

Case 2   U = 0.5 m/s

$$R_{el} = \frac{\rho_G U l}{\mu_G} = 6667$$

Case 3   U = 1 m/s

$$R_{el} = \frac{\rho_G U l}{\mu_G} = 13333$$

Stage 2: Calculation of the Grashof number (G_r)

The next parameter, called Grashof number (G_r), which, in conjunction with the Reynolds

number (R_{el}), indicates whether the heat transfer is occurring by natural convection or by

forced convection (Incropera and DeWitt, 2002; Shires et al., 1994). The Grashof number can

be calculated as follows (Incropera and DeWitt, 2002; Shires et al., 1994):

$$G_r = \frac{g * \beta * \Delta T * l^3 * \rho_G^2}{\mu_G{}^2} = \frac{9.8 * 3.2 * 10^{-3} * 10 * 0.2^3 * 1.2^2}{(1.8 * 10^{-5})^2} = 11.15 * 10^6$$

Stage 3: Determination of the nature of the convection heat transfer

Case 1 $G_r/R_{el}{}^2 = 25 >> 1$ Natural convection

Case 2 $G_r/R_{el}{}^2 = 0.25 \sim 1$ Natural + forced convection

Case 3 $G_r/R_{el}{}^2 = 0.06 << 1$ Forced convection

Stage 4: Determination of the Nusselt numbers

Case 1 $R_{al} = G_r * P_r = 8.02 * 10^6 \leq 10^9$ (laminar) $Nu_l = 0.54 * R_{al}^{\frac{1}{4}} = 28.73$ ($10^4 \leq$

$R_{al} \leq 10^7$)

Case 2 $R_{el} = 6667 \leq 5 * 10^5$ (laminar) $Nu_l = 0.664 * R_{el}^{\frac{1}{2}} * P_r^{\frac{1}{3}} = 48.60$

$(R_{el} \leq 5 * 10^5)$

Case 3 $R_{el} = 13333 \leq 5 * 10^5$ (laminar) $Nu_l = 0.664 * R_{el}^{\frac{1}{2}} * P_r^{\frac{1}{3}} = 68.71$

$(R_{el} \leq 5 * 10^5)$

Stage 5: Determination of the heat-transfer coefficients

Case 1 $h = \dfrac{Nu_l * k_G}{l} = \dfrac{28.73 * 0.02}{0.2} = 2.40 \ W/m^2/K$

Case 2 $h = \dfrac{Nu_l * k_G}{l} = \dfrac{48.60 * 0.02}{0.2} = 4.80 \ W/m^2/K$

Case 3 $h = \dfrac{Nu_l * k_G}{l} = \dfrac{68.71 * 0.02}{0.2} = 5.40 \ W/m^2/K$

5.12   Appendix 6A

Table 6.A1. Breakdown of the key materials required for the Oxford kiln with a 10 m³ load

capacity.

SL	Section (m X m)	Length/thickness (m)	Quantity	Description/components /materials	Reference
1	0.05 X 0.15	0.76	6	Vertical pillars/ north wall/timber	Figure 6.A1
2	0.05 X 0.15	2.33	6	Vertical pillars/ south wall/timber	Figure 6.A1
3	0.05 X 0.15	1.19	2	Vertical pillars/East and west walls//timber	Figure 6.A2
		1.66	2		
		2.12	2		
		2.69	2		
4	0.05 X 0.05	5	2	Horizontal supports/south wall//timber	Figure 6.A1
5	0.05 X 0.05	2.74	2	Horizontal supports/east and west walls//timber	Figure 6.A2
		4.17	2		
		5.51	2		
6	0.05 X0.05	4.61	6	North roof (longitudinal)	Figure 6.A3
7		1.67	5	South roof (longitudinal)	Figure 6.A3
8		5	6	North roof (transverse)	Figure 6.1
9		5	2	South roof (transverse)	Figure 6.1
10	0.15 X 0.10	5.51	2	Foundation frame (north to south)	Figure 6.1
		5	2	Foundation frame (east to west)	Figure 6.1

| SL	Section (m X m)	Length/thickness (m)	Quantity	Description/components /materials	Reference
1 1	5.51 X5	0.10	1	Floor/concrete	Figure 6.1
1 2	4.54 X 2.86	0.0006	1	North absorber/aluminium	Figure 6.1
1 3	4.54 X 2.80	0.0006	1	South absorber/aluminium	Figure 6.1
1 4	5.51 X 5	0.00102	1	Floor sheeting/polycarbonate	Figure 6.1
1 5	5 X 2.33	0.00102	2	South wall/polycarbonate	Figure 6.A1
1 6	5 X 0.76	0.005	2	North wall/polycarbonate	Figure 6.A1
1 7	5 X 1.67	0.005	2	South roof/polycarbonate	Figure 6.A3
1 8	5 X 4.61	0.005	2	North roof/polycarbonate	Figure 6.A3
1 7	11.67 (m^2)	0.005	4	East and West walls/polycarbonate	Figure 6.A2
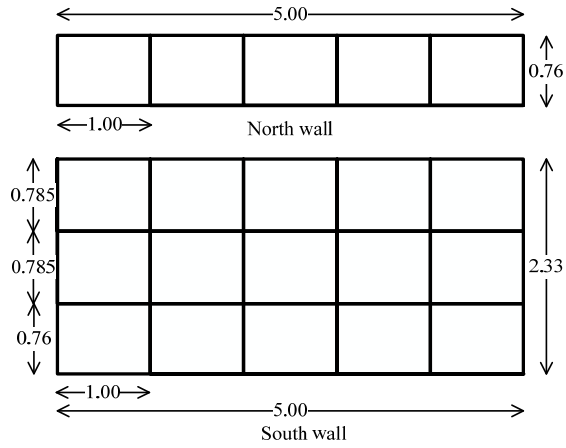
Figure 6.A1. Oxford north/south wall profile with support beams.
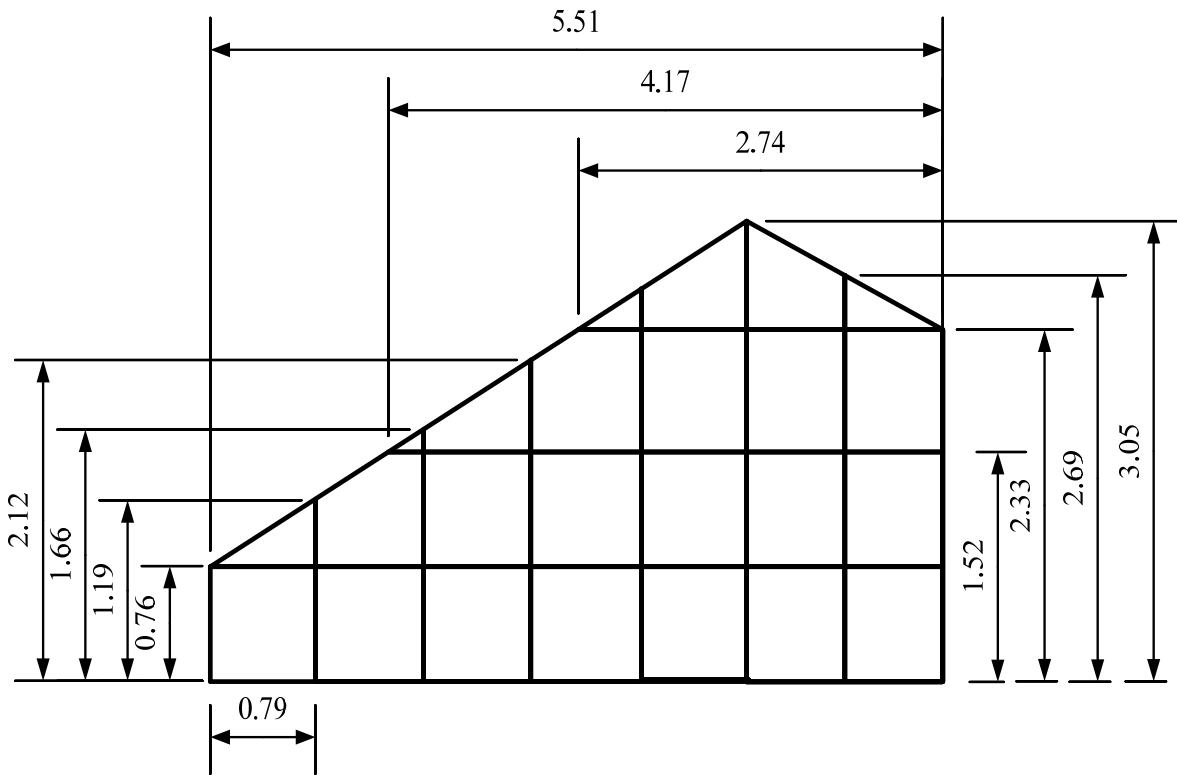

Figure 6.A2. Oxford kiln east/west side profile with support beams.

5.13   Appendix 6B

Table 6.B1. Breakdown of the key materials required for the Boral kiln with a 10 m³ load capacity.

SL	Section (m X m)	Length/thickness (m)	Quantity	Description/component s/ material	Reference
1		3.25	24	Vertical pillars/ all walls/aluminium	Figure 6.B1
4		5.6	16	Horizontal supports/all walls/ aluminium	Figure 6.B1
7	(0.04 * 0.04 – 0.36 * 0.36) m²	4.87	2	East/west roof sides supports/aluminium	Figure 6.B2
8		0.7	2	East/west vertical roof sides vertical pillars/aluminium	Figure 6.B2
		0.9	2		
		1	2		
9		5.6	7	Roof top east/west supports	Figure 6.B3
10		6.30	8	North/South roof (curved)	Figure 6.B3
11		5.6	4	Foundation frame	Figure 6.2
12	5.6 X 5.6	0.10	1	Floor/concrete	Figure 6.2
13	3.5 X 2.25	0.006	2	North/south absorbers/ tinplate	Figure 6.2
15	4.1 X 3.5	0.006	1	Roof absorber/tinplate	Figure 6.2
16	5.6 X 5.6	0.00102	1	Floor sheeting/polycarbonate	Figure 6.2

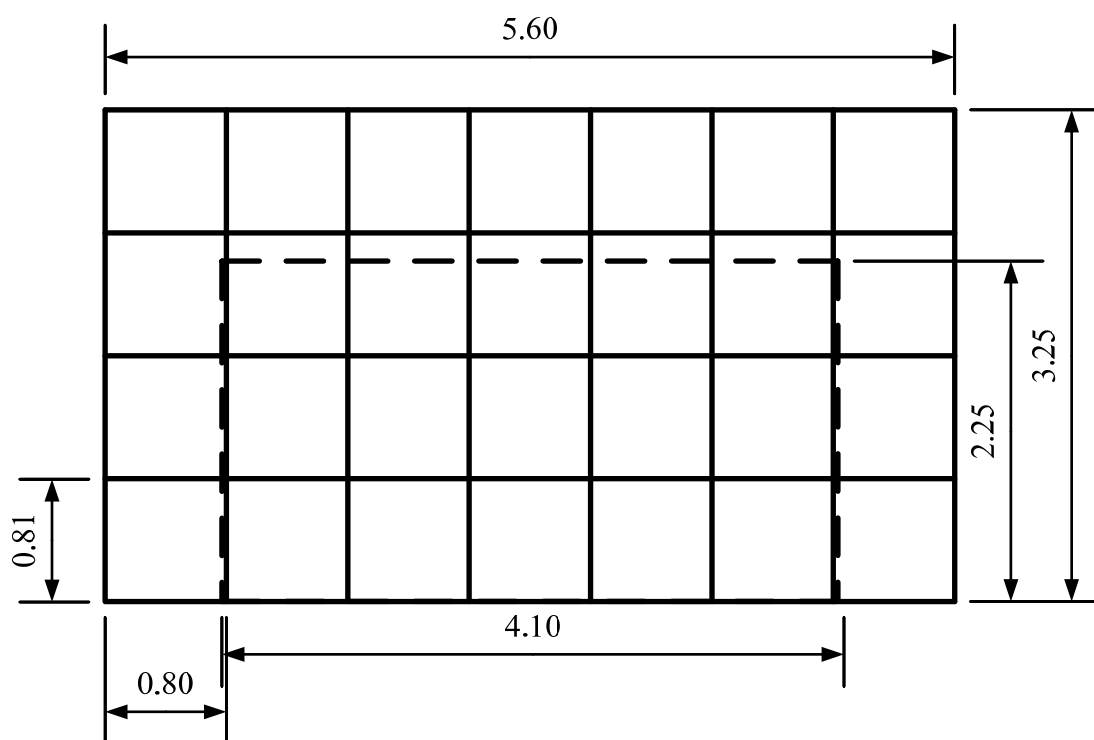| SL	Section (m X m)	Length/thickness (m)	Quantity	Description/components/ material	Reference
17	5.6 X 3.25	0.005	4	North/south walls/polycarbonate	Figure 6.B1
19	5.6 X 6.3	0.005	2	Roof/polycarbonate	Figure 6.B3

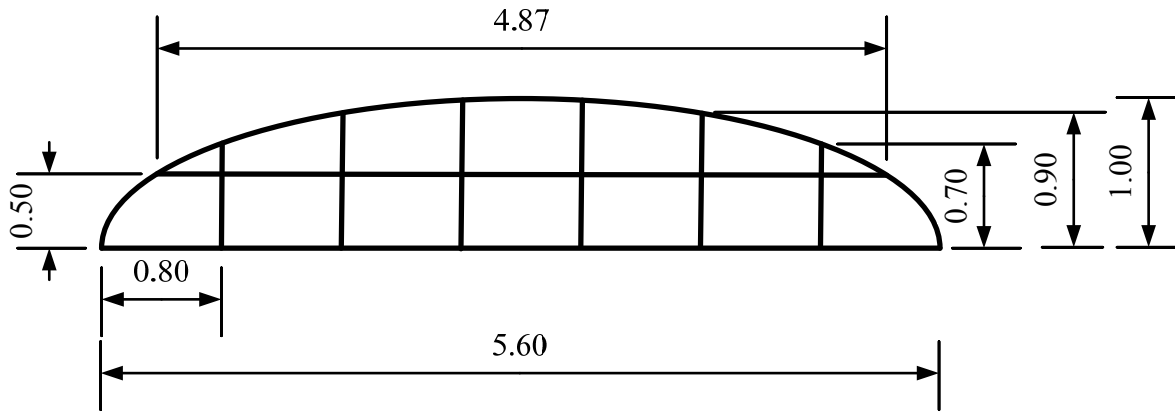Figure 6.B1. North/south/east/west walls profiles for the Boral kiln.

Figure 6.B2. Profiles of roof sides for the Boral kiln.

References

Adelard, L., Pignolet-Tardan, F., Mara, T., Lauret, P., Garde, F., Boyer, H., 1998. Sky temperature modelisation and applications in building simulation. Renewable Energy 15, 418-430.

Aktaş, M., Ceylan, İ., Yilmaz, S., 2009. Determination of drying characteristics of apples in a heat pump and solar dryer. Desalination 239, 266-275.

Altobelli, F., Condorí, M., Duran, G., Martinez, C., 2014. Solar dryer efficiency considering the total drying potential. Application of this potential as a resource indicator in north-western Argentina. Solar Energy 105, 742-759.

Alwan, Z., Jones, P., 2014. The importance of embodied energy in carbon footprint assessment. Structural Survey 32, 49-60.

Aravindh, M.A., Sreekumar, A., 2015. Solar Drying—A Sustainable Way of Food Processing, in: Sharma, A., Kar, K.S. (Eds.), Energy Sustainability Through Green Energy. Springer India, New Delhi, pp. 27-46.

Atwork Supplies. Industrial fans. 2015 [cited 2015 April, 10]; Available from: www.atworksupplies.com.au/industrial-ans.html?gclid=CMf9sL3s_8QCFUwIvAodwWIAIw.

AugVeg, 2014. Australian vegetable export opportunities, Victoria.

Australian Bureau of Agricultural and Resource Economics and Sciences. Agricultural commodity statistics. 2012a [cited 2015, May 25]; Available from: http://data.daff.gov.au/data/warehouse/agcstd9abcc002/agcstd9abcc0022012/ACS_2012_1.1.0.pdf.

Australian Bureau of Agricultural and Resource Economics and Sciences. Australian forest and wood products statistics 2012b [cited 2015, April 10]; Available from: http://www.agriculture.gov.au/abares/forestsaustralia/australian-forest-and-wood-products-statistics.

Australian Bureau of Agricultural and Resource Economics and Sciences. Australian vegetable growing farms: an economic survey, 2012-13 and 2013-14. 2014 [cited 2015 May 15]; Available from: http://data.daff.gov.au/data/warehouse/9aab/9aabf/2014/avfesd9absf20141114/AustVegGrwFrmEcoSurvey20141114_1.0.0.pdf.

Australian Bureau of Statistics. Household energy consumption survey (HECS). 2012a [cited 2015, February 20]; Available from: http://www.abs.gov.au/ausstats/abs@.nsf/Lookup/4670.0main+features100052012.

Australian Bureau of Statistics. Survey of Motor Vehicle Use 2012b [cited 2015, April 5]; Available from: http://www.abs.gov.au/ausstats/abs@.nsf/mf/9208.0/.

Australian Bureau of Statistics. Agricultural commodities, Australia. 2013 [cited 2015, May 5]; cat. no. 7121.0:[Available from: http://www.abs.gov.au/ausstats/abs@.nsf/Latestproducts/7121.0Main%20Features72012-2013?opendocument&tabname=Summary&prodno=7121.0&issue=2012-2013&num=&view=.

Australian Federal Chamber of Automotive Industries. National average carbon emission. 2011 [cited 2015, April 10]; Available from: http://www.fcai.com.au/environment/co2-emissions-and-climate-change.

Australian Life Cycle Assessment Society. Australian Life Cycle Inventory (AusLCI). 2009 [cited 2014, July 7]; Available from: http://alcas.asn.au/AusLCI/.

Awadalla, H.S.F., El-Dib, A.F., Mohamad, M.A., Reuss, M., Hussein, H.M.S., 2004. Mathematical modelling and experimental verification of wood drying process. Energy Conversion and Management 45, 197-207.

Baker, D., Fear, J., Denniss, R., 2009. What a waste: an analysis of household expenditure on food, Policy Brief.

Barrenjoey, T. Building Timber / Structural Pine. 2015 [cited 2015 March, 22]; Available from:

http://www.barrenjoeytimber.com.au/show.aspx?product=Structural+Pine+MPG10&number=53&cat=7&catb=0.

Bayart, J.-B., Bulle, C., Deschênes, L., Margni, M., Pfister, S., Vince, F., Koehler, A., 2010. A framework for assessing off-stream freshwater use in LCA. The International Journal of Life Cycle Assessment 15, 439-453.

Bejan, A., 2004. Convection heat transfer. Wiley, Hoboken, N.J.

Bentayeb, F., Bekkioui, N., Zeghmati, B., 2008. Modelling and simulation of a wood solar dryer in a Moroccan climate. Renewable Energy 33, 501-506.

Berger, M., Finkbeiner, M., 2013. Methodological Challenges in Volumetric and Impact-Oriented Water Footprints. Journal of Industrial Ecology 17, 79-89.

Berger, X., Buriot, D., Garnier, F., 1984. About the equivalent radiative temperature for clear skies. Solar Energy 32, 725-733.

Bergman, R.D., 2008. Operation and cost of a small dehumidification dry kiln.

Biggerstaff, T., 1965. Drying diffusion coefficients in wood as affected by temperature. Forest Product Journal 15, 127-133.

Bliss, R.W., 1961. Atmospheric radiation near the surface of the ground: A summary for engineers. Solar Energy 5, 103-120.

Blyth, W., Yang, M., Bradley, R., International Energy, A., Organisation for Economic, C.-o., Development, Iea, 2007. Climate policy uncertainty and investment risk. International Energy Agency, Paris.

Bodig, J. and B.A. Jayne. 1982. Mechanics of wood and wood composites. Van Nostrand Reinhold, New York. 712 pp.

Bramhall, G., 1976. Fick's law and bound-water diffusion. Wood Science 8, 153-161.

Bramhall, G., 1995. Diffusion and the drying of wood. Wood Science and Technology 29, 209-215.

Brooke, A., 1999. Optimisation of Hardwood Timber Drying Schedules, Chemical Engineering. The University of Sydney, Australia, p. 139.

Bucki, M., Perre, P., 2003. Physical formulation and numerical modeling of high frequency heating of wood. Drying Technology 21, 1151-1172.

Buonomano, A., Calise, F., Palombo, A., Vicidomini, M., 2015. Energy and economic analysis of geothermal–solar trigeneration systems: A case study for a hotel building in Ischia. Applied Energy 138, 224-241.

Bureau of Resources and Energy Economics. Australian Energy Resource Assessment. 2014 [cited 2015, August 20]; Second:[Available from:

http://www.ga.gov.au/webtemp/image_cache/GA21797.pdf.

Burke, R. Solar Dryers Australia. 2015a [cited 2015, July 29]; Available from: http://www.ats.business.gov.au/companies-and-technologies/environmental-technologies/clean-buildings/solar-dryers-australia.

Burke, R. Solar dryers Australia Pty Ltd. 2015b [cited 2015; Available from: http://www.solardry.com.au/solardry/.

Burns, K., Burke, B., 2012. ABARES national wood processing survey, 2010-11. Australian Bureau of Agricultural and Resource Economics, Canberra, A.C.T.

Cabardo, S.J., Langrish, T.A.G., Dickson, R., Joe, B., 2006. Variability in transport properties regarding drying behavior for blackbutt timber in New South Wales. Drying Technology 24, 211-224.

Carbajales-Dale, M., Barnhart, C.J., Brandt, A.R., Benson, S.M., 2014. A better currency for investing in a sustainable future. Nature Clim. Change 4, 524-527.

Carrington, M (1996) High-temperature seasoning of softwood boards. Determination of mechanical properties at elevated temperature. ME (Chem) Thesis, University of Canterbury, NZ.

Chadwick, W.B., Langrish, T.A.G., 1996. A comparison of drying time and timber quality in the continuous and cyclic drying of Australian turpentine timber. Drying Technology 14, 895-906.

Choong, E.T., 1965. Diffusion coefficients of softwoods by steady-state and theoretical methods. Forest Product Journal 15, 21-27.

Cleveland, C.J. Net energy analysis. 2013 [cited 2014, October 20]; Available from: http://www.eoearth.org/view/article/154821/.

Cloutier, A., Fortin, Y., 1993. A model of moisture movement in wood based on water potential and the determination of the effective water conductivity. Wood Science and Technology 27, 95-114.

Cloutier, A., Fortin, Y., 1994. Wood drying modelling based on the water potential concept: Hysteresis effects. Drying Technology 12, 1793-1814.

Cloutier, A., Fortin, Y., Dhatt, G., 1992. A wood drying finite-element model based on the water potential concept. Drying Technology 10, 1151-1181.

Commonwealth of Australia. Handbook of cost-benefit analysis. The Financial Management Guidance 2006 [cited 2015, March 20]; Available from:

http://www.finance.gov.au/finframework/docs/Handbook_of_CB_analysis.pdf.

Construction & Real Estate. Plastic building materials. 2015 [cited 2015 January, 15]; Available from: http://www.alibaba.com/product-detail/High-Quality-10-year-Warranty-ISO_60188346952.html.

Department of Energy and Water Supply. Current electricity prices. 2015 [cited 2015, April 24]; Available from: https://www.dews.qld.gov.au/energy-water-home/electricity/prices/current-prices.

Department of Infrastructure and Transport. Truck productivity: sources, trends and future prospects. Bureau of Infrastructure, Transport and Regional Economics 2011 [cited 2014 September 20]; Available from:

http://www.bitre.gov.au/publications/2011/files/report_123.pdf.

Department of the Environment. National greenhouse accounts factors. 2014 [cited 2015, August 15]; Available from:

http://www.environment.gov.au/system/files/resources/b24f8db4-e55a-4deb-a0b3-32cf763a5dab/files/national-greenhouse-accounts-factors-2014.pdf.

Department of the Prime Minister and Cabinet. Best practice regulation guidance note: Value of statistical life. 2014 December 1 [cited 2014 December 20]; Available from: https://www.dpmc.gov.au/sites/default/files/publications/Value_of_Statistical_Life_guidance_note.pdf.

Desch, H.E., Dinwoodie, J.M., 1996. Timber: Structure, Properties, Conversion and Use. Macmillan.

Dinwoodie, J.M., 2000. Timber, its nature and behaviour, 2nd ed. E & FN Spon, England;London;New York;.

Dixit, M.K., Culp, C.H., Lavy, S., Fernandez-Solis, J., 2014. Recurrent embodied energy and its relationship with service life and life cycle energy: A review paper. Facilities 32, 160-181.

Dixit, M.K., Fernández-Solís, J.L., Lavy, S., Culp, C.H., 2010. Identification of parameters for embodied energy measurement: A literature review. Energy and Buildings 42, 1238-1247.

Dixit, M.K., Fernández-Solís, J.L., Lavy, S., Culp, C.H., 2012. Need for an embodied energy measurement protocol for buildings: A review paper. Renewable and Sustainable Energy Reviews 16, 3730-3743.

Doe, P.D., Oliver, A.R., Booker, J.D., 1994. A non-linear strain and moisture content model of variable hardwood drying schedules, 4th IUFRO International Wood Drying Conference, Rotorua, New Zealand, pp. 203-210.

Dolan, W., Cummings, P., LeVan, M., 1989. Process optimization via simulated annealing: application to network design. AIChE Journal 35, 725-736.

Dossor, R., 2013. The future of the Australian processed food sector, in: Heriot, D. (Ed.), Parliamentary library briefing book: key issues for the 44th parliament. Parliament of Australia.

Duffie, J.A., Beckman, W.A., 1991. Solar engineering on thermal processes, Second ed. John Wiley & Sons, Inc. p. 10-95 USA.

Duffie, J.A., Beckman, W.A., 2006. Solar engineering of thermal processes. Wiley, Hoboken, NJ.

Ellwood, E.L., 1954. Properties of American Beech in Tension and Compression Perpendicular to the Grain and Their Relation to Drying. Yale University.

Fadhel, A., Kooli, S., Farhat, A., Bellghith, A., 2005. Study of the solar drying of grapes by three different processes. Desalination 185, 535-541.

Fadhel, M.I., Sopian, K., Daud, W.R.W., Alghoul, M.A., 2011. Review on advanced of solar assisted chemical heat pump dryer for agriculture produce. Renewable and Sustainable Energy Reviews 15, 1152-1168.

Fair Work Ombudsman. Pay calculator. 2015 [cited 2015 April, 24]; Available from: http://paycheck.fwo.gov.au/PayCheckPlus.aspx.

Falk, B., 2009. Wood as a sustainable building material. Forest Product Journal 59, 6-12.

Fernandes, B., Cunha, J., Ferreira, P., 2011. The use of real options approach in energy sector investments. Renewable and Sustainable Energy Reviews 15, 4491-4497.

Forest & Wood Products. Treated timber in Australia, p. 4. National Timber Development Program 2004 [cited 2015 January 10]; Available from: http://www.timber.net.au/images/downloads/exterior/outdoor_timber_cca_tech_report_5.pdf.

Fudholi, A., Ruslan, M.H. Technoeconomic analysis of solar drying system for seaweed in Malaysia. in Proc. of the 7th IASME/WSEAS Int. Conf. on Energy, Environment, Ecosystems and Sustainable Development (EEESD). 2011. Malaysia.

Fuller, R. Solar drying in Australia: a historical review. in Proceedings of the International Solar Energy Society conference, Adelaide. 2001.

Fuller, R.J., 2011. Solar industrial process heating in Australia – Past and current status. Renewable Energy 36, 216-221.

Giacomelli, G.A., Roberts, W.J., 1993. Greenhouse covering systems. HortTechnology 3, 50-58.

Grant, T., Peters, G., 2008. Best Practice Guide to Life Cycle Impact Assessment in Australia. Australian Life Cycle Scociety.

Green, David W.; Winandy, Jerrold E.; Kretschmann, David E. 1999. Mechanical properties of wood. Wood handbook : wood as an engineering material. Madison, WI : USDA Forest Service, Forest Products Laboratory, 1999. General technical report FPL ; GTR-113: Pages 4.1-4.45.

Guzman, J.A., Lauterbach, A., Jordan, R., 1985. Performance of wood solar kilns with box type collector. Energy in Agriculture 4, 243-252.

Guzman, J.A., Lauterbach, A., Jordan, R., 1987. Method for determining overall performance of solar kilns. Journal of Solar Energy Engineering, Transactions of the ASME 109, 26-29.

Hammond, G., Jones, C., 2008. Inventory of Carbon & Energy: ICE. Version 1.6a, 10-14, Sustainable Energy Research Team, Department of Mechanical Engineering, University of Bath, UK.

Hannon, B., 1982. Energy discounting. Technological Forecasting & Social Change 21, 281-300.

Hanson Heidelberg Cement Group. Products and services: pricing and ordering. 2015 [cited 2015 February, 20]; Available from: http://www.hanson.com.au/Productsandservices/Customersupport/Pricingandorderinge nquiries/QLD.aspx.

Haque, M.N., 2002. Modeling of solar kilns and the development of an optimized schedule for drying hardwood timber, Chemical Engineering. pp. 205-239, University of Sydney, Australia, p. 354.

Haque, M.N., Jangam, S.V., Mujumdar, A.S., 2014. Life cycle assessment of drying systems, Handbook of Industrial Drying, Fourth Edition. CRC Press, pp. 1229-1238.

Haque, M.N., Langrish, T.A.G., 2001. Stack-wide effects in the modeling of solar kilns for drying timber. Drying Technology 19, 99-114.

Haque, M.N., Langrish, T.A.G., 2003. Mathematical modelling of solar kilns for drying timber: Simulation and experimental validation. Drying Technology 21, 457-477.

Harrison, M., 2010. Valuing the Future: the social discount rate in cost-benefit analysis. Available at SSRN 1599963.

fHegner, S., 2007. An Assessment of Embodied Energy's Relevance for Energy Saving in the Swiss Residential Building Sector, Department of Environmental Science. pp. 1-5, ETH Zurich, Switzerland.

Helmer, W., Chen, P., Rosen, H., Wang, S. A theoretical model for solar-dehumidification drying of wood. in Proceedings... International Symposium on Drying. 1980.

Helwa, N.H., Khater, H.A., Enayet, M.M., Hashish, M.I., 2004. Experimental evaluation of solar kiln for drying wood. Drying Technology 22, 703-717.

Henriksen, J.E., 2006. The value of design in reducing energy use and co2-e impact over the life cycle of a detached dwelling in temperate climate, Faculty of Engineering and the Built Environment. University of Newcastle, Australia.

Herritsch, A., Dronfield, J., Nijdam, J.J., 2010. Intermittent and Continuous Drying of Red Beech Timber From the Green Condition. Drying Technology 28, 269-277.

Heun, M.K., de Wit, M., 2012. Energy return on (energy) invested (EROI), oil prices, and energy transitions. Energy Policy 40, 147-158.

Horticulture Australia Limited. Horticulture fact sheet. 2012 [cited 2015; Available from: http://www.agriculture.gov.au/Style%20Library/Images/DAFF/__data/assets/pdffile/0020/2109206/Horticulture_Fact_Sheet.pdf.

Hossain, M.A., Woods, J.L., Bala, B.K., 2005. Optimisation of solar tunnel drier for drying of chilli without color loss. Renewable Energy 30, 729-742.

Imre, L., 1986. Technical and economical evaluation of solar drying. Drying Technology 4, 503-512.

Incropera, F.P., DeWitt, D.P., 2002. Introduction to heat transfer. Wiley, New York.

Inflation Rate. Australian inflation rate history. 2015 [cited 2015 April, 24]; Available from: http://www.rateinflation.com/inflation-rate/australia-historical-inflation-rate.

Infrastructure Australia. Review of major infrastructure delivery. 2008 [cited 2014 December 20]; Available from: http://www.infrastructureaustralia.gov.au/publications/files/Review_of_Major_Infrastructure_Delivery_PWC.pdf.

International Federation of Institutes for Advanced Study, 1975. Workshop on Energy Analysis and Economics. International Federation of Institutes for Advanced Study, Energy Accounting Hearings, Lidingo, Sweden, p. 7.

Islam, H., Jollands, M., Setunge, S., Ahmed, I., Haque, N., 2014. Life cycle assessment and life cycle cost implications of wall assemblages designs. Energy and Buildings 84, 33-45.

Islam, H., Jollands, M., Setunge, S., Haque, N., Bhuiyan, M.A., 2015. Life cycle assessment and life cycle cost implications for roofing and floor designs in residential buildings. Energy and Buildings 104, 250-263.

ISO. ISO 14044: Environmental management — life cycle assessment — requirements and guidelines. 2006; Available from: https://www.iso.org/obp/ui/#iso:std:iso:14044:ed-1:v1:en.

Jairaj, K.S., Singh, S.P., Srikant, K., 2009. A review of solar dryers developed for grape drying. Solar Energy 83, 1698-1712.

Janjai, S., Bala, B.K., 2011. Solar drying technology. Food Engineering Reviews 4, 16-54.

Janjai, S., Intawee, P., Kaewkiew, J., Sritus, C., Khamvongsa, V., 2011. A large-scale solar greenhouse dryer using polycarbonate cover: Modeling and testing in a tropical environment of Lao People's Democratic Republic. Renewable Energy 36, 1053-1062.

Jambeck, J.R., 2004. The Disposal of CCA-Treated Wood in Simulated Landfills: Potential Impacts. PhD Dissertation, University of Florida, Gainesville, FL

Kakaç, S., Shah, R.K., Aung, W., 1987. Handbook of single-phase convective heat transfer. Wiley, chapter 2, 5, 12, 14 New York.

Kayihan, F., 1993. Adaptive control of stochastic batch lumber kilns. Computers and Chemical Engineering 17, 265-273.

Keep, L.B (1998). The determination of time-dependent strains in Pinus radiata under kiln – drying conditions. ME Thesis, University of Canterbury, Christchurch, NZ.

Keey, R.B., Walker, J.C.F., Langrish, T.A.G., 2000. Kiln-drying of lumber. Springer, New York; Berlin.

Kelleher, J.P., 2012. Energy Policy and the Social Discount Rate. Ethics, Policy & Environment 15, 45-50.

Khater, H.A., Helwa, N.H., Enayet, M.M., Hashish, M.I., 2004. Optimization of solar kiln for drying wood. Drying Technology 22, 677-701.

Khuntia, S., Parida, A., Misra, V.N., Technology Information, F., Council, A., Chapter, I.I.o.M.B., Scientific, C.o., Laboratory, I.R.R.R., 2003. Downsizing Technology for rural Development, Vol. 1. Allied Publishers.

Kollmann, F.F.P., 1968. Principles of wood science and technology [by] Franz F. P. Kollmann [and] Wilfred A. Cote, Jr. Springer-Verlag, Berlin, Heidelberg, New York.

Kushnir, D., Rokhlin, V., 2012. A highly accurate solver for stiff ordinary differential equations. Siam Journal on Scientific Computing 34, A1296-A1315.

Langrish, T.A.G., Bohm, N., 1997. An experimental assessment of driving forces for drying in hardwoods. Wood Science and Technology 31, 415-422.

Langrish, T.A.G., Brooke, A.S., Davis, C.L., Musch, H.E., Barton, G.W., 1997. An improved drying schedule for Australian ironbark timber: Optimisation and experimental validation. Drying Technology 15, 47-70.

Langrish, T.A.G., Keey, R.B., Kumar, M., 1992. Improving the quality of timber from red beech (N. Fusca) by intermittent drying. Drying Technology 10, 947-960.

Langrish, T.A.G., Thompson, F.B., Plumptre, R.A., 1993. The measurement of energy flows around a solar kiln used for drying timber. Commonwealth Forestry Review 72, 95-104.

Larbi, S., 2014. Heat and Mass Transfer with Condensation in Capillary Porous Bodies. The Scientific World Journal 2014, 8.

Lazarescu, C., Avramidis, S., Oliveira, L., 2009. Modeling Shrinkage Response to Tensile Stresses in Wood Drying: I. Shrinkage-Moisture Interaction in Stress-Free Specimens. Drying Technology 27, 1183-1191.

Leicester, R.H., 1971. A rheological model for mechano-sorptive deflections of beams. Wood Science and Technology 5, 211-220.

Lepik, U., 2009. Haar wavelet method for solving stiff differential equations. Mathematical Modelling and Analysis   14, 467-481.

Lippke, B., Oneil, E., Harrison, R., Skog, K., Gustavsson, L., Sathre, R., 2011. Life cycle impacts of forest management and wood utilization on carbon mitigation: Knowns and unknowns. Carbon Management 2, 303-333.

López-Vidaña, E.C., Méndez-Lagunas, L.L., Rodríguez-Ramírez, J., 2013. Efficiency of a hybrid solar–gas dryer. Solar Energy 93, 23-31.

Lovegrove, K., Dennis, M., 2006. Solar thermal energy systems in Australia. International Journal of Environmental Studies 63, 791-802.

Luikov, A.V., 1966. Heat and mass transfer in capillary-porous bodies / A V Lykov, London U6-ctx_ver=Z39.88-2004&ctx_enc=info%3Aofi%2Fenc%3AUTF-8&rfr_id=info:sid/summon.serialssolutions.com&rft_val_fmt=info:ofi/fmt:kev:mtx:book&rft.genre=book&rft.title=Heat+and+mass+transfer+in+capillary-

porous+bodies+%2F+A+V+Lykov&rft.date=1966&rft.externalDBID=n%2Fa&rft.externalDo cID=b42917736&paramdict=en-US U7 - Book.

Luna, D., Nadeau, J.P., Jannot, Y., 2009. Solar timber kilns: State of the art and foreseeable developments. Renewable and Sustainable Energy Reviews 13, 1446-1455.

Martin, M., Berdahl, P., 1984. Characteristics of infrared sky radiation in the United States. Solar Energy 33, 321-336.

Masters Home Improvement. Valspar Exterior Low Sheen Black 1L. 2015 [cited 2015 April, 1]; Available from: https://www.masters.com.au/product/100945108/valspar-exterior-low-sheen-black-1l.

McDougall, F.R., White, P., 2001. Integrated solid waste management: a life cycle inventory. Blackwell Science, Malden, MA.

Mekhilef, S., Saidur, R., Safari, A., 2011. A review on solar energy use in industries. Renewable and Sustainable Energy Reviews 15, 1777-1790.

Metalroofing. Corrugated iron colorbond® roofing sheets. 2015 [cited 2015 March, 15]; Available from: https://www.metalroofingonline.com.au/victoria/9-corrugated-colorbond-roofing-sheets.html.

Meteorology, B.o. Daily weather observations. 2013 [cited 2015 May 25]; Available from: http://www.bom.gov.au/climate/data/.

Milne, G., Reardon, C. Embodied energy. 2013 [cited 2014 August 28]; Available from: http://www.yourhome.gov.au/materials/embodied-energy.

Mujumdar, A.S., 2007. Handbook of industrial drying. CRC/Taylor & Francis, Boca Raton, FL.

Mundi, I. Aluminum Monthly Price. 2015 [cited 2015 January, 20]; Available from: http://www.indexmundi.com/commodities/?commodity=aluminum&currency=aud.

Musch, H.E., Barton, G.W., Langrish, T.A.G., Brooke, A.S., 1998. Nonlinear model predictive control of timber drying. Computers & Chemical Engineering 22, 415-425.

Newton, P.W., Hampson, K., Drogemuller, R., 2009. Technology, design and process innovation in the built environment. Spon Press, New York.

Nolan, G., Innes , T., Redman, A., McGavin, R., 2003. Australian hardwood drying best practice manual Part 1. Forest & Wood Products Research and Development Corporation Victoria, Australia.

Odonoghue, J., Fuller, R., 1999. Experiences with the australian version of the hohenheim solar tunnel dryer, Australian Solar Council Scientific Conference Australian Solar Council.

Oliver, A.R., University of, T., Civil, Mechanical Engineering, D., 1991. A model of the behaviour of wood as it dries : (with special reference to Eucalypt materials). Civil & Mechanical Engineering Dept., Faculty of Engineering, University of Tasmania, [Hobart].

Ong, K.S., 1997. Comparison between drying of timber in a solar dryer and in an electrically-heated kiln. Drying Technology 15, 1231-1237.

Ontario Construction Secretariat, 2001. A guide to construction cost sources. University of Toronto, Toronto, Canada, p. 120.

Origin Energy. QLD small business energy price fact sheet. 2015 [cited 2015 August, 15]; Available   from: http://www.originenergy.com.au/content/dam/origin/business/Documents/energy-price-fact-sheets/qld/QLD_Natural%20Gas_Small%20Business_Australian%20Gas%20Networks%20Brisbane_Business%20eSaver.PDF.

Ormarsson, S., Dahlblom, O., Petersson, H., 2000. A numerical study of the shape stability of sawn timber subjected to moisture variation. Wood Science and Technology 34, 207-219.

Othman, M.Y.H., Sopian, K., Yatim, B., Daud, W.R.W., 2006. Development of advanced solar assisted drying systems. Renewable Energy 31, 703-709.

OzHarvest, 2014. Australia takes part in global UN initiative to cut food waste, ECOS. CSIRO.

Pallet, D., 1988. Simulation and validation of a solar drying lumber model, International Drying Symposium. IDS, Versailles, France, p. 6 p.

Pandey, R.N., Srivastava, S.K., Mikhailov, M.D., 1999. Solutions of Luikov equations of heat and mass transfer in capillary porous bodies through matrix calculus: a new approach. International Journal of Heat and Mass Transfer 42, 2649-2660.

Pangavhane, D.R., Sawhney, R.L., 2002. Review of research and development work on solar dryers for grape drying. Energy Conversion and Management 43, 45-61.

PE International, 2012. Life cycle assessment of rough-sawn kiln-dried hardwood lumber, American Hardwood Export Council (AHEC), USA, p. 16.

Penman, T.D., Law, B.S., Ximenes, F., 2010. A proposal for accounting for biodiversity in life cycle assessment. Biodiversity and Conservation 19, 3245-3254.

Perré, P., Turner, I.W., 2002. A heterogeneous wood drying computational model that accounts for material property variation across growth rings. Chemical Engineering Journal 86, 117-131.

Peters, M.S., Timmerhaus, K.D., West, R.E., 2003. Plant design and economics for chemical engineers. McGraw-Hill, Boston.

Pirasteh, G., Saidur, R., Rahman, S.M.A., Rahim, N.A., 2014. A review on development of solar drying applications. Renewable & Sustainable Energy Reviews 31, 133-148.

Plank, R.J., 2005. Sustainable building construction for structural engineers. Structural Engineer 83, 30-33.

Pordage, L.J., Langrish, T.A.G., 1999. Simulation of the effect of air velocity in the drying of hardwood timber. Drying Technology 17, 237-255.

Prakash, O., Kumar, A., 2014. Solar greenhouse drying: A review. Renewable & Sustainable Energy Reviews 29, 905-910.

Rawlinsons Group, 2014. Rawlinsons construction cost guide: for housing, small commercial and industrial buildings, 22 ed, Perth, Australia.

Reuter, W.H., Szolgayová, J., Fuss, S., Obersteiner, M., 2012. Renewable energy investment: Policy and market impacts. Applied Energy 97, 249-254.

Rock, G. Using the time value of energy. 2006 [cited 2014, November 11]; Available from: http://www.hubbertpeak.com/netenergy/netenergyprofitratio_gregrock.pdf.

Romano, G., Kocsis, L., Farkas, I., 2009. Analysis of Energy and Environmental Parameters during Solar Cabinet Drying of Apple and Carrot. Drying Technology 27, 574-579.

Rosen, H.N., 1987. Recent advances in the drying of solid wood, in: Mujumdar, A.S. (Ed.), Advances in drying. Hemisphere, Washington, DC, USA, pp. 99-146.

Sabic Innovative Plastics. Product datasheet. 2008 [cited 2014 November 3]; Warranty conditions]. Available from: http://www.sabic-ip.com/resins/DataSheet/Internet/PDF/1002002131_1002003948_1002038287_SI.pdf.

Salin, J.G., 1992. Numerical prediction of checking during timber drying and a new mechanosorptive creep model. Holzals Rho-Und Werkstoff 50, 195-200.

Sandra, B., Kim, H., 2011. Water content of fruits and vegetables. Health Matters Program.

Sartori, I., Hestnes, A.G., 2007. Energy use in the life cycle of conventional and low-energy buildings: A review article. Energy & Buildings 39, 249-257.

Schaffner, R.D., 1981. Fundamental Aspects of Timber Seasoning. , Civil and Mechanical Engineering. University of Tasmania, p. 279.

Shampine, L.F., Reichelt, M.W., 1997. The MATLAB ODE suite. Siam Journal on Scientific Computing 18, 1-22.

Sharma, A., Chen, C.R., Vu Lan, N., 2009. Solar-energy drying systems: A review. Renewable & Sustainable Energy Reviews 13, 1185-1210.

Sherwood, T.K., 1929. The Drying of Solids—I. Industrial & Engineering Chemistry 21, 12-16.

Shires, G.L., Hewitt, G.F., Bott, T.R., 1994. Process heat transfer. CRC Press. 1042p., London, Boca Raton.

Shmulsky, R., Jones, P.D., 2011. Forest products and wood science: an introduction. Wiley-Blackwell, Ames, Iowa;Chichester, England;.

Simpson, W.T., 1993. Determination and use of moisture diffusion coefficient to characterize drying of northern red oak (Quercus rubra). Wood Science and Technology 27, 409-420.

Singh, S., Kumar, S., 2012. New approach for thermal testing of solar dryer: Development of generalized drying characteristic curve. Solar Energy 86, 1981-1991.

Skaar, C., 2012. Wood-water relations. Springer, New York.

Smitabhindu, R., Janjai, S., Chankong, V., 2008. Optimization of a solar-assisted drying system for drying bananas. Renewable Energy 33, 1523-1531.

Söderström, O., 1996. Surface conditions and Fick's law. Wood Science and Technology 30, 149-151.

Sodha, M.S., Chandra, R., 1994. Solar drying systems and their testing procedures: A review. Energy Conversion and Management 35, 219-267.

Solar Kilns. General specifications. 2014 [cited 2014, November 25]; Available from: http://www.solarkilns.com/solar_kilns/features_and_specifications/specification-matrix.htm.

Solo-Gabriele, H.M., Townsend, T.G., Messick, B., Calitu, V., 2002. Characteristics of chromated copper arsenate-treated wood ash. Journal of Hazardous Materials 89, 213-232.

Song, J., Dubey, B., Jang, Y.-C., Townsend, T., Solo-Gabriele, H., 2006. Implication of chromium speciation on disposal of discarded CCA-treated wood. Journal of Hazardous Materials 128, 280-288.

Srikiatden, J., Roberts, J.S., 2008. Predicting moisture profiles in potato and carrot during convective hot air drying using isothermally measured effective diffusivity. Journal of Food Engineering 84, 516-525.

Stamm, A.J., 1964. Wood and cellulose science. Ronald Press Co., New York.

Stanish, M.A., Schajer, G.S., Kayihan, F., 1986. A mathematical model of drying for hygroscopic porous media. AIChE Journal 32, 1301-1311.

Stefan, G., Hosahalli, S.R., Michele, M., 2003. Drying of Fruits, Vegetables, and Spices, Handbook of Postharvest Technology. CRC Press, pp. 653-695.

Suleiman, M.B., Musa, H., Ismail, F., Senu, N., 2013. A new variable step size block backward differentiation formula for solving stiff initial value problems. International Journal of Computer Mathematics, 1-18.

Swinbank, W.C., 1964. Long-wave radiation from clear skies. Quarterly Journal of the Royal Meteorological Society 90, 488-493.

Tharumaharajah, A., Grant, T. Australian national life cycle inventory database: moving forward. in 5th Australian Life Cycle Assesment Scociety Conference. 2006. Melbourne, Australia.

Thibeault, F., Marceau, D., Younsi, R., Kocaefe, D., 2010. Numerical and experimental validation of thermo-hygro-mechanical behaviour of wood during drying process. International Communications in Heat and Mass Transfer 37, 756-760.

Timber NSW. Hardwood industry. 2013   [cited 2015 April, 10]; Available from: http://timbernsw.com.au/our-industry/.

Trucks, C.L., 2008. EP20K PAC - EP25K PAC, EP30K PAC - EP35K PAC, Specifications, in: Trucks, C.L. (Ed.), p. 2.

Tsilingiris, P.T., 2010. Modeling heat and mass transport phenomena at higher temperatures in solar distillation systems – The Chilton–Colburn analogy. Solar Energy 84, 308-317.

Turner, I.W., Puiggali, J.R., Jomaa, W., 1998. A numerical investigation of combined microwave and convective Drying of a Hygroscopic Porous Material: A Study Based on Pine Wood. Chemical Engineering Research and Design 76, 193-209.

United States Environmental Protection Agency. U.S. greenhouse gas inventory report: 1990-2014. 2014 [cited 2016; Available from:

https://www3.epa.gov/climatechange/ghgemissions/usinventoryreport.html.

Visavale, G.L., 2012. Principles, Classification and Selection of Solar Dryers, in: Hii, C.L., Jangam, S.V., Ong, S.P., Mujumdar, A.S. (Eds.), Singapore, p. 14.

Walker, J.C.F., 2006. Primary wood processing: principles and practice. Springer, Dordrecht.

Wan, J., Langrish, T.A.G., 1995. A numerical simulation for solving the diffusion equations in the drying of hardware timber. Drying Technology 13, 783-799.

Wang, X., Lu, M., Mao, W., Ouyang, J., Zhou, B., Yang, Y., 2015. Improving benefit-cost analysis to overcome financing difficulties in promoting energy-efficient renovation of existing residential buildings in China. Applied Energy 141, 119-130.

Wengert, E.M., Meyer, D., 1993. Warp in drying: Causes and cures for warpage when drying lumber. School of Natural Resources, USA.

Winter, E.R.F., Viskanta, R., 1998. An efficient simulation of the heat and mass transfer processes during drying of capillary porous, hygroscopic materials. International Journal of Heat and Mass Transfer 41, 3611-3625.

Wu, Q., 1989. An investigation of some problems in drying of Tasmanian Eucalypt timbers, Civil and mechanical engineering. University of Tasmania, p. 237.

Wu, Q.L., Milota, M.R., 1995. Rheological behavior of douglas-fir perpendicular to the grain at elevated-temperatures. Wood and Fiber Science 27, 285-295.

Ximenes, F.A., Gardner, W.D., Cowie, A.L., 2008. The decomposition of wood products in landfills in Sydney, Australia. Waste Management 28, 2344-2354.

Ximenes, F.A., Grant, T., 2013. Quantifying the greenhouse benefits of the use of wood products in two popular house designs in Sydney, Australia. The International Journal of Life Cycle Assessment 18, 891-908.

Yang, M., Blyth, W., 2007. Modeling investment risks and uncertainties with real options approach.

Yee, T.F., Grossmann, I.E., 1990. Simultaneous optimization models for heat integration—II. Heat exchanger network synthesis. Computers & Chemical Engineering 14, 1165-1184.

Yee, T.F., Grossmann, I.E., 1991. A screening and optimization approach for the retrofit of heat-exchanger networks. Industrial & Engineering Chemistry Research 30, 146-162.

Yee, T.F., Grossmann, I.E., Kravanja, Z., 1990. Simultaneous optimization models for heat integration—I. Area and energy targeting and modeling of multi-stream exchangers. Computers & Chemical Engineering 14, 1151-1164.

Yung, P., Lam, K.C., Yu, C., 2013. An audit of life cycle energy analyses of buildings. Habitat International 39, 43-54.

Zachariah, J.A.L., 2003. Towards Sustainable Homes Through Optimization [microform] An Approach to Balancing Life Cycle Environmental Impacts and Life Cycle Costs in Residential Buildings. Thesis (Ph.D.)--University of Toronto.

Zaid, A., Paul, J., 2014. The importance of embodied energy in carbon footprint assessment. Structural Survey 32, 49-60.

Zhan, J.F., Gu, J.Y., Shi, S.Q., 2009. Rheological behavior of larch timber during conventional drying. Drying Technology 27, 1041-1050.

Zhang, X., Zhao, X., Smith, S., Xu, J., Yu, X., 2012. Review of R&D progress and practical application of the solar photovoltaic/thermal (PV/T) technologies. Renewable and Sustainable Energy Reviews 16, 599-617.